

UNIVERSITE DU QUEBEC A MONTREAL

ETUDE DE LA CIRCULATION DES EAUX SOUTERRAINES DES BASSES
TERRES DU SAINT-LAURENT : APPROCHE PAR LES ISOTOPES DE
L'HELIUM ET DE L'URANIUM

THESE

PRESENTEE

COMME EXIGENCE PARTIELLE

DU DOCTORAT EN SCIENCES DE LA TERRE ET DE L'ATMOSPHERE

PAR

PAULINE MEJEAN

MAI 2016

UNIVERSITÉ DU QUÉBEC À MONTRÉAL
Service des bibliothèques

Avertissement

La diffusion de cette thèse se fait dans le respect des droits de son auteur, qui a signé le formulaire *Autorisation de reproduire et de diffuser un travail de recherche de cycles supérieurs* (SDU-522 – Rév.07-2011). Cette autorisation stipule que «conformément à l'article 11 du Règlement no 8 des études de cycles supérieurs, [l'auteur] concède à l'Université du Québec à Montréal une licence non exclusive d'utilisation et de publication de la totalité ou d'une partie importante de [son] travail de recherche pour des fins pédagogiques et non commerciales. Plus précisément, [l'auteur] autorise l'Université du Québec à Montréal à reproduire, diffuser, prêter, distribuer ou vendre des copies de [son] travail de recherche à des fins non commerciales sur quelque support que ce soit, y compris l'Internet. Cette licence et cette autorisation n'entraînent pas une renonciation de [la] part [de l'auteur] à [ses] droits moraux ni à [ses] droits de propriété intellectuelle. Sauf entente contraire, [l'auteur] conserve la liberté de diffuser et de commercialiser ou non ce travail dont [il] possède un exemplaire.»

AVANT-PROPOS

Cette thèse a été rédigée sous forme de trois articles en anglais formant chacun un chapitre. Le premier a été publié dans *Applied Geochemistry*, revue internationale avec comité de lecture. Le deuxième article sera soumis prochainement dans *Geofluids*, une revue spécialisée internationale avec comité de lecture. Alors que le troisième article sera soumis *Geophysical Research Letters*, revue spécialisée internationale également avec comité de lecture. La mise en page de ces trois chapitres suit donc les directives du Guide de présentation des mémoires et thèses de l'UQAM. De plus, d'un chapitre à l'autre les références bibliographiques sont conservées selon les mêmes directives.

Ma contribution aux publications qui constituent le corps de cette thèse couvre la totalité du domaine analytique. Une partie des échantillons d'eaux souterraines ayant fait l'objet de cette thèse ont été prélevés au cours de l'été 2011. J'ai par la suite complété l'échantillonnage au cours de l'été 2012. J'ai également participé et organisé le prélèvement des échantillons interprétés dans les chapitres II et III. J'ai réalisé l'ensemble des analyses des isotopes de l'U dans le laboratoire de radiochronologie du GEOTOP à l'UQAM. Quant aux isotopes de l'hélium ^3He , ^4He des chapitres II et III je les ai analysés au laboratoire des gaz rares de l'Université de Tokyo, à l'institut *AORI*. L'analyse de l'ensemble des données, la composition des figures, l'interprétation des résultats et la rédaction des manuscrits aux fins de publication ont été réalisés sous la supervision de mon directeur de thèse, Daniele Pinti, et de ma co-directrice Marie Larocque.

Un article intitulé *U-Th dating of broken speleothems from Cacahuamilpa cave, Mexico : Are they recording past seismic events?* a également été réalisé pendant mon doctorat (voir annexe). Cet article a été publié dans la revue *Journal of South America Earth Sciences* en 2015 avec pour co-auteurs Victor-Hugo Garduno-Monroy, Daniele L. Pinti, Bassam Ghaleb, Laura Bouvier, Martha G. Gomez-Vasconcelos et Alain Tremblay. Ce travail ne cadrait pas dans le sujet principal de cette thèse, il n'est pas repris comme chapitre à part entière pour assurer l'homogénéité du document final. Enfin, je suis co-auteure du papier Vautour, Pinti, Méjean *et al.* (2015) paru dans *Chemical Geology*. Ce papier contient les premiers âges isotopiques publiés sur les eaux souterraines de la zone d'étude de Bécancour dans le Centre-du-Québec, et a servi de base à la recherche présentée aux chapitres I et II.

REMERCIEMENTS

« Il ne faut avoir aucun regret pour le passé, aucun remord pour le présent, et une confiance inébranlable pour l'avenir »

Jean Jaurès

Merci à mon directeur de thèse Daniele ainsi qu'à Bassam pour m'avoir accordé leur confiance tout au long de ces années. Vous m'avez ouvert d'incroyables horizons jusqu'au soleil levant et permis que chaque pas posé en terrain inconnu le soit dans les meilleures conditions. Tout ceci n'aurait pas été possible sans votre soutien.

Un grand merci

Aux jolies rencontres transformées en sincères amitiés, aux français nouvellement québécois et à ceux seulement de passage, aux coups de cœur locaux,

À mes colocs et ex-colocs que j'adore et qui m'ont supportée avec beaucoup de patience : Marie, Christine, Clemence, Sam, Morgann, Remi.

Big up à SDB, car comme vous le savez, l'acquisition n'est rien sans sa transmission. Pour la musique et les voyages, c'est la même chose! Aux bourlingueurs que vous êtes, à nos aventures passées et aux prochaines !

À Marinette et Mimilie, et à tous les amis de cœur qui ont toujours répondu présents pour les grands rendez-vous inter-sudistes à Montpellier (même si Calvison, c'est un peu le Nord).

Aux vieux amis de lycée et nouveaux parisiens et nîmois (Titoune, Pepette, les 2 Morues, Kate,...), comme si l'on ne s'était jamais quittés et avec qui chaque rencontre dans un joli lieu parisien garde la même saveur de nos naïves années...

A l'énergie retrouvée grâce aux échanges et rencontres qui rythmaient nos saisons.

Un immense merci

Aux responsables et aides de laboratoire : JF, André, Agnieszka, Julien, Raynald L. ... pour leur gentillesse et leur infaillible patience.

À l'ancienne équipe de recherche de Marie et à ceux qui sont encore là, qui ont toujours répondu présents pour rattraper nos boulettes ou bien, sur lesquels on pouvait tester nos hypothèses les plus loufoques avec d'en parler aux « Chefs »,

À la sagesse de Diogo, Sophie, Lucie, Matthieu D. : collègues de bureau, de ragots et de sucreries...

Jenny, JB, Laurence et Audrey qui ont toujours su glisser un mot rassurant au bon endroit au bon moment,

À tous les collègues de doc', pour les conversations plus ou moins scientifiques (James, Coco, David, Hugo, PM, Adelphine, Sophie, MC, Aurélie...) ;)

Bras serrés le long du corps, le buste incliné en avant un bref instant,

A Lou(ette), à Lou(is), à Lou(ie), aux Lou(piottes) qu'on ira bientôt accrocher ensemble, aux Lou(ps) que l'on croisera peut être dans les Pyrénées, au petit Lou(stique) avec qui on ira bientôt jouer à Perpignan,

Au soutien de ma mère et de mon père, qui ont accepté mes allers sans retour. Merci pour le nombre incalculable de colis qui ont sournoisement passé les frontières avec ce que notre région offre de plus réconfortant, presque aussi apaisant qu'une sieste

sous le soleil de Paulilles en écoutant le bruit des vagues qui viennent se briser sur notre Côte Rocheuse.

A Sophie, à Bruno et à Rominou, la distance, on s'en fiche ! Ça ne change rien ☺

Enfin, j'aimerais rappeler que « la vie c'est comme la bicyclette, il faut avancer pour ne pas perdre l'équilibre»

A. Einstein

TABLE DES MATIÈRES

AVANT-PROPOS	II
REMERCIEMENTS.....	III
TABLE DES MATIÈRES	VI
LISTE DES FIGURES	VI
ABSTRACT.....	XIV
RÉSUMÉ	XVI
INTRODUCTION	1
0.1 Problématique.....	1
0.2 Objectifs de la thèse	5
0.3 Région d'étude	6
0.4 Matériel	11
0.5 Approche méthodologique	12
0.6 Organisation de la thèse	18
REFERENCES	20
CHAPITRE I.....	24
PROCESSES CONTROLLING ^{234}U AND ^{238}U ISOTOPE FRACTIONATION AND HELIUM IN THE GROUNDWATER OF THE ST. LAWRENCE LOWLANDS, QUEBEC: THE POTENTIAL ROLE OF NATURAL ROCK FRACTURING	24
ABSTRACT.....	25
1.1 INTRODUCTION.....	27
1.2 STUDY AREA.....	30
1.2.1 Geology and hydrogeology.....	30
1.2.2 Groundwater chemistry and ages.....	32
1.3 SAMPLING AND ANALYTICAL PROCEDURES	34
1.4 RESULTS.....	36
1.5 DISCUSSION	38
1.5.1 Uranium mobilization and redox conditions in the aquifers.....	38
1.5.2 ^{234}U - ^{238}U fractionation an the chemical evolution of the water.....	39
1.5.3 He and U isotopes: groundwater mixing	41

1.5.4 Processes leading to ($^{234}\text{U}/^{238}\text{U}_{\text{act}}$) isotopic fractionation and radiogenic ^4He excesses	43
1.6 CONCLUSIONS	47
ACKNOWLEDGMENTS	48
REFERENCES	49
FIGURES	56
CHAPITRE II	70
DO WE ALWAYS NEED BASAL FLUXES TO EXPLAIN RADIogenic ^4HE EXCESSSES IN GROUNDWATER? A U AND HE ISOTOPE TALE FROM QUEBEC AQUIFERS.....	70
ABSTRACT.....	71
2.1 INTRODUCTION.....	72
2.2 HYDROGEOLOGY OF THE STUDY AREA	75
2.3 RESULTS AND DISCUSSION	77
2.3.1 Revisiting the U-Th isotope system in the St. Lawrence Lowlands	77
2.3.2 Enhanced release of ^{234}U and ^4He in groundwater: causes and processes	78
2.3.3 Modeling the release of ^{234}U and ^4He into groundwater: principles.....	80
2.3.4 Modeling the release of ^{234}U and ^4He into groundwater.....	83
2.4 CONCLUSIONS	86
ACKNOWLEDGMENTS	87
REFERENCES	88
FIGURES.....	93
CHAPITRE III	99
MANTLE-DERIVED ^3HE IN GROUNDWATER OF THE ST. LAWRENCE LOWLANDS: A FOSSIL RECORD OF THE NEW ENGLAND HOTSPOT?	99
ABSTRACT.....	100
3.1 INTRODUCTION.....	101
3.2 GEOLOGY AND HYDROGEOLOGY OF THE STUDY AREA	103
3.3 SAMPLING AND ANALYTICAL METHODS.....	106
3.4 RESULTS.....	107
3.5 DISCUSSION	109

3.5.1 Sources of mantle helium in groundwater	109
3.5.2 Magma aging model and the mantle source	110
CONCLUSIONS	115
ACKNOWLEDGMENTS	115
APPENDICE	115
REFERENCES	117
FIGURES	124
CONCLUSIONS GÉNÉRALES	100
BIBLIOGRAPHIE.....	120
ANNEXE A	120

LISTE DES FIGURES

Figure	Page
0.1 Volumes d'eau stockés dans les différents réservoirs qui constituent le cycle global de l'eau (Gleeson <i>et al.</i> , 2016).....	3
0.2 Carte de localisation des zones de gestion intégrée de Bécancour et de Vaudreuil-Soulanges. En rouge sont représentées les intrusions Montérégien...es.....	6
0.3 Coupe hydrostratigraphique du bassin versant de Bécancour NO-SE depuis le fleuve à la limite amont de la zone d'étude (repris de Larocque <i>et al.</i> , 2013). . . 9	9
0.4 Coupe topo-géologique de la zone de gestion de Vaudreuil-Soulanges avec les écoulements souterrains théoriques et les zones potentielles de recharge (repris de Larocque <i>et al.</i> , 2015). 10	10
0.5 Schéma de désintégration de ^{238}U . ^{234}Th est éjecté hors du système cristallin (a), ^{234}Th reste dans le minéral et ^{234}U produit sera en position préférentielle pour passer en solution (b) (modifié de Kigoshi, 1971). 14	14
0.6 Représentation schématique des âges ^3H - ^3He et des trois réservoirs : atmosphérique, crustal et mantellique. Sont également représentés les rapports ^3He / ^4He (R) associés..... 16	16
1.1 Simplified map of the Bécancour watershed, southern Quebec, with potentiometric head isolines of the regional fractured bedrock aquifer and the groundwater sampled wells of this study (diamonds: Quaternary granular aquifer; circles: Ordovician regional fractured bedrock aquifer) (modified from Larocque <i>et al.</i> , 2013). 56	56

1.2	Cross section illustrating shallow granular aquifers and deeper fractured aquifers with geological groups belonging to the St. Lawrence Platform and the Appalachian Mountains (modified from Larocque <i>et al.</i> , 2013).	57
1.3	Logarithmic plot of Sodium (Na^+) versus Calcium (Ca^{2+}) for groundwater that is under-saturated to saturated in calcite (black dots) and groundwater saturated to oversaturated with respect to calcite (white dots). Plotted values are the calcite saturation index (SI; Table 1).	58
1.4	Plot of sodium (Na^+) versus Chloride (Cl^-) concentrations, showing the evolution of groundwater composition: Ca-HCO ₃ (white dots) and Ca,NaSO ₄ (black squares) type achieved through rock dissolution, Na-HCO ₃ (black dots) through ionic exchange, and Na-HCO ₃ -Cl (black and white dots) through mixing with older mineralized waters.....	59
1.5	Measured uranium concentrations (in ppb) in Bécancour watershed groundwater, compared to data from other sedimentary aquifers with similar lithological and hydrological conditions.	60
1.6	Measured ($^{234}\text{U}/^{238}\text{U}$) _{act} in Bécancour watershed groundwater, compared to data from other sedimentary aquifers with similar lithological and hydrological conditions. Dotted vertical lines represent the ($^{234}\text{U}/^{238}\text{U}$) _{act} secular equilibrium value.	61
1.7	Statistical boxplots of ($^{234}\text{U}/^{238}\text{U}$) _{act} for Bécancour watershed groundwater samples as a function of the geological province (a), aquifer type (b), hydrogeological conditions of aquifer (c), and groundwater chemistry (d).	62
1.8	U/Cl molar ratios as a function of SO ₄ /Cl ratios in Bécancour watershed groundwater samples. The dotted lines represent the seawater U/Cl and SO ₄ /Cl ratios. Numbers in parentheses for BEC101, BEC119, and F9 are measured ($^{234}\text{U}/^{238}\text{U}$) _{act}	63

1.9	Measured $(^{234}\text{U}/^{238}\text{U})_{\text{act}}$ as a function of Na^+ . Diamonds represent groundwater from Quaternary granular aquifers. Circles represent groundwater from the Ordovician fractured bedrock, where samples whose chemistry is controlled by the dissolution of carbonates are shaded gray, and black symbols represents samples whose chemistry is controlled by ionic exchange processes.	64
1.10	Measured $(^{234}\text{U}/^{238}\text{U})_{\text{act}}$ as a function of Na^+ concentration (a), and alkalinity (b). Diamonds represent groundwater from Quaternary granular aquifers. Circles represent groundwater from the Ordovician fractured bedrock, where samples whose chemistry is controlled by the dissolution of carbonates are shaded gray, and black symbols represents samples whose chemistry is controlled by ionic exchange processes... ..	65
1.11	Measured $(^{234}\text{U}/^{238}\text{U})_{\text{act}}$ as a function of the ${}^3\text{He}/{}^4\text{He}$ ratios normalized to the same ratio measured in the air (Ra). Least-square mixing hyperbolas between an evolved water end-member, with $(^{234}\text{U}/^{238}\text{U})_{\text{act}}$ of 6.07 and ${}^3\text{He}/{}^4\text{He}$ ratio of 0.012Ra, and a tritiogenic-rich freshwater end-member, with $(^{234}\text{U}/^{238}\text{U})_{\text{act}}$ of ~1 and ${}^3\text{He}/{}^4\text{He}$ ratio of 3.109Ra, are also plotted. Values of hyperbola curvature, “r”, are reported for each mixing curve. Symbols are as in figure 8, 9 and 10.	66
2.1	Simplified map of the Bécancour watershed. Potentiometric head contour lines of the fractured bedrock aquifer and location of groundwater samples are reported (from Larocque <i>et al.</i> , 2013).	93
2.2	Cross section illustrating shallower Quaternary granular aquifers and deeper Ordovician fractured aquifer. Geological formations/groups belonging to the St. Lawrence Platform and the Appalachian Mountains Supergroups are reported (from Larocque <i>et al.</i> , 2013).	94

2.3	Plot of ${}^4\text{He}$ and $({}^{234}\text{U}/{}^{238}\text{U})_{\text{act}}$ with supposed groundwater end-members and mixing trends (dashed lines). End-members 1 and 3 correspond to two different recharge conditions while end-member 2 is mainly influenced by accumulation of both ${}^{234}\text{U}$ and ${}^4\text{He}$. See text for details.	95
2.4	Schematic representation of shallower fractures aquifer with a) condition of water circulation in the system during Laurentide Ice Sheet retreat ca. 12kyrs, and b) between 10.6 kyrs and the present-day.....	96
2.5	Simulation of $({}^{234}\text{U}/{}^{238}\text{U})_{\text{act}}$ evolution as a function of time, using $S = 5.746 \text{ cm}^2 \text{ cm}^{-3}$ calculated with eqn. 2.4.....	96
2.6	Simulated ${}^4\text{He}$ released into water as a function of time since ice retreat using eqn. 2.5 with diffusion coefficient $D_1=1 \times 10^{-18} \text{ cm}^2 \text{ s}^{-1}$ (black diamonds) and $D_2 = 1 \times 10^{-19} \text{ cm}^2 \text{ s}^{-1}$	96
3.1	Location map of the St. Lawrence Lowlands including the intrusions of the Cretaceous Monteregean Hills, the Bécancour region (BEC), the Nicolet and lower Saint-Francois River region (NSF), and the Vaudreuil-Soulanges watershed (VS). The percentage of mantle helium (fm) measured in each watershed is also indicated.	124
3.2	Geological map of the VS region with piezometric heads and location of the sampled wells.	125
3.3	Weise-type plot of measured helium ratios corrected for air bubble entrainment ($({}^3\text{He}/{}^4\text{He})_{\text{total}} - ({}^3\text{He}/{}^4\text{He})_{\text{ea}}$) vs. the relative amount of ${}^4\text{He}$ derived from solubility with respect to total He, corrected for air bubble entrainment (${}^4\text{He}_{\text{ea}}/({}^4\text{He}_{\text{tot}} - {}^4\text{He}_{\text{ea}})$) in VS groundwater. The black line represents the mixing between water at the recharge (Air Saturated Water or ASW). Dashed lines interpolated through samples represent the addition of 5, 18, 35 and 65 TU helium, mixed with the terrigenic	

	components having variable R_{terr} . The stars represent the ASW (R_{eq}) and terrigenic (R_{terr}) helium end-members.....	126
3.4	Evolution of the $[R/\text{Ra}]_{\text{magma}}$ as a function of time elapsed since the intrusion of the Precambrian syenite of Mont Rigaud (564^{+10}_{-8} Ma) using the “magma aging” model of Torgersen <i>et al.</i> (1995; eqn. 3.2) (bold line). Initial helium ratio R/Ra for a SLCM was fixed at 6.5 (grey star). Dashed lines represent evolution of the SLCM source taking into account uncertainties on the initial R/Ra . The R/Ra measured in VS108 (16.7% of total helium) is represented by a red star.....	127
3.5	Evolution of the $[R/\text{Ra}]_{\text{magma}}$ as a function of time elapsed since the intrusion of (a) Oka carbonatite 123 ± 2 Ma ago using the “magma aging” model of Torgersen <i>et al.</i> (1995; eqn. 3.2) (bold line). Dashed lines represent evolution of the OIB source taking into account uncertainties on the initial R/Ra . The R/Ra measured in VS108 (16.7% of total helium) is represented by a red star.	128
3.6	Evolution of the $[R/\text{Ra}]_{\text{magma}}$ as a function of time elapsed since the intrusion of (a) Oka carbonatite and (b) alnoïte 123 ± 2 Ma ago using the “magma aging” model of Torgersen <i>et al.</i> (1995; eqn. 3.2) (bold line). Dashed lines represent evolution of the OIB source taking into account uncertainties on the initial R/Ra . The R/Ra measured in VS108 (16.7% of total helium) is represented by a red star.	129

ABSTRACT

The residence time of groundwater is a fundamental parameter for estimating water resources that are available at the human time scale. Discriminating between “young” and “old” water provides crucial information for understanding how groundwater resources respond to climatic and anthropogenic stresses (i.e. pollution). The approach based on radiometric ages consists of using isotopes of radioactive elements that decay into daughter elements along the flow path, for example ${}^3\text{H}/{}^3\text{He}$ and $(\text{U}-\text{Th})/{}^4\text{He}$. However, several studies coupling $(\text{U-Th})/{}^4\text{He}$ water dating with other isotopic chronometers (such as ${}^{14}\text{C}$) have shown that the amount of ${}^4\text{He}$ in the water frequently exceeds the amount expected to be accumulated due to local *in situ* production from rocks composing the aquifers.

The objective of this thesis was to identify and quantify ${}^{3,4}\text{He}$ components: atmospheric component (${}^{3,4}\text{He}_{\text{ASW}}$), terrigenic component (crustal production of radiogenic ${}^4\text{He}$ or mantle ${}^{3,4}\text{He}$) or tritiogenic component (${}^3\text{He}_{\text{tri}}$) from total helium measured in groundwater samples to constrain ${}^3\text{H}/{}^3\text{He}$ and $(\text{U-Th})/{}^4\text{He}$ methods of datation. The research focuses on the fractured bedrock aquifer of two regions of the St. Lawrence Lowlands where groundwater characterization projects have been carried out: 1) the Bécancour and 2) the Vaudreuil-Soulanges watersheds.

The behavior of dissolved uranium isotopes (${}^{234}\text{U}$ and ${}^{238}\text{U}$) was studied in the Bécancour watershed. The results show that groundwater results from a mixing between two end-members: 1) low $({}^{234}\text{U}/{}^{238}\text{U})_{\text{act}}$, 1.14 ± 0.01 measured in Ca- HCO_3 -type freshwater from the shallow Quaternary aquifer. Here bulk dissolution of carbonates allows U to migrate into water with little ${}^{234}\text{U}-{}^{238}\text{U}$ isotopic fractionation; and 2) high $({}^{234}\text{U}/{}^{238}\text{U})_{\text{act}}$, up to 6.07 ± 0.14 in Na- $\text{HCO}_3\text{-Cl}$ -type groundwater contained in a confined part of the Paleozoic regional aquifer. Interestingly, there is an inverse relationship between $({}^{234}\text{U}/{}^{238}\text{U})_{\text{act}}$ and R/Ra (i.e. $({}^3\text{He}/{}^4\text{He})_{\text{water}}$ normalized

to that of the atmosphere (or ($^3\text{He}/^4\text{He}_{\text{air}}$)) underlining enrichment of both radiogenic ^4He and ^{234}U isotopes in the water. This suggests a common mechanism of release and enrichment of both isotopes in groundwater. The re-evaluation of the internal source of production of radiogenic ^4He was achieved using a coupled model of ^{234}U preferential solution and radiogenic ^4He released from grains into groundwater. This model assumes comminution (reduction of size) of the aquifer matrix's grains, by fracturation during the retreat of the Holocene Laurentides Ice Sheet and isostatic rebound and relaxation of the crust. The result of this study suggests that local sources of helium, in aquifers, have the potential to retain large amounts of radiogenic ^4He . This is an interesting and alternative explanation of radiogenic ^4He excess measured in hydrogeological settings worldwide explained by the occurrence of an external basal He flux.

In the Vaudreuil-Soulanges region helium isotopes shown a mantle helium component (up to 16.7 % of the total measured helium), which was, to a lesser extent, observed in the neighbouring watersheds of the Nicolet, Saint-François (8%), and Bécancour rivers (2%). It was postulated that groundwater acquired this fossil mantle helium locally, by leaching magmatic intrusions related to the emplacement of the Montréal Hills. Results of a model for "magma aging" suggest that Cretaceous intrusions related to the Oka Carbonatite Complex are the source of this derived helium. Simulations also suggest an initial R/Ra up to 58 which excludes subcontinental mantle as the source of the Montréal Hills, but favors the hypothesis of their emplacement during the passage of the New England hotspot. These results might constitute an alternative argument to resolve this end-less debate on the source of this magmatic province.

RÉSUMÉ

Le temps de résidence des eaux souterraines est un paramètre essentiel dans l'estimation des ressources disponibles pour alimenter en eau potable les populations. La différence entre une eau « jeune » et une eau « ancienne » est un critère crucial pour comprendre comment réagit un système aquifère face aux pressions climatiques et anthropiques. L'une des approches est basée sur la datation radiométrique qui est obtenue en quantifiant la décroissance d'éléments radioactifs en éléments fils le long des lignes d'écoulements, comme par exemple les méthodes $^3\text{H}/^3\text{He}$ et $(\text{U-Th})/^4\text{He}$. Néanmoins, plusieurs études ont montré que, couplées à d'autres méthodes de datation isotopiques (p.ex. âges ^{14}C), les âges calculés $(\text{U-Th})/^4\text{He}$ sont trop vieux, soit l'eau contient des excès en ^4He avec des teneurs qui dépassent de plusieurs ordres de grandeur les quantités prédictes par la production *in situ* des roches encaissantes.

L'objectif de cette thèse était d'identifier et de quantifier l'origine de toutes les composantes d'hélium présentes, soit la composante atmosphérique acquise à la recharge ($^3\text{He}_{\text{ASW}}$ et $^4\text{He}_{\text{ASW}}$), la composante terrigénique (production crustale de $^4\text{He}_{\text{terr}}$ ou mantellique de $^{3,4}\text{He}_{\text{terr}}$) et la composante tritiogénique ($^3\text{He}_{\text{tri}}$) dans les eaux souterraines afin de contraindre les méthodes de datation $^3\text{H}/^3\text{He}$ et $\text{U-Th}/^4\text{He}$. Ce travail a été mené sur les eaux souterraines prélevées dans les aquifères fracturés Paléozoïques et granulaires Quaternaires de deux bassins versants situées dans les Basses-Terres du Saint-Laurent où des projets de caractérisation sont menés : 1) Bécancour, 2) et Vaudreuil-Soulanges.

Dans la région de Bécancour, le comportement des isotopes de l'uranium dissous (^{234}U et ^{238}U) a été caractérisé, ce qui a permis de mettre en évidence des mélanges entre deux familles d'eaux : 1) des eaux de type Ca-HCO₃ nouvellement infiltrées et contenues dans les aquifères superficiels du Quaternaire avec des rapports d'activités

isotopiques ($^{234}\text{U}/^{238}\text{U}$)_{act} de 1.14 ± 0.01 . C'est la dissolution des carbonates qui a permis la mise en solution de l'uranium avec un rapport d'activité isotopique ($^{234}\text{U}/^{238}\text{U}$)_{act} peu fractionné ; et 2) des rapports ($^{234}\text{U}/^{238}\text{U}$)_{act} élevés jusqu'à 6.07 ± 0.14 dans des eaux de type Na-HCO₃-Cl dans l'aquifère fracturé Paléozoïque. Fait intéressant, il existe une relation inverse entre ($^{234}\text{U}/^{238}\text{U}$)_{act} et R/Ra (i.e. ($^3\text{He}/^4\text{He}$)_{eau} normalisé au rapport de l'atmosphère, ($^3\text{He}/^4\text{He}_{\text{air}}$)), ce qui souligne l'enrichissement conjoint de ^4He radiogénique et de l'isotope ^{234}U dans l'eau. La réévaluation de la production de l' ^4He radiogénique a été effectuée en couplant le modèle de mise en solution préférentielle de ^{234}U avec le modèle de relâche de ^4He depuis le grain dans l'eau souterraine en assumant une réduction de la taille des grains consécutivement au retrait du glacier Laurentidien.

Cette étude suggère que des mécanismes locaux pourraient être la cause des grandes quantités de ^4He radiogénique mesurées dans les eaux de ces bassins versants. Cette hypothèse permettrait de façon novatrice d'expliquer les quantités de ^4He parfois supérieures de plusieurs ordres de grandeur aux quantités produites par l'U et le Th des roches au sein de l'aquifère, jusqu'ici attribué à l'ajout d'un flux basal d'hélium extérieur à l'aquifère.

Dans la région de Vaudreuil-Soulanges, les résultats révèlent des valeurs élevées de la composante mantellique de l'hélium, jusqu'à 16.7%, avec une décroissance régionale en s'éloignant de Vaudreuil (8% sur les bassins versants des rivières Nicolet et Saint-François, et 2% sur le bassin versant de la rivière Bécancour). L'hypothèse est que les eaux auraient accumulé localement de l'hélium mantellique fossile par interactions avec des intrusions présentes dans la région. Le modèle de « vieillissement du magma » suggère que les intrusions Crétacées en lien avec la mise en place du complexe carbonaté d'Oka (Collines Montérégiennes) seraient la source de l'hélium mesuré dans les eaux. Le modèle montre également que des rapports initiaux R/Ra jusqu'à 58 excluent le manteau subcontinental comme source des collines

Montérégiennes mais alimente l'hypothèse de la mise en place de ces intrusions suite au passage du point chaud *New England*. Ces données pourraient donc constituer une preuve supplémentaire permettant de mettre fin au débat qui perdure depuis trente ans sur la source de cette province magmatique continentale.

Mots-clés : Temps de résidence des eaux souterraines; Basses-Terres de Saint-Laurent; Aquifères fracturés; Fractionnement ^{234}U - ^{238}U : Excès de ^4He radiogénique; Composante mantellique de l'hélium; Collines Montérégienne.

INTRODUCTION

0.1 Problématique

Le Canada possède 7% des ressources en eau douce renouvelables de la planète (Gouvernement du Canada ; 2016). Il puise majoritairement son eau potable dans les systèmes hydriques de surface (rivières et lacs). Les connaissances sur les réserves d'eau souterraine et sur leur vulnérabilité sont encore mal quantifiées sur la majorité du territoire du Canada, y compris dans les régions du pays proches de la frontière américaine où vit 70% de la population. Face aux pressions anthropiques et aux changements climatiques (Aeschbach-Hertig et Gleeson, 2012), les réserves hydriques de surface sont de plus en plus en danger et une évaluation plus précise des stocks d'eau souterraine est nécessaire pour assurer le développement économique et agricole du pays, ainsi que le maintien des écosystèmes dépendants des eaux souterraines.

En 2009, le Ministère du Développement durable, de l'Environnement et Lutte contre les changements climatiques (MDDELCC) a mis sur pied le *Programme d'acquisition de connaissances sur les eaux souterraines du Québec*. Le but de ce programme était de dresser un portrait réaliste et concret de la ressource en eaux souterraines des territoires municipalisés du Québec méridional dans le but ultime de protéger la ressource et d'en assurer la pérennité.

L'originalité des études réalisées dans ce programme se révèle par l'aspect multidisciplinaire qui a permis l'élaboration de rapports scientifiques de qualité. Ces rapports ont ensuite été rendus accessibles aux populations concernées par l'intermédiaire du Réseau québécois sur les eaux souterraines (RQES). Dans le cadre de ce vaste programme d'acquisition de données, plusieurs études scientifiques ont

participé au développement des méthodes de quantification des ressources en eau souterraine afin de comprendre leur vulnérabilité face aux pressions anthropiques.

Une de ces méthodes consiste à estimer l'âge de l'eau souterraine : à savoir le temps écoulé depuis l'infiltration des eaux de surface jusqu'au moment où un puits intercepte la nappe.

Un aquifère alimenté par des précipitations modernes se renouvelle plus rapidement (quelques dizaines d'années) qu'un aquifère captif ne recevant pas ou très peu de recharge. Ce dernier sera susceptible de se renouveler à une échelle de temps supérieure à celle humaine. Le temps de résidence de l'eau souterraine est un critère très important pour la gestion de la ressource en eau souterraine puisque l'aquifère le plus rapidement renouvelé sera également le plus vulnérable face aux pollutions anthropiques de surface (Bethke et Johnson, 2008).

La définition stricte de l'âge de l'eau rappelle qu'une eau n'est pas simplement une masse isolée qui aurait intégré un système aquifère depuis un certain temps, mais plutôt un mélange de différentes masses d'eau ayant eu des temps de résidence dans les aquifères plus ou moins longs (Phillips et Castro, 2003) impliquant des temps de contact eau-roche eux aussi différents. Une étude très récente de Gleeson *et al.* (2016) reprenant les résultats des datations des plus grands aquifères au monde a montré que sur les 22.6 millions de km³ d'eau souterraine présente dans les premiers 2 km de croûte terrestre, seulement 0.63 millions de km³ ont un âge inférieur à 100 ans (Fig. 0.1). L'eau restante a des âges allant de quelques milliers d'années (Aggarwal *et al.*, 2015) à des millions (Pinti et Marty, 1998) voire des centaines de millions d'années ; (Bottomley *et al.*, 2002; Lippmann-Pipke *et al.*, 2011; Pinti *et al.*, 2013).

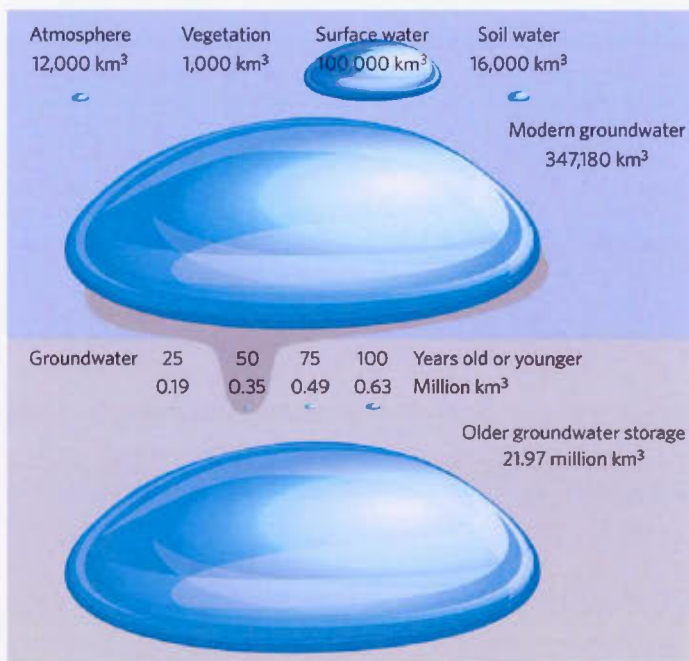


Figure 0.1 Volumes d'eau stockés dans les différents réservoirs qui constituent le cycle global de l'eau (Gleeson *et al.*, 2016).

Les processus d'interaction de l'eau avec les minéraux constitutifs d'un aquifère (hydrolyse, dissolution, précipitation, échanges ioniques, etc.) sont d'une grande importance car ils laissent une empreinte géochimique dans les eaux, participant ainsi à la minéralisation de l'eau souterraine qui conduit à l'individualisation de différents types d'eau (Mazor, 2003; Porcelli et Baskaran, 2012). Ces « empreintes géochimiques » sont de précieux outils pour estimer le temps de résidence des masses d'eaux souterraines dans un aquifère.

Pour les aquifères des Basses-Terres du Saint-Laurent dans le Québec méridional, les travaux récemment publiés ont permis d'adapter les approches isotopiques à la présence d'eaux ayant interagi avec différents réservoirs : atmosphère, croûte et manteau (Saby *et al.*, 2016; Vautour *et al.*, 2015). Ces masses d'eau ont des âges variés allant d'une eau d'âge moderne (où l'obtention d'âges tritiogéniques ${}^3\text{H}/{}^3\text{He}$

est possible pour des temps de résidence inférieurs à 60 ans), à une eau potentiellement très ancienne pour laquelle la présence de formation carbonatées met en évidence les limites d'utilisation de la méthode de datation ^{14}C (la dissolution de carbone mort entraînant un vieillissement artificiel des âges calculés). Une solution récemment proposée dans les Basses-Terres du Saint-Laurent par Vautour *et al.* (2015) est l'utilisation de la méthode de datation $(\text{U-Th})/{}^4\text{He}$ qui est basée sur la quantification de l' ${}^4\text{He}$ produit par désintégration radioactive de l'U et du Th des roches de l'aquifère puis son transfert dans l'eau porale. Cette méthode est utile pour étudier des eaux ayant entre un millier d'années jusqu'à des millions d'années (Torgersen et Stute, 2013).

Dans les Basses-Terres du Saint-Laurent, comme dans de nombreux autres bassins sédimentaires dans le monde, des teneurs en ${}^4\text{He}$ de plusieurs ordres de grandeur en excès par rapport à la production *in situ* ont été mesurées (Pinti et Marty, 1998). Les conditions de relâche de l' ${}^4\text{He}$ étant mal contraintes, ces excès entraînent un vieillissement des âges $(\text{U-Th})/{}^4\text{He}$ calculés qui divergent des âges estimés par d'autres méthodes de datation isotopiques (âge ${}^3\text{H}/{}^3\text{He}$ et ${}^{14}\text{C}$; Vautour *et al.*, 2015). À ces excès en ${}^4\text{He}$ ont également été associées des teneurs élevées en ${}^3\text{He}$ qui ne peuvent pas être expliqués par la production tritiogénique (${}^3\text{H} \rightarrow {}^3\text{He}$) ou radiogénique (${}^6\text{Li}(\text{n},\alpha){}^3\text{H}(\beta){}^3\text{He}$). Dans cette région, de l' ${}^3\text{He}$ d'origine mantellique a récemment été mesuré, ce qui rend indispensable la quantification précise des différentes sources d'hélium (atmosphérique, crustale, mantellique) afin d'optimiser l'utilisation des méthodes de datation ${}^3\text{H}/{}^3\text{He}$ et $(\text{U-Th})/{}^4\text{He}$.

0.2 Objectifs de la thèse

Le but de cette thèse est de comprendre l'origine des excès en hélium (^3He et ^4He) mesurés dans les eaux souterraines et de proposer une solution pour mieux contraindre les sources terrigéniques nécessaires à l'obtention des âges isotopiques $^3\text{H}/^3\text{He}$ et $(\text{U-Th})/^4\text{He}$. Plus spécifiquement, l'objectif de cette thèse est d'identifier et de quantifier l'origine de toutes les composantes d'hélium présentes, soit la composante atmosphérique acquise à la recharge ($^3\text{He}_{\text{ASW}}$ et $^4\text{He}_{\text{ASW}}$), la composante terrigénique (production crustale de $^4\text{He}_{\text{ter}}$ ou mantellique de $^{3,4}\text{He}_{\text{ter}}$), et la composante tritiogénique ($^3\text{He}_{\text{tri}}$) afin de contraindre les méthodes de datation $^3\text{H}/^3\text{He}$ et $\text{U-Th}/^4\text{He}$. Les objectifs spécifiques sont les suivants :

Identifier les masses d'eaux présentes dans l'aquifère des Basses-Terres du Saint-Laurent par la mise en évidence de pôles géochimiques à l'aide des rapports isotopiques de l'hélium ($^3\text{He}/^4\text{He}$) et de l'uranium ($^{234}\text{U}/^{238}\text{U}_{\text{act}}$,

Déterminer les processus contrôlant la mise en solution de l'uranium depuis la zone de recharge d'un bassin versant et les interactions eaux-roches le long des lignes d'écoulement grâce aux isotopes de l'uranium (^{234}U et ^{238}U) et à l'évolution du rapport d'activité isotopique ($^{234}\text{U}/^{238}\text{U}_{\text{act}}$,

Quantifier les processus de mise en solution de l' ^4He et de l' ^{234}U en fonction du temps de contact et des caractéristiques lithologiques des aquifères traversés afin de contraindre les temps de résidence de l'eau,

Relier l'histoire isotopique des eaux souterraines au contexte géologique associé au bassin sédimentaire des Basses Terres du Saint-Laurent.

0.3 Région d'étude

Les deux zones d'étude retenues pour cette thèse se situent au sud du Québec dans les Basses-Terres du Saint-Laurent, le long du fleuve Saint-Laurent : 1) la zone de gestion intégrée de l'eau de Bécancour ($2,924 \text{ km}^2$) dans le Centre-du-Québec, où 43% des municipalités assurent leur approvisionnement en eau potable à partir des eaux souterraines (Larocque *et al.*, 2013) et 2), la zone de gestion intégrée de l'eau de Vaudreuil-Soulanges (814 km^2), proche de la frontière ontarienne, où 62% de la population s'approvisionne à partir de puits captant les eaux souterraines (Larocque *et al.*, 2015) (Fig. 0.2).

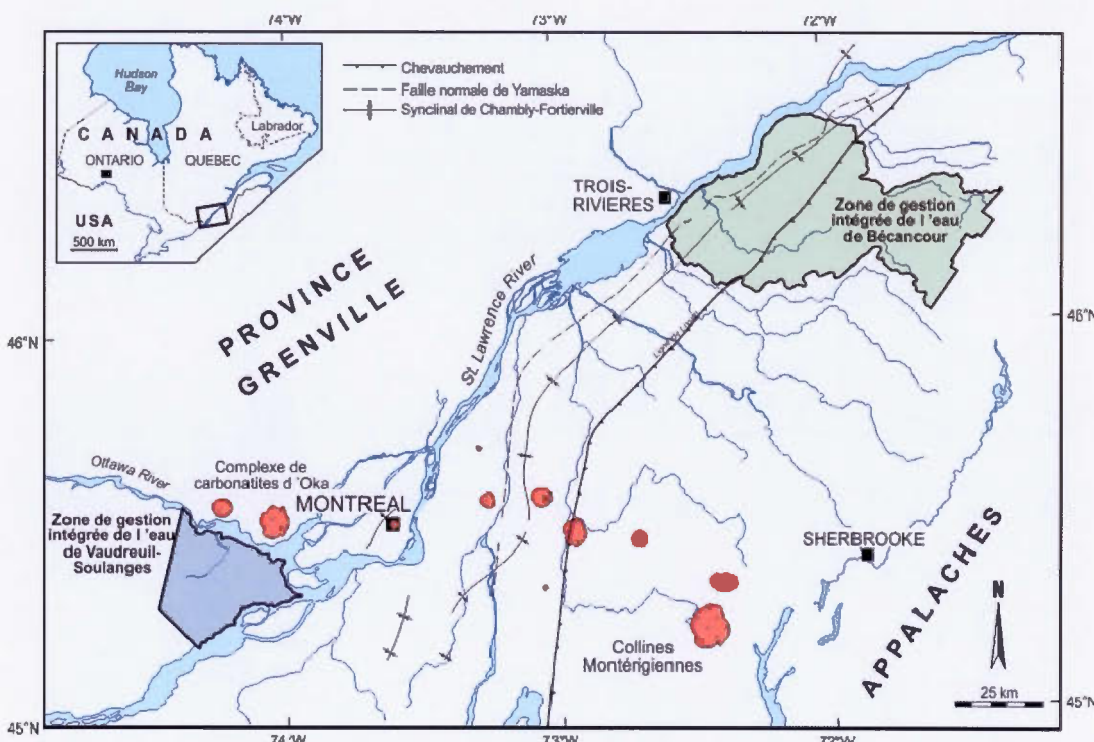


Figure 0.2 Carte de localisation des zones de gestion intégrée de Bécancour et de Vaudreuil-Soulanges. En rouge sont représentées les intrusions Montérégiennes.

Les Basses-Terres du Saint-Laurent s'étendent de la ville d'Ottawa jusqu'à Québec le long du fleuve Saint Laurent et couvrent une superficie de $20,000 \text{ km}^2$ sur le territoire

québécois (Globensky, 1987). Les roches sédimentaires qui les composent sont datées du Cambrien à l'Ordovicien. Elles sont généralement subhorizontales à légèrement plissées par la mise en place des Appalaches (Ordovicien) lors de la déformation Taconienne et lors de la déformation Acadienne. Cet épisode est marqué par la mise en place du synclinal de Chambly-Fortierville (Fig. 0.2). Les formations des Basses-Terres peuvent atteindre 3,000 m d'élévation et sont représentées à la base du Cambrien et au sommet de l'Ordovicien, par des formations continentales alors que la partie médiane est marine (Globensky, 1987). Les roches autochtones des Basses-Terres sont principalement de nature détritique : les grès du Potsdam déposés en discordance sur le socle Précambrien du Grenville. On retrouve ensuite les dolomies et grès du Beekmantown ainsi que des dolomies fossilières, calcaires cristallins et grès du groupe de Chazy (Ordovicien moyen). Ensuite les shale calcareux de l'Utica (Ordovicien moyen) déposés dans un bassin anoxique en fermeture. Grâce à leur richesse en matière organique, ces séries ont été identifiées comme des shales gazifères (Lavoie *et al.*, 2009; Séjourné *et al.*, 2013). Ces formations sont chevauchées par les shales, grès et calcaires du Groupe Lorraine (Ordovicien moyen), elles aussi potentiellement des shales gazifères, et les molasses (shale rouges et grès) du Groupe Queenston (Ordovicien supérieur).

Par-dessus les formations d'âge Ordovicien décrites auparavant, se sont déposées les séquences d'âge quaternaire avec des épaisseurs pouvant atteindre 100 m à proximité du Saint-Laurent. Elles sont séparées par des sédiments glacio-lacustres conséquents aux avancées et retraits des glaciers. À chaque couche de till sont associés des sédiments laminés glacio-lacustres provenant des lacs glaciaires formés consécutivement aux avancées et retraits du glacier créant un drainage des eaux vers le N-E. Ces sédiments sont sur-consolidés et leur arrangement granulométrique leur confère une grande imperméabilité.

La déglaciation de l’Inlandsis Laurentidien a permis les dépôts successifs de sédiments fluvioglaciaires et glacio-lacustres. La dépression pro-glaciaire laissée après le recul de l’inlandsis a été occupée par l’Océan Atlantique, créant la Mer de Champlain. La mer de Champlain a ennoyé les Basses-Terres de l’Outaouais et du Saint-Laurent en amont de Québec entre 13,100 et 10,600 ans B.P. (Occhietti et Richard, 2003) pour ensuite disparaître et se réduire en une série de lacs postglaciaires (comme le Lac de Champlain) quand le bouclier canadien est remonté par rebond isostatique. Le roc est principalement observé dans le secteur amont des zones étudiées au-dessus de 200 m et au niveau des hauteurs topographiques.

Dans les Basses-Terres, les eaux souterraines sont majoritairement présentes dans l’aquifère fracturé constitué dans les dépôts sédimentaires déposés en discordance sur le socle Grenvillien. Des aquifères locaux et de moindre importance sont également présents dans les dépôts meubles de surface consécutifs aux épisodes glaciaires. On notera que dans cette région, comme dans le reste du Québec, les échanges entre aquifères superficiels et profonds (voire très profonds) constituent une problématique complexe (Pinti *et al.*, 2011; 2014) qui sera prise compte dans cette thèse.

Dans les aquifères granulaires et fracturés de la zone d’étude de Bécancour, les eaux souterraines circulent régionalement depuis la zone préférentielle d’infiltration située au piedmont des Appalaches, où les formations sédimentaires affleurent, vers la rivière Saint-Laurent où l’aquifère devient captif sous des dépôts quaternaires peu perméables (Fig. 0.3). Les eaux souterraines acquièrent une chimie de type Ca-HCO₃ et Ca-SO₄ par dissolution du matériel encaissant lors de la recharge. Ces eaux évoluent vers une composition chimique de type Na-HCO₃ et Na-SO₄ par échange ionique entre Ca²⁺ dissous et Na⁺ de la matrice de l’aquifère (Meyzonnat *et al.*, 2016). Les eaux les plus évoluées ont des signatures de type Na-Cl grâce aux mélanges avec des eaux porales marines encavées dans les argiles déposées lors de l’épisode de la mer de Champlain (Cloutier *et al.*, 2006). De récents travaux ont mis en évidence la

présence conjointe de recharges récentes avec des âges $^{3}\text{H}/^{3}\text{He}$ entre 2 et 60 ans mélangées et des eaux ayant des âges corrigés ^{14}C jusqu'à plusieurs milliers d'années (Vautour *et al.*, 2015).

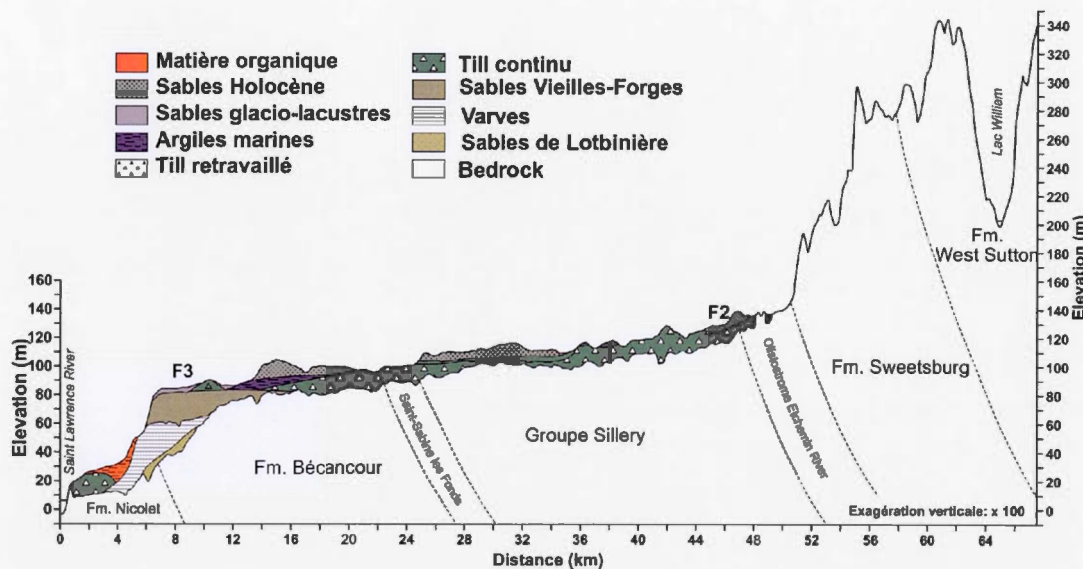


Figure 0.3 Coupe hydrostratigraphique du bassin versant de Bécancour NO-SE depuis le fleuve à la limite amont de la zone d'étude (repris de Larocque *et al.*, 2013).

Dans la zone d'étude du Vaudreuil-Soulanges, les hauts niveaux topographiques constituent les zones préférentielles d'infiltration (Mont Rigaud, buttes de Saint-Lazare et d'Hudson, esker de Saint-Telesphore) (Larocque *et al.*, 2015; fig. 04). Ces aquifères passent rapidement en condition de nappe captive au niveau de la plaine argileuse qui recouvre 76% de la zone d'étude. L'écoulement régional se fait ici vers la rivière des Outaouais et vers le fleuve Saint-Laurent (Fig. 0.4). L'évolution chimique des eaux est reliée à des processus similaires à ceux décrits précédemment dans la zone de Bécancour avec des eaux de type Ca-Mg-HCO₃ et Ca-SO₄ dans les zones de recharge vers une chimie de type Na-Cl dans la plaine argileuse.

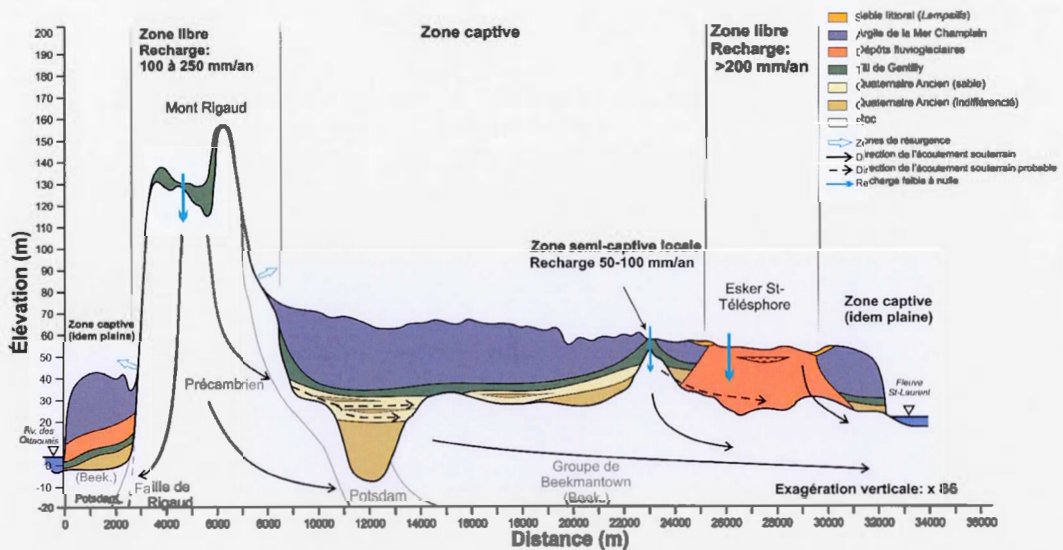


Figure 0.4 Coupe topo-géologique de la zone de gestion de Vaudreuil-Soulanges avec les écoulements souterrains théoriques et les zones potentielles de recharge (repris de Larocque et al., 2015).

0.4 Matériel

Les campagnes d'échantillonnages des eaux souterraines des zones d'études de Bécancour et de Vaudreuil-Soulanges ont eu lieu au cours des étés 2011 et 2012 (38 échantillons prélevés) et 2012 et 2013 respectivement (15 échantillons prélevés) dans les 100 premiers mètres des aquifères granulaires et fracturés. Les analyses ont porté sur les ions majeurs, mineurs, isotopes de l'eau ($\delta^{18}\text{O}$ et $\delta^2\text{H}$; GEOTOP, UQAM), gaz rares (${}^4\text{He}$, ${}^{20}\text{Ne}$, ${}^{36}\text{Ar}$, ${}^{84}\text{Kr}$, ${}^{132}\text{Xe}$; laboratoire GEOTOP-GRAM, UQAM), et isotopes de l'hélium ${}^3\text{He}/{}^4\text{He}$ (laboratoire *Atmosphere and Ocean Research Institute* AORI de l'Université de Tokyo). Ces échantillons proviennent de puits municipaux, de puits privés ainsi que de piézomètres mis en place dans le cadre du Projet de connaissances des eaux souterraines du bassin versant de la rivière Bécancour et de la MRC de Bécancour (Larocque *et al.*, 2013) et dans le cadre du projet PACES de la zone de Vaudreuil-Soulanges (Larocque *et al.*, 2015). Lors de travaux en commun avec les résultats publiés par Saby *et al.* (2016), le contenu en hélium de 26 échantillons d'eau prélevés dans la zone d'étude de Nicolet-Saint-François au cours de la campagne d'échantillonnage de l'été 2013 a également été analysé (${}^3\text{He}/{}^4\text{He}$; laboratoire *Atmosphere and Ocean Research Institute* AORI de l'Université de Tokyo) et fera l'objet d'un article synthétisant l'évolution de l'hélium à l'échelle régionale des Basses Terres (Saby, Méjean *et al.*, 2016, en prep.).

Parmi les échantillons prélevés sur la zone d'étude de Bécancour, 23 ont été sélectionnés afin d'y mesurer les concentrations en uranium dissous (particules $<0.07\mu\text{m}$) et le rapport d'activité isotopique, $({}^{234}\text{U}/{}^{238}\text{U})_{\text{act}}$ afin d'étudier l'évolution du fractionnement ${}^{234}\text{U}-{}^{238}\text{U}$ amont-aval et sur un transect médian au cœur du synclinal Chambly-Fortierville.

0.5 Approche méthodologique

L'uranium dissous et le rapport d'activité ($^{234}\text{U}/^{238}\text{U}$)_{act}

Il existe à l'état naturel trois chaînes de désintégration radioactive, chacune débutant avec un actinide (^{238}U , ^{235}U and ^{232}Th), ayant des demi-vies longues ($t_{1/2} > 0.7$ Gyr) et finissant avec un isotope stable du plomb. Dans une chaîne de désintégration, lorsque les descendants conservent un état non perturbé pendant environ six fois la demi-vie du nucléide intermédiaire, alors l'état d'équilibre séculaire est atteint. L'activité de l'isotope père ($A_{\text{père}} = N_{\text{père}} \times \lambda_{\text{père}}$; avec N le nombre d'atomes et λ constante de désintégration : $\lambda = \ln(2)/\text{demi-vie}$) égale alors celle de ses descendants de telle sorte que leur rapport d'activité est égal à 1 : $A_{\text{père}}/A_{\text{fils}} = 1$ (Bourdon *et al.*, 2003). L'intérêt d'étudier les différents isotopes d'une série de désintégration radioactive est qu'il existe plusieurs processus naturels capables de perturber cet état d'équilibre. Cette thèse focalise sur l' ^{238}U et son descendant ^{234}U et fait le lien entre la présence de ces ions en solution et les processus à l'origine du fractionnement $^{234}\text{U}-^{238}\text{U}$. Les résultats de mes travaux constituent au Québec les premières données isotopiques en uranium dans des eaux souterraines de la région.

En milieu aqueux, la particularité des chaînes de désintégration de l'uranium est que la mise en solution et le transport des nucléides dépend fortement des conditions physico-chimiques du milieu, des ions présents en solution ainsi que de la lithologie traversée par le fluide. Alors que l'uranium sera soluble en milieu oxydant et formera des complexes avec les carbonates, phosphates et chlorures aux pH généralement rencontrés dans les eaux souterraines peu profondes, le thorium aura tendance à se soustraire de la phase aqueuse par adsorption (Gascoyne, 1992). Le radium quant à lui verra sa mobilité augmenter avec la salinité des eaux et le radon demeurera inerte comme les autres gaz rares. Cette particularité constitue la première cause du fractionnement observé entre deux isotopes d'une même chaîne de désintégration à

une échelle de temps inférieure à celle de la demi-vie de l'isotope fils ($t_{1/2}$ (^{234}U) = 2.45×10^5 ans).

Un fractionnement entre deux nucléides peut également avoir lieu pendant la désintégration radioactive. Lors de la désintégration de type α de ^{238}U , les particules produites (^{234}Th et ^4He) sont chargées et émises avec une certaine énergie cinétique, ce qui entraîne leur déplacement, il s'agit du recul α . Dans un aquifère, lors de la désintégration de l'uranium contenu dans la roche, le ^{234}Th produit peut être directement éjecté de la phase minérale vers l'eau porale (Fig. 0.5a) puis adsorbé à la surface du grain. Deuxième possibilité, la distance de recul (R , estimé entre 30-100 nm selon la lithologie ; Harvey, 1962) est inférieure à la taille du grain et le ^{234}Th produit restera dans le réseau cristallin (Fig. 0.5b). Lors de la désintégration de ^{234}Th en ^{234}U , ce dernier sera en position préférentielle pour être complexé et passer en solution (Langmuir, 1978). Dans les deux situations le ^{238}U reste dans la surface cristalline ce qui entraîne des rapports d'activités ($^{234}\text{U}/^{238}\text{U}$)_{act} supérieurs à 1 dans les eaux souterraines.

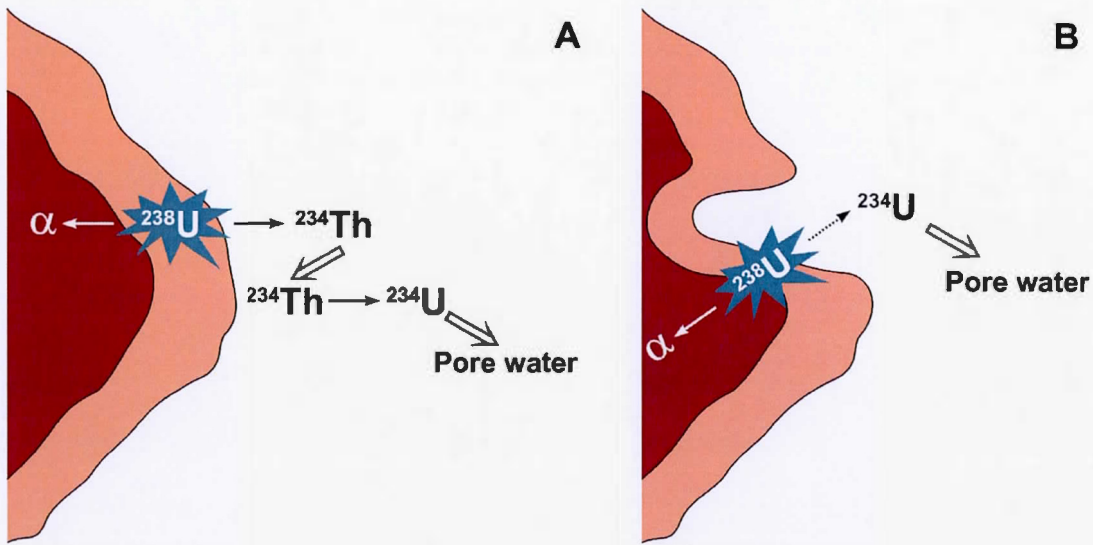


Figure 0.5 Schéma de désintégration de l' ^{238}U . ^{234}Th est éjecté hors du système cristallin (a), ^{234}Th reste dans le minéral et ^{234}U produit sera en position préférentielle pour passer en solution (b) (modifié de Kigoshi, 1971).

Les isotopes ^4He et ^{234}U provenant tous les deux d'une désintégration α , ce sont leurs conditions de mise en solution qui seront étudiées dans cette thèse.

Les gaz rares dans l'eau souterraine

Leur rareté dans la nature et leur inertie font des gaz rares d'excellents traceurs conservatifs en milieu aquatique (Kipfer *et al.*, 2002). Au sein d'un système aquifère, les gaz rares conservent les rapports isotopiques acquis à la source, permettant ainsi l'individualisation des réservoirs dont ils sont issus et l'étude des mélanges entre différentes masses d'eaux (Ballentine et Burnard, 2002).

Dans les eaux souterraines, l'hélium total mesuré ($^{3,4}\text{He}_{\text{tot}}$) est la somme de trois composantes : atmosphérique, crustale et mantellique, avec l'hélium passé en solution en équilibre avec l'atmosphère : « eq », l'hélium dissous en profondeur à partir de bulles d'air : « ea », la production à partir du tritium atmosphérique « tri » et la composante terrigénique composée de la production radiogénique à partir de U et Th ou Li « rad » et la part mantellique « mtl »):

$${}^3\text{He}_{\text{tot}} = {}^3\text{He}_{\text{eq}} + {}^3\text{He}_{\text{ea}} + {}^3\text{He}_{\text{tri}} + ({}^3\text{He}_{\text{rad}} + {}^3\text{He}_{\text{mtl}}) \quad (0.1)$$

$${}^4\text{He}_{\text{tot}} = {}^4\text{He}_{\text{eq}} + {}^4\text{He}_{\text{ea}} + ({}^4\text{He}_{\text{rad}} + {}^4\text{He}_{\text{mtl}}) \quad (0.2)$$

Le rapport isotopique entre ${}^3\text{He}$ et ${}^4\text{He}$, R, permet d'individualiser les trois principaux réservoirs : atmosphérique (R_a), crustal (R_c) et mantellique (R_m) (Fig. 0.6). L'apport radiogénique peut se faire par production *in situ* ou par remontée d'un flux basal (Aggarwal *et al.*, 2015). L'ajout d'hélium mantellique a été mis en évidence dans des zones tectoniques actives (Kulongska *et al.*, 2013), dans des zones d'amincissement lithosphérique en domaine d'extension (Torgersen, 1993) ou lors de la mise en place d'intrusions magmatiques (Torgersen *et al.*, 1994; 1995).

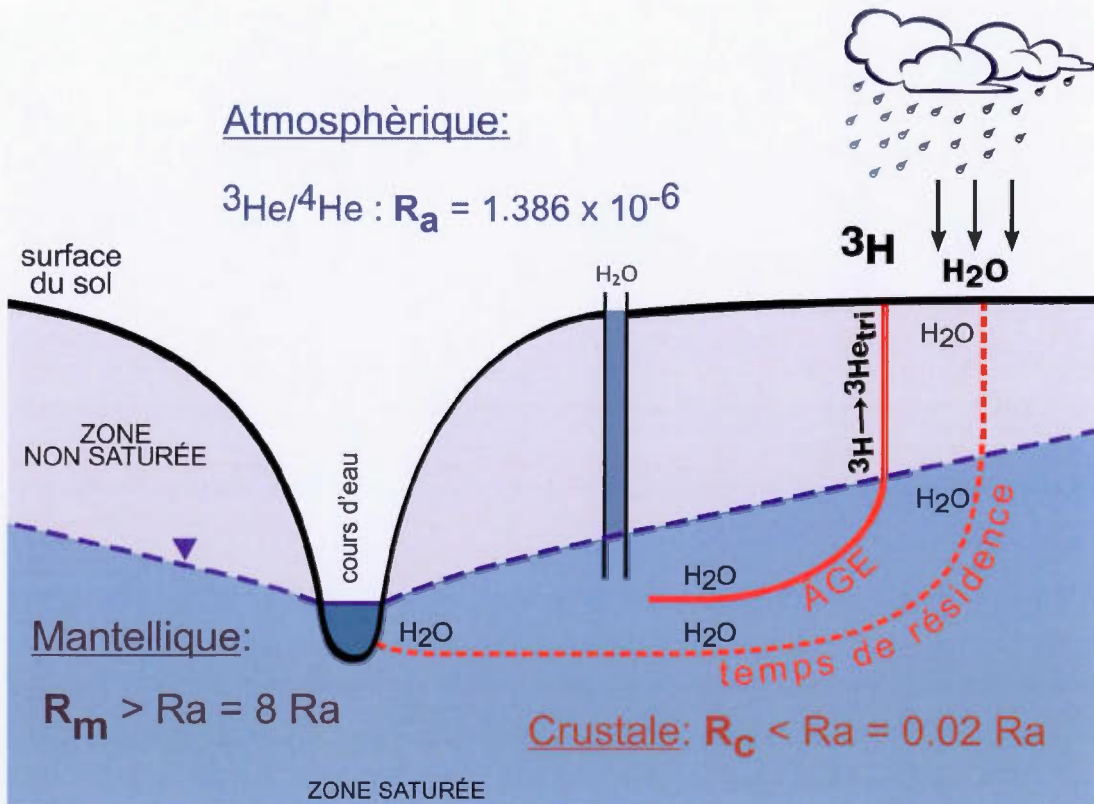


Figure 0.6 Représentation schématique des âges ${}^3\text{H}-{}^3\text{He}$ et des trois réservoirs : atmosphérique, crustal et mantellique. Sont également représentés les rapports ${}^3\text{He}/{}^4\text{He}$ (R) associés.

Une fois les composantes de l'hélium estimées, la quantification de la part tritiogénique de l' ${}^3\text{He}$ couplée aux teneurs en ${}^3\text{H}$ permet d'obtenir un âge ${}^3\text{H}-{}^3\text{He}$ (Schlosser *et al.*, 1989). Le calcul des âges $(\text{U-Th})/{}^4\text{He}$ quand à lui est le rapport entre l' ${}^4\text{He}$ d'origine radiogénique et la vitesse de relâchement dans l'eau porale de cet hélium suite à sa production depuis la roche. Rappelons que lors de chaque désintégration de type α , la particule α éjectée correspond à un atome ${}^4\text{He}$ (Torgersen et Clark, 1985).

Alors que la part radiogénique d' ^4He est estimée en utilisant l'équation 0.2, la vitesse de relâchement de l' ^4He tient compte des paramètres hydrogéologiques propres à chaque aquifère : le rapport entre les vides ($1-\emptyset/\emptyset$) (calculé à partir de la porosité de la roche \emptyset), la masse volumique ϕ (g.cm^{-3}), la production de ^4He par désintégration radioactive de type alpha des descendants des familles ^{238}U , ^{235}U et ^{232}Th ($P^4\text{He}$, en $\text{cm}^3.\text{groche}^{-1}.\text{an}^{-1}$), du facteur de relâchement de l'hélium Λ , généralement posé égal à 1, mais qui lui-même dépend de la relation entre la taille du grain et la distance de recul de l'atome fils produit lors d'une désintégration (Torgersen, 1980). L'âge ($\text{U-Th})^4\text{He}$ est obtenu en faisant le rapport entre la part radiogénique de l' ^4He et le taux d' ^4He produit et libéré dans l'eau porale (Torgersen et Clark, 1985) :

$$t = \frac{\left[^4\text{He}_{\text{terr}} \right]}{P^4\text{He} \times \Lambda \times \frac{1-\emptyset}{\emptyset} \times \phi} \quad (0.3)$$

0.6 Organisation de la thèse

La thèse se décline en trois chapitres majeurs rédigés en anglais, chacun correspondant à un article accepté (chapitre 1) ou en préparation pour soumission à une revue scientifique (chapitres 2 et 3).

Le *chapitre I* traite de la systématique de l'uranium dissous et de l'évolution de $(^{234}\text{U}/^{238}\text{U})_{\text{act}}$ dans l'eau souterraine des aquifères granulaires et fracturés de la zone d'étude de Bécancour. Les observations en uranium ont été couplées aux données géochimiques (Meyzonnat *et al.*, 2016) et aux âges $^3\text{H}/^3\text{He}$ et ^{14}C récemment estimés (Vautour *et al.*, 2015) afin de déterminer les conditions de mise en solution de l'uranium depuis l'infiltration des eaux de surface jusqu'à la partie aval de la zone d'étude où la présence d'eau marine a été démontrée. Alors que le fractionnement $^{234}\text{U}-^{238}\text{U}$ augmente avec le temps de contact eau-roche dans l'aquifère, une relation entre l' ^4He radiogénique et $(^{234}\text{U}/^{238}\text{U})_{\text{act}}$ a également été identifiée. Il existe une relation inverse entre le rapport $(^3\text{He}/^4\text{He})$ mesuré dans les eaux et $(^{234}\text{U}/^{238}\text{U})_{\text{act}}$ ce qui souligne la présence de mélanges entre familles d'eaux ayant des pôles isotopiques distincts. L'hypothèse avancée ici est que le processus de recul α pourrait soutenir les excès en ^4He radiogénique mesurés dans ces eaux souterraines. Cette relation entre ^4He radiogénique et $(^{234}\text{U}/^{238}\text{U})_{\text{act}}$ constitue le cœur de la réflexion du *chapitre II* où le modèle de mise en solution de ^{234}U développé par Andrews *et al.* (1982) a été couplé avec le modèle de relâchement de ^4He depuis un grain théoriquement sphérique (Solomon *et al.*, 1996). L'utilisation de ces modèles révèle l'étroite relation entre évolution de la taille du grain de la roche qui constitue l'aquifère et la relâche des isotopes ^{234}U et ^4He dans l'eau porale.

Dans le *chapitre III*, les observations dans la zone d'étude de Vaudreuil-Soulanges ont été combinées avec celles disponibles dans de travaux précédents (Vautour *et al.*, 2015 ; Saby *et al.*, 2016) pour mettre en évidence une augmentation de la composante mantellique dans les eaux souterraines d'est en ouest dans la région de Basses-Terres

du Saint-Laurent. Étant donné que l'activité tectonique est faible dans cette région, le signal mantellique contenu dans les eaux est donc fossile. Un modèle de vieillissement de cette signature mantellique est utilisé pour démontrer que les Collines Montérégiennes sont la source mantellique riche en ${}^3\text{He}$ à l'origine de la composante mantellique observée dans les eaux souterraines. Les conditions de mise en place de ces intrusions sont-elles mêmes sujet à débat pour trancher entre le passage du point chaud *New England* (Torgersen *et al.*, 1995), ou de la réactivation de failles NO-SE en lien avec l'ouverture de l'Océan Atlantique (Rouleau *et al.*, 2013) comme processus à l'origine des Collines Montérégiennes.

REFERENCES

- Aeschbach-Hertig W and Gleeson T 2012 Regional strategies for the accelerating global problem of groundwater depletion *Nature GeoSciences*, 5, 853–61.
- Aggarwal, P.K., Matsumoto, T., Sturchio, N.C., Chang, H.K., Gastmans, D., Araguas-Araguas, L.J., Jiang, W., Lu, Z.-T., Mueller, P., Yokochi, R., Purtschert, R. et Torgersen, T. (2015). Continental degassing of 4He by surficial discharge of deep groundwater. [Letter]. *Nature Geosciences*, 8(1), 35-39.
- Andrews, J.N., Giles, I.S., Kay, R.L.F., Lee, D.J., Osmond, J.K., Cowart, J.B., Fritz, P., Barker, J.F. et Gale, J. (1982). Radioelements, radiogenic helium and age relationships for groundwaters from the granites at Stripa, Sweden. *Geochimica et Cosmochimica Acta*, 46(9), 1533-1543.
- Ballentine, C.J. et Burnard, P.G. (2002). Production, release and transport of noble gases in the continental crust. *Reviews in mineralogy and geochemistry*, 47(1), 481-538.
- Bethke, C.M. et Johnson, T.M. (2008). Groundwater age and groundwater age dating. *Annu. Rev. Earth Planet. Sci.*, 36, 121-152.
- Bottomley, D.J., Renaud, R., Kotzer, T. et Clark, I.D. (2002). Iodine-129 constraints on residence times of deep marine brines in the Canadian Shield. *Geology*, 30(7), 587-590.
- Bourdon, B. Henderson, G.M., Lundstrom, C.C. et Turner S.P. (2003). Uranium-series Geochemistry, Geochemical Society Mineralogical Society of America, Washington 658 pp.
- Cloutier, V., Lefebvre, R., Savard, M.M., Bourque, É. et Therrien, R. (2006). Hydrogeochemistry and groundwater origin of the Basses-Laurentides sedimentary rock aquifer system, St. Lawrence Lowlands, Québec, Canada. *Hydrogeology Journal*, 14(4), 573-590.
- Gascoyne, M. (1992). Palaeoclimate determination from cave calcite deposits. *Quaternary Science Reviews*, 11(6), 609-632.
- Gleeson, T., Befus, K.M., Jasechko, S., Luijendijk, E. et Cardenas, M.B. (2016). The global volume and distribution of modern groundwater. *Nature Geosci*, 9, 161–167.
- Globensky, Y. (1987). Géologie des basses-terres du Saint-Laurent. : [Ministère de l'énergie et des ressources], Direction générale de l'exploration géologique et minérale, Direction de la recherche géologique, Service de la géologie.
- Harvey BG (1962) Introduction to Nuclear Physics and Chemistry. Prentice Hall Inc, New Jersey

- Kigoshi, K. (1971). Alpha-recoil thorium-234: dissolution into water and the uranium-234/uranium-238 disequilibrium in nature. *Science*, 173(3991), 47-48.
- Kipfer, R. et Peeters, F. (2002). Using transient conservative and environmental tracers to study water exchange in Lake Issyk-Kul. : Springer.
- Kulongoski, J.T., Hilton, D.R., Barry, P.H., Esser, B.K., Hillebrands, D. et Belitz, K. (2013). Volatile fluxes through the Big Bend section of the San Andreas Fault, California: Helium and carbon-dioxide systematics. *Chemical Geology*, 339, 92-102.
- Larocque, M., Gagné, S., Tremblay, L. et Meyzonnat, G. (2013). Projet de connaissance des eaux souterraines du bassin versant de la rivière Bécancour et de la MRC de Bécancour. Rapport final présenté au Ministère du Développement durable, de l'Environnement, de la Faune et des Parcs (219 pp.).
- Larocque, M., Meyzonnat, G., Barbacot, F., Pinti, D., Gagné, S., Barnetche, D., Ouellet, M. et Graveline, M. (2015). Projet de connaissance des eaux souterraines de la zone de Vaudreuil-Soulanges Rapport final présenté au Ministère du Développement durable, de l'Environnement, de la Faune et des Parcs (203pp.).
- Lavoie, D., Pinet, N., Castonguay, S., Hannigan, P., Dietrich, J., Hamblin, T. et Giller, P. (2009). Petroleum resource assessment, Paleozoic successions of the St. Lawrence Platform and Appalachians of eastern Canada. *Geological Survey of Canada*, 6174, 275.
- Lippmann-Pipke, J., Lollar, B.S., Niedermann, S., Stroncik, N.A., Naumann, R., Van Heerden, E. et Onstott, T.C. (2011). Neon identifies two billion year old fluid component in Kaapvaal Craton. *Chemical Geology*, 283(3), 287-296.
- Mazor, E. (2003). Chemical and isotopic groundwater hydrology. (Vol. 98) : CRC press.
- Meyzonnat, G., Larocque, M., Barbacot, F., Pinti, D. et Gagné, S. (2016). The potential of major ion chemistry to assess groundwater vulnerability of a regional aquifer in southern Quebec (Canada). *Environmental Earth Sciences*, 75(1), 1-12.
- Occhietti, S. et Richard, P.J. (2003). Effet réservoir sur les âges ^{14}C de la Mer de Champlain à la transition Pléistocène-Holocène: révision de la chronologie de la déglaciation au Québec méridional. *Géographie physique et Quaternaire*, 57(2-3), 115-138.
- Phillips, F. et Castro, M. (2003). Groundwater dating and residence-time measurements. *Treatise on geochemistry*, 5, 451-497.

- Pinti, D.L. et Marty, B. (1998). The origin of helium in deep sedimentary aquifers and the problem of dating very old groundwaters. Geological Society, London, Special Publications, 144(1), 53-68.
- Pinti, D.L., Béland-Otis, C., Tremblay, A., Castro, M.C., Hall, C.M., Marcil, J.-S., Lavoie, J.-Y. et Lapointe, R. (2011). Fossil brines preserved in the St-Lawrence Lowlands, Québec, Canada as revealed by their chemistry and noble gas isotopes. *Geochimica et Cosmochimica Acta*, 75(15), 4228-4243.
- Pinti, D.L., Castro, M.C., Shouakar-Stash, O., Tremblay, A., Garduño, V.H., Hall, C.M., Hélie, J.F. et Ghaleb, B. (2013). Evolution of the geothermal fluids at Los Azufres, Mexico, as traced by noble gas isotopes, $\delta^{18}\text{O}$, δD , $\delta^{13}\text{C}$ and $^{87}\text{Sr}/^{86}\text{Sr}$. *Journal of Volcanology and Geothermal Research* 249, 1-11.
- Pinti, D.L., Retailleau, S., Barnetche, D., Moreira, F., Moritz, A.M., Larocque, M., Gélinas, Y., Lefebvre, R., Hélie, J.-F., Valadez, A. (2014). 222Rn activity in groundwater of the St. Lawrence Lowlands, Quebec, eastern Canada: Relation with local geology and health hazard, *Journal of environmental radioactivity*, 136, 206-217.
- Porcelli, D. et Baskaran, M. (2012). An overview of isotope geochemistry in environmental studies. Dans Handbook of Environmental Isotope Geochemistry (11-32) : Springer.
- Rouleau, E. et Stevenson, R. (2013). Geochemical and isotopic (Nd–Sr–Hf–Pb) evidence for a lithospheric mantle source in the formation of the alkaline Montréal Province (Quebec). *Canadian Journal of Earth Sciences*, 50(6), 650-666.
- Saby, M., Larocque, M., Pinti, D.L., Barbicot, F., Sano, Y. et Castro, M.C. (2016). Linking groundwater quality to residence times and regional geology in the St. Lawrence Lowlands, southern Quebec, Canada. *Applied Geochemistry*, 65, 1-13.
- Schlosser, P., Stute, M., Sonntag, C. et Munnich, K. (1989). Tritiogenic ^3He in shallow groundwater. *Earth Planet. Sci. Lett.*, 94, 245-256.
- Solomon, D., Hunt, A. et Poreda, R. (1996). Source of radiogenic helium 4 in shallow aquifers: Implications for dating young groundwater. *Water Resources Research*, 32(6), 1805-1813.
- Torgersen, T. (1980). Controls on pore-fluid concentration of ^4He and 222Rn and the calculation of $^4\text{He}/222\text{Rn}$ ages. *Journal of Geochemical Exploration*, 13(1), 57-75.
- Torgersen, T. (1993). Torgersen, T. (1993). Defining the role of magmatism in extensional tectonics: Helium 3 fluxes in extensional basins. *Journal of Geophysical Research: Solid Earth* (1978–2012), 98(B9), 16257-16269.

- Torgersen, T. et Clarke, W.B. (1985). Helium accumulation in groundwater, I: An evaluation of sources and the continental flux of crustal 4He in the Great Artesian Basin, Australia. *Geochimica et Cosmochimica Acta*, 49(5), 1211-1218.
- Torgersen, T. et Stute, M. (2013). Helium (and other noble gases) as a tool for understanding long time-scale groundwater transport. Isotope methods for Dating old groundwater, IAEA, Vienna, 179-216.
- Torgersen, T., Drenkard, S., Farley, K., Schlosser, P. et Shapiro, A. (1994). Mantle helium in the groundwater of the Mirror Lake Basin, New Hampshire. USA In Noble Gas Geochemistry and Cosmochemistry, ed. J. Matsuda, 279-292 : Tokyo: Terra Scientific Publishing Co.
- Torgersen, T., Drenkard, S., Stute, M., Schlosser, P. et Shapiro, A. (1995). Mantle helium in ground waters of eastern North America: Time and space constraints on sources. *Geology*, 23(8), 675-678.
- Vautour, G., Pinti, D.L., Méjean, P., Saby, M., Meyzonnat, G., Larocque, M., Castro, M.C., Hall, C.M., Boucher, C., Roulleau, E., Barbecot, F., Takahata, N. et Sano, Y. (2015). $^3\text{H}/^3\text{He}$, ^{14}C and (U-Th)/ 4He groundwater ages in the St. Lawrence Lowlands, Quebec, Eastern Canada. *Chemical Geology*, 413, 94-106.
- Pinti, D.L. et Marty, B. (1998). The origin of helium in deep sedimentary aquifers and the problem of dating very old groundwaters. *Geological Society, London, Special Publications*, 144(1), 53-68.
- Séjourné, S., Lefebvre, R., Malet, X. et Lavoie, D. (2013). Synthèse géologique et hydrogéologique du Shale d'Utica et des unités sus-jacentes (Lorraine, Queenston et dépôts meubles), Basses-Terres du Saint-Laurent, Province de Québec; Commission géologique du Canada. Commission géologique du Canada, Dossier Public, 7338, 165.

CHAPITRE I

PROCESSES CONTROLLING ^{234}U AND ^{238}U ISOTOPE FRACTIONATION AND HELIUM IN THE GROUNDWATER OF THE ST. LAWRENCE LOWLANDS, QUEBEC: THE POTENTIAL ROLE OF NATURAL ROCK FRACTURING

Pauline Méjean¹, Daniele L. Pinti¹, Marie Larocque¹, Bassam Ghaleb¹, Guillaume Meyzonnat¹, Sylvain Gagné¹

¹GEOTOP and Département des sciences de la Terre et de l'atmosphère, Université du Québec à Montréal, CP888, Succ. Centre-Ville, Montréal, QC, H3C 3P8 Canada

Keywords: ($^{234}\text{U}/^{238}\text{U}$) activity ratio; helium isotopes; fractured aquifers; α -recoil; ^4He excess; St. Lawrence Lowlands.

Article publié dans Applied Geochemistry : doi 10.1016/j.apgeochem.2015.12.015

ABSTRACT

The goal of this study is to explain the origin of ^{234}U - ^{238}U fractionation in groundwater from sedimentary aquifers of the St. Lawrence Lowlands (Quebec, Canada), and its relationship with $^3\text{He}/^4\text{He}$ ratios, to gain insight regarding the evolution of groundwater in the region. ($^{234}\text{U}/^{238}\text{U}$) activity ratios, or ($^{234}\text{U}/^{238}\text{U}$)_{act}, were measured in 23 groundwater samples from shallow Quaternary unconsolidated sediments and from the deeper fractured regional aquifer of the Bécancour River watershed. The lowest ($^{234}\text{U}/^{238}\text{U}$)_{act}, 1.14 ± 0.014 , was measured in Ca-HCO₃-type freshwater from the Quaternary Shallower Aquifer, where bulk dissolution of the carbonate allows U to migrate into water with little ^{234}U - ^{238}U isotopic fractionation. The ($^{234}\text{U}/^{238}\text{U}$)_{act} increases to 6.07 ± 0.14 in Na-HCO₃-Cl-type groundwater. Preferential migration of ^{234}U into water by α -recoil is the underlying process responsible for this isotopic fractionation. An inverse relationship between ($^{234}\text{U}/^{238}\text{U}$)_{act} and $^3\text{He}/^4\text{He}$ ratios has been observed. This relationship reflects the mixing of newly recharged water, with ($^{234}\text{U}/^{238}\text{U}$)_{act} close to the secular equilibrium and containing atmospheric/tritiogenic helium, and mildly-mineralized older water (^{14}C ages of 6.6 kyr), with ($^{234}\text{U}/^{238}\text{U}$)_{act} of ≥ 6.07 and large amounts of radiogenic ^4He , in excess of the steady-state amount produced *in situ*. The simultaneous fractionation of ($^{234}\text{U}/^{238}\text{U}$)_{act} and the addition of excess ^4He could be locally controlled by stress-induced rock fracturing. This process increases the surface area of the aquifer matrix exposed to pore water, from which produced ^4He and ^{234}U can

be released by α -recoil and diffusion. This process would also facilitate the release of radiogenic helium at rates greater than those supported by steady-state U-Th production in the rock. Consequently, sources internal to the aquifers could cause the radiogenic ${}^4\text{He}$ excesses measured in groundwater.

1.1 INTRODUCTION

Knowledge of groundwater flow velocities and residence times is critical to the quantification of pollutant migration (Gascoyne, 2004) and aquifer vulnerability (Meyzonnat *et al.*, 2016). Flow velocities can be determined using *in situ* tracer tests (Geyh, 2005) or aquifer materials in the laboratory (Andersen *et al.*, 2009; Bonotto, et Andrews, 2000). Such methods provide local estimates of groundwater velocity and do not take the natural heterogeneity of an aquifer system at the regional scale into account. Studies performed at the watershed scale can partially account for this heterogeneity by integrating information from a large set of isotopic groundwater ages (Phillips et Castro, 2003). However, chronometers such as ^{14}C (Plummer et Glynn, 2013) can be affected by water-rock interactions and their chronological information can be altered or partially lost as a result.

In this regard, the ratio of ^{234}U and ^{238}U activities, $(^{234}\text{U}/^{238}\text{U})_{\text{act}}$, has the potential to quantify such water–rock (Riotte et Chabaux, 1999; Riotte *et al.*, 2003; Fröhlich, 2013; Paces et Wurster, 2014). Since the pioneering work of Cherdynsev *et al.* (1955), it has been shown that groundwater almost always has a $(^{234}\text{U}/^{238}\text{U})_{\text{act}}$ greater than one, the value corresponding to secular equilibrium, at which the activity of the daughter nuclide is equal to the activity of the parent nuclide. The physical process responsible for the ^{234}U - ^{238}U fractionation is the α -decay of ^{238}U . During decay, α -particles are emitted, transmitting kinetic energy to the ^{238}U -daughter nuclide, ^{234}Th . ^{234}Th is displaced 30 to 100 nm from its original site, and a fraction of the ^{234}Th is ejected from the mineral grain into the pore water. The insoluble ^{234}Th is rapidly adsorbed on the grain surface and decays to ^{234}U , with a half-life of 24.1 days. The resulting ^{234}U , now residing in damaged crystal lattice sites or on grain surfaces, will be transferred in its soluble form into the water phase (Kigoshi, 1971).

The extent of this ^{234}U - ^{238}U fractionation depends on numerous aquifer parameters, such as path lengths, grain surface of the porous media (Maher *et al.*, 2006; Tricca *et*

al., 2001), fracture surface and the duration of the recoil process (Andersen *et al.*, 2009; Andrews *et al.*, 1982), chemical aggression capacity, mineralogical composition of the rock in contact with water, the water/rock ratio (Riotte *et al.*, 1999; Paces *et al.*, 2002; Riotte *et al.*, 2003; Durand *et al.*, 2005), and/or the contact time between flowing water and the aquifer matrix (Elliot *et al.*, 2014). The behavior of ^{234}U compared with that of its parent, ^{238}U , is therefore useful for tracing groundwater flow patterns (Kronfeld *et al.*, 1979; Osmond et Cowart, 1976; 1982; 2000), determining mixing volumes and rates between waters of different ages (e.g., Andrews et Kay, 1983; Tricca *et al.*, 2000), and identifying groundwater inflow into surface waters (Plater *et al.*, 1992; Durand *et al.*, 2005).

Because of the long half-life of ^{234}U (2.46×10^5 yrs), many attempts have been made to apply the $(^{234}\text{U}/^{238}\text{U})_{\text{act}}$ to the dating of old groundwater up to hundreds of thousands of years in age (Osmond *et al.*, 1974; Andrews *et al.*, 1982; Andrews et Kay, 1983; Fröhlich et Gellermann, 1987; Ivanovitch *et al.*, 1991). However, the majority of these studies have shown that the excess decay of ^{234}U may not reflect groundwater residence times, but rather uranium redistribution between the aquifer matrix and the water phase. Consequently, to obtain reliable residence times, the method requires a detailed knowledge of the aquifer characteristics, such as matrix grain size and fracture openings (Andrews et Kay, 1983; Andrews *et al.*, 1982; Tricca *et al.*, 2001), as well as the adsorption of these isotopes onto the aquifer matrix (Fröhlich et Gellermann, 1987; Porcelli, Donald et Swarzenski, 2003).

Radiogenic helium isotopes in groundwater are produced by neutron reactions with Li (^3He) and α -decay of U and Th (^4He) contained in the aquifer rocks (Kulonogoski et Hilton, 2011). Compared with U-isotopes, He-isotopes are insensitive to redox conditions, chemical reactions, and adsorption processes, given that helium is a noble gas. The mixing of water masses with different ages and provenance primarily controls the helium isotopic variability in a groundwater system (e.g., Vautour *et al.*,

2015; Saby *et al.*, 2016). Groundwater ages, calculated from the radiogenic ${}^4\text{He}$ accumulation rate in water, are often higher than the hydrological ages, indicating an excess of ${}^4\text{He}$ (e.g., Pinti et Marty, 1998; Kulongski et Hilton, 2011; Torgersen et Stute, 2013). Additional sources of radiogenic ${}^4\text{He}$ could be related to He basal fluxes entering the aquifers (e.g., Torgersen et Clarke, 1985) or the release of ${}^4\text{He}$ from the aquifer rock at rates greater than those supported by steady-state U–Th production in rocks (Solomon *et al.*, 1996).

The objective of this study is to explain the cause of ${}^{234}\text{U}$ - ${}^{238}\text{U}$ fractionation in the St. Lawrence Lowlands (Fig. 1.1) aquifers, to better understand the evolution of groundwater in the region. It is one of the first attempts to examine the relationships between U and He isotopes, and how these may be linked in groundwater environments.

1.2 STUDY AREA

1.2.1 Geology and hydrogeology

The study area ($2,859 \text{ km}^2$) is located in southern Quebec (Fig. 1.1), encompassing the lower portion of the Bécancour River watershed, as well as eight smaller watersheds feeding the St. Lawrence River. The northwestern part of the watershed corresponds geographically to the St. Lawrence Lowlands, a flat area less than 150 m asl. The southeastern part of the watershed is located in the Appalachian Mountains, characterized by irregular topography reaching maximal elevations of approximately 500 m (Fig. 1.2). These two regions correspond geologically to the Cambro-Ordovician sedimentary St. Lawrence Platform and the Cambro-Devonian metasedimentary Appalachian Mountains respectively.

The St. Lawrence Platform is a 1,200 m-thick sequence of Cambrian-Early Ordovician siliciclastic and carbonate sediments, overlain by 1,800 m of Middle-Late Ordovician foreland carbonate-clastic-shale deposits (Lavoie, 2008). Ordovician geological units outcropping in the lower part of the Bécancour watershed are: 1) red shale interbedded with green sandstone and lenticular gypsum of the Queenston Group, and 2) mudstone, sandstone, and silty shale turbiditic units of the Lorraine and Sainte Rosalie Groups (Fig. 1.2). Dominant terrains in the Appalachian Mountains correspond to imbricated thrust sheets produced during the Taconian Orogeny: 1) Cambrian green and red shales (Sillery Group), 2) Ordovician bedded black and yellowish-weathered shaly matrix containing chaotic blocks of shales, cherts, and sandstone forming the “wildflysch” of the Etchemin River Olistostrome, and 3) Middle Ordovician dolomitic or calcitic schists of the Sweetsburg and the West Sutton Formation of the Oak Hill Group (Globensky, 1993) (Fig. 1.2).

Unconsolidated Quaternary sediments derived from the last two glaciation-deglaciation cycles unconformably cover the Cambrian-Ordovician sedimentary sequence of the St. Lawrence Platform (Lamothe, 1989). A nearly continuous till

sheet (Gentilly till) covers most of the area, separating the lacustrine and deltaic patches of sand deposited during marine regressions (Vieilles Forges and Lotbinière sands; Lamothe, 1989) from the uppermost clay units of the Champlain Sea (11.1 to 9.8 ka; Occhietti *et al.*, 2001; Occhietti et Richard, 2003).

During the last deglaciation, the retreat of the Laurentide Ice Sheet caused a marine invasion from the Gulf of St. Lawrence, called the Champlain Sea episode. This water is a mixture of meltwater from the Laurentide Ice Sheet and seawater (Hillaire-Marcel et Causse, 1989). Glacio-marine sediments of the Champlain Sea are found between the elevations of 175 and 65 m (Godbout, 2013; Parent et Occhietti, 1988). Generally encountered below 100 m elevation in ancient channels, the Champlain Sea clay can be more than 40 m thick in the Chambly-Fortierville syncline, close to the St. Lawrence River (Fig. 1.2). Glacio-marine deltaic sandy sediments are mainly found along the Bécancour River, at elevations between 65 and 100 m asl.

In the study area, two distinct aquifer systems are apparent: 1) a regional fractured bedrock aquifer in the Middle-Late Ordovician sedimentary units of the St. Lawrence Platform, and 2) discontinuous and localized perched aquifers in the fluvio-glacial sands of the Quaternary Vieilles Forges Formation (hereafter referred to as “granular aquifers”) (Larocque *et al.*, 2013). The main recharge zones of the regional fractured aquifer are located in the Appalachian Mountains. Local recharge has been observed in the lower part of the basin, downhill, where Champlain Sea clays are absent (Larocque *et al.*, 2013). Groundwater flows from the Appalachian Mountains northwesterly to the St. Lawrence River (Fig. 1.1). The Bécancour River acts as the main discharge for the regional fractured bedrock aquifer. The hydraulic conductivities of the fractured bedrock aquifer are low to moderate ($\sim 10^{-9}$ – 10^{-6} m s⁻¹). Effective porosity varies between 1 and 5% for the Ordovician fractured regional aquifer (Tran Ngoc *et al.*, 2014) and between 10 and 20% for the Quaternary granular aquifer (Benoit *et al.*, 2011).

1.2.2 Groundwater chemistry and ages

Groundwater chemistry shows the occurrence of low-salinity water with total dissolved solids (TDS) ranging from 0.06 to 0.78 g L⁻¹ (Table 1.1). Based on major ion concentrations, Meyzonnat *et al.* (2016) identified three water types in the Bécancour groundwater: 1) Ca-HCO₃, and Ca-HCO₃-SO₄ freshwater close to the recharge zone of the Appalachian mountains, 2) mixed water types (Na-HCO₃ and Na-HCO₃-SO₄) in the piedmont of the Appalachian Mountains and the St. Lawrence Plain, and 3) more highly mineralized waters (Ca-HCO₃-Cl,Na and Na-HCO₃-Cl types) closer to the St. Lawrence River (Meyzonnat *et al.*, 2016). The majority of water recharged in the Appalachian Mountains has a calcite saturation index (SI, with an uncertainty of ±0.1 units; Table 1.1) of 2.98 and -0.07, indicating that it ranges from under-saturated in calcite to close to saturation. From this, it can be concluded that the dissolution of calcite within the aquifers is the dominant process controlling the chemistry of these waters (Fig. 1.3). Groundwater reaches calcite saturation and evolves towards Na-HCO₃ type through ion exchange, where Ca²⁺_{water} exchanges with Na⁺_{mineral} in semi-confined aquifers (Cloutier *et al.*, 2006; Meyzonnat *et al.*, 2016). Groundwater finally evolves to a Na-Cl type (Fig. 1.4) through exchange with pore water of marine origin trapped in the Champlain Sea clays or in the fractured rock aquifers, especially in areas confined by thick marine clay and with limited water recharge (Meyzonnat *et al.*, 2016). These saline waters are found mainly in the Lorraine Group units, and waters are located in the lowermost part of the watershed, along the Chambly-Fortierville syncline, a narrow band of 10 km parallel to the St. Lawrence River. None of these Na-Cl waters were sampled for this study.

Mixing between a freshwater Ca-HCO₃ end-member and locally evolved Na-HCO₃-Cl water end-member is responsible for the geochemical character of the groundwater and its spatial distribution in the Bécancour watershed (Vautour *et al.*, 2015). This mixing is reflected in the apparently contradictory ³H/³He and ¹⁴C ages measured in the same water samples from Bécancour (Vautour *et al.*, 2015) and neighboring

watersheds (Saby *et al.*, 2016). $^3\text{H}/^3\text{He}$ ages span from 2 to 60 yrs, while the NETHPATH ^{14}C -adjusted ages for the same water ranges from 6.6 thousand years to present. This apparent contradiction in age results from the mixing of old groundwater with modern water, as clearly demonstrated by Saby *et al.* (2016) through a linear mixing trend between the ^3H and A^{14}C activities in the St. Lawrence Lowlands groundwater, including those from the Bécancour watershed.

1.3 SAMPLING AND ANALYTICAL PROCEDURES

Twenty-three groundwater samples were collected from municipal and domestic wells (named BEC in Figure 1.1 and Table 1.1; n = 17) and from instrumented wells drilled for monitoring purposes (named F1, F2, F4, F5, F7 and F9 in Fig. 1.1; n = 5). Sampling was done during the summers of 2012 and 2013. Twenty of the wells tap groundwater from the regional Ordovician fractured aquifer (with depths ranging from 15.0 to 64.6 m; Table 1.1). These are cased in the section crossing the unconsolidated Quaternary deposits and have open boreholes in the fractured bedrock. Three wells (BEC105, BEC117, and BEC118) have casings and a screen at their base, and tap groundwater from the shallower Quaternary sandy aquifer (with depths ranging from 6.1 to 15 m; Table 1.1).

Groundwater was collected from domestic wells using a Waterra® Inertial Pump System, which consists of a foot valve fixed to the bottom of a high-density polyethylene tube with a variable diameter of between 5/8" to 2" and an electric actuator Hydrolift-2® pump. Water was collected at the closest water faucet, prior to any intermediate reservoirs for the chemical treatment of the water. In municipal wells, water was collected directly at the wellhead. Water was purged from the wells until chemo-physical parameters (conductivity, pH, and temperature) stabilized. Samples were collected for uranium analyses in 1 L Nalgene® bottles filtered through 0.7 µm Millipore filters and acidified with nitric acid to a pH of around 2.

U extraction was performed at the Radioisotope laboratory of GEOTOP, following a method modified from that of Edwards *et al.* (1987). A known amount of spike (^{233}U - ^{236}U) was added to 75 ml of water sample to determine the U concentration by isotope dilution (Chen *et al.*, 1986). An aliquot was prepared with 150 ml of water sample following the same technique to measure $(^{234}\text{U}/^{238}\text{U})_{\text{act}}$. Approximately 3 mg of Fe carrier (FeCl_3 already purified of any trace of uranium) was added to this solution, and a $\text{Fe}(\text{OH})_3$ precipitate was created by adding a solution of ammonium

hydroxide until a pH of between 7 and 9 was obtained. The precipitate was recovered by centrifugation and then dissolved in 2 ml of 6 M HCl solution and loaded in 2 ml of AG-1X8 anionic resin bed. After washing the resin with 8 ml of 6M HCl, the U-Fe fractions were retrieved by elution with 8 ml of H₂O and evaporated to dryness. The resulting U separate was purified using 0.2 ml U-Teva (Eichrom Industries) resin. The Fe was eluted with 3 N HNO₃ and the U fraction with 0.02 N HNO₃.

The recovered U fraction was deposited on a Rhenium filament between two layers of graphite, and U isotopes were measured with a VG-SECTOR Thermo-Ionization Mass Spectrometer (TIMS) equipped with an ion counter. Uranium concentration was determined by peak jumping between ²³⁶U, ²³⁵U and ²³³U on the ion counter and corrected for mass fractionation using a double spike with a (²³⁶U/²³³U) of 1.132 and assuming a constant ²³⁸U/²³⁵U ratio of 137.88. To obtain ²³⁴U/²³⁸U activity ratios, we measured ²³⁴U, ²³⁵U, and ²³⁸U and their atomic ratios on un-spiked samples. The ²³⁴U/²³⁸U atomic ratio was converted to (²³⁴U/²³⁸U)_{act} using $\lambda^{238}/\lambda^{234} = 5.4887 \times 10^{-5}$. The analytical errors on the U concentrations were usually less than 1% (except for samples BEC138 and F4; table 1), at the 2 σ level. The errors on the (²³⁴U/²³⁸U)_{act} vary from 0.4 to 5 % with an average error of ~ 1.3 % at 2 σ level (except sample F1; Table 1.1).

Water samples for helium isotopic analyses were collected from the wells with 3/8-inch diameter, refrigeration-type copper tubes, cold-sealed with clamps, following standard procedures described in Vautour *et al.* (2015). Helium isotopes were measured at the Noble Gas Laboratory at the University of Michigan using a MAP-215 noble gas mass spectrometer. Details of the analytical procedures, uncertainties, and reproducibility are reported elsewhere (Castro *et al.*, 2009; Vautour *et al.*, 2015).

1.4 RESULTS

The uranium concentrations in ppb [U] and the activity ratios, $(^{234}\text{U}/^{238}\text{U})_{\text{act}}$, measured in this study are reported in Table 1, together with geological and water chemistry data for the same samples, previously reported by Meyzonnat *et al.* (2016) and Larocque *et al.* (2013). ^4He amount and helium isotopic ratios ($^3\text{He}/^4\text{He}$) are reported from Vautour *et al.* (2015). The measured [U] are very low and display a high degree of variability, with values ranging from 0.003 ± 0.00002 to 2.939 ± 0.012 ppb. The $(^{234}\text{U}/^{238}\text{U})_{\text{act}}$ ratios are greater than one (i.e., exceed secular equilibrium), ranging from 1.14 ± 0.01 to 6.07 ± 0.14 (Table 1.1). Table 1.1 also reports the $^3\text{He}/^4\text{He}$ ratios measured for the samples and reported previously in Vautour *et al.* (2015). ^4He amounts range from $5.36 \times 10^{-8} \text{ cm}^3\text{STP g}^{-1} \text{ H}_2\text{O}$ to $4.48 \times 10^{-5} \text{ cm}^3\text{STP g}^{-1} \text{ H}_2\text{O}$ (Table 1.1). The lowest amount is very close to that of atmospheric helium dissolved in freshwater at the recharge (ASW or Air Saturated Water at 10°C ; $4.59 \times 10^{-8} \text{ cm}^3\text{STP g}^{-1} \text{ H}_2\text{O}$) and increases to 3 orders of magnitude higher, indicating significant accumulations of radiogenic ^4He (Vautour *et al.*, 2015). The helium isotopic ratios ($^3\text{He}/^4\text{He}$) in groundwater, normalized to the ($^3\text{He}/^4\text{He}$) in the atmosphere (1.386×10^{-6} ; Ozima et Podosek, 1983), range from 2.005 ± 0.039 to 0.039 ± 0.003 . The ratios higher than the atmospheric value are explained by the addition of ^3H -produced ^3He , while the very low ratios reflect the large addition of radiogenic ^4He (Vautour *et al.*, 2015). A detailed discussion on the helium isotopic systematics is beyond the scope of this paper and is reported in Vautour *et al.* (2015).

Figures 1.5 and 1.6 compares the measured [U] and $(^{234}\text{U}/^{238}\text{U})_{\text{act}}$ in the current study area with those from other sedimentary aquifers characterized by similar lithologies and confinement conditions (except for confined oil brines; Kronfeld *et al.*, 1975; Banner *et al.*, 1990). Both measured [U] (Fig. 1.5) and $(^{234}\text{U}/^{238}\text{U})_{\text{act}}$ (Fig. 1.6) from the study area are within the range of values observed in other unconfined and confined sedimentary aquifers (Banner *et al.*, 1990; Bonotto et Andrews, 2000; Durand *et al.*, 2005; Hubert *et al.*, 2006; Reynolds *et al.*, 2003; Riotte and Chabaux,

1999; Tricca *et al.*, 2001), but are characterized by higher variability. When a simple statistical treatment of the data is carried out, the main parameters controlling the uranium behavior and the distribution of the $(^{234}\text{U}/^{238}\text{U})_{\text{act}}$ in the Bécancour groundwater system are revealed (Fig. 1.7a-d). Groundwater located in the main recharge zone of the Appalachians is characterized by lower $(^{234}\text{U}/^{238}\text{U})_{\text{act}}$ (median value of 2.64; n = 13 Fig. 1.7a) than those measured in the St. Lawrence Lowlands plain (median value of 3.79; n = 10 Fig. 1.7a), where groundwater discharges. Shallower granular aquifers show a $(^{234}\text{U}/^{238}\text{U})_{\text{act}}$ median value of 1.26 (n = 3), closer to the secular equilibrium value (i.e., 1) than groundwater in the deeper fractured bedrock aquifer, which shows higher $(^{234}\text{U}/^{238}\text{U})_{\text{act}}$ (median value of 3.03; n = 20 Fig. 1.7b). There is an increase in the $(^{234}\text{U}/^{238}\text{U})_{\text{act}}$ fractionation with hydrological conditions of the aquifer (Fig. 1.7c). Unconfined and semi-confined aquifers have lower $(^{234}\text{U}/^{238}\text{U})_{\text{act}}$ (median value of 2.64, n = 16 and 2.50, n = 3; Fig. 1.7c) than confined aquifers (median value of 4.08, n = 4; Fig. 1.7c). Most importantly, the $(^{234}\text{U}/^{238}\text{U})_{\text{act}}$ is found to progressively fractionate towards higher values in groundwater that is more chemically evolved (Fig. 1.7d). Ca-HCO₃ newly recharged water has the lowest $(^{234}\text{U}/^{238}\text{U})_{\text{act}}$, with a median value of 2.31 (n = 12). The value is even lower (1.22) if only the 3 samples from the shallowest granular aquifer with the youngest waters are considered. Older water, which exchanged Ca²⁺ with Na⁺, has a fractionated $(^{234}\text{U}/^{238}\text{U})_{\text{act}}$ median value of 3.41 (n = 3). Highly evolved Na-HCO₃-Cl water, representing post-glacial meltwater preserved in the fractured bedrock aquifer (Vautour *et al.*, 2015), has a median $(^{234}\text{U}/^{238}\text{U})_{\text{act}}$ value of 5.51 (n= 4). This water is slightly saline, with chlorine derived from trapped pore seawater (Meyzonnat *et al.*, 2016).

1.5 DISCUSSION

1.5.1 Uranium mobilization and redox conditions in the aquifers

The concentration of uranium in groundwater depends on aquifer redox conditions, which strongly impact the radionuclide transport in groundwater. The oxidized form, U^{+6} , reacts with O_2 -rich freshwater and forms UO_2^{2+} , a highly mobile dissolved cation (Langmuir, 1978). ^{234}U and ^{238}U are brought into the water phase through the formation of uranyl complexes or U-fluoride complexes with carbonates and hydroxides under reduced conditions and above pH 7 to 8 (Chabaux *et al.*, 2003). Under mildly reducing conditions, U^{+6} forms complexes with Cl and SO_4 in saline groundwater (Gascoyne, 1992). While progressing along its flow path and to confined conditions, groundwater becomes increasingly reduced by microbial aerobic respiration, which uses O_2 as an electron acceptor (Chapelle *et al.*, 1995). The reduced form, U^{+4} , is rapidly adsorbed on the mineral surface of the aquifer matrix (Langmuir, 1978; Porcelli et Swarzenski, 2003), and thus is removed from groundwater.

In the absence of measured Eh or dissolved oxygen in the sampled groundwater, the concentration of SO_4 can be used as proxy of an aquifer's redox conditions, SO_4 being converted into insoluble sulfides under reducing conditions. Figure 1.8 is a logarithmic plot of the measured SO_4/Cl versus U/Cl molar ratios, with Cl used to normalize values against dilution effects. There is a roughly linear trend, indicating that under increasingly reducing conditions, both SO_4 and U are removed from the groundwater system, the first by forming insoluble sulfides, which are then adsorbed on grain and mineral surfaces. It is interesting to note that the three water samples with the lowest SO_4 and U concentrations (figure 1.8) are BEC101, BEC119, and F9, which exhibit more fractionated $(^{234}U/^{238}U)_{act}$ (Table 1.1). The adsorbed U could constitute a local source of ^{234}U that is easily transferred in soluble form into the water phase, creating high $^{234}U-^{238}U$ fractionation (e.g., Ivanovich *et al.*, 1991).

However, the relationship between U- and He-isotopes seems to exclude this process as the one controlling the ^{234}U - ^{238}U fractionation. Indeed, the possible amount of adsorbed U would be by far insufficient to explain the amount of radiogenic ^4He found in these samples (Table 1.1; see section 5.3 for details).

1.5.2 ^{234}U - ^{238}U fractionation and the chemical evolution of the water

The following scenario might explain the observed trends in $(^{234}\text{U}/^{238}\text{U})_{\text{act}}$ with regards to geological context, aquifer type, hydrological conditions, and water chemistry in the Bécancour groundwater system (Figs. 1.7a-d). The main recharge zone in the Appalachian Mountains and the shallow granular aquifers (both in the Appalachian Mountains and in the plain) are dominated by recently recharged freshwater. This water dissolves carbonate minerals as it infiltrates, acquiring Ca-HCO₃ chemistry. Bulk dissolution of a mineral surface is a zero-order rate process that results in the incorporation of U having the same $(^{234}\text{U}/^{238}\text{U})_{\text{act}}$ as the bulk solid (Bonotto et Andrews, 1993), which is close to secular equilibrium. Along the flow path, water evolves into Na-HCO₃ type when Ca²⁺_{water} exchanges with Na⁺_{mineral} in semi-confined aquifers (Cloutier *et al.*, 2006; Meyzonnat *et al.*, 2016). Approaching the most confined portion of the fractured bedrock aquifer, water evolves to Na-HCO₃-Cl through exchange with saline pore water from the Champlain Sea clay (Cloutier *et al.*, 2010). Na⁺ is not a cation involved in the formation of complexes with uranium (uranyl ions), which might be responsible for transport of U into groundwater. However, there is a roughly linear trend between the measured $(^{234}\text{U}/^{238}\text{U})_{\text{act}}$ and Na⁺ in study area (Fig. 1.9), which might suggest a causative relationship. The relationship between Na⁺ and $(^{234}\text{U}/^{238}\text{U})_{\text{act}}$ might, however, simply indicate mixing between the little-evolved Ca-HCO₃ waters, dominated by the dissolution of carbonates and U with an activity ratio close to secular equilibrium (U bulk dissolution), and more evolved, Na-rich waters, where U isotopic fractionation is produced by the preferential release of ^{234}U by α -recoil. This mixing is also apparent

through the roughly linear relationship between the alkalinity of water (expressed here as mg L⁻¹ of HCO₃ equivalent; Table 1.1) and the (²³⁴U/²³⁸U)_{act} (Fig. 1.10).

The relationships between (²³⁴U/²³⁸U)_{act} and alkalinity, and (²³⁴U/²³⁸U)_{act} and Na concentration (Fig. 1.9, 1.10) could be interpreted either in terms of the time-dependent chemical evolution of the water and progressive accumulation of ²³⁴U or in terms of the mixing of distinct sources. The second hypothesis appears to be more plausible. Indeed, if (²³⁴U/²³⁸U)_{act} fractionation was a time-dependent process, an evolution along the flow path from the Appalachian recharge to the St. Lawrence River discharge would be expected, but this has been not observed. Well BEC118, which shows bulk dissolution and (²³⁴U/²³⁸U)_{act} close to the secular equilibrium, is located downgradient in the St. Lawrence Plain, while elevated (²³⁴U/²³⁸U)_{act} values have been observed both downgradient (BEC101) and upgradient (BEC126). This means that (²³⁴U/²³⁸U)_{act} evolved locally and discrete water masses with characteristic (²³⁴U/²³⁸U)_{act} then mixed together.

If this mixing scenario could explain the distribution of ²³⁴U-²³⁸U fractionations in the watershed, the cause of this fractionation requires an explanation. (²³⁴U/²³⁸U)_{act} ratios higher than 3 are generally observed in oxidizing groundwater with low circulation rates (small water/rock ratios) and with low etch rates (Bonotto. et Andrews, 2000; Paces *et al.*, 2002), or in deep reducing brines that have very low U concentrations where, in same rare cases, (²³⁴U/²³⁸U)_{act} values up to 16 have been measured (Banner *et al.*, 1990). In the Bécancour watershed, groundwater has very low salinity, between 61 and 780 mg.L⁻¹ (Table 1.1), which excludes porewater of marine origin from being the main source of ²³⁴U. Alternative processes producing ²³⁴U-²³⁸U fractionation in groundwater need to be explored.

1.5.3 He and U isotopes: groundwater mixing

Figure 1.11 shows the $(^{234}\text{U}/^{238}\text{U})_{\text{act}}$ plotted against the ${}^3\text{He}/{}^4\text{He}$ ratios (normalized to the atmospheric ratio, $\text{Ra} = 1.386 \times 10^{-6}$). This is one of the first times that these two sets of isotopes have been investigated together in a groundwater system (Tokarev *et al.*, 2006). The ${}^3\text{He}/{}^4\text{He}$ ratio would be atmospheric (1Ra) or higher for groundwater recharging the system between the mid-1950s and the present-day, with ${}^3\text{He}$ excesses derived from the decay of post-bomb tritium (${}^3\text{H}$) (Takaoka et Mizutani, 1987). Older water tends to have ${}^3\text{He}/{}^4\text{He}$ ratios of less than one because of the production of radiogenic ${}^4\text{He}$ from the decay of U and Th contained in the aquifer rock and its accumulation with time in the water (Torgersen et Clarke, 1985). The ratio-ratio plot presented in Fig. 1.11 shows the mixing between at least two groundwater sources having distinct U and He isotopic signatures. The first end-member is an old water having accumulated large amount of radiogenic ${}^4\text{He}$. The resulting ${}^3\text{He}/{}^4\text{He}$ ratio should be close to that expected for production from Li (${}^3\text{He}$), U, and Th (${}^4\text{He}$) present in local formations (0.012Ra; Pinti *et al.*, 2011; Saby *et al.*, 2016). The $(^{234}\text{U}/^{238}\text{U})_{\text{act}}$ of the evolved water end-member is assumed to be equal to that of BEC101, which is the highest measured in the Bécancour watershed. The second end-member is recently recharged water, containing ${}^3\text{He}$ in excess of its atmospheric concentration by production from tritium. The highest ${}^3\text{He}/{}^4\text{He}$ ratio measured in the Bécancour groundwater is 3.10 ± 0.07 (Vautour *et al.*, 2015), and is assumed in the current study to be the maximum reached in the watershed. The $(^{234}\text{U}/^{238}\text{U})_{\text{act}}$ of the recently recharged water end-member should be close to one (i.e., U in the water is isotopically at secular equilibrium). Here, we assume for simplicity that $(^{234}\text{U}/^{238}\text{U})_{\text{act}}$ is at secular equilibrium. Calculations on mixing hyperbola are not affected if a $(^{234}\text{U}/^{238}\text{U})_{\text{act}}$ slightly higher than 1 is assumed.

For a general binary mixing model (Fig. 1.11), mixing lines are hyperbolas with the numerical value “r” = $([\text{U}]/[\text{He}])_{\text{A}}/([\text{U}]/[\text{He}])_{\text{B}}$ defining the degree of curvature between the two end-members, A and B (Langmuir *et al.*, 1978). In Figure 1.11, end-

member A is the old water and end-member B is the recently recharged water. [U] and [He] are the uranium and helium concentrations (in molarity) measured in the two mixing end-members. Mixing curves will only be a straight line for the rare case where $r = 1$ (Langmuir *et al.*, 1978). It is worth noting that samples with Ca-HCO₃ type chemistry resulting from the dissolution of carbonate aquifer rocks (white circles; Fig. 1.11) are closer to the recently recharged water end-member, while mineralized Na-HCO₃ waters affected by ionic exchange are closer to the BEC101 end-member (black circles; Fig. 1.11).

With the exception of BEC102, BEC105, BEC107, BEC118, and BEC126, all other data define a common mixing trend, passing through the newly recharged and the older water end-members (Fig. 1.11). Using an inverse fitting method, as described in Albarède (1995; page 262), the resulting least-square mixing hyperbola has a curvature of 0.18. BEC126, BEC105, BEC107, and BEC118 lie on a different mixing hyperbola with a curvature of 0.01. BEC102 can be explained by a mixing hyperbola with a curvature of 1.2 (Fig. 1.11). The two primary mixing trends revealed in Figure 1.11 appear to be approximately similar to those observed by Vautour *et al.* (2015) in a plot of ³He/⁴He vs uncorrected ¹⁴C ages. Water samples BEC126, BEC105, BEC107, and BEC118 defined a mixing trend alone between old and newly recharged waters. All the other samples defined a second mixing trend between BEC101 and BEC138 (Vautour *et al.*, 2015). In terms of ²³⁴U-²³⁸U fractionation (Fig. 11), these trends might indicate the mixing of old water with newly recharged water infiltrated under different recharge conditions in terms of lithology (Chabaux *et al.*, 2003) and/or infiltration rates (Tricca *et al.*, 2001).

The obtained “r” values can add some insight as to the expected amounts of U in the older groundwater source, if the other concentrations are held fixed. Newly recharged waters are too young (³H/³He ages of less than 50 yrs; Vautour *et al.*, 2015) to have accumulated radiogenic ⁴He produced from the aquifer rock. Here, we assume that

the ${}^4\text{He}$ content in the freshwater is purely atmospheric in origin and is dissolved in water at the average temperature of the aquifer (ASW value at 10°C of $4.59 \times 10^{-8} \text{ cm}^3\text{STP g}^{-1}\text{H}_2\text{O}$). The [U] amount in the newly recharged water end-member should be lower than the amount measured in water samples (BEC138, BEC118) located on the right side of Figure 1.11, i.e. $< 0.0275 \text{ ppb}$. The [He] amount in the older water end-member is more difficult to estimate and could be highly variable. BEC101, which best represents the older water end-member (Fig. 1.7), has a ${}^4\text{He}$ concentration of $1.16 \times 10^{-5} \text{ cm}^3\text{STP g}^{-1}\text{H}_2\text{O}$. BEC126 has highly variable concentrations, which might result from mixing with the theoretical older water end-member. Vautour *et al.* (2015) measured concentrations ranging from 2.6 to $4.5 \times 10^{-5} \text{ cm}^3\text{STP g}^{-1}\text{H}_2\text{O}$ (Table 1.1). Here, we assume that the old water end-member could have [He] concentrations ranging from 1.2 to $4.5 \times 10^{-5} \text{ cm}^3\text{STP g}^{-1}\text{H}_2\text{O}$. From the calculated curvature factors, “r”, the U content in the old water end-member could range from between 0.07 and 0.3 ppb ($r = 0.01$) to between 1.3 and 4.9 ppb ($r = 0.18$). These values are within the range of or slightly higher than those measured in the Bécancour watershed groundwater (Table 1). The amount of U needed to explain the relatively high $({}^{234}\text{U}/{}^{238}\text{U})_{\text{act}}$ measured in BEC102 would be excessively high, from 8.8 to 32.4 ppb. It is likely that this water sample is not a mixture of the two end-members defined above, but that it acquires this relatively high $({}^{234}\text{U}/{}^{238}\text{U})_{\text{act}}$ of 2.50 locally.

1.5.4 Processes leading to $({}^{234}\text{U}/{}^{238}\text{U})_{\text{act}}$ isotopic fractionation and radiogenic ${}^4\text{He}$ excesses

Vautour *et al.* (2015) observed that the amount of radiogenic ${}^4\text{He}$ measured in both BEC101 and BEC126 cannot be derived from the *in situ* decay of U and Th contained in the aquifer rocks. To obtain enough ${}^4\text{He}$ in groundwater from *in situ* production rates in fractured bedrock ($3.5 \times 10^{-13} \text{ cm}^3\text{STP g}^{-1}\text{H}_2\text{O yr}^{-1}$; Vautour *et al.*, 2015), groundwater ages need to range from 379 ka for BEC101 to 1.45 Ma for BEC126,

while ^{14}C adjusted ages are of 6.6 and 2.5 kyrs respectively (Vautour *et al.*, 2015). Alternatively, assuming the ^{14}C -adjusted ages of BEC101 and BEC126 to be 6.6 and 2.5 kyrs, the bulk U and Th contents in the aquifer rocks should be on the order of 90-900 ppm [U] and 300-3000 ppm [Th] to produce the measured radiogenic ^4He . These amounts are 10-100 times higher than average bulk U and Th amounts of 1.5 and 5.7 ppm measured in the aquifer rocks by Vautour *et al.* (2015).

The causal relationship between radiogenic ^4He and U isotopes in groundwater end-members requires a process able to simultaneously fractionate ^{234}U from ^{238}U as well as decrease the initial $^3\text{He}/^4\text{He}$ by adding large amounts of radiogenic ^4He . Stress-induced fracturing of the rock might be the cause of this process (Andrews *et al.*, 1982; Andrews et Kay, 1983; Torgersen et O'Donnell, 1991). An increase in rock fracturing could have taken place following ice retreat and the accelerated phase of isostatic rebound from 12 kyrs to 6.7 kyrs (Lamarche *et al.*, 2007), increasing the permeability (Aquilina *et al.*, 2015; Person *et al.*, 2007), and shaping the hydrological network of the St. Lawrence Lowlands close to that observed at present (e.g., Lamarche *et al.*, 2007; Saby *et al.*, 2016).

Radiogenic helium is usually released by diffusion and α - recoil from the rock (Torgersen, 1980). If the aquifer rock grain size is much larger than the distance of α -recoil (30-100 nm; Torgersen, 1980) or than that of diffusion length, only a fraction of the produced ^4He will be released to the water phase, while the majority will accumulate into the rock for a long time (Solomon *et al.*, 1996). Torgersen et O'Donnell (1991) have suggested that the progressive fracturing of a rock slab increases the specific surface exposed to water and therefore that the ^4He accumulated in the rock can be instantaneously released into the water. A 1-D model of rock fracturing showed that stress-induced macro-fracturing every 10 m along a 1 km wide rock slab would allow the release of ^4He otherwise accumulated over 15 Myrs in only 1500 years (Torgersen et O'Donnell, 1991).

Increasing the aquifer matrix surface area exposed to water by fracturing would also enhance the release of ^{234}U by α -recoil and thus shift the initial ($^{234}\text{U}/^{238}\text{U}$)_{act} towards higher values. This process can be modeled following equation (1) of Andrews *et al.* (1982) (see also Andrews et Kay, 1983):

$$\left(\frac{^{234}\text{U}}{^{238}\text{U}}\right)_{act}^{final} = 1 + \left[\left(\frac{^{234}\text{U}}{^{238}\text{U}}\right)_{act}^{initial} - 1 \right] \cdot e^{(-^{234}\lambda t)} + 0.235 \cdot \rho \cdot S \cdot R \cdot [1 - e^{(-^{234}\lambda t)}] \cdot \frac{[U]_{rock}}{[U]_{water}} \quad (1.1)$$

In this equation, the first term is the decay of ^{234}U , while the second term is the production of ^{234}U in the rock (Andrews *et al.*, 1982). $\left(\frac{^{234}\text{U}}{^{238}\text{U}}\right)_{act}^{final}$ is the final activity ratio measured for BEC101 (6.07) and $\left(\frac{^{234}\text{U}}{^{238}\text{U}}\right)_{act}^{initial}$ is the initial activity ratio assumed to be close or equal to the secular equilibrium value; $^{234}\lambda$ is the decay constant of ^{234}U ($2.785 \times 10^{-6} \text{ yr}^{-1}$); ρ is the rock density (2.72 g cm^{-3} for carbonates); R is the recoil length of ^{234}Th in the rock ($3 \times 10^{-6} \text{ cm}$) (Andrews et Kay, 1983); $[U]$ is the uranium concentration in ppm in the rock (1.19 ppm for BEC101; Vautour *et al.*, 2015) and in the water (0.0442 ppb for BEC101; Table 1); t is the groundwater residence time, reported here as the NETPATH adjusted ^{14}C age of 6,696 yrs for BEC101 (Vautour *et al.*, 2015); S is the fracture surface area (cm^2/cm^3), which is the rock surface in contact with a volume unit of groundwater (Andrews et Kay, 1983). It is proportional to the fracture width w ($w = 2/S$) and it is an indirect index of the extent of rock fracturing (Andrews et Kay, 1983; Elliot *et al.*, 2014).

The extent of the $^{234}\text{U}-^{238}\text{U}$ isotopic fractionation measured in BEC101 ($(^{234}\text{U}/^{238}\text{U})_{act} = 6.07 \pm 0.14$) can be explained by a density of fracturing $S = 5296 \text{ cm}^2 \text{ cm}^{-3}$, equivalent to a w of $3.8 \mu\text{m}$. This fracture opening is consistent with the hydraulic conductivities measured during well pumping tests (Larocque *et al.*, 2013). Fracture

opening (w) is related to hydraulic conductivity (K_f) following the relationship (Witherspoon, 2010):

$$K_f = \frac{[(w^2) \times \phi \times g]}{12 \times \mu} \quad (1.2)$$

Where μ is the kinematic viscosity of water at aquifer temperatures (0.0013 kg/m/s); ρ is the density of water (assumed equal to 1); and g is the gravity acceleration. Calculated K_f is 2.4×10^{-8} m s⁻¹ for BEC101, within the values measured in the Bécancour fractured bedrock of 0.5 to 80×10^{-8} m s⁻¹ during well pumping tests (Larocque *et al.*, 2013).

1.6 CONCLUSIONS

The goal of this study was to investigate the systematics of ^{234}U and ^{238}U isotopes in groundwater from the aquifers of the St. Lawrence Lowlands, to improve understanding of the chemical evolution of its waters. Results of this study showed that the measured variability in the $^{234}\text{U}/^{238}\text{U}$ activity ratios, which range from 1.145 ± 0.014 to 6.07 ± 0.14 , is related to mixing of waters with distinct $(^{234}\text{U}/^{238}\text{U})_{\text{act}}$, acquired locally.

The relationship between $^3\text{He}/^4\text{He}$ and $(^{234}\text{U}/^{238}\text{U})_{\text{act}}$ reveal the occurrence of distinct water types with separate evolutionary origins: 1) modern freshwater located in the upper granular aquifer, poorly mineralized and with a $(^{234}\text{U}/^{238}\text{U})_{\text{act}}$ close to the secular equilibrium, and 2) a mineralized older water from the fractured aquifer with a higher $(^{234}\text{U}/^{238}\text{U})_{\text{act}}$ of 6.07.

The inverse causal relationship between helium isotope ($^3\text{He}/^4\text{He}$) and U isotope ($^{234}\text{U}/^{238}\text{U}$)_{act} ratios (Fig. 1.11) suggests a unique common process, able to simultaneously fractionate $(^{234}\text{U}/^{238}\text{U})_{\text{act}}$ toward higher values and lower the $^3\text{He}/^4\text{He}$ ratios, through a concomitant release of ^{234}U and ^4He . The underlying process might be rock fracturing, which is able to increase the surface area of rock exposed to α -recoil of ^{234}U and to α -recoil and diffusion of radiogenic ^4He , both mechanisms favoring the release of these two nuclides into the water phase. In future work, it would prove highly valuable to verify whether this He-U relationship exists in other hydrogeological contexts. Future work should also investigate the hypothesis that rock fracturing favors the release of large amounts of radiogenic helium from internal aquifer sources (Carey *et al.*, 2004; Solomon *et al.*, 1996), rather than being derived from the addition of helium basal fluxes from sources external to aquifers (Torgersen *et al.*, 1985).

ACKNOWLEDGMENTS

We wish to thank the handling editor, Luc Aquilina, as well as J. Paces (USGS) and two anonymous reviewers for their thoughtful comments that greatly improved the manuscript. We also thank G.B. Johnson for correcting English. The authors thank the Quebec Ministry of Environment (*Ministère du Développement durable, de l'Environnement, des Parcs et de la Lutte contre les changements climatiques*), the Quebec Research Fund (“Fonds de recherche du Québec - Nature et Technologies”), the Bécancour River Watershed Organization (“organisme de bassin versant GROBEC”), and the municipalities that contributed funding to this research (Cré Centre-du-Québec, MRC d’Arthabaska, MRC de Bécancour, MRC de l’Erable, MRC de Nicolet-Yamaska, AGTCQ, Céged Thetford).

REFERENCES

- Andersen, M.B., Erel, Y. et Bourdon, B. (2009). Experimental evidence for ^{234}U - ^{238}U fractionation during granite weathering with implications for $^{234}\text{U}/^{238}\text{U}$ in natural waters. *Geochimica et Cosmochimica Acta*, 73(14), 4124-4141.
- Andrews, J.N., Giles, I.S., Kay, R.L.F., Lee, D.J., Osmond, J.K., Cowart, J.B., Fritz, P., Barker, J.F. et Gale, J. (1982). Radioelements, radiogenic helium and age relationships for groundwaters from the granites at Stripa, Sweden. *Geochimica et Cosmochimica Acta*, 46(9), 1533-1543.
- Andrews, J.N. et Kay, R.L.F. (1983). The U contents and $^{234}\text{U}/^{238}\text{U}$ activity ratios of dissolved uranium in groundwaters from some Triassic Sandstones in England. *Chemical Geology*, 41, 101-117.
- Aquilina, L., Vergnaud-Ayraud, V., Les Landes, A.A., Pauwels, H., Davy, P., Pételet-Giraud, E., Labasque, T., Roques, C., Chatton, E. et Bour, O. (2015). Impact of climate changes during the last 5 million years on groundwater in basement aquifers. *Scientific reports*, 5.
- Ballentine, C.J. et Burnard, P.G. (2002). Production, release and transport of noble gases in the continental crust. *Reviews in mineralogy and geochemistry*, 47(1), 481-538.
- Banner, J.L., Wasserburg, G., Chen, J.H. et Moore, C.H. (1990). ^{234}U - ^{238}U - ^{230}Th - ^{232}Th systematics in saline groundwaters from central Missouri. *Earth and Planetary Science Letters*, 101(2), 296-312.
- Benoît, N., Blanchette, D., Nasterv, M. et Molson, J.N. (2011). *Groundwater geochemistry of the Lower Chaudière River Watershed, Québec*. Proceedings of the International Association of Hydrogeologists-Canadian National Chapter (IAH-CNC)/Canadian Quaternary Association (CANQUA) Conference: GeoHydro 2011.
- Bonotto, D.M. et Andrews, J.N. (1993). The mechanism of $^{234}\text{U}/^{238}\text{U}$ activity ratio enhancement in karstic limestone groundwater. *Chemical Geology*, 103, 193-206.
- Bonotto, D.M. et Andrews, J.N. (2000). The transfer of uranium isotopes ^{234}U and ^{238}U to the waters interacting with carbonates from Mendip Hills area (England). *Applied Radiation and Isotopes*, 52(4), 965-983.
- Bourdon, B., Henderson, G.M., Lundstrom, C.C. et Turner S.P. (2003). Uranium-series Geochemistry, Geochemical Society Mineralogical Society of America, Washington 658 pp.
- Carey, A.E., Dowling, C.B. et Poreda, R.J. (2004). Alabama Gulf Coast groundwaters: ^4He and ^{14}C as groundwater-dating tools. *Geology*, 32(4), 289-292.

- Castro, M.C., Ma, L. et Hall, C.M. (2009). A primordial, solar He–Ne signature in crustal fluids of a stable continental region. *Earth and Planetary Science Letters*, 279(3), 174-184.
- Chabaux, F., Riotte, J. et Dequincey, O. (2003). U-Th-Ra fractionation during weathering and river transport. *Reviews in Mineralogy and Geochemistry*, 52(1), 533-576.
- Chapelle, F.H., McMahon, P.B., Dubrovsky, N.M., Fujii, R.F., Oaksford, E.T. et Vroblesky, D.A. (1995). Deducing the distribution of terminal electron-accepting processes in hydrologically diverse groundwater systems. *Water Resources Research*, 31(2), 359-371.
- Chen, J.H., Lawrence Edwards, R. et Wasserburg, G.J. (1986). ^{238}U , ^{234}U and ^{232}Th in seawater. *Earth and Planetary Science Letters*, 80(3–4), 241-251.
- Cherdynsev, V., Chalov, P. et Khitrik, M. (1955). On isotopic composition of radio-elements in natural objects and problems of geochronology. *Trans. 3rd Session Commiss. Determ. Abs. age geol. Formns*, 175-233.
- Cloutier, V., Lefebvre, R., Savard, M.M., Bourque, É. et Therrien, R. (2006). Hydrogeochemistry and groundwater origin of the Basses-Laurentides sedimentary rock aquifer system, St. Lawrence Lowlands, Québec, Canada. *Hydrogeology Journal*, 14(4), 573-590.
- Cloutier, V., Lefebvre, R., Savard, M.M. et Therrien, R. (2010). Desalination of a sedimentary rock aquifer system invaded by Pleistocene Champlain Sea water and processes controlling groundwater geochemistry. *Environmental Earth Sciences*, 59(5), 977-994.
- Durand, S., Chabaux, F., Rihs, S., Duringer, P. et Elsass, P. (2005). U isotope ratios as tracers of groundwater inputs into surface waters: example of the Upper Rhine hydrosystem. *Chemical Geology*, 220(1), 1-19.
- Edwards, R.L., Chen, J. et Wasserburg, G. (1987). ^{238}U - ^{234}U - ^{230}Th - ^{232}Th systematics and the precise measurement of time over the past 500,000 years. *Earth and Planetary Science Letters*, 81(2), 175-192.
- Elliot, T., Bonotto, D.M. et Andrews, J.N. (2014). Dissolved uranium, radium and radon evolution in the Continental Intercalaire aquifer, Algeria and Tunisia. *Journal of Environmental Radioactivity*, 137, 150-162.
- Fröhlich, K. (2013). Dating of old groundwater using uranium isotopes-principles and applications. Chapter 7. Dans *Isotope methods for dating old groundwater*.
- Fröhlich, K. et Gellermann, R. (1987). On the potential use of uranium isotopes for groundwater dating. *Chemical Geology: Isotope Geoscience section*, 65(1), 67-77.

- Gascoyne, M. (1992). Palaeoclimate determination from cave calcite deposits. *Quaternary Science Reviews*, 11(6), 609-632.
- Gascoyne, M. (2004). Hydrogeochemistry, groundwater ages and sources of salts in a granitic batholith on the Canadian Shield, southeastern Manitoba. *Applied Geochemistry*, 19(4), 519-560.
- Geyh, M. (2005). *Dating of old groundwater—history, potential, limits and future.* : Springer.
- Globensky, Y. (1987). Géologie des basses-terres du Saint-Laurent. : [Ministère de l'énergie et des ressources], Direction générale de l'exploration géologique et minérale, Direction de la recherche géologique, Service de la géologie.
- Globensky, Y. (1993). *Lexique stratigraphique canadien. Volume VB: région des Appalaches, des Basses-Terres du Saint-Laurent et des îles de la Madeleine.* : [Québec]: Direction générale de l'exploration géologique et minérale.
- Godbout, P.-M. (2013). Géologie du quaternaire et hydrostratigraphie des dépôts meubles du bassin versant de la rivière Bécancour et des zones avoisinantes, Québec.
- Harvey BG (1962) Introduction to Nuclear Physics and Chemistry. Prentice Hall Inc, New Jersey
- Hillaire-Marcel, C. et Causse, C. (1989). Chronologie Th/U des concrétions calcaires des varves du lac glaciaire de Deschaillons (Wisconsinien inférieur). *Canadian Journal of Earth Sciences*, 26(5), 1041-1052.
- Hubert, A., Bourdon, B., Pili, E. et Meynadier, L. (2006). Transport of radionuclides in an unconfined chalk aquifer inferred from U-series disequilibria. *Geochimica et Cosmochimica Acta*, 70(22), 5437-5454.
- Ivanovich, M., Fröhlich, K. et Hendry, M. (1991). Uranium-series radionuclides in fluids and solids, Milk River aquifer, Alberta, Canada. *Applied Geochemistry*, 6(4), 405-418.
- Kigoshi, K. (1971). Alpha-recoil thorium-234: dissolution into water and the uranium-234/uranium-238 disequilibrium in nature. *Science*, 173(3991), 47-48.
- Kipfer, R. et Peeters, F. (2002). *Using transient conservative and environmental tracers to study water exchange in Lake Issyk-Kul.* : Springer.
- Kronfeld, J., Gradsztajn, E., Müller, H.W., Radin, J., Yaniv, A. et Zach, R. (1975). Excess ^{234}U : an aging effect in confined waters. *Earth Planetary Sciences Letter*, 27, 342-345.

- Kronfeld, J., Gradsztajn, E. et Yaniv, A. (1979). A flow pattern deduced from uranium disequilibrium studies for the Cenomanian carbonate aquifer of the Beersheva region, Israel. *Journal of Hydrology*, 44(3), 305-310.
- Kulongoski, J.T. et Hilton, D.R. (2011). Applications of groundwater helium. In: Baskaran, M. (Ed.), *Handbook of Environmental Isotope Geochemistry, Advances in Isotope Geochemistry*. Springer-Verlag, Berlin Heidelberg, pp. 285–303.
- Lamarche, L., Bondue, V., Lemelin, M.-J., Lamothe, M. et Roy, A. (2007). Deciphering the Holocene evolution of the St. Lawrence River drainage system using luminescence and radiocarbon dating. *Quaternary Geochronology*, 2(1), 155-161.
- Lamothe, M. (1989). A new framework for the Pleistocene stratigraphy of the central St. Lawrence Lowland, Southern Québec. *Géographie physique et Quaternaire*, 43(2), 119-129.
- Langmuir, D. (1978). Uranium solution-mineral equilibria at low temperatures with applications to sedimentary ore deposits. *Geochimica et Cosmochimica Acta*, 42(6, Part A), 547-569.
- Lavoie, D. (2008). Appalachian foreland basin of Canada. *Sedimentary basins of the world*, 5, 65-103.
- Lavoie, D., Pinet, N., Castonguay, S., Hannigan, P., Dietrich, J., Hamblin, T. et Giller, P. (2009). Petroleum resource assessment, Paleozoic successions of the St. Lawrence Platform and Appalachians of eastern Canada. *Geological Survey of Canada*, 6174, 275.
- Maher, K., Steefel, C.I., DePaolo, D.J. et Viani, B.E. (2006). The mineral dissolution rate conundrum: Insights from reactive transport modeling of U isotopes and pore fluid chemistry in marine sediments. *Geochimica et Cosmochimica Acta*, 70(2), 337-363.
- Meyzonnat, G., Larocque, M., Barbicot, F., Pinti, D. et Gagné, S. (2016). The potential of major ion chemistry to assess groundwater vulnerability of a regional aquifer in southern Quebec (Canada). *Environmental Earth Sciences*, 75(1), 1-12.
- Occhietti, S., Parent, M., Shilts, W.W., Dionne, J.-C., Govare, E. et Harmand, D. (2001). Late Wisconsinan glacial dynamics, deglaciation, and marine invasion in southern Québec. *SPECIAL PAPERS-GEOLOGICAL SOCIETY OF AMERICA*, 243-270.
- Occhietti, S. et Richard, P.J. (2003). Effet réservoir sur les âges ^{14}C de la Mer de Champlain à la transition Pléistocène-Holocène: révision de la chronologie de

- la déglaciation au Québec méridional. *Géographie physique et Quaternaire*, 57(2-3), 115-138.
- Osmond, J. et Cowart, J. (1976). The theory and uses of natural uranium isotopic variations in hydrology. *Atomic Energy Review*, 14(4), 620-679
- Osmond, J.K. et Cowart, J. (1982). Natural uranium and thorium serie disequilibrium: new approaches to geochemical problems. *Nucl. Sci. Appl. B* 1, 303e352.
- Osmond, J.K. et Cowart, J.B. (2000). U-series nuclides as tracers in groundwater hydrology. In: Cook, P., Herczeg, A. (Eds.), *Environmental Tracers in Subsurface Hydrology*. Kluwer Academic Publishers, Boston, pp. 145e174.
- Osmond, J., Kaufman, M.I. et Cowart, J. (1974). Mixing volume calculations, sources and aging trends of Floridan aquifer water by uranium isotopic methods. *Geochimica et Cosmochimica Acta*, 38(7), 1083-1100.
- Ozima, M. et Podosek, F. (1983). *Noble gas chemistry*: Cambridge, United Kingdom : Cambridge Univ. Press.
- Paces, J.B., Ludwig, K.R., Peterman, Z.E. et Neymark, L.A. (2002). $^{234}\text{U}/^{238}\text{U}$ evidence for local recharge and patterns of ground-water flow in the vicinity of Yucca Mountain, Nevada, USA. *Applied Geochemistry*, 17(6), 751-779.
- Paces, J.B., Wurster, F.C., 2014. Natural uranium and strontium isotope tracers of water sources and surface water-groundwater interactions in arid wetlands-Pahranagat Valley, Nevada, USA. *Journal of Hydrology*. 517, 213-225.
- Parent, M. et Occhietti, S. (1988). Late Wisconsinan deglaciation and Champlain sea invasion in the St. Lawrence valley, Québec. *Géographie physique et Quaternaire*, 42(3), 215-246.
- Person, M., McIntosh, J., Bense, V. et Remenda, V. (2007). Pleistocene hydrology of North America: the role of ice sheets in reorganizing groundwater flow systems. *Reviews of Geophysics*, 45(3).
- Phillips, F. et Castro, M. (2003). Groundwater dating and residence-time measurements. *Treatise on geochemistry*, 5, 451-497.
- Pinti, D.L. et Marty, B. (1998). The origin of helium in deep sedimentary aquifers and the problem of dating very old groundwaters. *Geological Society, London, Special Publications*, 144(1), 53-68.
- Pinti, D.L., Béland-Otis, C., Tremblay, A., Castro, M.C., Hall, C.M., Marcil, J.-S., Lavoie, J.-Y. et Lapointe, R. (2011). Fossil brines preserved in the St-Lawrence Lowlands, Québec, Canada as revealed by their chemistry and noble gas isotopes. *Geochimica et Cosmochimica Acta*, 75(15), 4228-4243.

- Plater, A., Ivanovich, M. et Dugdale, R. (1992). Uranium series disequilibrium in river sediments and waters: the significance of anomalous activity ratios. *Applied Geochemistry*, 7(2), 101-110.
- Plummer, L. et Glynn, P. (2013). Radiocarbon dating in groundwater systems. *Isotope Methods for Dating Old Groundwater, International Atomic Energy Agency (IAEA), Vienna*, 33-90.
- Porcelli, D. et Swarzenski, P.W. (2003). The behavior of U-and Th-series nuclides in groundwater. *Reviews in Mineralogy and Geochemistry*, 52(1), 317-361.
- Reynolds, B., Wasserburg, G. et Baskaran, M. (2003). The transport of U-and Th-series nuclides in sandy confined aquifers. *Geochimica et Cosmochimica Acta*, 67(11), 1955-1972.
- Riotte, J. et Chabaux, F. (1999). ($^{234}\text{U}/^{238}\text{U}$) activity ratios in freshwaters as tracers of hydrological processes: the Strengbach watershed (Vosges, France). *Geochimica et Cosmochimica Acta*, 63(9), 1263-1275.
- Riotte, J., Chabaux, F., Benedetti, M., Dia, A., Gérard, M., Boulègue, J. et Etamé, J. (2003). Uranium colloidal transport and origin of the $^{234}\text{U}-^{238}\text{U}$ fractionation in surface waters: new insights from Mount Cameroon. *Chemical Geology*, 202(3), 365-381.
- Saby, M., Larocque, M., Pinti, D.L., Barbecot, F., Sano, Y. et Castro, M.C. (2016). Linking groundwater quality to residence times and regional geology in the St. Lawrence Lowlands, southern Quebec, Canada. *Applied Geochemistry*, 65, 1-13.
- Solomon, D., Hunt, A. et Poreda, R. (1996). Source of radiogenic helium 4 in shallow aquifers: Implications for dating young groundwater. *Water Resources Research*, 32(6), 1805-1813.
- Takaoka, N. et Mizutani, Y. (1987). Tritiogenic ^3He in groundwater in Takaoka. *Earth and Planetary Science Letters*, 85(1), 74-78.
- Tokarev, I., Zubkov, A., Rumynin, V.G., Polyakov, V., Kuznetsov, V.Y. et Maksimov, F. (2006). Origin of high $^{234}\text{U}/^{238}\text{U}$ ratio in post-permafrost aquifers. Dans *Uranium in the Environment* (p. 847-856) : Springer.
- Torgersen, T. (1980). Controls on pore-fluid concentration of ^4He and ^{222}Rn and the calculation of $^4\text{He}/^{222}\text{Rn}$ ages. *Journal of Geochemical Exploration*, 13(1), 57-75.
- Torgersen, T. et Clarke, W.B. (1985). Helium accumulation in groundwater, I: An evaluation of sources and the continental flux of crustal ^4He in the Great Artesian Basin, Australia. *Geochimica et Cosmochimica Acta*, 49(5), 1211-1218.

- Torgersen, T. et O'Donnell, J. (1991). The degassing flux from the solid earth: release by fracturing. *Geophysical Research Letters*, 18(5), 951-954.
- Torgersen, T. et Stute, M. (2013). Helium (and other noble gases) as a tool for understanding long time-scale groundwater transport. Isotope methods for *Dating old groundwater*, IAEA, Vienna, 179-216.
- Tran Ngoc, T., Lefebvre, R., Konstantinovskaya, E. et Malo, M. (2014). Characterization of deep saline aquifers in the Bécancour area, St. Lawrence Lowlands, Québec, Canada: Implications for CO₂ geological storage. *Environmental geology*, 72(1), 119-146.
- Tricca, A., Porcelli, D. et Wasserburg, G. (2000). Factors controlling the groundwater transport of U, Th, Ra, and Rn. *Journal of Earth System Science*, 109(1), 95-108.
- Tricca, A., Wasserburg, G., Porcelli, D. et Baskaran, M. (2001). The transport of U- and Th-series nuclides in a sandy unconfined aquifer. *Geochimica et Cosmochimica Acta*, 65(8), 1187-1210.
- Vautour, G., Pinti, D.L., Méjean, P., Saby, M., Meyzonnat, G., Larocque, M., Castro, M.C., Hall, C.M., Boucher, C., Roulleau, E., Barbicot, F., Takahata, N. et Sano, Y. (2015). ³H/³He, ¹⁴C and (U-Th)/He groundwater ages in the St. Lawrence Lowlands, Quebec, Eastern Canada. *Chemical Geology*, 413, 94-106.
- Witherspoon, P. (2010). Validity of cubic law for fluid flow in a deformable rock fracture. *Lawrence Berkeley National Laboratory*. Water Resources Research, LBNL Paper LBL-9557

FIGURES

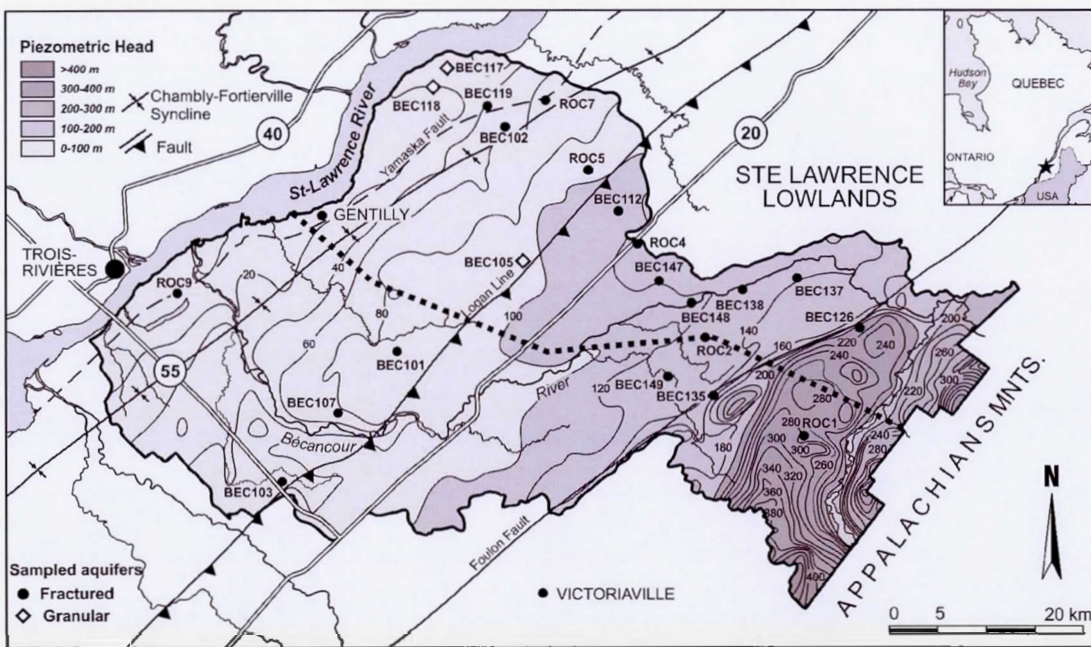


Figure 1.1 Simplified map of the Bécancour watershed, southern Quebec, with potentiometric head isolines of the regional fractured bedrock aquifer and the groundwater sampled wells of this study (diamonds: Quaternary granular aquifer; circles: Ordovician regional fractured bedrock aquifer) (modified from Larocque *et al.*, 2013).

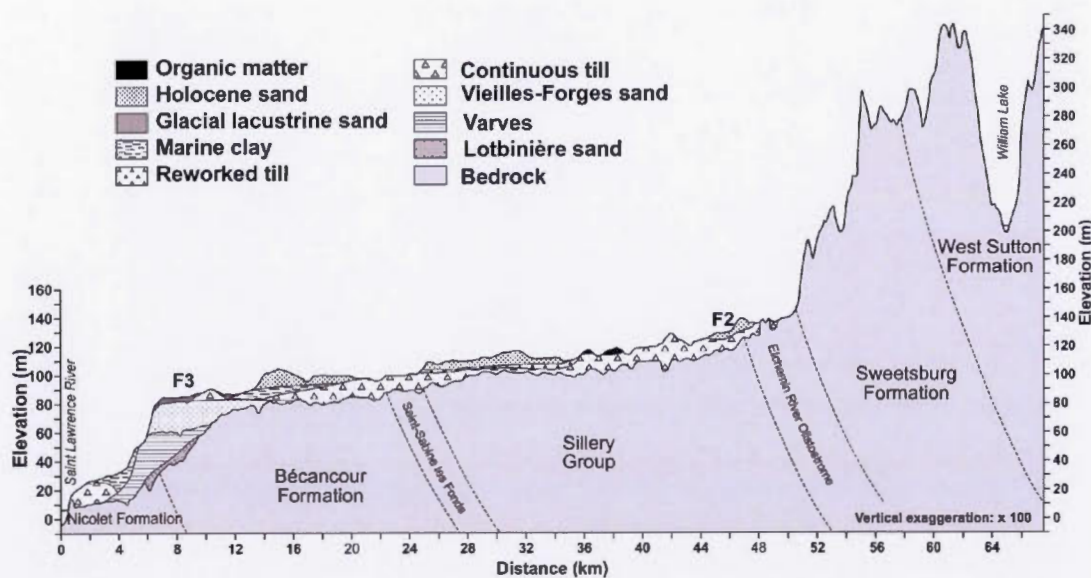


Figure 1.2 Cross section illustrating shallow granular aquifers and deeper fractured aquifers with geological groups belonging to the St. Lawrence Platform and the Appalachian Mountains (modified from Larocque *et al.*, 2013).

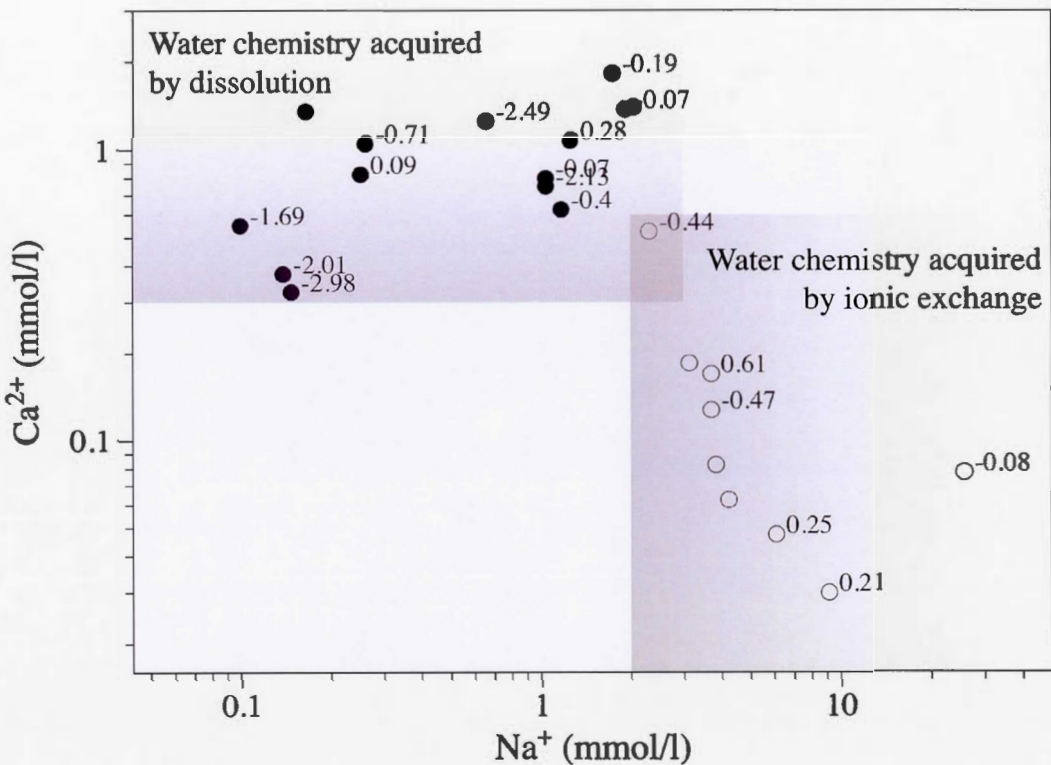


Figure 1.3 Logarithmic plot of Sodium (Na^+) versus Calcium (Ca^{2+}) for groundwater that is under-saturated to saturated in calcite (black dots) and groundwater saturated to oversaturated with respect to calcite (white dots). Plotted values are the calcite saturation index (SI; Table 1).

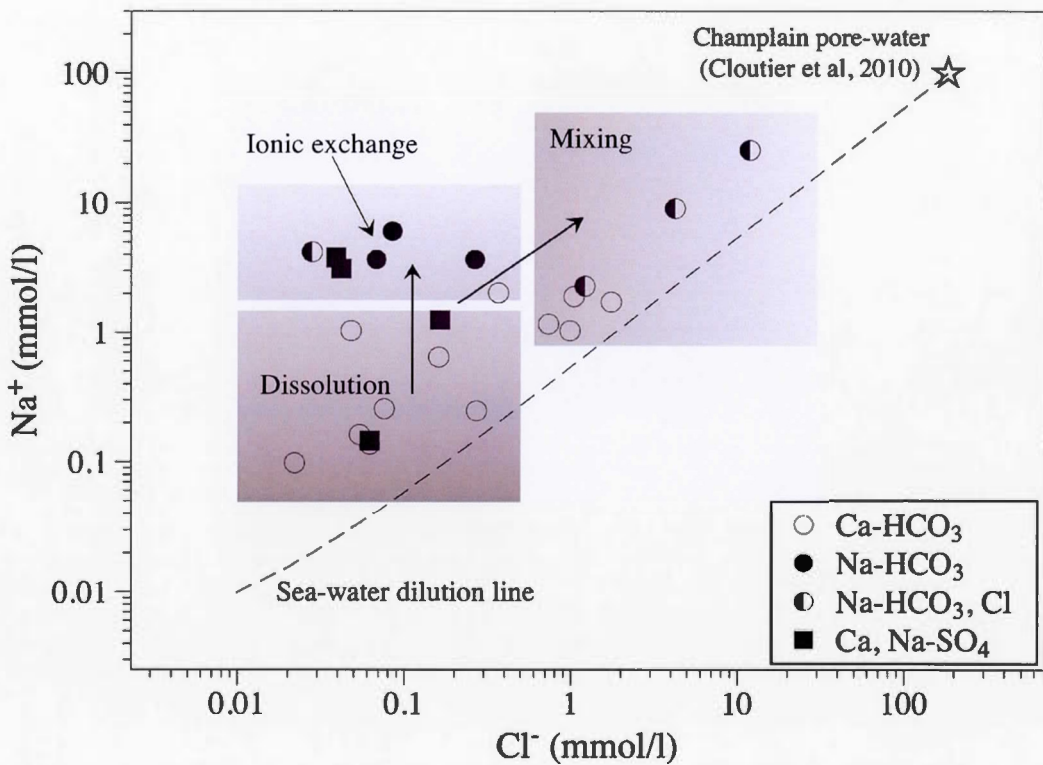


Figure 1.4 Plot of sodium (Na^+) versus Chloride (Cl^-) concentrations, showing the evolution of groundwater composition: Ca-HCO_3 (white dots) and Ca,NaSO_4 (black squares) type achieved through rock dissolution, Na-HCO_3 (black dots) through ionic exchange, and $\text{Na-HCO}_3\text{-Cl}$ (black and white dots) through mixing with older mineralized waters.

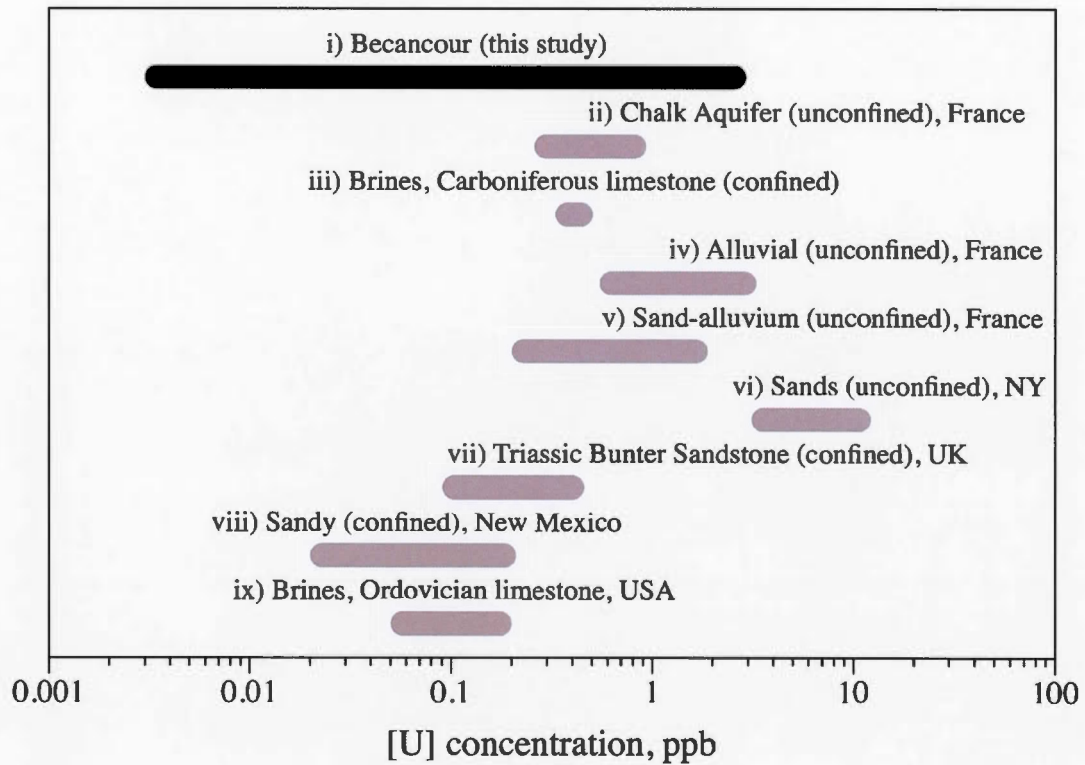


Figure 1.5 Measured uranium concentrations (in ppb) in Bécancour watershed groundwater, compared to data from other sedimentary aquifers with similar lithological and hydrological conditions.

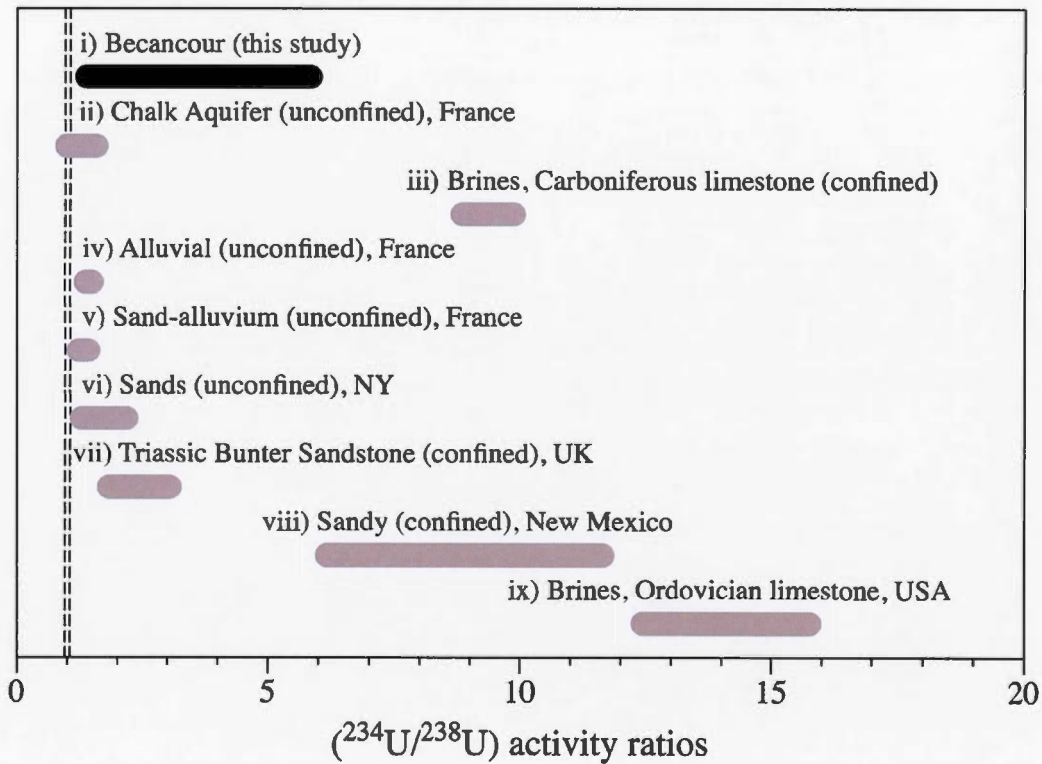


Figure 1.6 Measured $(^{234}\text{U}/^{238}\text{U})_{\text{act}}$ in Bécancour watershed groundwater, compared to data from other sedimentary aquifers with similar lithological and hydrological conditions. Dotted vertical lines represent the $(^{234}\text{U}/^{238}\text{U})_{\text{act}}$ secular equilibrium value.

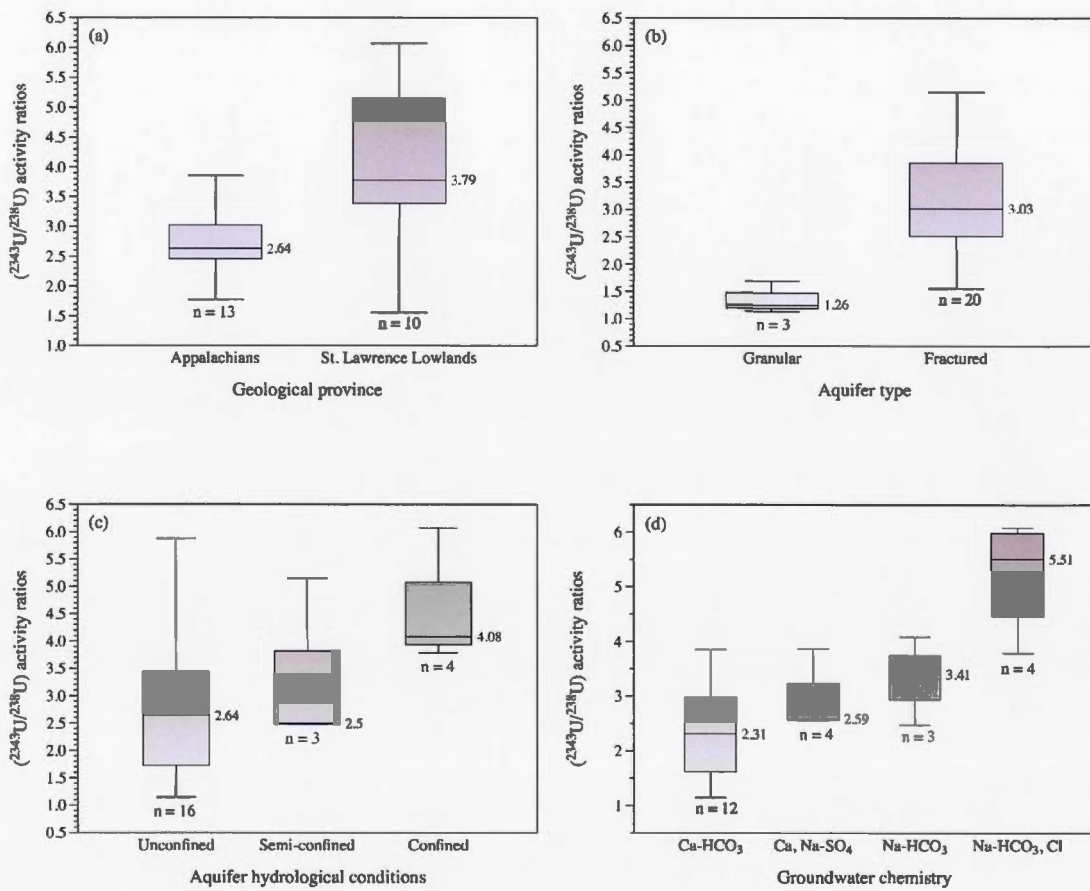


Figure 1.7 Statistical boxplots of $(^{234}\text{U}/^{238}\text{U})_{\text{act}}$ for Bécancour watershed groundwater samples as a function of the geological province (a), aquifer type (b), hydrogeological conditions of aquifer (c), and groundwater chemistry (d).

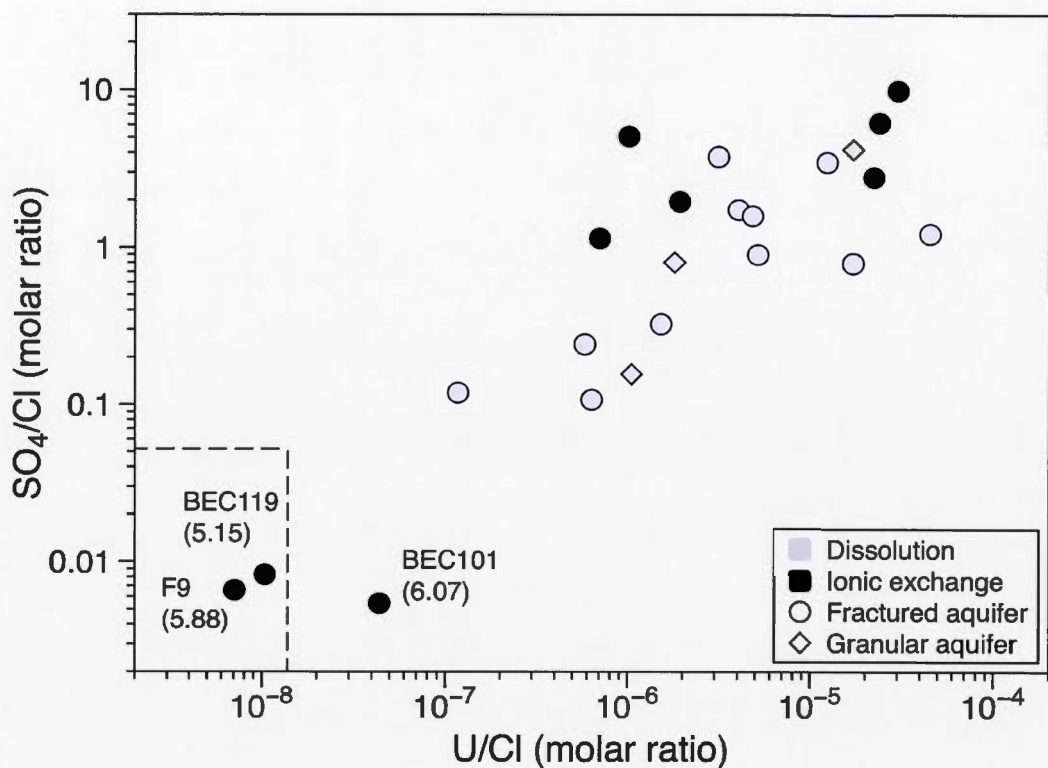


Figure 1.8 U/Cl molar ratios as a function of SO₄/Cl ratios in Bécancour watershed groundwater samples. The dotted lines represent the seawater U/Cl and SO₄/Cl ratios. Numbers in parentheses for BEC101, BEC119, and F9 are measured (²³⁴U/²³⁸U)_{act}.

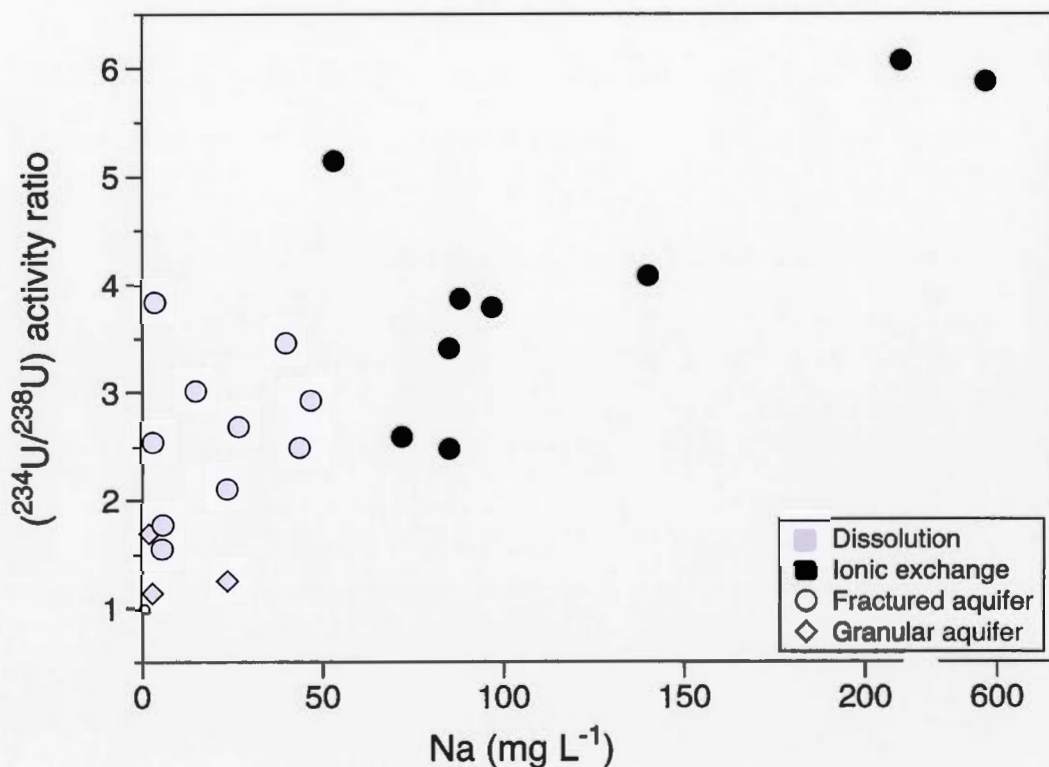


Figure 1.9 Measured $(^{234}\text{U}/^{238}\text{U})_{\text{act}}$ as a function of Na^+ . Diamonds represent groundwater from Quaternary granular aquifers. Circles represent groundwater from the Ordovician fractured bedrock, where samples whose chemistry is controlled by the dissolution of carbonates are shaded gray, and black symbols represents samples whose chemistry is controlled by ionic exchange processes.

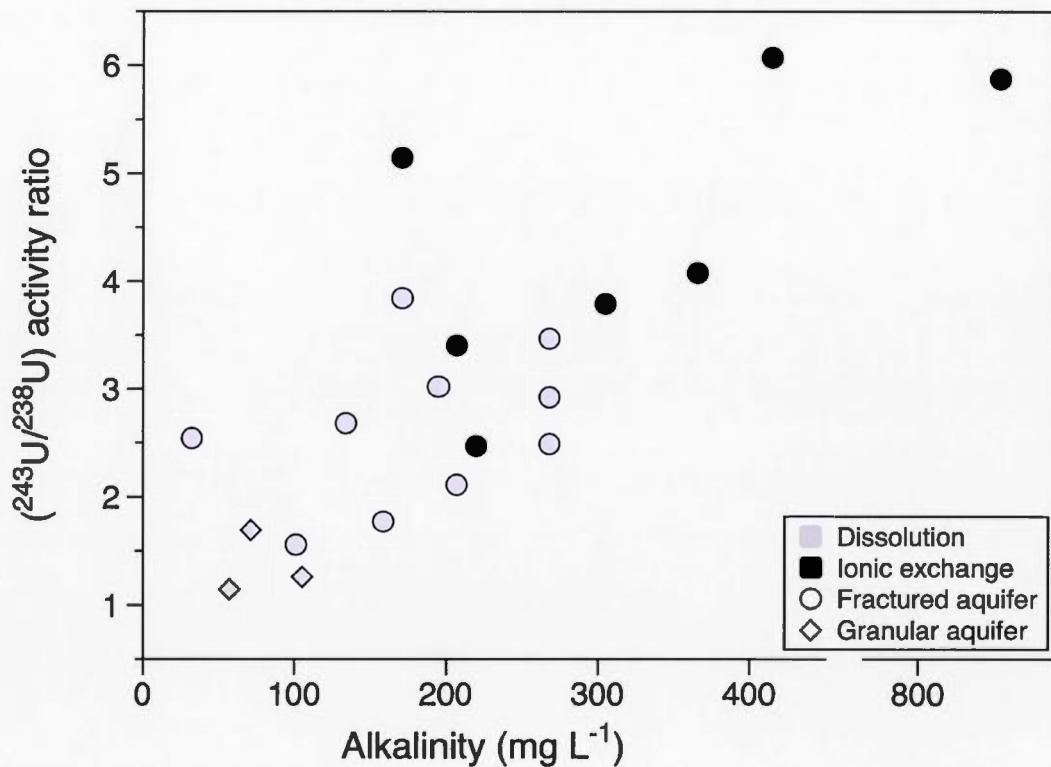


Figure 1.10 Measured $(^{234}\text{U}/^{238}\text{U})_{\text{act}}$ as a function of Na^+ concentration (a), and alkalinity (b). Diamonds represent groundwater from Quaternary granular aquifers. Circles represent groundwater from the Ordovician fractured bedrock, where samples whose chemistry is controlled by the dissolution of carbonates are shaded gray, and black symbols represents samples whose chemistry is controlled by ionic exchange processes.

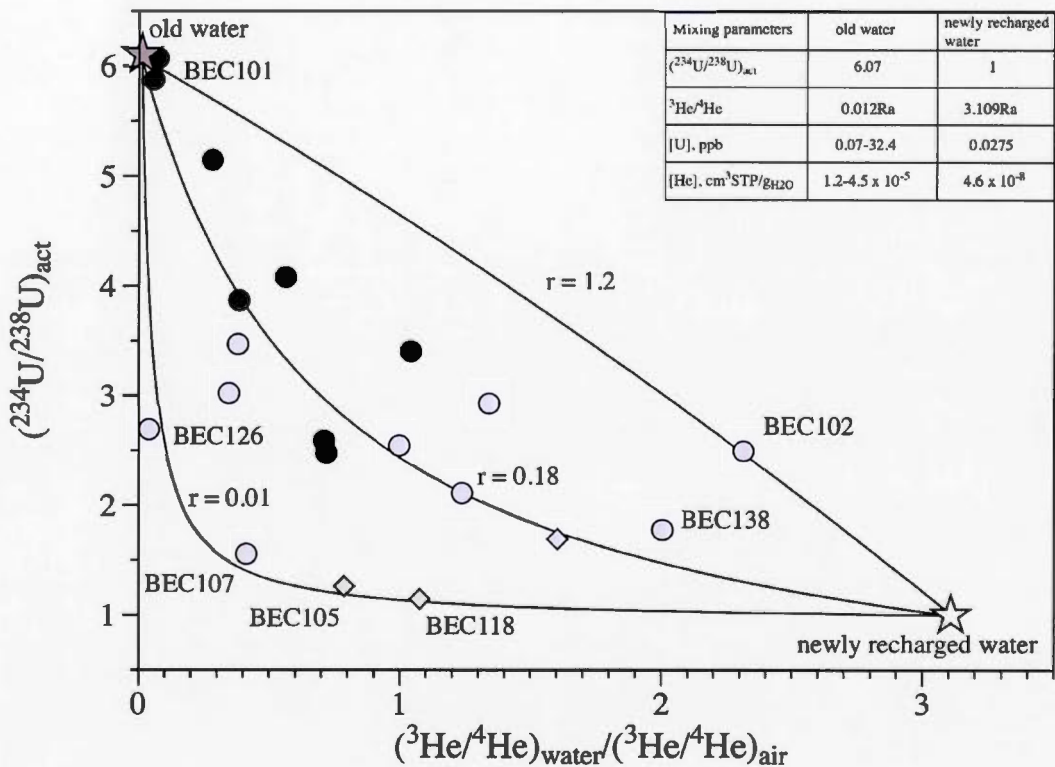


Figure 1.11 Measured $(^{234}\text{U}/^{238}\text{U})_{\text{act}}$ as a function of the $^{3}\text{He}/^{4}\text{He}$ ratios normalized to the same ratio measured in the air (Ra). Least-square mixing hyperbolas between an evolved water end-member, with $(^{234}\text{U}/^{238}\text{U})_{\text{act}}$ of 6.07 and $^{3}\text{He}/^{4}\text{He}$ ratio of 0.012Ra, and a tritiogenic-rich freshwater end-member, with $(^{234}\text{U}/^{238}\text{U})_{\text{act}}$ of ~1 and $^{3}\text{He}/^{4}\text{He}$ ratio of 3.109Ra, are also plotted. Values of hyperbola curvature, “r”, are reported for each mixing curve. Symbols are as in figure 8, 9 and 10.

Tableau 1.1 Hydrogeological characteristics of the groundwater sampled in the Bécancour River watershed together with U-series isotopic data.

Sample	Water chemistry	Hydrological conditions	Depth m	Geological Province	Geology Group/Fm.	Temp °C
BEC101 (F)	Na-HCO ₃ ,Cl	confined	47.2	SL Platform	Lorraine	12
BEC102 (F)	Ca-HCO ₃	semi-confined	21.6	SL Platform	Queenston	8.9
BEC103 (F)	Ca-HCO ₃	unconfined	43.6	SL Platform	Sainte-Rosalie	9.6
BEC105 (G)	Ca-HCO ₃	unconfined	7.0	SL Platform	Sainte-Rosalie	9.4
BEC107 (F)	Ca-HCO ₃	unconfined	36.6	SL Platform	Lorraine	13.3
BEC110 (F)	Ca-Na ₂ SO ₄	confined	37.8	SL Platform	Queenston	8.9
BEC112 (F)	Ca-HCO ₃	unconfined	38.1	Appalachian Mts	Stanbridge	8.6
BEC117 (G)	Ca-HCO ₃	unconfined	15.2	SL Platform	Lorraine	7.4
BEC118 (G)	Ca-HCO ₃	unconfined	6.1	SL Platform	Lorraine	9.9
BEC119 (F)	Na-HCO ₃ ,Cl	semi-confined	45.7	SL Platform	Lorraine	12.0
BEC126* (F)	Ca-HCO ₃	unconfined	49.1	Appalachian Mts	Olistostrome *	8.8
BEC135 (F)	Ca-HCO ₃	unconfined	44.2	Appalachian Mts	Sillery	8.9
BEC137 (F)	Na-HCO ₃	semi-confined	23.7	Appalachian Mts	Sillery	8.6
BEC138 (F)	Ca-HCO ₃	unconfined	32.0	Appalachian Mts	Sillery	8.9
BEC147 (F)	Ca-HCO ₃	unconfined	32.0	Appalachian Mts	Olistostrome *	9.9
BEC148 (F)	Ca, Na ₂ SO ₄	unconfined	64.6	Appalachian Mts	Sillery	10.4
BEC149 (F)	Ca-HCO ₃	unconfined	54.9	Appalachian Mts	Sillery	9.5
F1 (F)	Ca-Na ₂ SO ₄	unconfined	30.0	Appalachian Mts	Oak hill	8.5
F2 (F)	Ca-Na ₂ SO ₄	unconfined	42.0	Appalachian Mts	Sillery	7.2
F4 (F)	Na-HCO ₃	unconfined	36.6	SL Platform	Stanbridge	8.5
F5 (F)	Na-HCO ₃	confined	47.2	SL Platform	Lorraine	8.0
F7 (F)	Na-HCO ₃ ,Cl	confined	48.8	SL Platform	Lorraine	n.d.
F9 (F)	Na-HCO ₃ ,Cl	unconfined	35.7	SL Platform	Lorraine	8.5

Notes :

(F) = Ordovician fractured bedrock aquifer; (G) Quaternary granular aquifer

SL Platform = St. Lawrence Platform; * Olistostrome de la Rivière Etchemin Group; n.d.: not determined

pH	[U] ppb	±	(²³⁴ U/ ²³⁸ U) _{act}	±	[⁴ He] cm ³ STP g ⁻¹	±	(³ He/ ⁴ He) _{sample} (³ He/ ⁴ He) _{air}	±
----	------------	---	--	---	---	---	---	---

x 10-8								
9.17	0.044	0.0004	6.07	0.14	1169.41	17.54	0.074	0.003
7.44	0.029	0.0003	2.50	0.01	7.95	0.12	2.316	0.048
7.21	0.244	0.004	3.47	0.02	63.35	0.95	0.381	0.011
6.00	0.247	0.002	1.26	0.01	9.23	1.40	0.788	0.021
8.13	2.939	0.012	1.55	0.005	39.65	0.59	0.412	0.009
8.03	0.122	0.001	n.d.	n.d.	60.65	0.91	0.172	0.008
7.76	0.046	0.0002	2.11	0.02	6.70	0.10	1.238	0.041
6.83	0.090	0.0003	1.69	0.02	5.36	0.08	1.604	0.010
6.17	0.027	0.0002	1.14	0.01	6.04	0.09	1.077	0.037
7.38	0.003	0.00002	5.15	0.15	62.92	0.94	0.283	0.014
7.71	0.111	0.001	2.69	0.14	2662-4482	67.23	0.039	0.003
5.06	0.159	0.001	3.85	0.03	n.d.	n.d.	n.d.	n.d.
8.13	0.044	0.0003	2.47	0.04	11.32	0.17	0.720	0.019
7.10	0.028	0.003	1.77	0.02	7.72	0.12	2.005	0.039
7.63	1.502	0.009	2.93	0.08	7.51	0.11	1.341	0.033
8.81	0.237	0.001	2.59	0.03	12.38	0.19	0.711	0.014
5.16	0.198	0.001	3.03	0.02	97.84	1.47	0.344	0.010
5.99	0.071	0.001	2.55	0.69	77.28	1.16	0.996	0.019
9.38	0.278	0.001	3.87	0.02	21.22	0.32	0.386	0.010
9.12	0.016	0.001	3.40	0.08	62.30	0.93	1.043	0.038
9.10	0.039	0.0002	4.08	0.05	12.77	0.19	0.564	0.020
9.29	0.148	0.001	3.79	0.01	14.40	0.24	n.d.	n.d.

n.d.: not determined

Helium amounts and isotopic ratios are reported from Vautour et al. (2015) (${}^3\text{He}/{}^4\text{He}_{\text{air}} = 1.386 \times 10^{-6}$) (Ozima and Podosek, 1993)

Alkalinity mg L ⁻¹ HCO ₃	TDS	Ca	Mg	K	Na mg L ⁻¹	Cl	SO ₄	HCO ₃ ⁻	SI calcite
414.8	780	1.2	0.29	1.1	210	150.0	2.2	414.8	0.21
268.4	427	55.0	8.3	2.4	44	37.0	12.0	268.4	-0.07
268.4	501	73.0	13	3.1	40	62.0	41.0	268.4	-0.19
104.9	213	30.0	3.2	1.2	24	35.0	15.0	104.9	-2.13
101.3	188	33.0	5.4	0.82	5.8	9.6	32.0	101.3	0.09
160.0	346	43.0	11	1.8	29	5.8	60.0	195.2	0.28
207.4	286	32.0	11	2	24	1.7	8.1	207.4	-0.07
70.8	84	22.0	2	0.53	2.3	0.8	8.8	57.3	-1.69
57.3	298	15.0	1.5	0.29	3.2	2.2	4.8	170.8	-2.01
170.8	471	21.0	6.9	2.6	53	43.0	1.0	292.8	-0.44
134.2	227	25.0	6.2	0.9	27	26.0	7.6	134.2	-0.4
170.8	85	54.0	6.1	0.97	3.8	1.9	18.0	170.2	nd
219.6	350	5.1	0.41	1.6	85	9.4	29.0	219.6	-0.47
158.6	216	42.0	3.3	1.4	6	2.7	2.4	158.6	-0.71
268.4	157	56.0	6.9	5.6	47	13.0	28.0	268.4	nd
n.d.	109	7.4	1.3	1.4	72	1.5	25.0	nd	nd
195.2	286	50.0	4	2	15	5.7	14.0	195.2	-2.49
31.7	62	13.0	2	0.64	3.4	2.2	9.5	31.7	-2.98
n.d.	131	3.3	0.7	0.99	88	1.4	37.0	n.d.	nd
207.4	339	6.8	3.3	0.83	85	2.4	33.0	207.4	0.61
366.0	529	1.9	0.53	1.6	140	3.0	16.0	366.0	0.25
305.0	150	2.5	0.67	1.1	97	1.0	7.5	303.8	nd
829.6	222	3.1	2.6	3.4	590	420.0	7.5	134.2	-0.08

n.d.: not determined

CHAPITRE II

DO WE ALWAYS NEED BASAL FLUXES TO EXPLAIN RADIogenic ^4He EXCESSES IN GROUNDWATER? A U AND HE ISOTOPE TALE FROM QUEBEC AQUIFERS

Pauline Méjean¹, Daniele L. Pinti¹, Marie Larocque¹, Bassam Ghaleb¹

¹GEOTOP and Département des sciences de la Terre et de l'atmosphère, Université du Québec à Montréal, CP888, Succ. Centre-Ville, Montréal, QC, H3C 3P8 Canada

Préparé pour soumission dans Geofluids

Keywords: ^{234}U - ^{238}U fractionation, radiogenic helium excess, rock fracturing; Laurentide Ice sheet retreat.

ABSTRACT

Large amounts of radiogenic ${}^4\text{He}$ up to $4.48 \times 10^{-5} \text{ cm}^3 \text{ STP g}_{\text{H}_2\text{O}}^{-1}$ were measured in an Ordovician fractured regional aquifer from the Bécancour watershed in the St. Lawrence Lowlands (Quebec, Canada). These amounts are 10^4 times higher than those expected for U-Th *in situ* steady-state production from aquifer rocks of $3.5 \times 10^{-13} \text{ cm}^3 \text{ STP g}_{\text{H}_2\text{O}}^{-1} \text{ yr}^{-1}$. Previous studies suggested that a basal flux of helium enters the aquifer creating this ${}^4\text{He}$ excess in groundwater. This study shows that the ${}^4\text{He}$ concentration in groundwater is related to the U activity ratios $({}^{234}\text{U}/{}^{238}\text{U})_{\text{act}}$. The increase of the ${}^4\text{He}$ concentration in water is accompanied by $({}^{234}\text{U}/{}^{238}\text{U})_{\text{act}}$ deviating from the secular equilibrium with activity ratios up to 6. This suggests that a common process controls the local preferential release of ${}^{234}\text{U}$ and ${}^4\text{He}$ in groundwater. This process has been identified in mechanical rock fracturing and grain comminution after the Laurentide Ice Sheet retreat, 12-6.7 kyrs ago. Using a simple model of helium diffusion from a crystal grain it is demonstrated that following the retreat of the Laurentide inlandsis, accumulated ${}^4\text{He}$ in aquifer rocks has been released at mean rates from $2.18 \times 10^{-8} \text{ cm}^3 \text{ STP g}_{\text{H}_2\text{O}}^{-1} \text{ yr}^{-1}$ to $6.26 \times 10^{-8} \text{ cm}^3 \text{ STP g}_{\text{H}_2\text{O}}^{-1} \text{ yr}^{-1}$ which are 10^5 times higher than steady-state production rates. The integration of ${}^4\text{He}$ release rates over the time elapsed since the ice retreat yields a radiogenic ${}^4\text{He}$ content in groundwater between $1.55 \times 10^{-5} \text{ cm}^3 \text{ STP g}_{\text{H}_2\text{O}}^{-1}$ and $2.52 \times 10^{-5} \text{ cm}^3 \text{ STP g}_{\text{H}_2\text{O}}^{-1}$, i.e. 10 times higher than that found in groundwater samples. Thus a local source of radiogenic helium can explain this excess in groundwater without calling for external basal fluxes. The results from this study suggest that the U-He relation could be the key to correctly identifying helium sources in a groundwater system. Quantifying the internal source of helium could contribute to improving the (U-Th/ ${}^4\text{He}$) method for dating old groundwater and resolve the apparent age contradiction between different water chronometers.

2.1 INTRODUCTION

Groundwater is the largest component of freshwater accessible for human use (Kotwicki *et al.*, 2009). Of the 22.6 Mkm³ of groundwater in the first 2 km of the upper crust, only 0.63 Mkm³ are less than 100 years old (Gleeson *et al.*, 2016). The rest has ages spanning from a few thousand years (Aggarwal *et al.*, 2015) to potentially hundreds of million years (e.g., Bottomley *et al.*, 2002; Lippmann-Pipke *et al.*, 2011; Pinti *et al.*, 2011; Holland *et al.*, 2013). The age of this large body of groundwater needs to be constrained to estimate the sustainability of current and future groundwater use.

Groundwater with ages of less than 60 years old can be identified by the presence of tritium (³H) introduced into the hydrological cycle by the fallout of atmospheric nuclear weapon tests during the 1960s. Because ³H decays to ³He with a half-life of 12.32 years, ³H/³He is a good chronometer of modern water (e.g., Tolstikhin et Kamensky, 1969; Takaoka et Mizutani, 1987). Dating groundwater older than 100 years is a challenge (Philips et Castro, 2003; Aggarwal, 2013) because the initial concentration of radionuclides can be altered by water-rock interactions. An example is ¹⁴C (half-life = 5,730 yrs), primarily introduced into groundwater in the soil zone through biological processes. Along the flow path, ¹⁴C concentrations decrease according to radioactive decay (Plummer et Glynn, 2013). However, dilution of ¹⁴C-free carbonate, exchange with carbonates (Fontes, 1992), loss, or addition of ¹⁴C from old organic matter or CH₄ (Aravena *et al.*, 1995) can significantly alter the original ¹⁴C concentration, resulting in older apparent ages.

Radiogenic ⁴He produced by decay of ^{238,235}U and ²³²Th contained in aquifer rocks and released into groundwater has a great potential for dating groundwater with ages ranging from 1,000 years up to hundreds million years (Marine, 1979; Torgersen, 1980; Andrews et Kay, 1983). However, in numerous hydrological studies (e.g., Pinti et Marty, 1998) U-Th/⁴He ages are constantly older than hydrological ages. This

difference - the so-called ${}^4\text{He}$ excess (Torgersen et Clarke, 1985; Kulongoski et Hilton, 2011) - is interpreted as an additional source of radiogenic helium, external to the aquifer.

In a study of the Great Artesian Basin (GAB) of Australia, Torgersen and Clarke (1985) calculated that the measured He excess was equivalent to the addition of the total crustal production of He beneath the basin. Mazor (1995) and Tolstikhin *et al.* (1996) contested this model, suggesting that aquifers are largely heterogeneous in terms of conductivity and then connate (stagnant) water can exist, accumulating large amounts of radiogenic helium (Pinti *et al.*, 1997; Pinti et Marty, 1998). Mixing of stagnant water with recently recharged water might cause these ${}^4\text{He}$ excesses (Tolstikhin *et al.*, 1996). Solomon *et al.* (1996) noticed that in numerous aquifers, radiogenic ${}^4\text{He}$ is released into water at rates greater than supported by U/Th production. These authors developed a model to demonstrate that only a small portion of the He produced, close to the surface of the aquifer matrix, can be released at steady state by diffusion and/or α -recoil. During fracturing of rocks, the specific surface exposed to water increases and thus the ${}^4\text{He}$ accumulated in the rock during geological times can be rapidly released into the groundwater creating the excess in dissolved radiogenic helium.

Recently, Méjean *et al.* (2016) have found an inverse causal relationship between the ${}^{234}\text{U}/{}^{238}\text{U}$ activity ratios, or $({}^{234}\text{U}/{}^{238}\text{U})_{\text{act}}$, and the ${}^3\text{He}/{}^4\text{He}$ ratios measured in groundwater circulating in sedimentary aquifers of the St. Lawrence Lowlands, Quebec (Canada). Newly recharged water devoid of radiogenic helium showed $({}^{234}\text{U}/{}^{238}\text{U})_{\text{act}}$ close to 1, i.e. the secular equilibrium. Older groundwater is progressively enriched in radiogenic helium (i.e. the ${}^3\text{He}/{}^4\text{He}$ ratio decreases) and the $({}^{234}\text{U}/{}^{238}\text{U})_{\text{act}}$ increases up to 6. The ${}^{234}\text{U}-{}^{238}\text{U}$ fractionation (i.e. $({}^{234}\text{U}/{}^{238}\text{U})_{\text{act}} \gg 1$) is controlled by the ejection of ${}^{234}\text{U}$ by α -recoil into the water while its parent element ${}^{238}\text{U}$ is firmly trapped into the solid phase (Kigoshi, 1971). Méjean *et al.* (2016)

suggested that the opening of new fractures might provide surfaces from which both ^{234}U and ^4He migrates by α -recoil into water at high rates.

The objective of this study is to show that the U- He relationship could be the key to demonstrate that internal sources to the aquifers can provide the radiogenic ^4He excess often found in groundwater. Data from Méjean *et al.* (2016) and Vautour *et al.* (2015) are revisited and integrated in a coupled model of ^{234}U - ^{238}U fractionation and radiogenic ^4He release into groundwater by fracturing using equations developed by Andrews *et al.* (1982) and Solomon *et al.* (1996).

2.2 HYDROGEOLOGY OF THE STUDY AREA

The hydrogeological description of the studied area is only briefly reported here to highlight the context of this work. More details can be found in Vautour *et al.* (2015) and Méjean *et al.* (2016). The Bécancour River study area ($2,859 \text{ km}^2$) is located in the St. Lawrence Lowlands in southern Quebec, Canada (Fig. 2.1). The main aquifer is located in the fractured bedrock composed of Middle-Late Ordovician foreland carbonate-clastic-shale deposits (Lavoie, 2008). Recharge for this aquifer occurs in the Appalachian Mountains where Cambrio-Devonian siccilastic and metasedimentary rocks (“wildflysch”, shales, calcitic schists) outcrops (Larocque *et al.*, 2013). Unconsolidated Quaternary fluvioglacial, deltaic and lacustrine sands (Vieilles Forges and Lobtinière sands; Lamothe, 1989) occur in the middle to lower portion of the study area. These deposits are of limited extent and thickness. Partially buried under, thick deposits of marine clay were deposited during marine transgression-regression cycles when the retreat of the Laurentide Ice Sheet caused a marine invasion from the Gulf of St. Lawrence known as the Champlain Sea episode (9,750 BP; Occhietti *et al.*, 2001).

The regional groundwater flows from the main recharge area in the Appalachian Mountains to the St. Lawrence River (Fig. 2.2; Larocque *et al.*, 2013). Groundwater mainly discharges as base flows in the Bécancour River and its tributaries. Local recharge occurs in the lower part of the watershed, where Champlain Sea clays are discontinuous (Larocque *et al.*, 2013; Vautour *et al.*, 2015; Méjean *et al.*, 2016). The hydraulic conductivities of the Ordovician fractured bedrock aquifer are low to moderate ($\sim 10^{-9}\text{--}10^{-6} \text{ m s}^{-1}$) while those of the Quaternary aquifer are moderate ($\sim 10^{-6}\text{--}10^{-5} \text{ m s}^{-1}$). Effective porosities vary between 1 and 5% for the Ordovician fractured regional aquifer (Tran Ngoc *et al.*, 2014) and between 10 and 20% for the Quaternary granular aquifer (Benoît *et al.*, 2011). Groundwater has a low salinity between 0.06 to 0.78 g L⁻¹. Groundwater types are as follows (Meyzonnat *et al.*, 2016): 1) Ca-HCO₃, and Ca-HCO₃-SO₄ freshly recharged water; Na-HCO₃ and Na-

$\text{HCO}_3\text{-SO}_4$ evolved water with $\text{Ca}^{2+}_{\text{dissolved}}$ exchanged with $\text{Na}^+_{\text{mineral}}$; 3) slightly mineralized waters ($\text{Ca-HCO}_3\text{-Cl,Na}$ and $\text{Na-HCO}_3\text{-Cl}$ types) close to the St. Lawrence River, where chlorine is derived from marine-glacial porewater originating from the Champlain Sea episode. Recently recharged groundwater containing tritium has been dated to be less than 60 years (Vautour *et al.*, 2015). More evolved waters show NETPATH ^{14}C -adjusted ages up to 6.6 kyrs (Vautour *et al.*, 2015). The data used in this paper are from Vautour *et al.* (2015) and Méjean *et al.* (2016). Details of the sampling methods can be found in these publications.

2.3 RESULTS AND DISCUSSION

2.3.1 Revisiting the U-Th isotope system in the St. Lawrence Lowlands

The distribution of the data in Fig. 2.3 suggests that ${}^4\text{He}$ and $({}^{234}\text{U}/{}^{238}\text{U})_{\text{act}}$ in groundwater originated from a three-component mixing, two of these having been identified by Méjean *et al.* (2016). The first one is recently recharged water (end member 1, white star; Fig. 2.3) containing ${}^4\text{He}$ close to *ASW* (Air Saturated Water; $4.6 \times 10^{-8} \text{ cm}^3\text{STP g}_{\text{H}_2\text{O}}^{-1}$; Smith et Kennedy, 1983) and $({}^{234}\text{U}/{}^{238}\text{U})_{\text{act}} \approx 1$. Freshwater from well BEC118 is the best representative of this end-member with a ${}^4\text{He} = 6.04 \times 10^{-8} \text{ cm}^3\text{STP g}_{\text{H}_2\text{O}}^{-1}$ and a $({}^{234}\text{U}/{}^{238}\text{U})_{\text{act}} = 1.14$ (Méjean *et al.*, 2016). This sample has a chemical composition (Ca-HCO₃ water type) mainly controlled by dissolution of superficial material during infiltration of water in the unconfined part of the aquifer (Vautour *et al.*, 2015; Méjean *et al.*, 2016). Bulk dissolution of carbonates causes the $({}^{234}\text{U}/{}^{238}\text{U})_{\text{act}}$ to be close to the secular equilibrium, i.e. the activity ratio in the rock.

The second end-member is older groundwater having accumulated both large amounts of radiogenic ${}^4\text{He}$ ($2.5\text{-}4.5 \times 10^{-5} \text{ cm}^3\text{STP g}_{\text{H}_2\text{O}}^{-1}$) and having highly fractionated $({}^{234}\text{U}/{}^{238}\text{U})_{\text{act}}$, higher than 6 (end member 2, black star; Fig. 2.3). This evolved water was identified in BEC101, which has similar helium and uranium composition to the expected end-member. Interestingly this water has a Na-HCO₃ chemistry indicating a higher degree of evolution by water-rock interactions (mineral-water cation exchange; Meyzonnat *et al.*, 2016). This groundwater was sampled in the confined part of the fractured bedrock where dissolution processes are negligible and where ${}^{234}\text{U}$ - ${}^{238}\text{U}$ fractionation is dominated by α -recoil processes (Méjean *et al.*, 2016). The majority of the samples plots on a mixing line between the end-members 1 and 2.

To explain the scattered points that do not lie on this mixing curve, a third end-member is necessary. Two samples (BEC105, BEC107) plot on a mixing line between end-member 1 and a newly identified third end-member having large

amounts of radiogenic ${}^4\text{He}$ ($2.5\text{--}4.5 \times 10^{-5} \text{ cm}^3\text{STP g}_{\text{H}_2\text{O}}^{-1}$) but only slightly fractionated (${}^{234}\text{U}/{}^{238}\text{U}_{\text{act}}$) up to 1.6. It is unusual to find ${}^4\text{He}$ -enriched groundwater in a recharge area associated with low isotopic ratio (${}^{234}\text{U}/{}^{238}\text{U}_{\text{act}}$). This end-member could represent a situation where bulk dissolution of carbonate rocks, close to the recharge liberates instantaneously the ${}^4\text{He}$ produced in the grain and accumulated during a long span of time. As for end-member 1, bulk dissolution allows U to migrate into water with little ${}^{234}\text{U}$ - ${}^{238}\text{U}$ isotopic fractionation. The occurrence of this third end-member, enriched in radiogenic helium would support the model of Solomon *et al.* (1996) which suggest that aquifer grains accumulate large amounts of radiogenic ${}^4\text{He}$ for long geological periods, this ${}^4\text{He}$ being only partially released into water by diffusion or α -recoil close to the grain boundaries. Bulk dissolution and instantaneous release of the accumulated helium into water would create the apparent ${}^4\text{He}$ excess in groundwater.

2.3.2 Enhanced release of ${}^{234}\text{U}$ and ${}^4\text{He}$ in groundwater: causes and processes

The potential process of U and He enrichment is here assumed to be rock fracturing. Radiogenic helium is usually released by diffusion and α -recoil from the rock (Torgersen, 1980). If the aquifer rock grain size is much larger than the distance of α -recoil (30–100 nm; Harvey, 1962) or than that of diffusion length, only a fraction of the produced ${}^4\text{He}$ will be released to the water, while the majority will accumulate within the rock over time (Solomon *et al.*, 1996). Torgersen et O'Donnell (1991) have suggested that the progressive fracturing of a rock slab increases the specific surface exposed to water and therefore increasing the probability that ${}^4\text{He}$ close to the grain boundaries can be released into the water at rates greater than those supported by steady-state U–Th production in the rock (Solomon *et al.*, 1996). A 1-D model of rock fracturing showed that stress-induced macro-fracturing every 10 m along a 1 km

wide rock slab would allow the release of ^4He otherwise accumulated over 15 Myrs in only 1,500 years (Torgersen et O'Donnell, 1991).

Increasing the aquifer matrix surface area exposed to water by fracturing would also enhance the release of ^{234}U by α -recoil and thus shift the initial ($^{234}\text{U}/^{238}\text{U}$)_{act} towards higher values. During decay of ^{238}U , α -particles transmits kinetic energy to the ^{238}U -daughter nuclide (^{234}Th). A fraction of the ^{234}Th is ejected from the mineral grain into the pore water. Being insoluble, ^{234}Th is rapidly adsorbed on the grain surface and decays to ^{234}U . ^{234}U , now residing in damaged crystal lattice sites or onto grain surfaces, will be transferred in soluble form into the water phase while ^{238}U will be mainly retained in the crystal lattice (Kigoshi, 1971). As for helium, the larger surface area exposed to water increases the probability that ^{234}U is close to the grain boundaries facilitating its release into pore water.

In the study area, the deglaciation that occurred 12,000 years ago could be the main cause of induced stress changes and associated mechanical fracturing of the bedrock aquifer. This fracturing could have favored the release of ^{234}U and ^4He in groundwater. Gravitational loading by glacial ice can significantly affect near-surface stress magnitudes. Each cycle of deglaciation could produce additional sub-vertical tensile fractures, which could then be used by groundwater as flow-paths (Lemieux *et al.*, 2008).

This situation and the consequences for ^{234}U - ^{238}U fractionation and radiogenic ^4He release are illustrated in Figs. 2.4a,b. The presence of continental ice sheets played an important role in the subsurface hydrology of North America over the last 2 Ma (Mc Intosh et Walter, 2005; 2006; Neuzil, 2012; Mc Intosh *et al.*, 2011; Person *et al.*, 2012). Ice sheet loading and unloading possibly led to the development of anomalously high and low pressures within low-permeability confining units. As the Laurentide Ice Sheet started to retreat, the large amounts of subglacial water introduced into the system induced bulk dissolution of the bedrock, releasing U into

water with little ^{234}U - ^{238}U isotopic fractionation ($(^{234}\text{U}/^{238}\text{U})_{\text{act}} \approx 1$) (Fig. 2.4a). The enhanced bedrock dissolution also caused an accumulation of ^4He in the bedrock to be liberated at rates greater than those supported by steady-state U-Th production (Fig. 2.4a). This situation is illustrated by the supposed end-member 3 in Fig. 2.3.

The near-surface stress induced by the ice sheet retreat at 12 kyrs increased fracture density as a consequence of the overpressure and high horizontal stresses caused by both the retreat of ice sheet and unbending of the lithosphere (Grollimund et Zoback, 2000) (Fig. 2.4b). Between 10,600 and 6,700 yrs before present, the studied area was affected by the main phase of isostatic rebound (Lamarche *et al.*, 2007). At 6.7 kyrs, the hydrographic network of the St. Lawrence Valley reached a configuration close to that observed at present (Fig. 2.4b). The invasion of subglacial water terminated, newly recharged water started to flow into a higher fractured aquifer and to accumulate ^{234}U and ^4He released through the newly formed surfaces in the deeper reduced and confined part of the aquifer. This situation is illustrated by fractionated $(^{234}\text{U}/^{238}\text{U})_{\text{act}}$ ratios up to 6 accompanied by large amounts of radiogenic ^4He occurring in 6.6 Kyrs old groundwater from BEC101 (end-member 2 in Fig. 2.3).

2.3.3 Modeling the release of ^{234}U and ^4He into groundwater: principles

To quantify the release of both radiogenic ^4He and ^{234}U isotopes in groundwater, a coupled model of ^{234}U - ^{238}U -fractionation and ^4He release was developed using relevant equations from Andrews *et al.* (1982) and Solomon *et al.* (1996).

In order to quantify the ejection and accumulation rate of ^{234}U in groundwater, Andrews *et al.* (1982) simulated the relationship between stress-induced fracturing of the aquifer matrix with the formation of new surface of exchanges where α -recoil process can preferentially takes place. This model assumes that groundwater acquires dissolved U close to the recharge and may undergo further change in its uranium

concentration by water-rock interactions or, after U deposition, by ejection of ^{234}U caused by ^{234}Th recoil.

For a groundwater in a reducing environment with an initial $(^{234}\text{U}/^{238}\text{U})_{\text{initial,act}}$ entering the α -recoil zone (i.e. an aquifer at reducing conditions where α -recoil dominated on bulk dissolution), the evolution of the activity ratio with the age of the groundwater $(^{234}\text{U}/^{238}\text{U})_{\text{act,final}}$, can be estimated with the following relation of Andrews *et al.* (1982):

$$\left(\frac{^{234}\text{U}}{^{238}\text{U}}\right)_{\text{act,final}} = 1 + \left[\left(\frac{^{234}\text{U}}{^{238}\text{U}}\right)_{\text{act,initial}} - 1 \right] \cdot e^{(-^{234}\lambda t)} + 0.235 \cdot \rho \cdot S \cdot R \cdot [1 - e^{(-^{234}\lambda t)}] \cdot \frac{[U]_{\text{rock}}}{[U]_{\text{water}}} \quad (2.1)$$

The first term in eqn. (2.1) represents the decay of the ^{234}U excess accumulated before that groundwater encountered reducing conditions. The second term evaluates the α -recoil effect on the $(^{234}\text{U}/^{238}\text{U})_{\text{act}}$ for a groundwater which has entered a reducing zone (Andrews *et al.*, 1982). S the specific surface area in $\text{cm}^2 \cdot \text{cm}^{-3}$ (i.e. the extent of rock in contact with water); ρ is the rock density ($2.72 \text{ g} \cdot \text{cm}^{-3}$ as mean value of carbonate-dominated lithology in the studied area); the constant 0.235 is the probability that ^{234}Th atoms actually escape from the surface into water (Bonotto et Andrews, 1993); $^{234}\lambda$ is the decay constant of ^{234}U ($2.82 \times 10^{-6} \text{ yr}^{-1}$); and R is the recoil distance of ^{234}Th in the rock matrix (3.10^{-6} cm ; Andrews et Kay, 1983).

The boundary conditions for the model are: 1) $(^{234}\text{U}/^{238}\text{U})_{\text{act,final}}$ depends on $(^{234}\text{U}/^{238}\text{U})_{\text{act,initial}}$ at $t = 0$ and corresponds to the activity ratio recorded in the water when entering the α -recoil dominated zone and corresponds to the shallow groundwater sampled in the study area (BEC118 : $(^{234}\text{U}/^{238}\text{U})_{\text{act}} = 1.14$; Méjean *et al.*, 2016); 2) $[U]_{\text{rock}}$ is the mean value of 1.14 ppm measured in aquifer samples by Vautour *et al.* (2015) and $[U]_{\text{water}} = 0.04 \text{ ppb}$ is the mean uranium concentration measured in groundwater samples from the semi-confined and confined part of the

aquifer ($n = 7$; Méjean *et al.*, 2016); 3) t is the residence time of the groundwater. In the first simulation we obtained the highest $(^{234}\text{U}/^{238}\text{U})_{\text{act}}$ calculated in the aquifer when decay of ^{234}U excess is equilibrated by alpha-recoil ejection of ^{234}U . In a second simulation, the specific surface required to obtain $(^{234}\text{U}/^{238}\text{U})_{\text{act}}$ was estimated at 6.07 in a 6.6 Kyr old groundwater, here assumed to be the oldest age in the aquifer, as calculated in Vautour *et al.*, 2015 (Fig. 2.3).

The fracture surface area, S , per unit volume of interstitial water ($\text{cm}^2 \cdot \text{cm}^{-3}$) is obtained from eqn. 2.1:

$$S = \frac{\left(\frac{^{234}\text{U}}{^{238}\text{U}} \right)_{\text{act,final}} - \left(\left(\frac{^{234}\text{U}}{^{238}\text{U}} \right)_{\text{act,initial}} - 1 \right) \times e^{(-^{234}\lambda t)}}{0.235 \times \rho \times R \times (1 - e^{(-^{234}\lambda t)})} \quad (2.2)$$

From the specific surface S and assuming an aquifer matrix composed of grains produced by stress-induced fracturing, the mean grain size r (cm) is deduced from the relation of Bonotto et Andrews (1993):

$$r = \frac{3}{\phi \times S} \quad (2.3)$$

where ϕ is the mean matrix porosity (3% for the fractured bedrock aquifer; Vautour *et al.*, 2015).

The model developed by Solomon *et al.* (1996) is based on the helium diffusion out of a spherical grain. Fick's first law of diffusion allows to calculate the diffusive flux of radiogenic ${}^4\text{He}$ from a single grain. Solomon *et al.* (1996) developed the equation to obtain the release of helium per unit of weight of solids N ($\text{cm}^3 \text{STP g}_{\text{rock}}^{-1}$):

$$N = 6 \times \lambda \times (C_o - C_w K_{ws}) \times \Sigma \exp(-\lambda n^2 \pi^2) \quad (2.4)$$

where λ (s^{-1}) is the leakage coefficient that determines the rate at which previously accumulated He diffuses from the aquifer solids into groundwater; r is the geometric mean grain size (cm); C_o , the initial concentration in the grain, corresponding to the radiogenic ${}^4\text{He}$ produced in the grain since its deposition ($4.5 \times 10^{-4} \text{ cm}^3 \text{STP g}_{\text{rock}}^{-1}$ assuming a He production rate of $3.4 \times 10^{-13} \text{ cm}^3 \text{STP g}_{\text{rock}}^{-1} \text{ yr}^{-1}$ and an age of 4.45×10^8 yrs for the ordovician fractured bedrock); C_w , is the ${}^4\text{He}$ concentration measured in the groundwater; K_{ws} is the partition coefficient for He in a water-solid system, assumed 1 (Solomon *et al.*, 1996).

The leakage coefficient λ in turn depends on the grain size of the aquifer matrix through the relationship:

$$\lambda = \frac{D_s}{r^2} \quad (2.5)$$

where D_s is the solid-state diffusion coefficient (i.e. diffusion initiated in a solid phase by the occurrence of surface defects which include grain boundaries; $\text{cm}^2 \text{ s}^{-1}$). Two values were chosen $D_{s1} = 1.0 \times 10^{-18} \text{ cm}^2 \text{ s}^{-1}$ and $D_{s2} = 1.0 \times 10^{-19} \text{ cm}^2 \text{ s}^{-1}$ for the model to represent all lithologies encountered in the studied area, mainly carbonate-rich shales (experimental values obtained in carbonates at ambient temperature, $D_s = 3 \times 10^{-19} \text{ cm}^2 \text{ s}^{-1}$; Pinti *et al.*, 2012 and using grain quartz at 21°C : $D_s = 1.2 \times 10^{-18} \text{ cm}^2 \text{ s}^{-1}$; Salomon *et al.*, 1996).

2.3.4 Modeling the release of ${}^{234}\text{U}$ and ${}^4\text{He}$ into groundwater

Once groundwater becomes reducing enough that chemical leaching of ${}^{234}\text{U}$ ceases, $({}^{234}\text{U}/{}^{238}\text{U})_{\text{act}}$ may evolve in time as a balance between the ${}^{234}\text{U}$ physical leaching and the decay. The consequences for the $({}^{234}\text{U}/{}^{238}\text{U})_{\text{act}}$ evolution can be seen in a diagram

where the $(^{234}\text{U}/^{238}\text{U})_{\text{act}}$ is plotted against groundwater residence time (Fig. 2.5). The simulation is based on eqn. 2.1 and was calculated using an initial $(^{234}\text{U}/^{238}\text{U})_{\text{act}} = 1.14$ (BEC118; representing the activity ratio recorded in the water before entering the confined part of the aquifer) and a final value $(^{234}\text{U}/^{238}\text{U})_{\text{act}} = 6.07$ (BEC101; the maximum value measured in groundwater from the deeper Ordovician aquifer) after a contact time of 6.6 kyrs (Vautour et al., 2015).

Using the relation described above and eqn. 2.2, a specific surface $S = 5,746 \text{ cm}^2 \cdot \text{cm}^{-3}$ was estimated. The calculated specific surface represents the extent of rock surface in contact with water. The relation between specific surface and the grain size described in the part 3.3 (eqn. 2.3) is used and a mean grain radius of $17\mu\text{m}$ is calculated. The grain size calculated is smaller than the distance of α -recoil (30-100nm). This means that ${}^4\text{He}$ produced by U and Th in the grain will not be retained in the grain and should be released from grain providing a ${}^4\text{He}$ input into the aquifer.

The calculated mean grain size radius of $17\mu\text{m}$ was used to estimate the release of helium per unit of weight of solids N (eqn. 2.4; Solomon et al., 1996). In this equation the initial ${}^4\text{He}$ was fixed at a value of $1.51 \times 10^{-4} \text{ cm}^3 \text{STP g}_{\text{rock}}^{-1}$ which corresponds to the ${}^4\text{He}$ produced since the formation of the aquifer, 445 Ma ago (Ordovician age), using the mean helium production rate in the study area of $3.4 \times 10^{-13} \text{ cm}^3 \text{STP g}_{\text{rock}}^{-1}$ (Vautour et al., 2015). The range of calculated release rates therefore represents the highest possible values.

Higher release rates of radiogenic ${}^4\text{He}$ in water were calculated using $D_1 = 1 \times 10^{-18} \text{ cm}^2 \text{ s}^{-1}$ than using $D_2 = 1 \times 10^{-19} \text{ cm}^2 \text{ s}^{-1}$ with $N_1 = 2.6 \times 10^{-7} \text{ cm}^3 \text{STP g}_{\text{H}_2\text{O}}^{-1} \text{ yr}^{-1}$ and $N_2 = 8.4 \times 10^{-8} \text{ cm}^3 \text{STP g}_{\text{H}_2\text{O}}^{-1} \text{ yr}^{-1}$ respectively (Fig. 2.6). Release rate decreases faster using D_1 than with D_2 and after 100 kyrs (after 800 ka using D_2), the ${}^4\text{He}$ released rate N_1 is lower than ${}^4\text{He}$ *in situ* production calculated in the St. Lawrence Lowlands ($3.5 \times 10^{-13} \text{ ccSTP g}_{\text{rock}}^{-1}$; Pinti et al., 2011; Vautour et al., 2015). Those authors calculated

the ${}^4\text{He}$ production rate using U and Th contents measured in local rocks. They further assume that all ${}^4\text{He}$ produced in the grain is immediately released into pore-water. This is contrary to the assumption used here of a recent release of ${}^4\text{He}$ accumulated since the deposition of the sedimentary formations constituting the aquifers. Neglecting ${}^4\text{He}$ loss by diffusion over time, the accumulated radiogenic ${}^4\text{He}$ will be released only after the ice retreat. This ${}^4\text{He}$ component will be perceptible in groundwater depending on diffusion coefficient of the rock.

The total amount of ${}^4\text{He}$ released in water since the ice retreat can be estimated by integrating the mean ${}^4\text{He}$ release rate ($N = 6.26 \times 10^{-8} \text{ g}_{\text{H}_2\text{O}}^{-1}$ using D_{s1} and $N = 2.18 \times 10^{-8} \text{ g}_{\text{H}_2\text{O}}^{-1}$ using D_{s2}) over the time maximum time contact between groundwater and rock aquifer (maximum ${}^{14}\text{C}$ ages calculate in Bécancour; $t = 6.6 \text{ ka}$). This yields an estimation of values between $1.52 \times 10^{-5} \text{ cm}^3\text{STP g}_{\text{H}_2\text{O}}^{-1}$ and $2.55 \times 10^{-5} \text{ cm}^3\text{STP g}_{\text{H}_2\text{O}}^{-1}$ as a result of grain size reduction by stress-induced ice retreat. These values are in the same range of the radiogenic ${}^4\text{He}$ excess measured in the Bécancour groundwater (maximum ${}^4\text{He}$ measured in Bécancour is $4.48 \times 10^{-5} \text{ cm}^3 \text{ g}_{\text{H}_2\text{O}}^{-1}$) and likely reflect the maximum values estimated for the interval of total ${}^4\text{He}$ rapidly released. An important implication of the spherical diffusion model is that the fractured aquifer will release ${}^4\text{He}$ at a higher rate than the steady-state U-Th production for thousands of years. It can be assumed that large ${}^4\text{He}$ released during the last 12 kyr since the last deglaciation could explain radiogenic ${}^4\text{He}$ currently measured if this ${}^4\text{He}$ is conserved in the aquifer and if the ${}^4\text{He}$ lost by groundwater transport and diffusion between layers is limited.

2.4 CONCLUSIONS

The objective of this work was to re-evaluate the internal source of production of radiogenic ${}^4\text{He}$ using a coupled model of ${}^{234}\text{U}$ preferential solution and ${}^4\text{He}$ released from grains following the Laurentide Ice Sheet retreat, 12,000 yrs ago.

The results confirm that the large amounts of radiogenic ${}^4\text{He}$ found in the bedrock aquifer of the Bécancour watershed (up to ${}^4\text{He} = 4.48 \times 10^{-5} \text{ cm}^3 \text{ g}_{\text{H}_2\text{O}}^{-1}$) could be derived from instantaneous release of accumulated helium from the host rock, estimated to be between $1.52 \times 10^{-5} \text{ cm}^3 \text{ STP g}_{\text{H}_2\text{O}}^{-1}$ and $2.55 \times 10^{-5} \text{ cm}^3 \text{ STP g}_{\text{H}_2\text{O}}^{-1}$. This was caused by the intense fracturing which increased the surface area exposed to water for a rapid release of ${}^4\text{He}$ (and ${}^{234}\text{U}$). This means that in the St. Lawrence watersheds, the source of excess radiogenic helium could be internal to the aquifers and not supported by an external basal flux as previously suggested by Vautour *et al.* (2015).

This conclusion supports the hypothesis that excess radiogenic ${}^4\text{He}$ can be caused by internal sources, in this case by the release of helium at rates greater than those supported by steady-state U-Th production in the rock as observed in several periglacial aquifers worldwide (Solomon *et al.*, 1996).

It will now be important to investigate if similar relationships between the ${}^{234}\text{U}$ - ${}^{238}\text{U}$ fractionation and helium isotopes exist in other basins. This relationship could be the key to demonstrate that in other hydrogeological settings, helium excesses do not require sources external to the aquifer. Internal sources can also explain the apparent contradiction found between calculated (U-Th/ ${}^4\text{He}$) ages and those from other water chronometers.

ACKNOWLEDGMENTS

The authors thank the Quebec Ministry of Environment (*Ministère du Développement durable, de l'Environnement, des Parcs et de la Lutte contre les changements climatiques*), the Quebec Research Fund (“Fonds de recherche du Quebec - Nature et Technologies”), the Bécancour River Watershed Organization (“organisme de bassin versant GROBEC”), and the municipalities that contributed funding to this research (Cré Centre-du-Québec, MRC d’Arthabaska, MRC de Bécancour, MRC de l’Érable, MRC de Nicolet-Yamaska, AGTCQ, Céged Thetford).

REFERENCES

- Aggarwal, P.K., Matsumoto, T., Sturchio, N.C., Chang, H.K., Gastmans, D., Araguas-Araguas, L.J., Jiang, W., Lu, Z.-T., Mueller, P., Yokochi, R., Purtschert, R. et Torgersen, T. (2015). Continental degassing of ${}^4\text{He}$ by surficial discharge of deep groundwater. *Nature Geosci*, 8(1), 35-39.
- Andrews, J. et Kay, R.L.F. (1978). The evolution of enhanced ${}^{234}\text{U}/{}^{238}\text{U}$ activity ratios for dissolved uranium and groundwater dating. *US Geological Survey Open-File Rep*, 78(701), 11-13.
- Andrews, J.N. et Kay, R.L.F. (1982). ${}^{234}\text{U}/{}^{238}\text{U}$ activity ratios of dissolved uranium in groundwaters from a jurassic limestone aquifer in England. *Earth and Planetary Science Letters*, 57(1), 139-151.
- Andrews, J.N. et Kay, R.L.F. (1983). The U contents and ${}^{234}\text{U}/{}^{238}\text{U}$ activity ratios of dissolved uranium in groundwaters from some Triassic Sandstones in England. *Chemical Geology*, 41, 101-117.
- Andrews, J.N., Giles, I.S., Kay, R.L.F., Lee, D.J., Osmond, J.K., Cowart, J.B., Fritz, P., Barker, J.F. et Gale, J. (1982). Radioelements, radiogenic helium and age relationships for groundwaters from the granites at Stripa, Sweden. *Geochimica et Cosmochimica Acta*, 46(9), 1533-1543.
- Aravena, R., Wassenaar, L.I. et Plummer, L.N. (1995). Estimating ${}^{14}\text{C}$ groundwater ages in a methanogenic aquifer. *Water Resources Research*, 31(9), 2307-2317.
- Benoît, N., Blanchette, D., Nastev, M., Cloutier, V., Marcotte, D., Brun Kone, M et Molson, J.W. (2011). Groundwater geochemistry of the Lower Chaudière River Watershed, Québec. Proceedings of the International Association of Hydrogeologists-Canadian National Chapter (IAH-CNC)/Canadian Quaternary Association (CANQUA) Conference: GeoHydro 2011.
- Bonotto, D.M. et Andrews, J. (1993). The mechanism of ${}^{234}\text{U}/{}^{238}\text{U}$ activity ratio enhancement in karstic limestone groundwater. *Chemical geology*, 103(1), 193-206.
- Bottomley, D.J., Renaud, R., Kotzer, T. et Clark, I.D. (2002). Iodine-129 constraints on residence times of deep marine brines in the Canadian Shield. *Geology*, 30(7), 587-590.
- Fontes, J.-C. (1992). Chemical and isotopic constraints on ${}^{14}\text{C}$ dating of groundwater. Dans *Radiocarbon after four decades* (p. 242-261) : Springer.
- Gleeson, T., Befus, K.M., Jasechko, S., Luijendijk, E. et Cardenas, M.B. (2016). The global volume and distribution of modern groundwater. *Nature Geosci*, 9, 161–167

- Grollimund, B. et Zoback, M.D. (2000). Post glacial lithospheric flexure and induced stresses and pore pressure changes in the northern North Sea. *Tectonophysics*, 327(1–2), 61-81.
- Harvey BG (1962). *Introduction to Nuclear Physics and Chemistry*. Prentice Hall Inc, New Jersey.
- Holland, G., Lollar, B.S., Li, L., Lacrampe-Couloume, G., Slater, G. et Ballentine, C. (2013). Deep fracture fluids isolated in the crust since the Precambrian era. *Nature*, 497(7449), 357-360.
- Kigoshi, K. (1971). Alpha-recoil thorium-234: dissolution into water and the uranium-234/uranium-238 disequilibrium in nature. *Science*, 173(3991), 47-48.
- Kotwicki, T., Negrini, S., Grivas, T.B., Rigo, M., Maruyama, T., Durmala, J. et Zaina, F. (2009). Methodology of evaluation of morphology of the spine and the trunk in idiopathic scoliosis and other spinal deformities-6th SOSORT consensus paper. *Scoliosis*, 4(26), 1748-7161.
- Kulongoski, J.T. et Hilton, D.R. (2011). Applications of groundwater helium. In: Baskaran, M. (Ed.), *Handbook of Environmental Isotope Geochemistry, Advances in Isotope Geochemistry*. Springer-Verlag, Berlin Heidelberg, pp. 285–303.
- Lamarche, L., Bondue, V., Lemelin, M.-J., Lamothe, M. et Roy, A. (2007). Deciphering the Holocene evolution of the St. Lawrence River drainage system using luminescence and radiocarbon dating. *Quaternary Geochronology*, 2(1), 155-161.
- Lamothe, M. (1989). A new framework for the Pleistocene stratigraphy of the central St. Lawrence Lowland, Southern Québec. *Géographie physique et Quaternaire*, 43(2), 119-129.
- Larocque, M., Gagné, S., Tremblay, L. et Meyzonnat, G. (2013). Projet de connaissance des eaux souterraines du bassin versant de la rivière Bécancour et de la MRC de Bécancour. *Rapport final présenté au Ministère du Développement durable, de l'Environnement, de la Faune et des Parcs* (219 pp.).
- Lavoie, D. (2008). Appalachian foreland basin of Canada. *Sedimentary basins of the world*, 5, 65-103.
- Lemieux, J.M., Sudicky, E., Peltier, W. et Tarasov, L. (2008). Dynamics of groundwater recharge and seepage over the Canadian landscape during the Wisconsinian glaciation. *Journal of Geophysical Research: Earth Surface* (2003–2012), 113(F1).

- Lippmann-Pipke, J., Lollar, B.S., Niedermann, S., Stroncik, N.A., Naumann, R., van Heerden, E. et Onstott, T.C. (2011). Neon identifies two billion year old fluid component in Kaapvaal Craton. *Chemical Geology*, 283(3), 287-296.
- Marine, I. (1979). The use of naturally occurring helium to estimate groundwater velocities for studies of geologic storage of radioactive waste. *Water Resources Research*, 15(5), 1130-1136.
- Mazor, E. (1995). Stagnant aquifer concept Part 1. Large-scale artesian systems—Great Artesian Basin, Australia. *Journal of Hydrology*, 173(1), 219-240.
- McIntosh, J. et Walter, L. (2005). Volumetrically significant recharge of Pleistocene glacial meltwaters into epicratonic basins: Constraints imposed by solute mass balances. *Chemical Geology*, 222(3), 292-309.
- McIntosh, J. et Walter, L. (2006). Paleowaters in Silurian-Devonian carbonate aquifers: Geochemical evolution of groundwater in the Great Lakes region since the Late Pleistocene. *Geochimica et Cosmochimica Acta*, 70(10), 2454-2479.
- McIntosh, J., Garven, G. et Hanor, J. (2011). Impacts of Pleistocene glaciation on large-scale groundwater flow and salinity in the Michigan Basin. *Geofluids*, 11(1), 18-33.
- Méjean, P., Pinti, D.L., Larocque, M., Ghaleb, B., Meyzonnat, G. et Gagné, S. (2016). Processes controlling ^{234}U and ^{238}U isotope fractionation and helium in the groundwater of the St. Lawrence Lowlands, Quebec: the potential role of natural rock fracturing. *Applied Geochemistry* 66, 198-209.
- Meyzonnat, G., Larocque, M., Barbicot, F., Pinti, D. et Gagné, S. (2016). The potential of major ion chemistry to assess groundwater vulnerability of a regional aquifer in southern Quebec (Canada). *Environmental Earth Sciences*, 75(1), 1-12.
- Neuzil, C. (2012). Hydromechanical effects of continental glaciation on groundwater systems. *Geofluids*, 12(1), 22-37.
- Occhietti, S., Chartier H, M., Hillaire-Marcel, C., Cournoyer, M., Cumbaa, S.L. et Harington, R. (2001). Paléoenvironnements de la Mer de Champlain dans la région de Québec, entre 11 300 et 9750 BP: le site de Saint-Nicolas. *Géographie physique et Quaternaire*, 55(1), 23-46.
- Person, M., Butler, D., Gable, C.W., Villamil, T., Wavrek, D. et Schelling, D. (2012). Hydrodynamic stagnation zones: A new play concept for the Llanos Basin, Colombia. *AAPG bulletin*, 96(1), 23-41.
- Phillips, F. et Castro, M. (2003). Groundwater dating and residence-time measurements. *Treatise on Geochemistry*, 5, 451-497.

- Pinti, D.L., Marty, B. et Andrews, J.N. (1997). Atmosphere-derived noble gas evidence for the preservation of ancient waters in sedimentary basins. *Geology*, 25(2), 111-114.
- Pinti, D.L. et Marty, B. (1998). The origin of helium in deep sedimentary aquifers and the problem of dating very old groundwaters. *Geological Society, London, Special Publications*, 144(1), 53-68.
- Pinti, D.L., Béland-Otis, C., Tremblay, A., Castro, M.C., Hall, C.M., Marcil, J.-S., Lavoie, J.-Y. et Lapointe, R. (2011). Fossil brines preserved in the St-Lawrence Lowlands, Québec, Canada as revealed by their chemistry and noble gas isotopes. *Geochimica et Cosmochimica Acta*, 75(15), 4228-4243.
- Plummer, L. et Glynn, P. (2013). Radiocarbon dating in groundwater systems. *Isotope Methods for Dating Old Groundwater, International Atomic Energy Agency (IAEA), Vienna*, 33-90.
- Smith, S. et Kennedy, B. (1983). The solubility of noble gases in water and in NaCl brine. *Geochimica et Cosmochimica Acta*, 47(3), 503-515.
- Solomon, D., Hunt, A. et Poreda, R. (1996). Source of radiogenic helium-4 in shallow aquifers: Implications for dating young groundwater. *Water Resources Research*, 32(6), 1805-1813.
- Takaoka, N. et Mizutani, Y. (1987). Tritiogenic ^3He in groundwater in Takaoka. *Earth and Planetary Science Letters*, 85(1), 74-78.
- Tolstikhin, I. et Kamenskiy, I. (1969). Determination of ground-water ages by the T^3He Method. *Geochemistry International*, 6, 810-811.
- Tolstikhin, I., Lehmann, B., Loosli, H. et Gautschi, A. (1996). Helium and argon isotopes in rocks, minerals, and related ground waters: A case study in northern Switzerland. *Geochimica et cosmochimica acta*, 60(9), 1497-1514.
- Tolstikhin, I. et Marty, B. (1998). The evolution of terrestrial volatiles: a view from helium, neon, argon and nitrogen isotope modelling. *Chemical Geology*, 147(1), 27-52.
- Torgersen, T. (1980). Controls on pore-fluid concentration of ^4He and ^{222}Rn and the calculation of $^4\text{He}/^{222}\text{Rn}$ ages. *Journal of Geochemical Exploration*, 13(1), 57-75.
- Torgersen, T. et Clarke, W.B. (1985). Helium accumulation in groundwater, I: An evaluation of sources and the continental flux of crustal ^4He in the Great Artesian Basin, Australia. *Geochimica et Cosmochimica Acta*, 49(5), 1211-1218. doi:
- Torgersen, T. et O'Donnell, J. (1991). The degassing flux from the solid earth: release by fracturing. *Geophysical Research Letters*, 18(5), 951-954.

- Tran Ngoc, T., Lefebvre, R., Konstantinovskaya, E. et Malo, M. (2014). Characterization of deep saline aquifers in the Bécancour area, St. Lawrence Lowlands, Québec, Canada: Implications for CO₂ geological storage. *Environmental geology*, 72(1), 119-146.
- Vautour, G., Pinti, D.L., Méjean, P., Saby, M., Meyzonnat, G., Larocque, M., Castro, M.C., Hall, C.M., Boucher, C., Roulleau, E., Barbecot, F., Takahata, N. et Sano, Y. (2015). ³H/³He, ¹⁴C and (U-Th)/⁴He groundwater ages in the St. Lawrence Lowlands, Quebec, Eastern Canada. *Chemical Geology*, 413, 94-106.

FIGURES

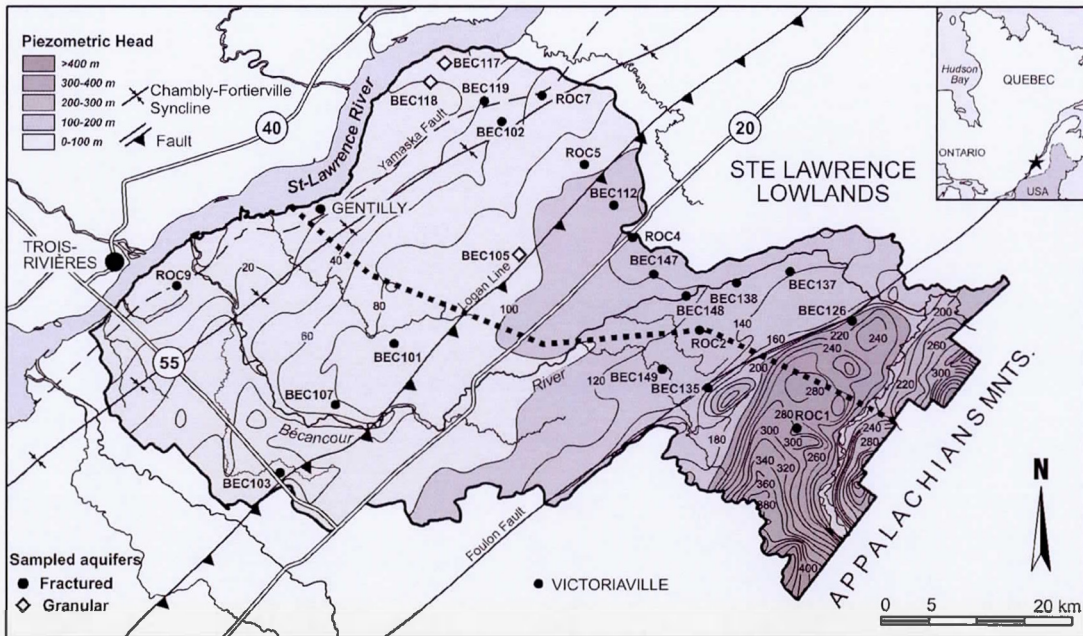


Figure 2.1 Simplified map of the Bécancour watershed. Potentiometric head contour lines of the fractured bedrock aquifer and location of groundwater samples are reported (from Larocque *et al.*, 2013).

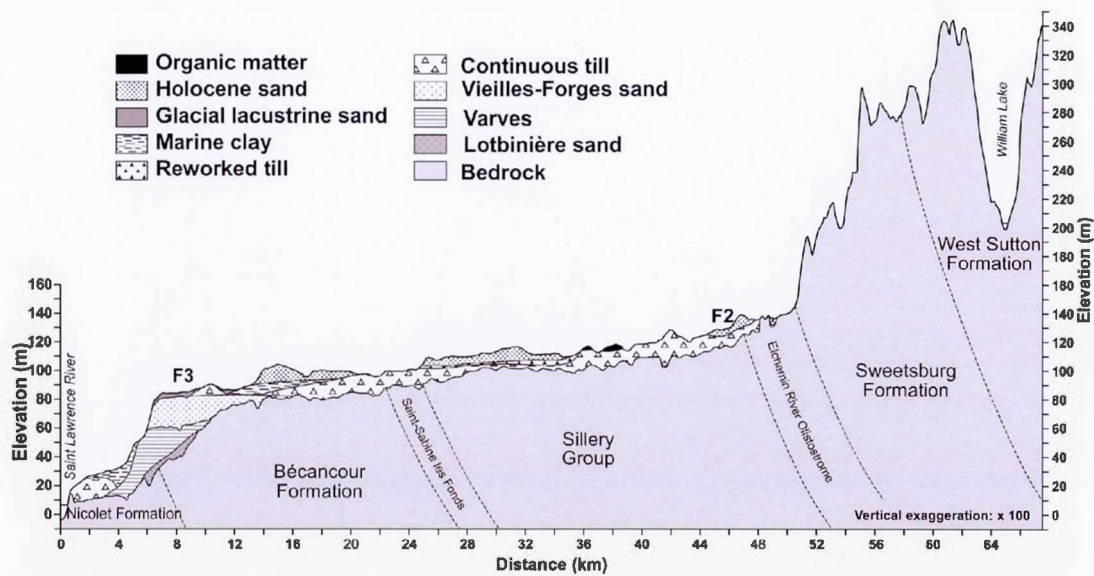


Figure 2.2 Cross section illustrating shallower Quaternary granular aquifers and deeper Ordovician fractured aquifer. Geological formations/groups belonging to the St. Lawrence Platform and the Appalachian Mountains Supergroups are reported (from Larocque *et al.*, 2013).

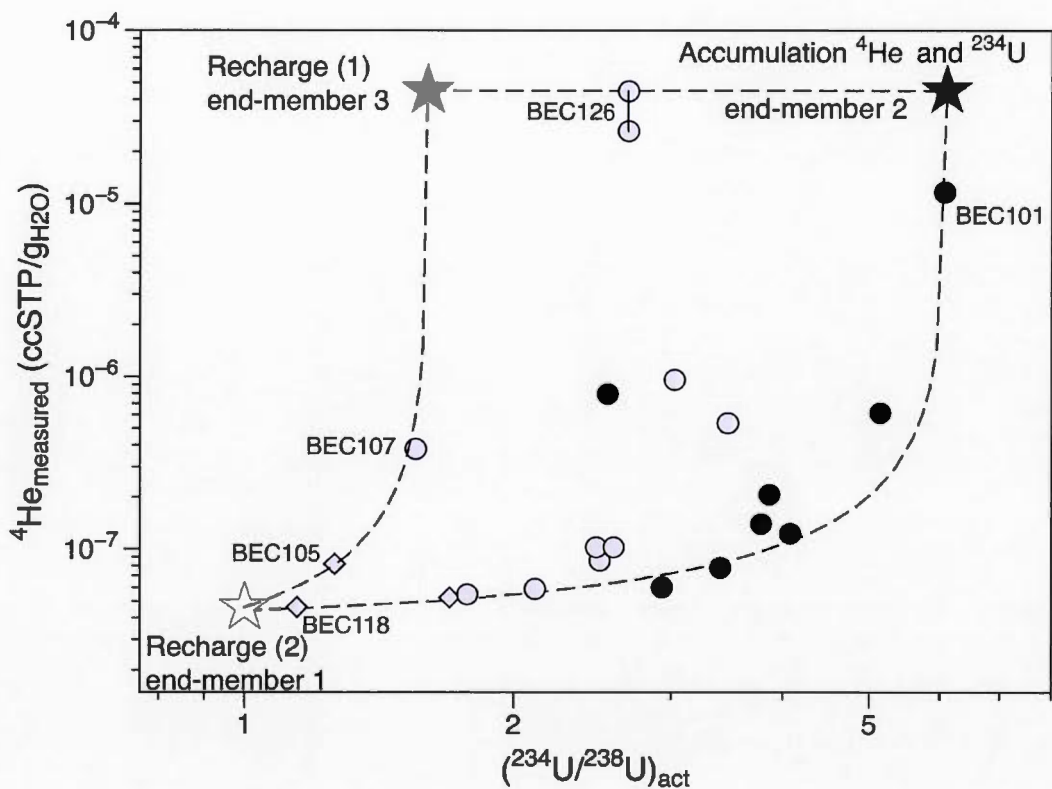


Figure 2.3 Plot of ${}^4\text{He}$ and $({}^{234}\text{U}/{}^{238}\text{U})_{\text{act}}$ with supposed groundwater end-members and mixing trends (dashed lines). End-members 1 and 3 correspond to two different recharge conditions while end-member 2 is mainly influenced by accumulation of both ${}^{234}\text{U}$ and ${}^4\text{He}$. See text for details.

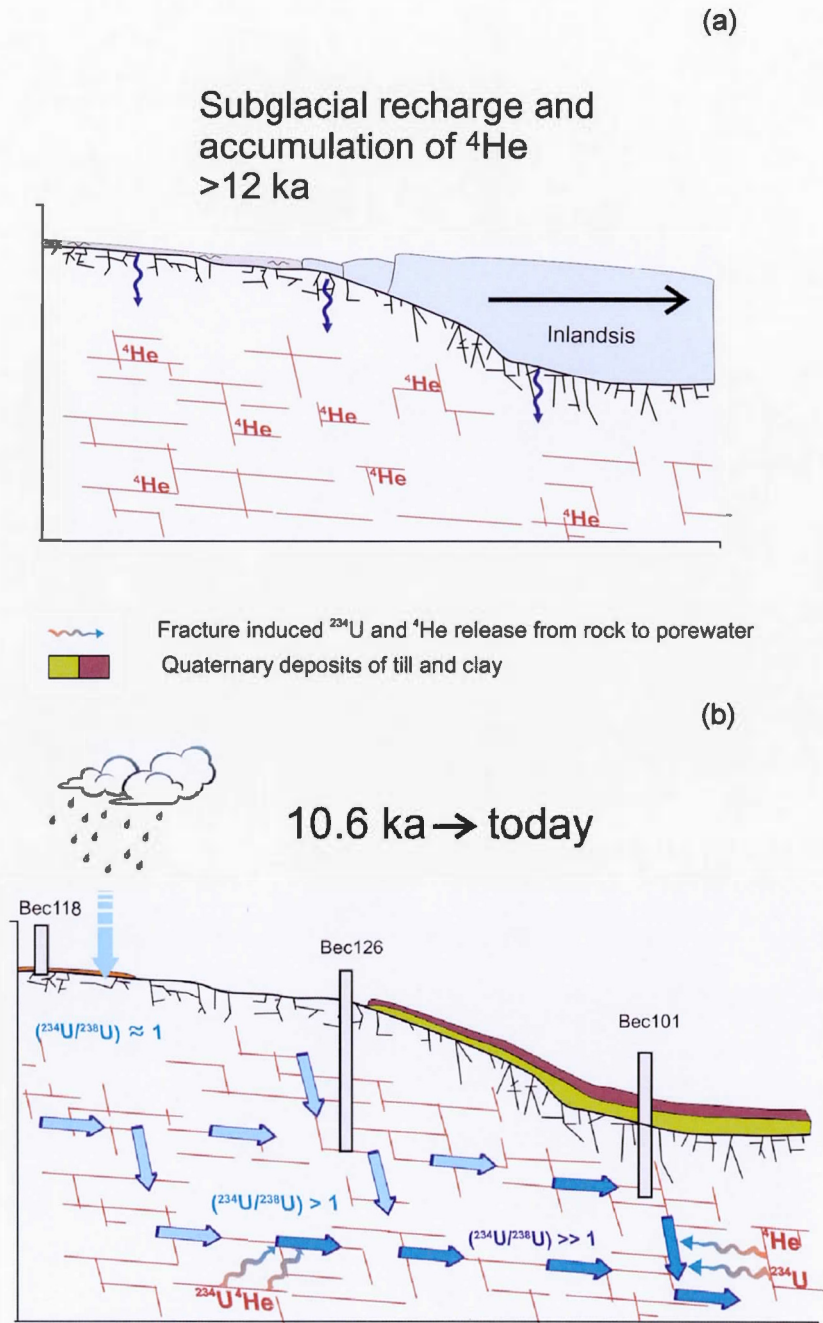


Figure 2.4 Schematic representation of shallower fractures aquifer with a condition of water circulation in the system during Laurentide Ice Sheet retreat ca. 12kyrs, and b) between 10.6 kyrs and the present-day.

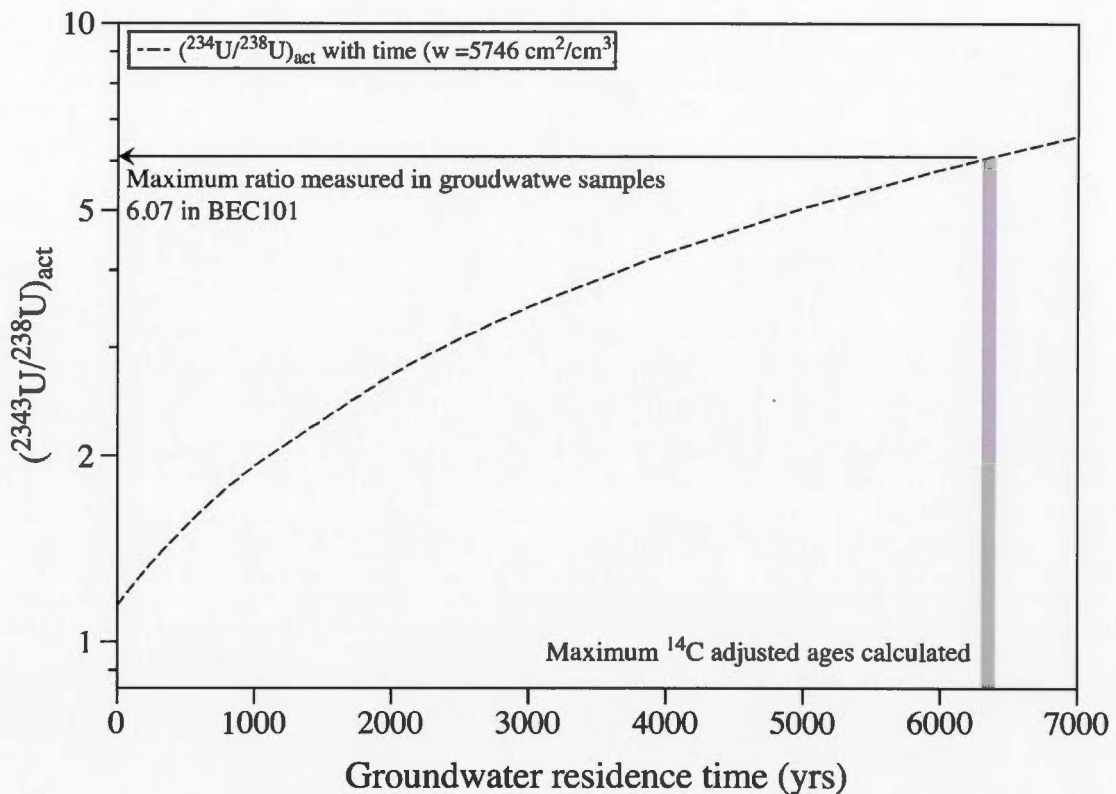


Figure 2.5 Simulation of $(^{234}\text{U}/^{238}\text{U})_{\text{act}}$ evolution as a function of time, using $S = 5,746 \text{ cm}^2 \text{ cm}^{-3}$ calculated with eqn.2.4.

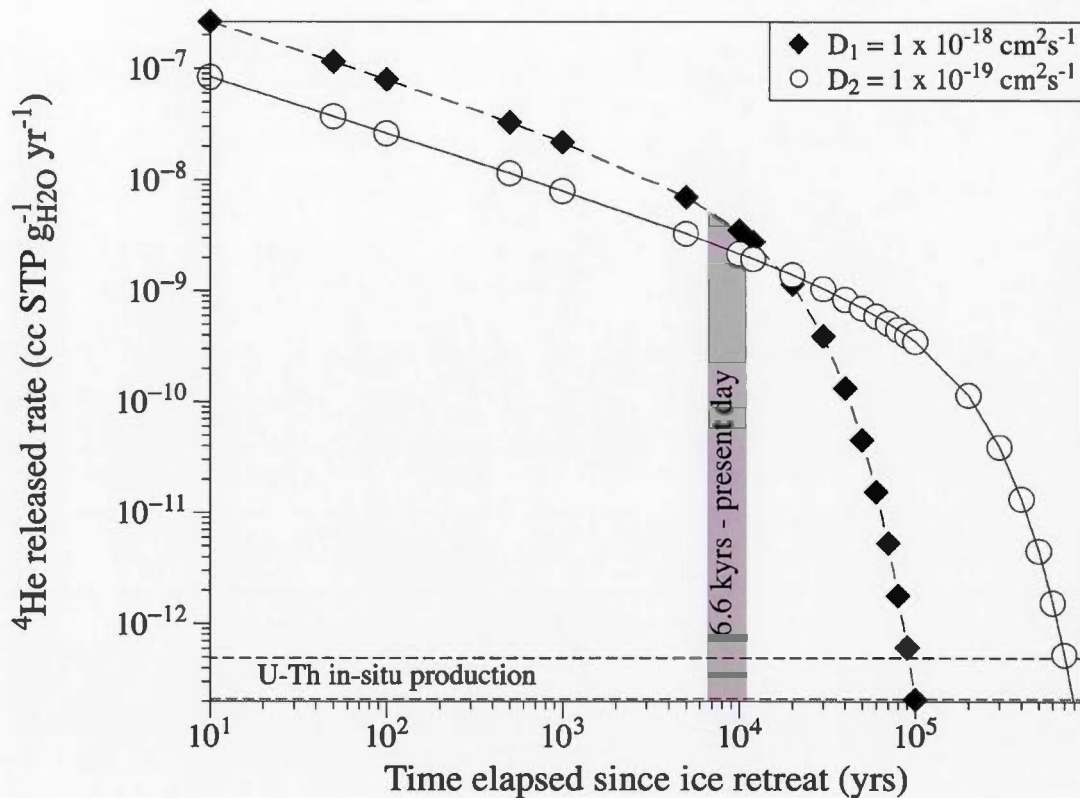


Figure 2.6 Simulated ${}^4\text{He}$ released into water as a function of time since ice retreat using eqn.2.5 with diffusion coefficient $D_1=1 \times 10^{-18} \text{ cm}^2 \text{s}^{-1}$ (black diamonds) and $D_2=1 \times 10^{-19} \text{ cm}^2 \text{s}^{-1}$ (white circles).

CHAPITRE III

MANTLE-DERIVED ^3He IN GROUNDWATER OF THE ST. LAWRENCE LOWLANDS: A FOSSIL RECORD OF THE NEW ENGLAND HOTSPOT?

Pauline MÉJEAN¹, Daniele L. PINTI¹, Marie Larocque¹, Takanori Kagoshima²,
Naoto TAKAHATA², Yuji SANO²

¹GEOTOP et département des Sciences de la terre et de l'Atmosphère, Université du Québec à Montréal, C.P.8888, Succ. Centre-Ville, Montréal, Qc, H3C 3P8 Canada

2- Atmosphere and Ocean Research Institute, the University of Tokyo, Kashiwa, Chiba 277-8564, Japan

Préparé pour soumission à Geophysical Research Letters

Keywords: mantle helium; groundwater; St. Lawrence Lowlands (Quebec, Canada); Monteregian Hills; New England (Great Meteor) hotspot.

ABSTRACT

Helium isotopic ratios ${}^3\text{He}/{}^4\text{He}$ were measured in groundwater from the fractured aquifer of Vaudreuil-Soulanges watershed, Quebec. This groundwater typically exhibits either ${}^3\text{He}/{}^4\text{He}$ (R) ratios higher than the atmospheric value ($\text{Ra} = 1.386 \cdot 10^{-6}$), indicating an excess of tritiogenic ${}^3\text{He}$, or lower than Ra, indicating an excess of radiogenic ${}^4\text{He}$. Interestingly, up to a third of the helium may be of mantle origin (16.7 % of the total). This could be due to groundwater acquiring mantle helium by leaching while moving through local magmatic intrusions. Magmatism occurred in this region during the Grenvillian orogeny at 564 Ma (Mont Rigaud syenite) and during the emplacement of the Monteregian Hills Province at ca. 123 Ma. A model of “magma aging” suggests that the younger Cretaceous intrusions related to the Oka Carbonatite Complex are the source of this mantle-derived helium. Modelling suggests an initial R/Ra up to 58, which excludes subcontinental mantle as the source of the Monteregian Hills but favors the hypothesis of their emplacement during the passage of the New England hotspot.

3.1 INTRODUCTION

Groundwater contains noble gases derived from the atmosphere, the crust and the mantle. In continental environments, mantle-derived noble gases are generally observed in regions of active volcanism and hydrothermalism (Gardner *et al.*, 2010; Pinti *et al.*, 2013) or in basins affected by extensional tectonic (Ballentine et O’Nions, 1992; Marty *et al.*, 1993; Morikawa *et al.*, 2008). The processes that control the release of mantle-derived volatiles to the subsurface are likely sub-continental magma intrusions and underplating with episodic advective transport in the crust (Torgersen, 1993). Mantle-derived ${}^3\text{He}/{}^4\text{He}$ ratio from 1.1×10^{-5} for a MORB-like source (Graham, 2002) and up to 8.3×10^{-5} for an non-degassed OIB-like source (Stuart *et al.*, 2003). The mantle source sharply contrasts with the atmospheric ${}^3\text{He}/{}^4\text{He}$ ratio (Ra) of 1.386×10^{-6} (Ozima et Podosek, 1983) and the crustal ${}^3\text{He}/{}^4\text{He}$ ratio of 2×10^{-8} (Pinti et Marty, 1998).

In the last 30 years, several studies identified fossil mantle helium in groundwater from eastern North America, which is surprisingly because it is a stable continental margin setting. In New Hampshire, Torgersen *et al.* (1994) identified the presence of helium with a substantial mantle helium component ($\approx 12\%$, ${}^3\text{He}/{}^4\text{He} = 1.2\text{Ra}$) in the young and shallow groundwater collected in the Mirror Lake Basin, where there has been no volcanism since Jurassic to Early Cretaceous time (190-95 Ma ago). Torgersen *et al.* (1995) related this mantle helium component to the passage of the New England hotspot that created the younger White Mountains plutonism (Eby, 1985a; Sleep, 1990). Castro *et al.* (2009) observed the presence of solar-like He and Ne in the deeper groundwater systems of the intracratonic Michigan Basin. These authors argued that the occurrence of a primordial noble gas signature does not necessarily indicate the presence of non-degassed OIB-type reservoir, related to the passage of a mantle plume. Indeed, there is no superficial magmatic evidence or seismic low-velocity anomaly that could indicate a fossil hotspot track in the region

(Aktas et Eaton, 2006). Castro *et al.* (2009) suggested that this primordial signature could be accounted for by a shallow refractory reservoir in the Archean subcontinental lithospheric mantle underneath the Michigan Basin. More recently, Pinti *et al.* (2011) identified a very small mantle helium component ($\approx 3\%$) in hundreds of millions of years old brines located in the deeper sedimentary aquifers of the Bécancour region of the St. Lawrence Lowlands, Quebec, Canada (BEC, Fig. 3.1). Saby *et al.* (2016) also found a mantle helium component in the shallow groundwater of the Nicolet-Saint-Francois watersheds ($\approx 8\%$, ${}^3\text{He}/{}^4\text{He} = 4.02 \times 10^{-6}$; NSF region in the Fig. 3.1). Neither of these two Quebec-focused studies discusses the source of this mantle helium.

The objective of the study was to identify the possible sources of helium to perform isotopic ages (U-Th) $/{}^4\text{He}$ in shallow aquifers. To evaluate the possible sources of mantle helium in the St-Lawrence Lowlands aquifers, the helium isotopic ratios ${}^3\text{He}/{}^4\text{He}$ were analyzed in 18 groundwater samples collected in the fractured aquifer of Vaudreuil-Soulanges watershed close to one of the most enigmatic Monteregian Hills, the Oka Carbonatite complex. The source of this fossil mantle helium retained in groundwater was assessed using a “magma aging” model (Torgersen *et al.*, 1995). Resolving the source of mantle helium in this region should help constrain the highly debated source of the Monteregian Hills, i.e hotspot vs. subcontinental lithospheric mantle (SCLM).

3.2 GEOLOGY AND HYDROGEOLOGY OF THE STUDY AREA

The Vaudreuil-Soulanges (814 km^2) is the westernmost region of the St. Lawrence Lowlands (Fig. 3.1). The St. Lawrence Lowlands are composed of ca. 1200 m-thick Cambrian–Lower Ordovician siliciclastic and carbonate platform sediments, overlain by ca. 1800 m of Middle–Late Ordovician foreland carbonate-clastic deposits. These sedimentary sequences uncomfortably overlay the granite-gneiss-anorthositic basement of the Mesoproterozoic (1250–980 Ma) Grenville Orogeny. Major tectonic events recorded in this region are (1) the opening of the Iapetus Ocean and the formation of the St. Lawrence Rift System around 550 Ma ago (Cawood *et al.*, 2001); (2) the formation of the Appalachians between 470 and 360 Ma (Tremblay et Castonguay, 2002); (3) Middle-Late Jurassic (200–150 Ma) reactivation of the Iapetus faults during the opening of the North Atlantic Ocean (Tremblay *et al.*, 2013); and (4) a Cretaceous magmatic event that produced a series of alkaline intrusions oriented approximately WNW-ESE and referred to as the Monteregian Hills (Eby, 1985a) (Fig. 3.1).

Crough *et al.* (1981) and Sleep (1990) suggested that the Monteregian Hills are the result of the passage of a mantle plume: the New England hotspot (also called the Great Meteor hotspot) a long-lived volcanic hotspot presently overridden by the Mid-Atlantic Ridge. The migration of the North-American craton over this plume is suggested to have created a series of kimberlite fields in Northern Ontario between 214 and 134 Ma, the Monteregian Hills at around 123 ± 2 Ma (Foland *et al.*, 1988) and the younger White Mountains series in New Hampshire at 139–117 Ma (Eby, 1985a). The alkaline character of the MH and their Sr (0.7032–0.7040) and Nd (0.5125–0.5127) isotopic ratios, which are similar to those measured in Oceanic Island Basalts (OIBs) supported a plume-related mantle source (Foland *et al.*, 1986). (McHone, 1996) showed that there is no evidence of age progression among the different magmatic provinces, as expected in a hotspot track, arguing for the involvement of heterogeneous SCLM melts rather than plume material. Some authors have ascribed

Monteregian Hills plutonism to melting of the lithospheric mantle through NW-SE Iapetus-related faults reactivated at the time of the opening of North Atlantic Ocean (Faure *et al.*, 1996; Wen *et al.*, 1987). Roulleau *et al.* (2012) observed an inverse relation between $^{206}\text{Pb}/^{204}\text{Pb}$ and $\text{N}_2/^{36}\text{Ar}$ ratios interpreted as the mixing between a recycled component (HIMU) and an ambiguous mantle source that could be either a plume source or the depleted mantle. Roulleau and Stenvenson (2013) have shown a geochemical and isotopic (Nd-Sr-Hf-Pb) evidence for a lithospheric mantle source in response to lithospheric extension related to opening of the North Atlantic Ocean.

The Vaudreuil-Soulanges region consists of Cambrian fluvio-marine quartzitic sandstone of the Potsdam Group and Early Ordovician shelf-carbonate and dolostone of the Beekmantown Group (Tran Ngoc *et al.*, 2014). These sequences are covered by a 120 m-thick sequence of Quaternary glacial till and clays from the marine transgression episode of the Champlain Sea that occurred between 12 and 9 kyrs ago (Occhietti *et al.*, 2001). The higher topography of the area is the syeno-granitic intrusion of Mont Rigaud with a U-Pb age of 564^{+10}_{-8} Ma (Malka *et al.*, 2000). K-rich alnoïtes intrude the sedimentary cover in the central eastern part of the watershed (Fig. 3.2; Chen et Simonetti, 2013; Eby, 1985a). They are related to the same cretaceous magmatic event (123 Ma ago) that led to the emplacement of the Oka carbonatitic Complex, north of the watershed (Fig. 3.2). The origin of the Oka Complex is also controversial. Recently, Chen et Simonetti (2015) suggested on the basis of a Pb, Sr, Nd, C, O multi-isotopic study that Oka carbonatite derived from sampling of a heterogeneous plume-related mantle source.

The main bedrock aquifer sampled in the current study is hosted by the Cambrian-early Ordovician rocks. Recharge is mainly from high permeability eskers (St-Telesphore) and sand hills of (St-Lazare and Hudson) where there are windows in the glacial till and Champlain Sea clays (Fig. 3.2). Lower recharge was observed from Mont Rigaud syenite due to the low permeability of the intrusion. Regional

groundwater flows from these topographic highs to the Ottawa River in the northern part of the area, and to the S-SE direction to the St. Lawrence River and Lake Saint-Francois in the southern part of the basin. Groundwater acquires Ca-Mg-HCO₃ and Ca-SO₄ chemistry by dissolution of Quaternary till, Ordovician carbonates and gypsum. It evolves to Na-HCO₃ and Na-SO₄ types by ionic exchange between Ca²⁺ dissolved and Na⁺ of minerals and finally to Na-Cl by exchange with saline pore water contained in Champlain Sea clays (Larocque *et al.*, 2015).

3.3 SAMPLING AND ANALYTICAL METHODS

Eighteen groundwater samples were collected in the fractured bedrock aquifer during summer 2014 at depths ranging between 20 m to 96 m from open bedrock municipal wells, domestic wells and piezometers. Groundwater was collected directly at the wellhead in municipal wells and at a water faucet in domestic wells, taking precautions to avoid intermediate reservoirs where the water could undergo degassing. After purging, water was collected in a cold-clamped 3/8-inch diameter, refrigeration-type copper tube following method described in Vautour *et al.* (2015). Helium isotopic ratios $^3\text{He}/^4\text{He}$ were measured at the University of Tokyo using a VG Helix SFT and compared to the HESJ standard (Helium Standard of Japan; Matsuda *et al.*, 2002) with a 2σ precision of $\pm 0.2\%$ (Sano *et al.*, 2008). ^4He and ^{20}Ne concentrations were measured on a Pfeiffer QMS PrismaTM connected to the purification line. Details on the analytical procedure at the University of Tokyo can be found in Vautour *et al.* (2015).

Three rock samples were collected, two in the Oka Complex and one from an alnöite located at the Ile Cadieux (Fig. 3.2). They were analyzed for whole rock geochemistry at ACME Lab in Vancouver by ICP for major elements and ICP-MS for minor elements. The ^4He amounts in the sampled rocks were estimated at the University of Tokyo using a two stage analytical process involving first degassing an aliquot by heating it at 1800°C to melt them in a Mo-Ta furnace, and measuring its ^4He content using the VG Helix SFT (Burnard *et al.*, 2013).

3.4 RESULTS

The atmosphere-normalized ${}^3\text{He}/{}^4\text{He}$ ratios R/Ra range from 0.18 to 2.33, pointing to the presence of both ${}^3\text{He}$ -enriched and ${}^4\text{He}$ -enriched groundwater samples (Table 3.1). Dissolved ${}^4\text{He}$ concentrations varies over three orders of magnitude from a value of 6.15×10^{-8} ccSTP/g_{H2O} (VS104) close to the solubility equilibrium with the atmosphere (Air Saturated Water at 10°C: 4.70×10^{-8} ccSTP/g_{H2O}) up to 1.32×10^{-5} ccSTP/g_{H2O} (VS114). The ${}^3\text{He}/{}^4\text{He}$ ratios measured in rock samples of the alnoïte and from the Oka carbonatite range from 0.06 ± 0.03 to 0.6 ± 0.01 . The total amount of ${}^4\text{He}$ measured in alnoïte and carbonatite ranges from 4.33×10^{-5} ccSTP/g_{H2O} to 5.83×10^{-5} ccSTP/g_{H2O} (Table 3.2). U and Th contents in alnoïtes are 3.3 ppm and 9.9 ppm while for carbonatite-1 they are 15.4 ppm and 40.9 ppm. These values are comparable to those found usually in other carbonatites (e.g., U between 0.2 ppm and 10 ppm in the carbonatites of Kola region, Russia; Marty *et al.*, 1998). Carbonatite-2 was sampled from the core of the Oka complex where niobium ores contain high contents of pyrochlore containing anomalous U contents of up to 28 wt% (Zurevinski et Mitchell, 2004). Thus it is concluded that the carbonatite-2 U contents (Table 3.2) are not representative of the bulk amount of U in the magma. He isotopic data measured in mineral separates from the Oka carbonatites from (Sasada *et al.*, 1997) are also reported in Table 2 for comparison.

The measured helium isotope ratios were corrected for excess-air helium (He_{ea}) resulting from air bubbles entering the water table and dissolved in groundwater (Heaton and Vogel, 1981). Resulting $({}^3\text{He}_{\text{tot}} - {}^3\text{He}_{\text{ea}})/({}^4\text{He}_{\text{tot}} - {}^4\text{He}_{\text{ea}})$ ratios are plotted against the ratio of the ASW helium (${}^4\text{He}_{\text{eq}}$) to the total helium corrected for the excess-air component (${}^4\text{He}_{\text{tot}} - {}^4\text{He}_{\text{ea}}$) in a Weise-type plot (Fig. 3.3; Weise and Moser, 1987). If the helium is purely atmospheric, these two ratios will be equal to 0.983Ra and 1, respectively. If only tritiogenic ${}^3\text{He}_{\text{tri}}$ occurs the samples will plot along the right-hand side Y-axis from an initial ASW composition ($R_{\text{eq}} = \text{Ra} \times 0.983$; Benson et Krause, 1980). If radiogenic ${}^4\text{He}$ produced by U and Th decay in the crust is added,

the samples will move closer to the left-bottom corner of the plot (R/Ra of 0.012; Fig. 3.3). Finally, if mantle-derived ${}^3\text{He}$ and ${}^4\text{He}$ occur, the sample will plot on the left-side Y-axis. Mixing between these components appears on this plot as straight lines governed by the equation (Weise et Moser, 1987):

$$\frac{\left(\frac{{}^3\text{He}_{tot} - {}^3\text{He}_{ea}}{4\text{He}_{tot} - {}^4\text{He}_{ea}}\right)}{Y} = \underbrace{\left(R_{eq} - R_{terr} + \frac{{}^3\text{He}_{tri}}{{}^4\text{He}_{eq}}\right)}_m \cdot \frac{{}^4\text{He}_{eq}}{\underbrace{{}^4\text{He}_{tot} - {}^4\text{He}_{ea}}_X} + \underbrace{R_{terr}}_b \quad (3.1)$$

where R_{terr} is the ${}^3\text{He}/{}^4\text{He}$ of the terrigenic source which corresponds either to the crustal helium or the mantle-derived helium or both.

Groundwater samples from VS are aligned along mixing line representing complete decay of 5TU, 18 TU, 35TU and 65TU and addition of R_{terr} ranging between 2.01×10^{-7} to 1.83×10^{-6} . These ratios are higher than the ratios of 0.45 to 1.8×10^{-8} that are expected from local production of ${}^3\text{He}$ from ${}^6\text{Li}$ and of ${}^4\text{He}$ from ${}^{238,235}\text{U}$ and ${}^{232}\text{Th}$ in St. Lawrence Lowlands sedimentary rocks or in rocks from the Grenville basement (Pinti *et al.*, 2011). The difference between the pure crustal R_{terr} and the calculated R_{terr} from the Weise-plot (Fig. 3.3) suggests the addition from 2% to 16.7% of mantle-derived helium. This is the highest mantle helium amount ever reported in the St. Lawrence Lowlands and higher than the 2-8% estimated by Pinti *et al.* (2011) and Saby *et al.* (2016), respectively. The VS108 and VS112 wells, where the highest mantle-derived ${}^3\text{He}$ signals have been measured in groundwater from the deeper portion of the Potsdam Group sandstone aquifer, which is in contact with the Grenville basement.

3.5 DISCUSSION

3.5.1 Sources of mantle helium in groundwater

The mantle helium component found in VS108 and VS 112 could be a fossil mantle source preserved in old brines within the sedimentary sequence of the St. Lawrence Lowlands or a fossil source preserved in magmatic intrusions released recently in groundwater. If the first hypothesis is valid, then old groundwater of at least the age of the Montréal Hills intrusions (123 ± 2 Ma) should have been preserved in the VS watershed. Although Pinti *et al.* (2011) have found such brines in the Potsdam Group in the Bécancour region, the groundwater chemistry at VS indicates a Ca-HCO₃ type freshwater for VS112 and a NaCl type for VS108. Salinity values of 237 and 710 mg/L for these two samples has been acquired locally by exchange with glacio-marine porewater from the Champlain Sea clays (Cloutier *et al.*, 2006; Meyzonnat *et al.*, 2016). The calculated ³H/⁴He age (see Appendix for detail on calculations) for VS112 from a tritium activity of 6.6 TU is 43 ± 1.5 yrs. The tritium amount measured in VS108 is 0.8 TU, a value equal to the detection limit of tritium measured at Waterloo University (see Appendix). Groundwater from VS108 water is therefore probably from groundwater recharged before the bomb-peak of the 1960s. The U-Th/⁴He ages calculated for the two samples on the basis of an *in situ* accumulation rate of ⁴He of 4.1×10^{-13} cm³STP/gH₂O/yr with a porosity of 3% (Tran Ngoc *et al.*, 2014) and using relevant equations from Torgersen and Clarke (1985) provides ages of $45(\pm 50\%)$ kyr corresponding to the previous glaciation (see Appendix). The occurrence of fossil brines in the VS region therefore appears to be unlikely.

Another explanation for the mantle helium component found in VS108 and VS 112 could be a mantle “aged” source preserved in magmatic intrusions and recently released into groundwater by leaching. Torgersen *et al.* (1995) showed that only a local, near-surface-emplaced, gas-rich magma that has retained significant volatiles (e.g., in fluid inclusions) is likely to retain a mantle memory. In the studied area, (Sasada *et al.*, 1997) measured ³He/⁴He ratios of 0.34 to 3.52Ra in mineral separates

from the Oka carbonatitic Complex (Table 3.2). In the current study, the measured values ${}^3\text{He}/{}^4\text{He}$ values in bulk rock samples are lower (0.06 to 0.60Ra). However, atmospheric helium contained in the interstitial matrix could have lowered the initial helium ratios from particular mineral and fluid inclusions. The hypothesis of an “aged” magma source appears to be a viable explanation.

3.5.2 Magma aging model and the mantle source

Torgersen et Jenkins (1982) developed a simple model of “magma aging”, which was later improved by Torgersen *et al.* (1995) and Sano *et al.* (2006). This model describes the evolution of an initial magmatic ${}^3\text{He}/{}^4\text{He}$ ratio in a magma body by the addition of radiogenic ${}^4\text{He}$ produced in situ by U and Th decay. Torgersen *et al.* (1995) determine the rate of change of helium concentration in the magma (J_{He}) as a result of crustal radiogenic ${}^4\text{He}$ production:

$$J_{\text{He}} = (0.2355 \times 10^{-12}) \times [U] \times \left(1 + 0.123 \left(\frac{[Th]}{U} \right) - 4 \right) \quad (3.2)$$

where $[U]$ and $[Th]$ are concentrations in ppm and J_{He} is in $\text{cm}^3\text{STP/g}_{\text{rock}}/\text{yr}$. U and Th determine the rate of change of the helium concentration of rock while the initial concentration of helium in an emplaced magma determining the change in the isotope ratio of helium $({}^3\text{He}/{}^4\text{He})_{\text{magma}}/({}^3\text{He}/{}^4\text{He})_{\text{air}}$ (i.e. $[R/Ra]_{\text{magma}}$).

This model is used here to determine whether one of the magmatic episodes that affected the region might have left a fossil mantle-derived helium signal that could have been then released into groundwater. Two main magmatic episodes occurred in VS area: (1) the intrusion of the Precambrian syenite of Mont Rigaud with an age of 564^{+10}_{-8} Ma and (2) the emplacement of the Oka carbonatites and the associated alnoïtic intrusions at 123 ± 2 Ma. In Eqn (3.2), ${}^3\text{He}$ was fixed ($7.8 \times 10^{-12} \text{ ccSTP/g}_{\text{rock}}$)

and R/Ra ratio changes with time depending on J_{He} . The loss of helium by diffusion and/or α -recoil with time since the magma intrusion was neglected. The production of nucleogenic 3He by neutron reaction with lithium (Morrison et Pine, 1955) was also neglected because the production of radiogenic 4He is dominant in a rock compared to that of 3He .

To verify if the fossil mantle-helium is preserved in the Mont Rigaud syenites, it was necessary to assume a value for the initial helium isotopic ratio for the Mont Rigaud syenites. The value used here was $6.5 \pm 1 Ra$ corresponding to a crustal rift signature (Gautheron *et al.*, 2009) which best represents the tectonic setting for the emplacement of Mont Rigaud. We used U and Th concentrations of 3.4 ppm and 11.3 ppm respectively measured in typical syenites (Cooper, 1958). Helium in the syenite was not measured but it is assumed that an initial $^4He = 6.7 \times 10^{-6}$ ccSTP/g_{H2O} corresponding to a MORB-like gas-rich source is realistic (Torgersen *et al.*, 1995). The decrease of the initial mantle signature $[R/Ra]_{magma} = 6.5$ (bold line; Fig. 3.4) is represented with its uncertainty of $\pm 1 Ra$ (dashed lines) from the emplacement of the Mont Rigaud intrusion ($t=0$) up to present day (red star; $(^3He/^4He)_{VS108}/(^3He/^4He)_{air} = 1.38 \pm 0.01$ measured in VS108; Table 3.1).

After 564 Ma, the final $[R/Ra]_{magma}$ is equal to 0.20 and is much lower than the value of the measured groundwater. Indeed after only 8 Ma since the emplacement, the radiogenic 4He addition completely masks the fossil mantle memory. This simple calculation excludes Mt Rigaud intrusion as the local source of fossil mantle helium in the VS groundwater.

In the second simulation, the final $[R/Ra]_{magma} = 1.38 \pm 0.01$ (i.e. VS108) was fixed and the initial ratio of the magma during emplacement of the Oka Carbonatite and alnoïte intrusions was estimated using the relation deduced from eqn.3.2. The initial $[R/Ra]_{magma}$ is unknown because of the uncertainties surrounding the origin of this magma (Chen et Simonetti, 2015; Eby, 1985b; Roulleau *et al.*, 2012). If the

hypothesis of a subcontinental mantle is true, then an initial $[R/Ra]_{magma}$ of 6.5 to 7.5Ra is expected (Dunai et Baur, 1995; Gautheron et Moreira, 2002). If the hypothesis of a mantle-plume related source is accepted, then any R/Ra value higher than 6.5Ra should be assumed.

$$\left(\frac{R_{magma}}{R_{air}} \right)_{initial} = \left[\left(\frac{R_{magma}}{R_{air}} \right)_{VS108} \times ({}^4He_{initial} + J^4He \times t \times 10^6) \right] / {}^4He_{initial} \quad (3.3)$$

J^4He is equal to 2.24×10^{-12} ccSTP/g_{rock}, t is the time elapsed since magma intrusion (we used t = 123 ± 2 Ma). We used [U] and [Th] of 3.3 ppm to 15.4 ppm, and 9.9 ppm to 40.9 ppm measured on the alnoïte and carbonatite-1 samples respectively (Table 3.2). We assume an initial 4He amount of 6.7×10^{-6} ccSTP/g_{rock} similar to that to for a MORB-like source. Torgersen et al. (1995) suggested that this value is also a good approximation of the helium amount in OIB-type mantle sources. This value is lower than the measured present values in the intrusions (Table 3.2) which represent the total helium including the radiogenic amount added since the time of their formation. The initial $[R/Ra]_{magma}$ estimated for the age of the Monteregian Hills is 58.0 ± 3.2 for the Oka intrusion (Fig. 3.5) and 21.9 ± 3.2 (Fig. 3.6) for the alnoïte intrusion. In both simulations (Fig. 3.5 and 3.6) the initial helium ratio estimated is greater than $[R/Ra]_{magma}$ measured in the SCLM (6.5Ra). The initial $[R/Ra]_{magma}$ of 58.0 and 21.9 indicate that a depleted OIB-like source related to a plume (the New England hotspot) can be considered the most viable explanation for the fossil mantle signal measured in VS108.

3.6 CONCLUSIONS

The simple model of magma aging used in our simulation shows that a fossil mantle signal could have been preserved in magma intrusions related to the Monteregian Hills Province and acquired by local groundwater. Because the mantle source is located within or in close proximity to the studied watershed, dilution of the mantle signal by addition of local groundwater is minimal and the mantle signal was not weakened during dispersion along the flow path. However, taking into account the relative high radioactivity of the Oka carbonatites and surrounding rock, only a ${}^3\text{He}$ -rich mantle source could have preserved the mantle signal. The results of our simulations suggest that the New England hotspot is responsible for the emplacement of at least of the Oka Complex. However future surveys of helium within aquifers and lakes close to or within the other Monteregian Hills plutons are needed to confirm our hypothesis and strength our magma aging model.

ACKNOWLEDGMENTS

The authors thank the Quebec Ministry of Environment (*Ministère du Développement durable, de l'Environnement, des Parcs et de la Lutte contre les changements climatiques*), the Quebec Research Fund (“Fonds de recherche du Quebec - Nature et Technologies”), the Bécancour River Watershed Organization (“organisme de bassin versant COBAVER-VS ”), and the municipalities that contributed funding to this research (MRC of Vaudreuil-Soulanges) and GEOMONT.

APPENDICE

$^3\text{H}/^4\text{He}$ method of datation

Estimation of ${}^3\text{He}_{\text{tri}}$ is given by Schlosser et al. (1989) is required to calculate ${}^3\text{H}/{}^4\text{He}$ ages:

$$\begin{aligned} {}^3\text{He}_{\text{tri}} = & {}^4\text{He}_{\text{tot}} \times (R_{\text{tot}} - R_{\text{terr}}) - {}^4\text{He}_{\text{eq}} \times (R_{\text{eq}} - R_{\text{ter}}) - \left(\frac{{}^4\text{He}}{{}^{20}\text{Ne}} \right)_{\text{ea}} \quad (\text{A.1}) \\ & \times ({}^{20}\text{Ne}_{\text{tot}} - {}^{20}\text{Ne}_{\text{eq}}) \times (R_{\text{ea}} - R_{\text{terr}}) \end{aligned}$$

where R_{tot} is the measured ${}^3\text{He}/{}^4\text{He}$ ratio; R_{eq} is the result of the fractionation factor (0.983) with R_{atm} the atmospheric ratio ($R_{\text{atm}} = 1.386 \times 10^{-8}$ ccSTP/g_{H2O}); $({}^4\text{He}/{}^{20}\text{Ne})_{\text{ea}}$ and R_{ea} are assumed to be atmospheric value.

${}^4\text{He}_{\text{tot}}$ and ${}^{20}\text{Ne}_{\text{tot}}$ are total amount measured in water samples; ${}^4\text{He}_{\text{eq}}$ and ${}^{20}\text{Ne}_{\text{eq}}$ were calculated using the relation between water temperature and solubility of the gas (Smith et Kennedy, 1983) with temperature measured in the wells during sampling.

$U\text{-Th}/{}^4\text{He}$ method of datation

Assuming that the measured radiogenic ${}^4\text{He}$ is produced from U and Th decay contained in the aquifer rocks (in situ production), the U-Th/ ${}^4\text{He}$ groundwater residence times can be calculated as follows (Torgersen et Clark, 1985):

$$t = \frac{[{}^4\text{He}_{\text{terr}}]}{P_4\text{He} \times \Lambda_4\text{He} \times \left(\frac{1-\phi}{\phi} \right) \times \varphi} \quad (\text{A2})$$

where $[{}^4\text{He}_{\text{tent}}]$ is the measured radiogenic ${}^4\text{He}$ concentration in groundwater ($\text{cm}^3 \text{STP g/water}$; Table 2); $P_4\text{He}$ is the radiogenic ${}^4\text{He}$ production rate in the fractured bedrock ($\text{cm}^3 \text{STP/g}_{\text{rock}}$); $\Lambda_4\text{He}$ is the He retention factor (${}^4\text{He}_{\text{released}}/{}^4\text{He}_{\text{produced}}$) taken as 1 (Torgersen, 1980; Sano et al., 2008); $(1-\phi/\phi)$ is the void ratio where ϕ is the fractional effective porosity; and ρ is the aquifer matrix density (assumed to be 2.72 g/cm^3 for a dominant carbonate matrix). Effective porosities of the Ordovician of the regional fractured aquifer from 1 to 5% have been estimated from pumping well tests (Larocque et al., 2013a) and measured on core samples (Tran Ngoc et al., 2014). ${}^4\text{He}$ production rate ($P_4\text{He}$) was calculated using U and Th measured in surrounding basin ($U = 2 \text{ ppm}$ and $\text{Th} = 6 \text{ ppm}$; Vautour et al., 2015). We obtained $P_4\text{He} = 4.1 \times 10^{-13} \text{ cm}^3 \text{STP/g}_{\text{rock}}/\text{yr}$, assuming secular equilibrium among the U and Th descendants (Ballentine et Burnard, 2002).

REFERENCES

- Aktas, K. et Eaton, D.W. (2006). Upper-mantle velocity structure of the lower Great Lakes region. *Tectonophysics*, 420(1), 267-281.
- Ballentine, C.J. et Burnard, P.G. (2002). Production, release and transport of noble gases in the continental crust. *Reviews in mineralogy and geochemistry*, 47(1), 481-538.
- Ballentine, C.J. et O'Nions, R.K. (1992). The nature of mantle neon contributions to Vienna Basin hydrocarbon reservoirs. *Earth and Planetary Science Letters*, 113(4), 553-567.
- Benson, B.B. et Krause Jr, D. (1980). Isotopic fractionation of helium during solution: A probe for the liquid state. *Journal of Solution Chemistry*, 9(12), 895-909.
- Bethke, C.M. et Johnson, T.M. (2008). Groundwater age and groundwater age dating. *Annu. Rev. Earth Planet. Sci.*, 36, 121-152.
- Burnard, P., Zimmermann, L. et Sano, Y. (2013). The noble gases as geochemical tracers: history and background. In: Burnard, P. (Ed.), *The Noble Gases as Geochemical Tracers*. Springer, Berlin, Heidelberg, 1–15.
- Castro, M.C., Ma, L. et Hall, C.M. (2009). A primordial, solar He–Ne signature in crustal fluids of a stable continental region. *Earth and Planetary Science Letters*, 279(3), 174-184.
- Cawood, P.A., McCausland, P.J. et Dunning, G.R. (2001). Opening Iapetus: constraints from the Laurentian margin in Newfoundland. *Geological Society of America Bulletin*, 113(4), 443-453.
- Chen, W. et Simonetti, A. (2013). In-situ determination of major and trace elements in calcite and apatite, and U–Pb ages of apatite from the Oka carbonatite complex: Insights into a complex crystallization history. *Chemical Geology*, 353, 151-172.
- Chen, W. et Simonetti, A. (2015). Isotopic (Pb, Sr, Nd, C, O) evidence for plume-related sampling of an ancient, depleted mantle reservoir. *Lithos*, 216–217, 81-92.
- Cloutier, V., Lefebvre, R., Savard, M.M., Bourque, É. et Therrien, R. (2006). Hydrogeochemistry and groundwater origin of the Basses-Laurentides sedimentary rock aquifer system, St. Lawrence Lowlands, Québec, Canada. *Hydrogeology Journal*, 14(4), 573-590.
- Cooper, W.S. (1958). Coastal sand dunes of Oregon and Washington. *Geological Society of America Memoirs*, 72, 1-162.

- Crough, S.T. (1981). Mesozoic hotspot epeirogeny in eastern North America. *Geology*, 9(1), 2-6.
- Dunai, T. et Baur, H. (1995). Helium, neon, and argon systematics of the European subcontinental mantle: Implications for its geochemical evolution. *Geochimica et Cosmochimica Acta*, 59(13), 2767-2783.
- Eby, G.N. (1985a). Age relations, chemistry, and petrogenesis of mafic alkaline dikes from the Monteregian Hills and younger White Mountain igneous provinces. *Canadian Journal of Earth Sciences*, 22(8), 1103-1111.
- Eby, G.N. (1985b). Sr and Pb isotopes, U and Th chemistry of the alkaline Monteregean and White Mountain igneous provinces, eastern North America. *Geochimica et Cosmochimica Acta*, 49(5), 1143-1153.
- Farley, K.A. (2002). (U-Th)/He dating: Techniques, calibrations, and applications. *Reviews in Mineralogy and Geochemistry*, 47(1), 819-844.
- Faure, S., Tremblay, A. et Angelier, J. (1996). State of intraplate stress and tectonism of northeastern America since Cretaceous times, with particular emphasis on the New England-Quebec igneous province. *Tectonophysics*, 255(1), 111-134.
- Foland, K., Gilbert, L.A., Sebring, C.A. et Jiang-Feng, C. (1986). $^{40}\text{Ar}/^{39}\text{Ar}$ ages for plutons of the Monteregean Hills, Quebec: Evidence for a single episode of Cretaceous magmatism. *Geological Society of America Bulletin*, 97(8), 966-974.
- Foland, K., Jiang-Feng, C., Gilbert, L.A. et Hofmann, A. (1988). Nd and Sr isotopic signatures of Mesozoic plutons in northeastern North America. *Geology*, 16(8), 684-687.
- Ford, K.L., Savard, M., Dessau, J.-C., Pellerin, E., Charbonneau, B.W. et Shives, B. (2001). The role of gamma-ray spectrometry in radon risk evaluation: a case history from Oka, Quebec. *Geoscience Canada*, 28(2).
- Gardner, W.P., Susong, D.D., Solomon, D.K. et Heasler, H.P. (2010). Using noble gases measured in spring discharge to trace hydrothermal processes in the Norris Geyser Basin, Yellowstone National Park, U.S.A. *Journal of Volcanology and Geothermal Research*, 198(3-4), 394-404.
- Gautheron, C. et Moreira, M. (2002). Helium signature of the subcontinental lithospheric mantle. *Earth and Planetary Science Letters*, 199(1), 39-47.
- Gautheron, C., Tassan-Got, L.; Barbarand, J. et Pagel, M. (2009). Effect of alpha-damage annealing on apatite (U-Th)/He thermochronology. *Chemical Geology*, 266(3-4), 157-170.

- Graham, D.W. (2002). Noble gas isotope geochemistry of mid-ocean ridge and ocean island basalts: Characterization of mantle source reservoirs. *Reviews in Mineralogy and Geochemistry*, 47(1), 247-317.
- Heaton, T. et Vogel, J. (1981). "Excess air" in groundwater. *Journal of Hydrology*, 50, 201-216.
- Hilton, D.R., Fischer, T.P. et Marty, B. (2002). Noble gases and volatile recycling at subduction zones. *Reviews in mineralogy and geochemistry*, 47(1), 319-370.
- Kipfer, R. et Peeters, F. (2002). *Using transient conservative and environmental tracers to study water exchange in Lake Issyk-Kul.* : Springer.
- Larocque, M., Gagné, S., Tremblay, L. et Meyzonnat, G. (2013). Projet de connaissance des eaux souterraines du bassin versant de la rivière Bécancour et de la MRC de Bécancour. *Rapport final présenté au Ministère du Développement durable, de l'Environnement, de la Faune et des Parcs* (219 pp.).
- Larocque, M., Meyzonnat, G., Barbecot, F., Pinti, D., Gagné, S., Barnetche, D., Ouellet, M. et Graveline, M. (2015). Projet de connaissance des eaux souterraines de la zone de Vaudreuil-Soulanges *Rapport final présenté au Ministère du Développement durable, de l'Environnement, de la Faune et des Parcs* (203pp.)
- Lemieux, J.M., Sudicky, E., Peltier, W. et Tarasov, L. (2008). Dynamics of groundwater recharge and seepage over the Canadian landscape during the Wisconsinian glaciation. *Journal of Geophysical Research: Earth Surface* (2003–2012), 113(F1).
- Malka, E., Stevenson, R.K. et David, J. (2000). Sm - Nd geochemistry and U - Pb geochronology of the Mont Rigaud stock, Quebec, Canada: a late magmatic event associated with the formation of the Iapetus rift. *The Journal of Geology*, 108(5), 569-583.
- Marty, B., Torgersen, T., Meynier, V., O'Nions, R.K. et Marsily, G. (1993). Helium isotope fluxes and groundwater ages in the Dogger Aquifer, Paris Basin. *Water resources research*, 29(4), 1025-1035.
- Marty, B., Tolstikhin, I., Kamensky, I.L., Nivin, V., Balaganskaya, E. et Zimmermann, J.-L. (1998). Plume-derived rare gases in 380 Ma carbonatites from the Kola region (Russia) and the argon isotopic composition in the deep mantle. *Earth and Planetary Science Letters*, 164(1), 179-192.
- Matsuda, J., Matsumoto, T., Sumino, H., Nagao, K., Yamamoto, J., Miura, Y., Kaneoka, I., Takahata, N. et Sano, Y. (2002). The ${}^3\text{He}/{}^4\text{He}$ ratio of the new internal He Standard of Japan (HESJ). *Geochemical Journal*, 36(2), 191-195.

- McHone, J.G. (1996). Broad-terrane Jurassic flood basalts across northeastern North America. *Geology*, 24(4), 319-322.
- Meyzonnat, G., Larocque, M., Barbecot, F., Pinti, D. et Gagné, S. (2016). The potential of major ion chemistry to assess groundwater vulnerability of a regional aquifer in southern Quebec (Canada). *Environmental Earth Sciences*, 75(1), 1-12.
- Morikawa, A., Suzuki, T., Kanazawa, T., Kikuta, K., Suda, A. et Shinjo, H. (2008). A new concept in high performance ceria-zirconia oxygen storage capacity material with Al_2O_3 as a diffusion barrier. *Applied Catalysis B: Environmental*, 78(3), 210-221.
- Morrison, P. et Pine, J. (1955). Radiogenic origin of the helium isotopes in rock. *Annals of the New York Academy of Sciences*, 62(3), 71-92.
- Occhietti, S., Parent, M., Shilts, W.W., Dionne, J.-C., Govare, E. et Harmand, D. (2001). Late Wisconsinan glacial dynamics, deglaciation, and marine invasion in southern Québec. *Special papers-geological society of america*, 243-270.
- Ozima, M. et Podosek, F. (1983). *Noble gas chemistry*: Cambridge, United Kingdom : Cambridge Univ. Press.
- Pinti, D.L. et Marty, B. (1998). Separation of noble gas mixtures from petroleum and their isotopic analysis by mass spectrometry. *Journal of Chromatography A*, 824(1), 109-117.
- Pinti, D.L., Béland-Otis, C., Tremblay, A., Castro, M.C., Hall, C.M., Marcil, J.-S., Lavoie, J.-Y. et Lapointe, R. (2011). Fossil brines preserved in the St-Lawrence Lowlands, Québec, Canada as revealed by their chemistry and noble gas isotopes. *Geochimica et Cosmochimica Acta*, 75(15), 4228-4243.
- Pinti, D.L., Castro, M.C., Shouakar-Stash, O., Tremblay, A., Garduño, V.H., Hall, C.M., Hélie, J.F. et Ghaleb, B. (2013). Evolution of the geothermal fluids at Los Azufres, Mexico, as traced by noble gas isotopes, $\delta^{18}\text{O}$, δD , $\delta^{13}\text{C}$ and $87\text{Sr}/86\text{Sr}$. *Journal of Volcanology and Geothermal Research* 249, 1-11.
- Pinti, D.L., Retailleau, S., Barnetche, D., Moreira, F., Moritz, A.M., Larocque, M., Gélinas, Y., Lefebvre, R., Hélie, J.-F., Valadez, A. (2014). 222Rn activity in groundwater of the St. Lawrence Lowlands, Quebec, eastern Canada: Relation with local geology and health hazard, *Journal of environmental radioactivity*, 136, 206-217.
- Pinti, D.L., Béland-Otis, C., Tremblay, A., Castro, M.C., Hall, C.M., Marcil, J.-S., Lavoie, J.-Y. et Lapointe, R. (2011). Fossil brines preserved in the St-Lawrence Lowlands, Québec, Canada as revealed by their chemistry and noble gas isotopes. *Geochimica et Cosmochimica Acta*, 75(15), 4228-4243.

- Roulleau, E., Pinti, D.L., Stevenson, R.K., Takahata, N., Sano, Y. et Pitre, F. (2012). N, Ar and Pb isotopic co-variations in magmatic minerals: Discriminating fractionation processes from magmatic sources in Montréal Hills, Québec, Canada. *Chemical Geology*, 326–327, 123-131.
- Roulleau, E. et Stevenson, R. (2013). Geochemical and isotopic (Nd–Sr–Hf–Pb) evidence for a lithospheric mantle source in the formation of the alkaline Montréal Province (Quebec). *Canadian Journal of Earth Sciences*, 50(6), 650-666.
- Saar, M., Castro, M., Hall, C., Manga, M. et Rose, T. (2005). Quantifying magmatic, crustal, and atmospheric helium contributions to volcanic aquifers using all stable noble gases: Implications for magmatism and groundwater flow. *Geochemistry, Geophysics, Geosystems*, 6(3).
- Saby, M., Larocque, M., Pinti, D.L., Barbecot, F., Sano, Y. et Castro, M.C. (2016). Linking groundwater quality to residence times and regional geology in the St. Lawrence Lowlands, southern Quebec, Canada. *Applied Geochemistry*, 65, 1-13.
- Sano, Y., Horiguchi, K., Takahata, N., Shirai, K., Oda, S. et Gamo, T. (2006). Helium isotopes of seawater in adjacent sea of Japan. *Geochimica et Cosmochimica Acta*, 70(18, Supplement), A555.
- Sano, Y., Tokutake, T. et Takahata, N. (2008). Accurate measurement of atmospheric helium isotopes. *Analytical Sciences*, 24(4), 521-525.
- Sasada, T., Hiyagon, H., Bell, K. et Ebihara, M. (1997). Mantle-derived noble gases in carbonatites. *Geochimica et cosmochimica acta*, 61(19), 4219-4228.
- Schlosser, P., Stute, M., Sonntag, C. et Munnich, K. (1989). Tritiogenic ^3He in shallow groundwater. *Earth Planet. Sci. Lett*, 94, 245-256.
- Sleep, N.H. (1990). Montréal hotspot track: A long - lived mantle plume. *Journal of Geophysical Research: Solid Earth* (1978–2012), 95(B13), 21983-21990.
- Smith, S. et Kennedy, B. (1983). The solubility of noble gases in water and in NaCl brine. *Geochimica et Cosmochimica Acta*, 47(3), 503-515.
- Stuart, F.M., Lass-Evans, S., Fitton, J.G. et Ellam, R.M. (2003). High $^3\text{He}/^4\text{He}$ ratios in picritic basalts from Baffin Island and the role of a mixed reservoir in mantle plumes. *Nature*, 424(6944), 57-59.
- Torgersen, T. (1980). Controls on pore-fluid concentration of ^4He and ^{222}Rn and the calculation of $^4\text{He}/^{222}\text{Rn}$ ages. *Journal of Geochemical Exploration*, 13(1), 57-75.

- Torgersen, T. (1993). Defining the role of magmatism in extensional tectonics: Helium 3 fluxes in extensional basins. *Journal of Geophysical Research: Solid Earth* (1978–2012), 98(B9), 16257-16269.
- Torgersen, T. et Clarke, W.B. (1985). Helium accumulation in groundwater, I: An evaluation of sources and the continental flux of crustal ${}^4\text{He}$ in the Great Artesian Basin, Australia. *Geochimica et Cosmochimica Acta*, 49(5), 1211-1218.
- Torgersen, T. et Jenkins, W. (1982). Helium isotopes in geothermal systems: Iceland, the geysers, raft river and steamboat springs. *Geochimica et Cosmochimica Acta*, 46(5), 739-748.
- Torgersen, T., Drenkard, S., Farley, K., Schlosser, P. et Shapiro, A. (1994). Mantle helium in the groundwater of the Mirror Lake Basin, New Hampshire. USA In *Noble Gas Geochemistry and Cosmochemistry*, ed. J. Matsuda, 279-292 : Tokyo: Terra Scientific Publishing Co.
- Torgersen, T., Drenkard, S., Stute, M., Schlosser, P. et Shapiro, A. (1995). Mantle helium in ground waters of eastern North America: Time and space constraints on sources. *Geology*, 23(8), 675-678.
- Tran Ngoc, T., Lefebvre, R., Konstantinovskaya, E. et Malo, M. (2014). Characterization of deep saline aquifers in the Bécancour area, St. Lawrence Lowlands, Québec, Canada: Implications for CO_2 geological storage. *Environmental geology*, 72(1), 119-146.
- Tremblay, A. et Castonguay, S. (2002). Structural evolution of the Laurentian margin revisited (southern Quebec Appalachians): Implications for the Salinian orogeny and successor basins. *Geology*, 30(1), 79-82.
- Tremblay, A., Roden-Tice, M.K., Brandt, J.A. et Megan, T.W. (2013). Mesozoic fault reactivation along the St. Lawrence rift system, eastern Canada: Thermochronologic evidence from apatite fission-track dating. *Geological Society of America Bulletin*, 125(5-6), 794-810.
- Vautour, G., Pinti, D.L., Méjean, P., Saby, M., Meyzonnat, G., Larocque, M., Castro, M.C., Hall, C.M., Boucher, C., Roulleau, E., Barbecot, F., Takahata, N. et Sano, Y. (2015). ${}^3\text{H}/{}^3\text{He}$, ${}^{14}\text{C}$ and (U-Th)/He groundwater ages in the St. Lawrence Lowlands, Quebec, Eastern Canada. *Chemical Geology*, 413, 94-106.
- Weise, S. et Moser, H. (1987). Groundwater dating with helium isotopes. *Isotope techniques in water resources development. IAEA, Vienna*, 105-126.
- Wen, J., Bell, K. et Blenkinsop, J. (1987). Nd and Sr isotope systematics of the Oka complex, Quebec, and their bearing on the evolution of the sub-continental upper mantle. *Contributions to Mineralogy and Petrology*, 97(4), 433-437.

Zurevinski, S.E. et Mitchell, R.H. (2004). Extreme compositional variation of pyrochlore-group minerals at the Oka carbonatite complex, Quebec: evidence of magma mixing? *The Canadian Mineralogist*, 42(4), 1159-1168.

FIGURES

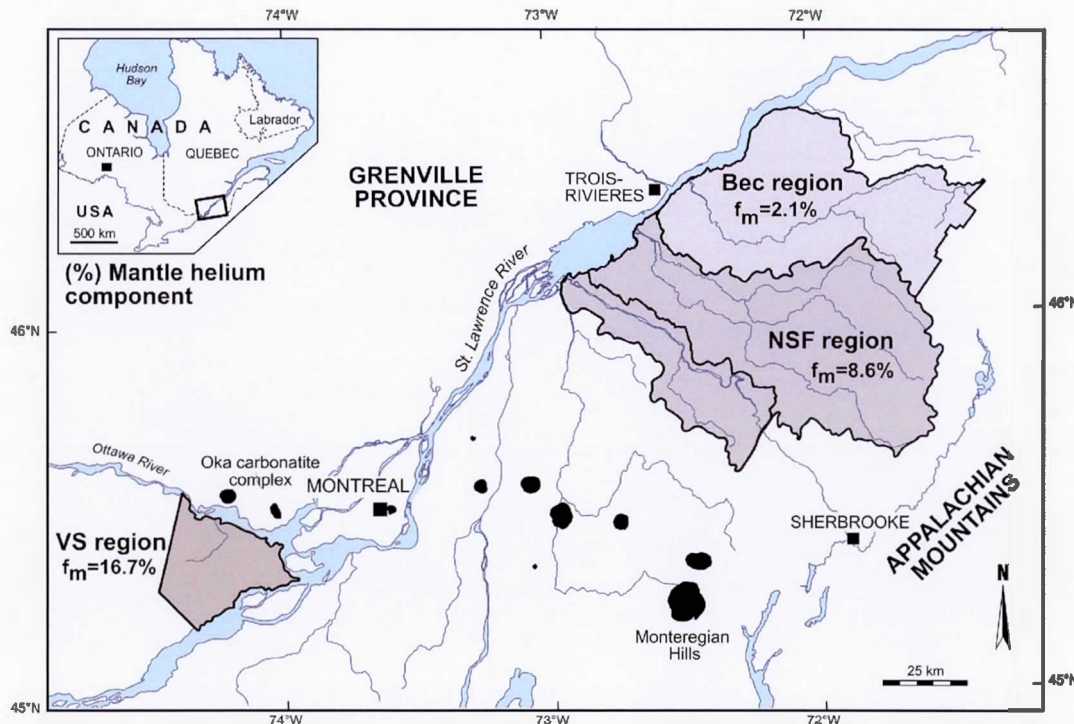


Figure 3.1 Location map of the St. Lawrence Lowlands including the intrusions of the Cretaceous Montréal Hills, the Bécancour region (BEC), the Nicolet and lower Saint-François River region (NSF), and the Vaudreuil-Soulanges watershed (VS). The percentage of mantle helium (f_m) measured in each watershed is also indicated.

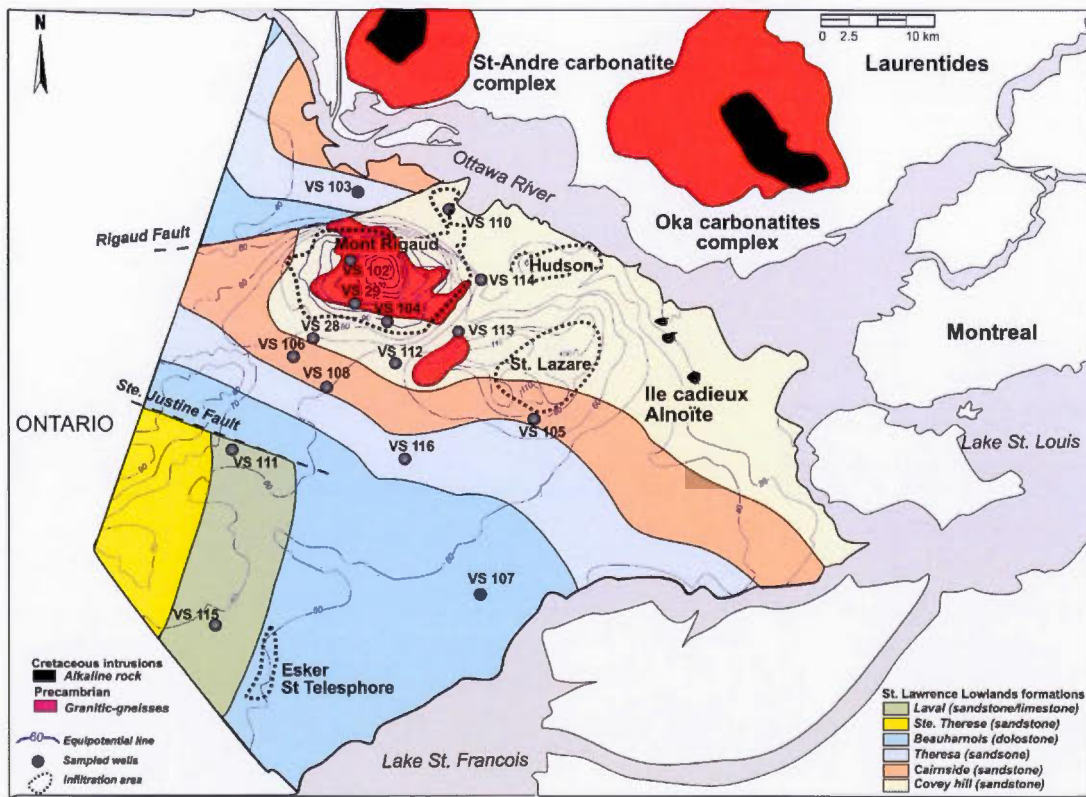


Figure 3.2 Geological map of the VS region with piezometric heads and location of the sampled wells.

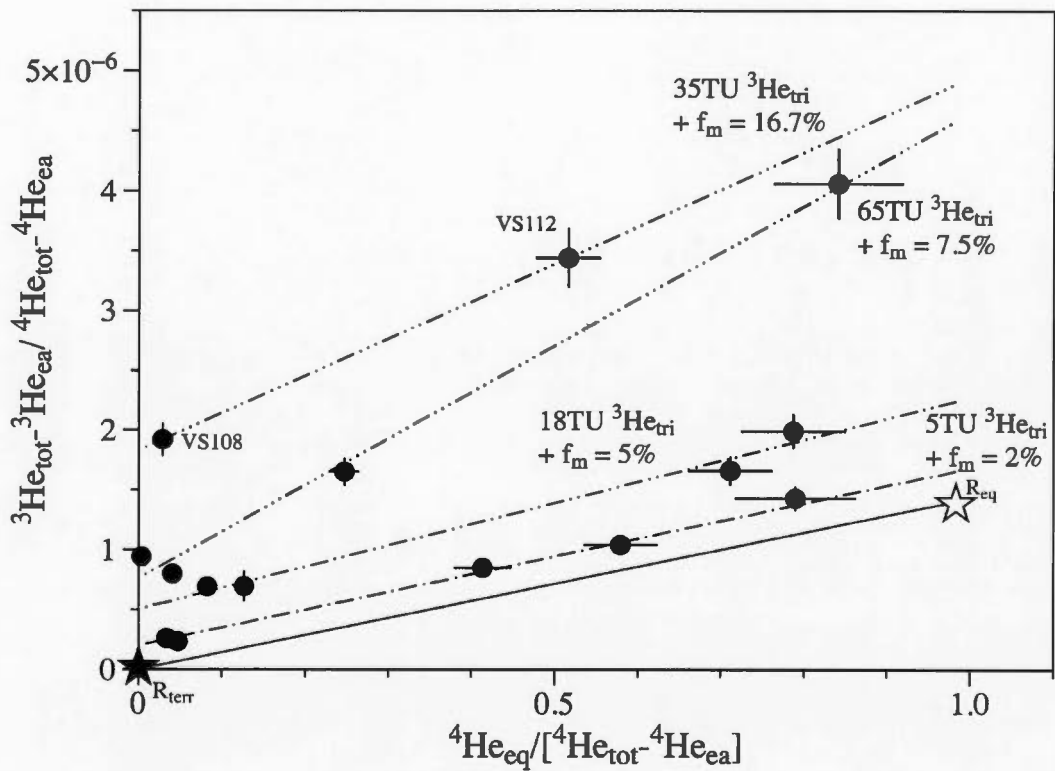


Figure 3.3 Weise-type plot of measured helium ratios corrected for air bubble entrainment ($({}^3\text{He} / {}^4\text{He})_{\text{total}} - ({}^3\text{He} / {}^4\text{He})_{\text{ea}}$) vs. the relative amount of ${}^4\text{He}$ derived from solubility with respect to total He, corrected for air bubble entrainment (${}^4\text{He}_{\text{ea}} / ({}^4\text{He}_{\text{tot}} - {}^4\text{He}_{\text{ea}})$) in VS groundwater. The black line represents the mixing between water at the recharge (Air Saturated Water or ASW). Dashed lines interpolated through samples represent the addition of 5, 18, 35 and 65 TU helium, mixed with the terrigenic components having variable R_{terr} . The stars represent the ASW (R_{eq}) and terrigenic (R_{terr}) helium end-members.

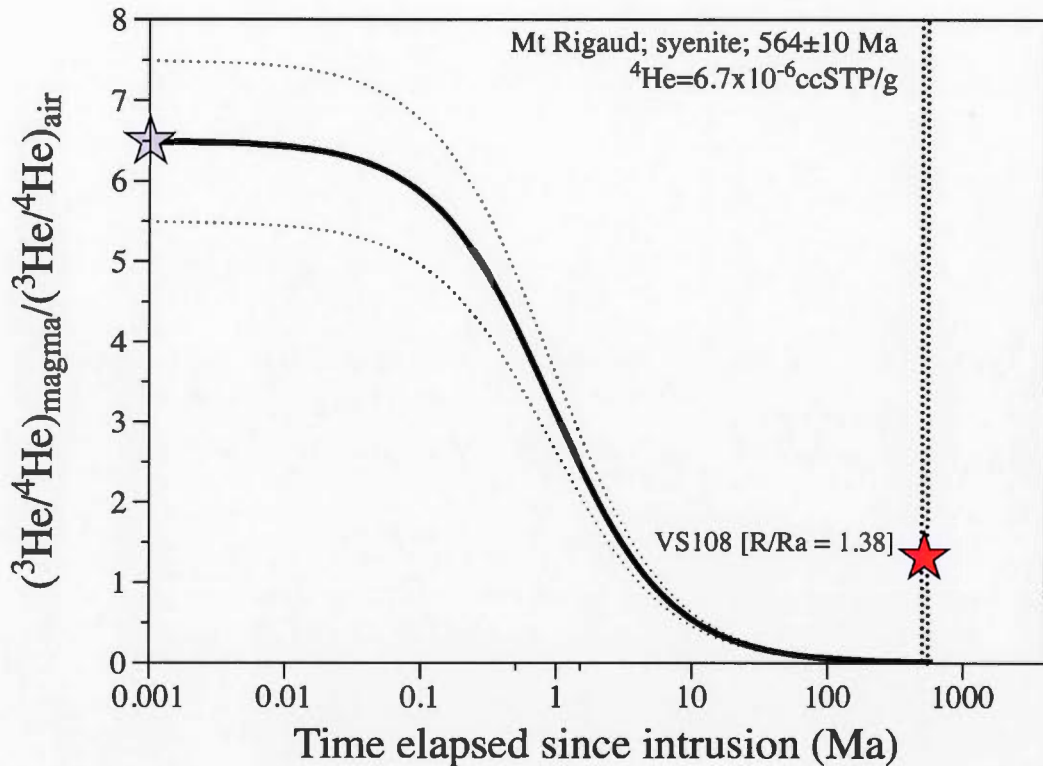


Figure 3.4 Evolution of the $[\text{R/Ra}]_{\text{magma}}$ as a function of time elapsed since the intrusion of the Precambrian syenite of Mont Rigaud (564^{+10}_{-8} Ma) using the “magma aging” model of Torgersen et al. (1995; eqn. 3.2) (bold line). Initial helium ratio R/Ra for a SLCM was fixed at 6.5 (grey star). Dashed lines represent evolution of the SLCM source taking into account uncertainties on the initial R/Ra . The R/Ra measured in VS108 (16.7% of total helium) is represented by a red star.

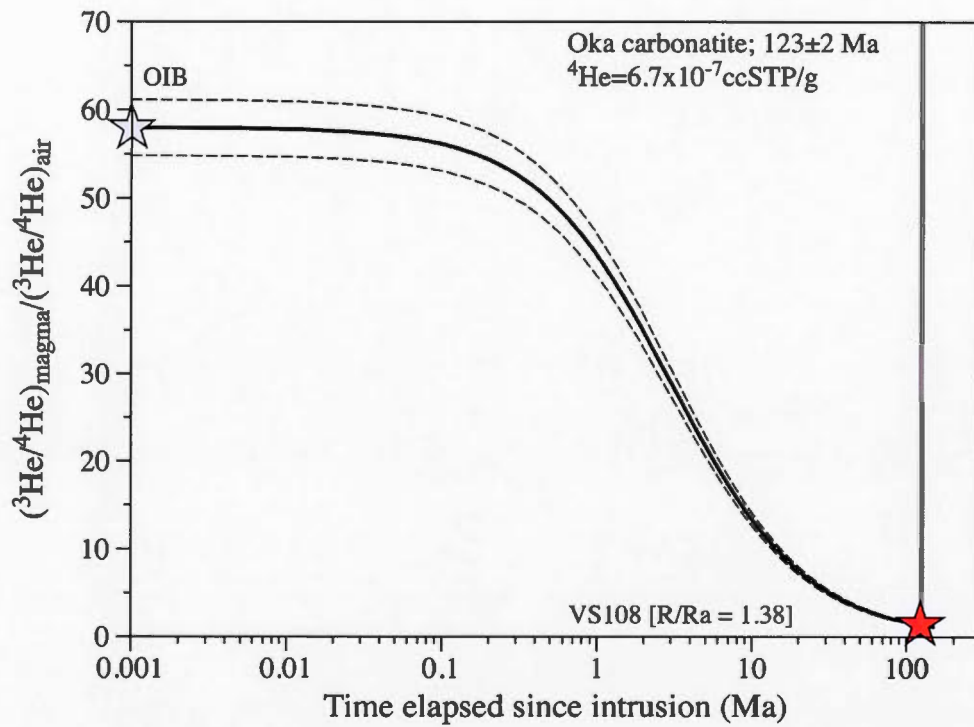


Figure 3.5 Evolution of the $[\text{R/Ra}]_{\text{magma}}$ as a function of time elapsed since the intrusion of (a) Oka carbonatite 123±2 Ma ago using the “magma aging” model of Torgersen *et al.* (1995; eqn. 3.2) (bold line). Dashed lines represent evolution of the OIB source taking into account uncertainties on the initial R/Ra. The R/Ra measured in VS108 (16.7% of total helium) is represented by a red star.

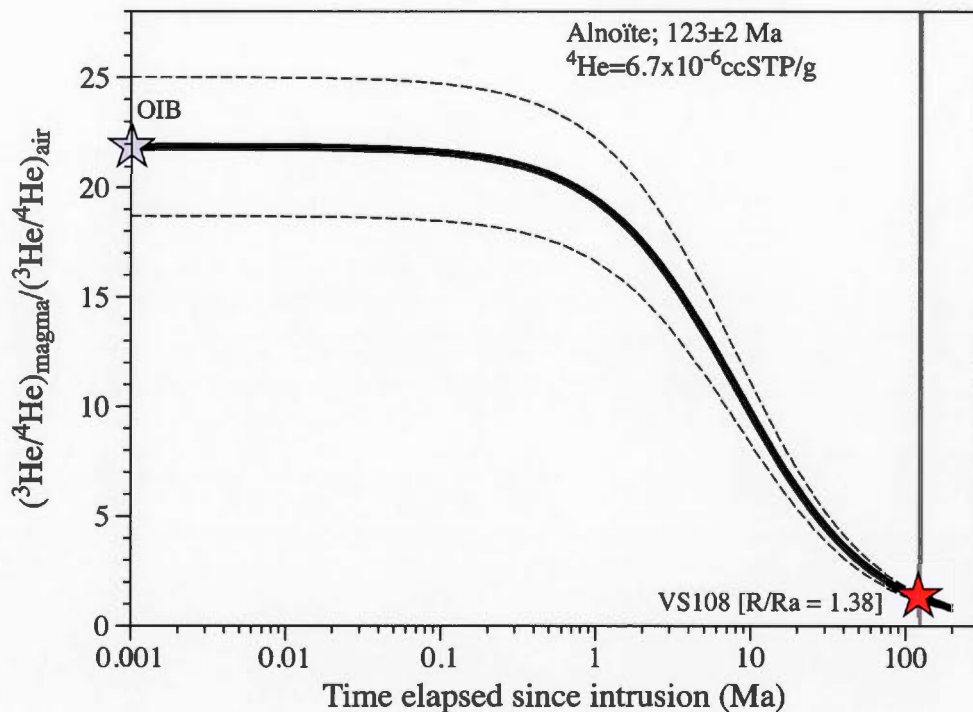


Figure 3.6 Evolution of the $[\text{R/Ra}]_{\text{magma}}$ as a function of time elapsed since the intrusion of (a) Oka carbonatite and (b) alnoïte 123 ± 2 Ma ago using the “magma aging” model of Torgersen *et al.* (1995; eqn. 3.2) (bold line). Dashed lines represent evolution of the OIB source taking into account uncertainties on the initial R/Ra. The R/Ra measured in VS108 (16.7% of total helium) is represented by a red star.

Tableau 3.1 Hydrogeological characteristics of the groundwaters sampled in VS region together with helium isotopic data.

Sample	Water chemistry	Depth m	Geology Group	Temp °C	pH	TDS mg/L
VS102 (M)	Ca-HCO ₃	62.0	Grenville basement	9.3	7.2	323.7
VS103 (M)	Na-Cl	50.3	Beekmantown	9.6	7.7	1186.2
VS104 (M)	Ca-HCO ₃	42.0	Potsdam	9.7	8.1	325.1
VS105 (PZ)	Ca-HCO ₃	52.4	Potsdam	9.8	8.5	256.7
VS106 (PZ)	Na-HCO ₃	32.9	Potsdam	9.1	7.1	467.0
VS107 (PZ)	Ca-HCO ₃	20.4	Beekmantown	10.8	7.7	676.2
VS108 (P)	Na-Cl	96.0	Potsdam	10.2	7.3	861.7
VS110 (P)	Ca-HCO ₃	49.0	Potsdam	11.0	7.8	560.1
VS111 (P)	Ca-HCO ₃	58.0	Laval	11.4	7.6	572.9
VS112 (P)	Ca-HCO ₃	41.8	Potsdam	10.1	8.3	256.4
VS113 (P)	Na-HCO ₃	91.0	Potsdam	10.0	8.1	786.8
VS114 (P)	Na-Cl	54.9	Potsdam	10.0	8.5	783.6
VS115 (P)	Ca-SO ₄	27.0	Laval	10.5	7.2	1482.1
VS116 (P)	Na-Cl	62.0	Beekmantown	10.1	8.3	686.2
VS28 (P)	Mg-HCO ₃	42.7	Potsdam	10.8	8.8	341.5
VS29 (P)	Na-HCO ₃	67.0	Grenville basement	13.7	8.2	312.8

Notes :

M: municipal well; P: private well; PZ: instrumented piezometer.

(³He/⁴He)air = 1.386 x 10⁻⁶ (Ozima et Podosek, 1993)

Tableau 3.1 suite

	${}^4\text{He}$ $\text{cm}^3\text{STP/g}$	\pm $\times 10^{-8}$	${}^{20}\text{Ne}$ $\text{cm}^3\text{STP/g}$	\pm $\times 10^{-7}$	$({}^3\text{He}/{}^4\text{He})_{\text{sample}}$	\pm
VS102 (M)	9.28	0.46	2.87	0.14	1.02	0.01
VS103 (M)	116.10	5.81	2.11	0.11	0.58	0.01
VS104 (M)	6.15	0.31	1.72	0.09	1.20	0.02
VS105 (PZ)	8.81	0.44	2.83	0.14	2.23	0.02
VS106 (PZ)	19.46	0.97	1.95	0.10	1.19	0.01
VS107 (PZ)	7.46	0.37	2.28	0.11	1.35	0.02
VS108 (P)	166.64	8.33	2.79	0.14	1.38	0.01
VS110 (P)	9.26	0.46	2.17	0.11	0.78	0.01
VS111 (P)	133.98	6.70	1.75	0.09	0.19	0.01
VS112 (P)	10.19	0.51	2.16	0.11	2.33	0.02
VS113 (P)	4.41	0.22	1.87	0.09	0.41	0.01
VS114 (P)	1323.18	66.16	1.78	0.09	0.68	0.01
VS115 (P)	100.56	5.03	2.25	0.11	0.18	0.01
VS116 (P)	39.39	1.97	2.54	0.13	0.53	0.01
VS28 (P)	15.19	0.76	3.01	0.15	0.71	0.01
VS29 (P)	135.59	6.78	1.34	0.07	0.28	0.01

Notes :

M: municipal well; P: private well; PZ: instrumented piezometer.

 $({}^3\text{He}/{}^4\text{He})_{\text{air}} = 1.386 \times 10^{-6}$ (Ozima et Podosek, 1993)

Tableau 3.1 suite

${}^4\text{He}$	\pm	${}^{20}\text{Ne}$	\pm	$({}^3\text{He}/{}^4\text{He})_{\text{sample}}$	\pm
cm ³ STP/g		cm ³ STP/g		$({}^3\text{He}/{}^4\text{He})_{\text{air}}$	
x 10 ⁻⁸		x 10 ⁻⁷			
9.28	0.46	2.87	0.14	1.02	0.01
116.10	5.81	2.11	0.11	0.58	0.01
6.15	0.31	1.72	0.09	1.20	0.02
8.81	0.44	2.83	0.14	2.23	0.02
19.46	0.97	1.95	0.10	1.19	0.01
7.46	0.37	2.28	0.11	1.35	0.02
166.64	8.33	2.79	0.14	1.38	0.01
9.26	0.46	2.17	0.11	0.78	0.01
133.98	6.70	1.75	0.09	0.19	0.01
10.19	0.51	2.16	0.11	2.33	0.02
4.41	0.22	1.87	0.09	0.41	0.01
1323.18	66.16	1.78	0.09	0.68	0.01
100.56	5.03	2.25	0.11	0.18	0.01
39.39	1.97	2.54	0.13	0.53	0.01
15.19	0.76	3.01	0.15	0.71	0.01
135.59	6.78	1.34	0.07	0.28	0.01

Notes :

M: municipal well; P: private well; PZ: instrumented piezometer.

 $({}^3\text{He}/{}^4\text{He})_{\text{air}} = 1.386 \times 10^{-6}$ (Ozima et Podosek, 1993)

Tableau 3.2 Hydrogeological characteristics of the groundwaters sampled in VS region together with helium isotopic data.

Sample	Phase	Temp °C	$^{3}\text{He}/^{4}\text{He}$	± Ra	[^{4}He] cm $^3\text{STP/g}$	±
Alnoite	Bulk		0.06	0.03	4.33E-05	
Oka carbonatite -1	Bulk		0.60	0.01	5.83E-05	
Oka carbonatite -2	Bulk		n.d		n.d	
Oka carbonatite *	Diopside	800	0.34	0.1	8.20E-06	
Oka carbonatite *	Diopside	1400	3.52	0.35	1.13E-06	
Oka carbonatite *	Monticellite	1000	0.43	0.13	1.16E-05	

* Data from Sasada et al. (1997).

[^{3}He] cm $^3\text{STP/g}$	±	[U] ppm	±	[Th] ppm	±
3.60E-12		3.3	0.1	15.4	0.2
4.85E-11		9.9	0.1	40.9	0.2
n.d		110.0	0.1	8.0	0.2
3.86E-12		n.d		n.d	
5.51E-12		n.d		n.d	
6.91E-12		n.d		n.d	

CONCLUSIONS GÉNÉRALES

Cette thèse s'inscrit dans une vaste démarche d'acquisition de connaissances sur les eaux souterraines du Québec méridional et en particulier des systèmes hydrogéologiques des Basses-Terres du Saint-Laurent. Cette région, la plus peuplée au Québec utilise l'eau souterraine principalement pour des fins agricoles, industrielles et comme source d'eau potable.

L'objectif de cette thèse était d'identifier et de quantifier l'origine de toutes les composantes d'hélium présentes, soit la composante terrigénique (production crustale de ${}^4\text{He}_{\text{ter}}$ ou mantélique de ${}^3\text{He}_{\text{ter}}$), la composante atmosphérique acquise à la recharge (${}^3\text{He}_{\text{ASW}}$ et ${}^4\text{He}_{\text{ASW}}$) et la composante tritiogénique (${}^3\text{He}_{\text{tri}}$) afin de contraindre les méthodes de datation ${}^3\text{H}/{}^3\text{He}$ et U-Th/ ${}^4\text{He}$. Le calcul de ces âges isotopiques nécessite d'identifier et de quantifier l'origine de toutes les composantes de l'hélium présent, soit la composante terrigénique (production crustale de ${}^4\text{He}_{\text{ter}}$ ou mantélique de ${}^3\text{He}_{\text{ter}}$), la composante atmosphérique acquise lors de la recharge (${}^3\text{He}_{\text{ASW}}$ et ${}^4\text{He}_{\text{ASW}}$) et la composante tritiogénique (${}^3\text{He}_{\text{tri}}$).

La particularité de ces méthodes de datation réside dans la complémentarité des gammes d'âges qu'elles couvrent, allant de la dizaine d'années pour la méthode ${}^3\text{H}/{}^3\text{He}$, jusqu'à plusieurs centaines de milliers d'années, voire potentiellement des millions d'années, pour la méthode (U-Th)/ ${}^4\text{He}$. Deux approches ont été menées ici, lorsque seulement la composante radiogénique de ${}^4\text{He}$ était en excès, le rapport en hélium ${}^3\text{He}/{}^4\text{He}$ (R) a été couplé au rapport d'activité isotopique (${}^{234}\text{U}/{}^{238}\text{U}$)_{act} afin d'identifier les masses d'eaux présentes et de mettre en évidence les processus d'interaction eaux-roches qui ont permis la minéralisation des eaux, de même que la mise en solution de l'isotope ${}^4\text{He}$ et des isotopes de l'uranium (${}^{234}\text{U}$ et ${}^{238}\text{U}$). Ce sont

ici les phénomènes de dissolution de la roche ainsi que de mise en solution préférentielle de ^{234}U qui ont été observés depuis la zone de recharge des eaux jusqu'à leur résurgence.

En présence d'excès d' ^3H d'origine mantellique, la présence d'intrusions magmatiques potentiellement porteuses d'une signature mantellique a été testé afin d'évaluer si la signature mantellique a conservé suffisamment d' ^3He mantellique face aux contaminations crustales (production ^4He par désintégration de U et Th) pour être transmise aux eaux souterraines.

Dans la région de Bécancour, les précédents travaux ont révélé la présence d'excès en ^4He qui ne peuvent s'expliquer ni par une production locale, ni par un flux crustal. Dans le premier volet de la thèse, une relation inverse entre le rapport $^3\text{He}/^4\text{He}$ de l'échantillon normalisé au rapport de l'atmosphère $(^3\text{He}/^4\text{He})_{\text{éch}}/(^3\text{He}/^4\text{He})_{\text{atm}}$ (i.e. R/Ra) et le rapport $(^{234}\text{U}/^{238}\text{U})_{\text{act}}$ a été mis en évidence pour la première fois dans des échantillons d'eaux souterraines provenant d'aquifères granulaires et fracturés de la région de Bécancour. Les eaux les plus jeunes (contenant de ^3He tritiogénique ; R=3.1Ra) ont les rapports $(^{234}\text{U}/^{238}\text{U})_{\text{act}}$ les plus faibles (≈ 1.1), correspondant à la dissolution de la roche encaissante lors de l'infiltration des eaux. En revanche, les eaux les plus anciennes (ayant accumulé de l' ^4He radiogénique ; R=0.012Ra) ont les rapports $(^{234}\text{U}/^{238}\text{U})_{\text{act}}$ les plus élevés, jusqu'à 6.07. Les eaux souterraines auraient donc accumulé à la fois du ^4He et l'isotope ^{234}U le long des lignes d'écoulement. L'ensemble des échantillons étudiés s'explique par un mélange entre ces deux pôles isotopiques. Ces excès sont interprétés comme provenant d'une source locale dans l'aquifère, qui serait le ^4He produit et accumulé dans la roche, relâché de façon rapide dans l'eau porale grâce à l'augmentation de la densité de fractures dans l'aquifère (i.e. la surface de contact eau-roche) suite au dernier retrait glaciaire (≈ 12 ka).

Pour vérifier cette hypothèse, un modèle de mise en solution préférentielle de ^{234}U et un modèle tenant compte de la relâche de ^4He par augmentation de la surface de

contact eau-roche et par diminution de la taille des grains ont été combinés dans le deuxième volet de la thèse. Le premier modèle prédit l'évolution de $(^{234}\text{U}/^{238}\text{U})_{\text{act}}$ à partir du moment où la nappe devient captive. Dans ce cas $(^{234}\text{U}/^{238}\text{U})_{\text{act}}$ évoluera en fonction de la désintégration de ^{234}U en excès dans l'eau et de sa production par désintégration du ^{234}Th , en considérant les paramètres hydrogéologiques de l'aquifère. La surface spécifique ($S = 5746 \text{ cm}^2.\text{cm}^{-3}$) associée à une taille de grain ($r = 17\mu\text{m}$) nécessaires pour obtenir un rapport $(^{234}\text{U}/^{238}\text{U})_{\text{act}} = 6.07$ en 6.6 kyrs ont été estimés. Cette taille de grain a ensuite été utilisée dans le second modèle pour estimer la quantité totale de ^4He produit puis relâché dans l'eau à partir de l'uranium et du thorium contenu dans la roche. La quantité de ^4He relâchée depuis la dernière déglaciation a été estimée entre $1.55 \times 10^{-5} \text{ ccSTP.g}_{\text{rock}}^{-1}$ et $2.52 \times 10^{-5} \text{ ccSTP.g}_{\text{rock}}^{-1}$. C'est ici une valeur maximale qui ne tient pas compte des processus de pertes de ^4He par diffusion et pas dispersion dans les eaux au cours du temps.

Le troisième volet de la thèse a étudié les eaux de l'aquifère fracturé de la zone de Vaudreuil-Soulanges où la composante mantellique de l'hélium la plus élevée du Québec a été mesurée (16.7% de l'hélium total). Le vieillissement d'une signature mantellique acquise par les intrusions mantelliennes présentes dans la région (Mont-Rigaud : 564 Ma et intrusions montérégienennes : 123 Ma) comme sources potentielle d'hélium mantellique a été testé. En tenant compte de la production locale de ^4He par désintégration de U et Th contenus dans les roches, les résultats ont montré que le Mont Rigaud, issu du manteau appauvri avec une signature initial $R/R = 6.5 \pm 1$, ne peut pas aujourd'hui avoir conservé une signature mantellique fossile assez élevée pour être à l'origine du rapport $R/R = 1.38 \pm 0.01$ mesuré dans l'eau souterraine. Afin de tester l'implication des intrusions montérégienennes dans les excès en ^3He d'origine mantellique, deux échantillons de carbonatite provenant du complexe de carbonatite d'Oka situé à nord de la zone d'étude ainsi qu'un échantillon d'alnoïte provenant d'une intrusion située sur notre zone d'étude ont également été prélevés. En utilisant l'hypothèse que l'intrusion d'Oka était la source mantellique des eaux de Vaudreuil,

le rapport R/Ra de l'intrusion au moment de sa mise en place il y a environ 123 Ma a été estimé pour la carbonatite ainsi que pour l'alnoïte. Fait intéressant, un rapport initial pour la carbonatite de $R/Ra = 58 \pm 3.2$ et un rapport pour l'alnoïte de $R/Ra = 21.9 \pm 3.2$ ont été obtenus. Ces rapports isotopiques initiaux en hélium sont nettement supérieurs aux rapports impliqués dans la mise en place d'un manteau lithosphérique sub-continental ($R/Ra = 6.5-7.5$), ce qui l'exclut comme étant à l'origine de la mise en place des collines montérégienennes. Par contre, les rapports isotopiques nettement plus élevés ici calculés correspondent bien à un manteau profond non dégazé comme source des montérégienennes. Ce manteau est celui à l'origine des points chauds. Ces nouveaux résultats relancent le débat ouvert depuis plusieurs années quant à savoir qui du manteau supérieur appauvri lié à la réactivation du rift Saint-Laurent ou bien de la source mantellique profonde liée au passage du point chaud *Great Meteor* en Amérique du Nord est à l'origine de la mise en place des collines montérégienennes.

Afin de poursuivre la quantification des excès en ${}^4\text{He}$ radiogéniques relâchés depuis les roches sédimentaires d'un bassin, il serait pertinent de mieux contraindre l'estimation des paramètres reliés aux fractures (surface spécifique, ouverture de fracture, taille de grains) en couplant l'approche théorique avec des observations de terrains de ces mêmes fractures et leur étude plus détaillée en laboratoire afin de juger la crédibilité des données calculées.

Les modèles présentés ici constituent une première approximation des sources potentielles internes au système aquifère qui pourrait être suffisantes pour expliquer les excès en ${}^4\text{He}$ radiogénique qui viennent surestimés les âges (U-Th)/ ${}^4\text{He}$ calculés. Une deuxième approche théorique complémentaire pour être de tester le modèle de Torgersen et O'Donnell (1991) qui considère strictement la relâche de ${}^4\text{He}$ par l'augmentation de la densité de fractures.

Le fort potentiel de ce modèle pourra prouver sa pertinence dans d'autres types de formations post-glaciaires comme par exemple les dépôts sableux des eskers et moraines où des excès en ${}^4\text{He}$ ont eux aussi été mis en évidence.

Concernant la source mantellique identifiée dans l' ${}^3\text{He}$ total mesuré dans les eaux des Basses-Terres du Saint-Laurent, l'implication des intrusions magmatiques offre une nouvelle interprétation sur leurs conditions de mise en place en apportant une approche complémentaire aux études géochimiques strictement appliquée sur les roches constitutives. Il faudra pour renforcer l'étude présentée ici considérer une gamme plus large de valeurs de ${}^4\text{He}$ initial dans la roche qui est un paramètre important dans le modèle de vieillissement de la signature R/Ra du magma. Afin de tester la robustesse du modèle reliant la mise en place des intrusions montérégienennes avec une source mantellique profonde, un échantillonnage devrait être mené dans les eaux souterraines proches des autres intrusions pour compléter les données existantes en hélium dans les roches.

En conclusion, la caractérisation isotopique des eaux souterraines des aquifères fracturés au Québec aura apporté des connaissances permettant de contraindre l'application des méthodes de datation ${}^3\text{H}/{}^3\text{He}$ et $(\text{U-Th})/{}^4\text{He}$ afin d'estimer le plus précisément possible le temps de résidences des eaux sur une large gamme d'âges isotopiques. L'approche multi-isotopique s'est révélée un outil puissant pour comprendre l'origine des excès en hélium mesurée et estimer les interactions eaux-roches que subissent les eaux souterraines durant leur séjour dans les aquifères toujours en lien avec les événements géologiques qui ont modelés les paysages québécois. Il serait intéressant d'étendre ces approches isotopiques aux autres bassins versants du Québec afin d'avoir un regard plus général sur la dynamique des aquifères de l'est du Canada.

BIBLIOGRAPHIE

- Aggarwal, P.K., Matsumoto, T., Sturchio, N.C., Chang, H.K., Gastmans, D., Araguas-Araguas, L.J., Jiang, W., Lu, Z.-T., Mueller, P., Yokochi, R., Purtschert, R. et Torgersen, T. (2015). Continental degassing of 4He by surficial discharge of deep groundwater. *Nature Geosci*, 8(1), 35-39.
- Aktas, K. et Eaton, D.W. (2006). Upper-mantle velocity structure of the lower Great Lakes region. *Tectonophysics*, 420(1), 267-281.
- Andersen, M.B., Erel, Y. et Bourdon, B. (2009). Experimental evidence for ^{234}U - ^{238}U fractionation during granite weathering with implications for $^{234}\text{U}/^{238}\text{U}$ in natural waters. *Geochimica et Cosmochimica Acta*, 73(14), 4124-4141.
- Andrews, J. et Kay, R. (1978). The evolution of enhanced $^{234}\text{U}/^{238}\text{U}$ activity ratios for dissolved uranium and groundwater dating. *US Geological Survey Open-File Rep*, 78(701), 11-13.
- Andrews, J.N., Giles, I.S., Kay, R.L.F., Lee, D.J., Osmond, J.K., Cowart, J.B., Fritz, P., Barker, J.F. et Gale, J. (1982). Radioelements, radiogenic helium and age relationships for groundwaters from the granites at Stripa, Sweden. *Geochimica et Cosmochimica Acta*, 46(9), 1533-1543.
- Andrews, J.N. et Kay, R.L.F. (1982). $^{234}\text{U}/^{238}\text{U}$ activity ratios of dissolved uranium in groundwaters from a jurassic limestone aquifer in England. *Earth and Planetary Science Letters*, 57(1), 139-151.
- Andrews, J.N. et Kay, R.L.F. (1983). The U contents and $^{234}\text{U}/^{238}\text{U}$ activity ratios of dissolved uranium in groundwaters from some Triassic Sandstones in England. *Chemical Geology*, 41, 101-117.
- Aquilina, L., Vergnaud-Ayraud, V., Les Landes, A.A., Pauwels, H., Davy, P., Pételet-Giraud, E., Labasque, T., Roques, C., Chatton, E. et Bour, O. (2015). Impact of climate changes during the last 5 million years on groundwater in basement aquifers. *Scientific reports*, 5.
- Aravena, R., Wassenaar, L.I. et Plummer, L.N. (1995). Estimating ^{14}C groundwater ages in a methanogenic aquifer. *Water Resources Research*, 31(9), 2307-2317.
- Ballentine, C.J. et Burnard, P.G. (2002). Production, release and transport of noble gases in the continental crust. *Reviews in mineralogy and geochemistry*, 47(1), 481-538.

- Ballentine, C.J. et O'Nions, R.K. (1992). The nature of mantle neon contributions to Vienna Basin hydrocarbon reservoirs. *Earth and Planetary Science Letters*, 113(4), 553-567.
- Banner, J.L., Wasserburg, G., Chen, J.H. et Moore, C.H. (1990). ^{234}U - ^{238}U - ^{230}Th - ^{232}Th systematics in saline groundwaters from central Missouri. *Earth and Planetary Science Letters*, 101(2), 296-312.
- Benson, B.B. et Krause Jr, D. (1980). Isotopic fractionation of helium during solution: A probe for the liquid state. *Journal of Solution Chemistry*, 9(12), 895-909.
- Benoît, N., Blanchette, D., Nasterv, M. et Molson, J.N. (2011). *Groundwater geochemistry of the Lower Chaudière River Watershed, Québec*. Proceedings of the International Association of Hydrogeologists-Canadian National Chapter (IAH-CNC)/Canadian Quaternary Association (CANQUA) Conference: GeoHydro 2011.
- Bonotto, D.M. et Andrews, J.N. (1993). The mechanism of $^{234}\text{U}/^{238}\text{U}$ activity ratio enhancement in karstic limestone groundwater. *Chemical Geology*, 103, 193-206.
- Bonotto, D.M. et Andrews, J.N. (2000). The transfer of uranium isotopes ^{234}U and ^{238}U to the waters interacting with carbonates from Mendip Hills area (England). *Applied Radiation and Isotopes*, 52(4), 965-983.
- Bottomley, D.J., Renaud, R., Kotzer, T. et Clark, I.D. (2002). Iodine-129 constraints on residence times of deep marine brines in the Canadian Shield. *Geology*, 30(7), 587-590.
- Burnard, P., Zimmermann, L. et Sano, Y., 2013. The noble gases as geochemical tracers: history and background. In: Burnard, P. (Ed.), *The Noble Gases as Geochemical Tracers*. Springer, Berlin, Heidelberg, 1–15.
- Carey, A.E., Dowling, C.B. et Poreda, R.J. (2004). Alabama Gulf Coast groundwaters: ^4He and ^{14}C as groundwater-dating tools. *Geology*, 32(4), 289-292.
- Castro, M.C., Ma, L. et Hall, C.M. (2009). A primordial, solar He-Ne signature in crustal fluids of a stable continental region. *Earth and Planetary Science Letters*, 279(3), 174-184.
- Cawood, P.A., McCausland, P.J. et Dunning, G.R. (2001). Opening Iapetus: constraints from the Laurentian margin in Newfoundland. *Geological Society of America Bulletin*, 113(4), 443-453.
- Chabaux, F., Riotte, J. et Dequincey, O. (2003). U-Th-Ra fractionation during weathering and river transport. *Reviews in Mineralogy and Geochemistry*, 52(1), 533-576.

- Chapelle, F.H., McMahon, P.B., Dubrovsky, N.M., Fujii, R.F., Oaksford, E.T. et Vroblesky, D.A. (1995). Deducing the distribution of terminal electron-accepting processes in hydrologically diverse groundwater systems. *Water Resources Research*, 31(2), 359-371.
- Chen, J.H., Lawrence Edwards, R. et Wasserburg, G.J. (1986). ^{238}U , ^{234}U and ^{232}Th in seawater. *Earth and Planetary Science Letters*, 80(3–4), 241-251.
- Chen, W. et Simonetti, A. (2013). In-situ determination of major and trace elements in calcite and apatite, and U-Pb ages of apatite from the Oka carbonatite complex: Insights into a complex crystallization history. *Chemical Geology*, 353, 151-172.
- Chen, W. et Simonetti, A. (2015). Isotopic (Pb, Sr, Nd, C, O) evidence for plume-related sampling of an ancient, depleted mantle reservoir. *Lithos*, 216–217, 81-92. Cherdynsev, V., Chalov, P. et Khitrik, M. (1955). On isotopic composition of radio-elements in natural objects and problems of geochronology. *Trans. 3rd Session Commiss. Determ. Abs. age geol. Formns*, 175-233.
- Cloutier, V., Lefebvre, R., Savard, M.M., Bourque, É. et Therrien, R. (2006). Hydrogeochemistry and groundwater origin of the Basses-Laurentides sedimentary rock aquifer system, St. Lawrence Lowlands, Québec, Canada. *Hydrogeology Journal*, 14(4), 573-590.
- Cloutier, V., Lefebvre, R., Savard, M.M. et Therrien, R. (2010). Desalination of a sedimentary rock aquifer system invaded by Pleistocene Champlain Sea water and processes controlling groundwater geochemistry. *Environmental Earth Sciences*, 59(5), 977-994.
- Cooper, W.S. (1958). Coastal sand dunes of Oregon and Washington. *Geological Society of America Memoirs*, 72, 1-162.
- Crough, S.T. (1981). Mesozoic hotspot epeirogeny in eastern North America. *Geology*, 9(1), 2-6.
- Dunai, T. et Baur, H. (1995). Helium, neon, and argon systematics of the European subcontinental mantle: Implications for its geochemical evolution. *Geochimica et Cosmochimica Acta*, 59(13), 2767-2783.
- Durand, S., Chabaux, F., Rihs, S., Düringer, P. et Elsass, P. (2005). U isotope ratios as tracers of groundwater inputs into surface waters: example of the Upper Rhine hydrosystem. *Chemical Geology*, 220(1), 1-19.
- Eby, G.N. (1985a). Age relations, chemistry, and petrogenesis of mafic alkaline dikes from the Montereian Hills and younger White Mountain igneous provinces. *Canadian Journal of Earth Sciences*, 22(8), 1103-1111.

- Eby, G.N. (1985b). Sr and Pb isotopes, U and Th chemistry of the alkaline Monteregean and White Mountain igneous provinces, eastern North America. *Geochimica et Cosmochimica Acta*, 49(5), 1143-1153.
- Edwards, R.L., Chen, J. et Wasserburg, G. (1987). ^{238}U - ^{234}U - ^{230}Th - ^{232}Th systematics and the precise measurement of time over the past 500,000 years. *Earth and Planetary Science Letters*, 81(2), 175-192.
- Elliot, T., Bonotto, D.M. et Andrews, J.N. (2014). Dissolved uranium, radium and radon evolution in the Continental Intercalaire aquifer, Algeria and Tunisia. *Journal of Environmental Radioactivity*, 137, 150-162.
- Farley, K.A. (2002). (U-Th)/He dating: Techniques, calibrations, and applications. *Reviews in Mineralogy and Geochemistry*, 47(1), 819-844.
- Faure, S., Tremblay, A. et Angelier, J. (1996). State of intraplate stress and tectonism of northeastern America since Cretaceous times, with particular emphasis on the New England-Quebec igneous province. *Tectonophysics*, 255(1), 111-134.
- Foland, K., Gilbert, L.A., Sebring, C.A. et Jiang-Feng, C. (1986). $^{40}\text{Ar}/^{39}\text{Ar}$ ages for plutons of the Monteregean Hills, Quebec: Evidence for a single episode of Cretaceous magmatism. *Geological Society of America Bulletin*, 97(8), 966-974.
- Foland, K., Jiang-Feng, C., Gilbert, L.A. et Hofmann, A. (1988). Nd and Sr isotopic signatures of Mesozoic plutons in northeastern North America. *Geology*, 16(8), 684-687.
- Ford, K.L., Savard, M., Dessau, J.-C., Pellerin, E., Charbonneau, B.W. et Shives, B. (2001). The role of gamma-ray spectrometry in radon risk evaluation: a case history from Oka, Quebec. *Geoscience Canada*, 28(2).
- Fontes, J.-C. (1992). Chemical and isotopic constraints on ^{14}C dating of groundwater. Dans *Radiocarbon after four decades* (p. 242-261) : Springer.
- Fröhlich, K. (2013). Dating of old groundwater using uranium isotopes-principles and applications. Chapter 7. Dans *Isotope methods for dating old groundwater*.
- Fröhlich, K. et Gellermann, R. (1987). On the potential use of uranium isotopes for groundwater dating. *Chemical Geology: Isotope Geoscience section*, 65(1), 67-77.
- Gascoyne, M. (1992). Palaeoclimate determination from cave calcite deposits. *Quaternary Science Reviews*, 11(6), 609-632.
- Gascoyne, M. (2004). Hydrogeochemistry, groundwater ages and sources of salts in a granitic batholith on the Canadian Shield, southeastern Manitoba. *Applied Geochemistry*, 19(4), 519-560.

- Gardner, W.P., Susong, D.D., Solomon, D.K. et Heasler, H.P. (2010). Using noble gases measured in spring discharge to trace hydrothermal processes in the Norris Geyser Basin, Yellowstone National Park, U.S.A. *Journal of Volcanology and Geothermal Research*, 198(3–4), 394-404.
- Gautheron, C. et Moreira, M. (2002). Helium signature of the subcontinental lithospheric mantle. *Earth and Planetary Science Letters*, 199(1), 39-47.
- Gautheron, C., Tassan-Got, L.; Barbarand, J. et Pagel, M. (2009). Effect of alpha-damage annealing on apatite (U-Th)/He thermochronology. *Chemical Geology*, 266(3–4), 157–170.
- Geyh, M. (2005). *Dating of old groundwater—history, potential, limits and future*. : Springer.
- Gleeson, T., Befus, K.M., Jasechko, S., Luijendijk, E. et Cardenas, M.B. (2016). The global volume and distribution of modern groundwater. *Nature Geosci*, 9, 161–167
- Globensky, Y. (1987). Géologie des basses-terres du Saint-Laurent. : [Ministère de l'énergie et des ressources], Direction générale de l'exploration géologique et minérale, Direction de la recherche géologique, Service de la géologie.
- Globensky, Y. (1993). *Lexique stratigraphique canadien. Volume VB: région des Appalaches, des Basses-Terres du Saint-Laurent et des îles de la Madeleine*. : [Québec]: Direction générale de l'exploration géologique et minérale.
- Godbout, P.-M. (2013). Géologie du quaternaire et hydrostratigraphie des dépôts meubles du bassin versant de la rivière Bécancour et des zones avoisinantes, Québec (MSc Thesis). Université du Québec à Montréal.
- Graham, D.W. (2002). Noble gas isotope geochemistry of mid-ocean ridge and ocean island basalts: Characterization of mantle source reservoirs. *Reviews in Mineralogy and Geochemistry*, 47(1), 247-317.
- Harvey BG (1962) Introduction to Nuclear Physics and Chemistry. Prentice Hall Inc, New Jersey.
- Heaton, T. et Vogel, J. (1981). “Excess air” in groundwater. *Journal of Hydrology*, 50, 201-216.
- Hillaire-Marcel, C. et Causse, C. (1989). Chronologie Th/U des concrétions calcaires des varves du lac glaciaire de Deschaillons (Wisconsinien inférieur). *Canadian Journal of Earth Sciences*, 26(5), 1041-1052.
- Hilton, D.R., Fischer, T.P. et Marty, B. (2002). Noble gases and volatile recycling at subduction zones. *Reviews in mineralogy and geochemistry*, 47(1), 319-370.

- Holland, G., Lollar, B.S., Li, L., Lacrampe-Couloume, G., Slater, G. et Ballentine, C. (2013). Deep fracture fluids isolated in the crust since the Precambrian era. *Nature*, 497(7449), 357-360.
- Hubert, A., Bourdon, B., Pili, E. et Meynadier, L. (2006). Transport of radionuclides in an unconfined chalk aquifer inferred from U-series disequilibria. *Geochimica et Cosmochimica Acta*, 70(22), 5437-5454.
- Ivanovich, M., Fröhlich, K. et Hendry, M. (1991). Uranium-series radionuclides in fluids and solids, Milk River aquifer, Alberta, Canada. *Applied Geochemistry*, 6(4), 405-418.
- Kigoshi, K. (1971). Alpha-recoil thorium-234: dissolution into water and the uranium-234/uranium-238 disequilibrium in nature. *Science*, 173(3991), 47-48.
- Kipfer, R. et Peeters, F. (2002). *Using transient conservative and environmental tracers to study water exchange in Lake Issyk-Kul.* : Springer.
- Kotwicki, T., Negrini, S., Grivas, T.B., Rigo, M., Maruyama, T., Durmala, J. et Zaina, F. (2009). Methodology of evaluation of morphology of the spine and the trunk in idiopathic scoliosis and other spinal deformities-6th SOSORT consensus paper. *Scoliosis*, 4(26), 1748-7161.
- Kronfeld, J., Gradsztajn, E., Müller, H.W., Radin, J., Yaniv, A. et Zach, R. (1975). Excess ^{234}U : an aging effect in confined waters. *Earth Planetary Sciences Letter*, 27, 342-345.
- Kronfeld, J., Gradsztajn, E. et Yaniv, A. (1979). A flow pattern deduced from uranium disequilibrium studies for the Cenomanian carbonate aquifer of the Beersheva region, Israel. *Journal of Hydrology*, 44(3), 305-310.
- Kulongoski, J.T. et Hilton, D.R. (2011). Applications of groundwater helium. In: Baskaran, M. (Ed.), *Handbook of Environmental Isotope Geochemistry, Advances in Isotope Geochemistry*. Springer-Verlag, Berlin Heidelberg, pp. 285–303.
- Kulongoski, J.T., Hilton, D.R., Barry, P.H., Esser, B.K., Hillegonds, D. et Belitz, K. (2013). Volatile fluxes through the Big Bend section of the San Andreas Fault, California: Helium and carbon-dioxide systematics. *Chemical Geology*, 339, 92-102.
- Lamarche, L., Bondue, V., Lemelin, M.-J., Lamothe, M. et Roy, A. (2007). Deciphering the Holocene evolution of the St. Lawrence River drainage system using luminescence and radiocarbon dating. *Quaternary Geochronology*, 2(1), 155-161.

- Lamothe, M. (1989). A new framework for the Pleistocene stratigraphy of the central St. Lawrence Lowland, Southern Québec. *Géographie physique et Quaternaire*, 43(2), 119-129.
- Langmuir, D. (1978). Uranium solution-mineral equilibria at low temperatures with applications to sedimentary ore deposits. *Geochimica et Cosmochimica Acta*, 42(6, Part A), 547-569.
- Larocque, M., Gagné, S., Tremblay, L. et Meyzonnat, G. (2013). Projet de connaissance des eaux souterraines du bassin versant de la rivière Bécancour et de la MRC de Bécancour. *Rapport final présenté au Ministère du Développement durable, de l'Environnement, de la Faune et des Parcs* (219 pp.).
- Larocque, M., Meyzonnat, G., Barbecot, F., Pinti, D., Gagné, S., Barnetche, D., Ouellet, M. et Graveline, M. (2015). Projet de connaissance des eaux souterraines de la zone de Vaudreuil-Soulanges *Rapport final présenté au Ministère du Développement durable, de l'Environnement, de la Faune et des Parcs* (203pp.)
- Lemieux, J.M., Sudicky, E., Peltier, W. et Tarasov, L. (2008). Dynamics of groundwater recharge and seepage over the Canadian landscape during the Wisconsinian glaciation. *Journal of Geophysical Research: Earth Surface* (2003–2012), 113(F1).
- Lippmann-Pipke, J., Lollar, B.S., Niedermann, S., Stroncik, N.A., Naumann, R., van Heerden, E. et Onstott, T.C. (2011). Neon identifies two billion year old fluid component in Kaapvaal Craton. *Chemical Geology*, 283(3), 287-296.
- Lavoie, D. (2008). Appalachian foreland basin of Canada. *Sedimentary basins of the world*, 5, 65-103.
- Lavoie, D., Pinet, N., Castonguay, S., Hannigan, P., Dietrich, J., Hamblin, T. et Giller, P. (2009). Petroleum resource assessment, Paleozoic successions of the St. Lawrence Platform and Appalachians of eastern Canada. *Geological Survey of Canada*, 6174, 275.
- Malka, E., Stevenson, R.K. et David, J. (2000). Sm-Nd geochemistry and U-Pb geochronology of the Mont Rigaud stock, Quebec, Canada: a late magmatic event associated with the formation of the Iapetus rift. *The Journal of Geology*, 108(5), 569-583.
- Maher, K., Steefel, C.I., DePaolo, D.J. et Viani, B.E. (2006). The mineral dissolution rate conundrum: Insights from reactive transport modeling of U isotopes and pore fluid chemistry in marine sediments. *Geochimica et Cosmochimica Acta*, 70(2), 337-363.

- Marine, I. (1979). The use of naturally occurring helium to estimate groundwater velocities for studies of geologic storage of radioactive waste. *Water Resources Research*, 15(5), 1130-1136.
- Marty, B., Torgersen, T., Meynier, V., O'Nions, R.K. et Marsily, G. (1993). Helium isotope fluxes and groundwater ages in the Dogger Aquifer, Paris Basin. *Water resources research*, 29(4), 1025-1035.
- Marty, B., Tolstikhin, I., Kamensky, I.L., Nivin, V., Balaganskaya, E. et Zimmermann, J.-L. (1998). Plume-derived rare gases in 380 Ma carbonatites from the Kola region (Russia) and the argon isotopic composition in the deep mantle. *Earth and Planetary Science Letters*, 164(1), 179-192.
- Matsuda, J., Matsumoto, T., Sumino, H., Nagao, K., Yamamoto, J., Miura, Y., Kaneoka, I., Takahata, N. et Sano, Y. (2002). The $^3\text{He}/^4\text{He}$ ratio of the new internal He Standard of Japan (HESJ). *Geochemical Journal*, 36(2), 191-195.
- McHone, J.G. (1996). Broad-terrane Jurassic flood basalts across northeastern North America. *Geology*, 24(4), 319-322.
- Mazor, E. (1995). Stagnant aquifer concept Part 1. Large-scale artesian systems—Great Artesian Basin, Australia. *Journal of Hydrology*, 173(1), 219-240.
- Mazor, E. (2003). Chemical and isotopic groundwater hydrology. (Vol. 98) : CRC press.
- McIntosh, J., Garven, G. et Hanor, J. (2011). Impacts of Pleistocene glaciation on large-scale groundwater flow and salinity in the Michigan Basin. *Geofluids*, 11(1), 18-33.
- McIntosh, J. et Walter, L. (2005). Volumetrically significant recharge of Pleistocene glacial meltwaters into epicratonic basins: Constraints imposed by solute mass balances. *Chemical Geology*, 222(3), 292-309.
- McIntosh, J. et Walter, L. (2006). Paleowaters in Silurian-Devonian carbonate aquifers: Geochemical evolution of groundwater in the Great Lakes region since the Late Pleistocene. *Geochimica et Cosmochimica Acta*, 70(10), 2454-2479.
- Méjean, P., Pinti, D.L., Larocque, M., Ghaleb, B., Meyzonnat, G. et Gagné, S. (2016). Processes controlling ^{234}U and ^{238}U isotope fractionation and helium in the groundwater of the St. Lawrence Lowlands, Quebec: the potential role of natural rock fracturing. *Applied Geochemistry* 66, 198-209.
- Meyzonnat, G., Larocque, M., Barbecot, F., Pinti, D. et Gagné, S. (2016). The potential of major ion chemistry to assess groundwater vulnerability of a regional aquifer in southern Quebec (Canada). *Environmental Earth Sciences*, 75(1), 1-12.

- Morikawa, A., Suzuki, T., Kanazawa, T., Kikuta, K., Suda, A. et Shinjo, H. (2008). A new concept in high performance ceria-zirconia oxygen storage capacity material with Al_2O_3 as a diffusion barrier. *Applied Catalysis B: Environmental*, 78(3), 210-221.
- Morrison, P. et Pine, J. (1955). Radiogenic origin of the helium isotopes in rock. *Annals of the New York Academy of Sciences*, 62(3), 71-92.
- Neuzil, C. (2012). Hydromechanical effects of continental glaciation on groundwater systems. *Geofluids*, 12(1), 22-37.
- Occhietti, S., Parent, M., Shilts, W.W., Dionne, J.-C., Govare, E. et Harmand, D. (2001). Late Wisconsinan glacial dynamics, deglaciation, and marine invasion in southern Québec. *Special papers-geological society of america*, 243-270.
- Occhietti, S. et Richard, P.J. (2003). Effet réservoir sur les âges ^{14}C de la Mer de Champlain à la transition Pléistocène-Holocène: révision de la chronologie de la déglaciation au Québec méridional. *Géographie physique et Quaternaire*, 57(2-3), 115-138.
- Osmond, J. et Cowart, J. (1976). The theory and uses of natural uranium isotopic variations in hydrology. *Atomic Energy Review*, 14(4), 620-679
- Osmond, J.K. et Cowart, J. (1982). Natural uranium and thorium serie disequilibrium: new approaches to geochemical problems. *Nucl. Sci. Appl. B* 1, 303e352.
- Osmond, J.K. et Cowart, J.B. (2000). U-series nuclides as tracers in groundwater hydrology. In: Cook, P., Herczeg, A. (Eds.), *Environmental Tracers in Subsurface Hydrology*. Kluwer Academic Publishers, Boston, pp. 145e174.
- Osmond, J., Kaufman, M.I. et Cowart, J. (1974). Mixing volume calculations, sources and aging trends of Floridan aquifer water by uranium isotopic methods. *Geochimica et Cosmochimica Acta*, 38(7), 1083-1100.
- Ozima, M. et Podosek, F. (1983). *Noble gas chemistry*: Cambridge, United Kingdom : Cambridge Univ. Press.
- Paces, J.B., Ludwig, K.R., Peterman, Z.E. et Neymark, L.A. (2002). $^{234}\text{U}/^{238}\text{U}$ evidence for local recharge and patterns of ground-water flow in the vicinity of Yucca Mountain, Nevada, USA. *Applied Geochemistry*, 17(6), 751-779.
- Paces, J.B., Wurster, F.C., 2014. Natural uranium and strontium isotope tracers of water sources and surface water-groundwater interactions in arid wetlands-Pahranagat Valley, Nevada, USA. *Journal of Hydrology*. 517, 213-225.
- Parent, M. et Occhietti, S. (1988). Late Wisconsinan deglaciation and Champlain sea invasion in the St. Lawrence valley, Québec. *Géographie physique et Quaternaire*, 42(3), 215-246.

- Person, M., McIntosh, J., Bense, V. et Remenda, V. (2007). Pleistocene hydrology of North America: the role of ice sheets in reorganizing groundwater flow systems. *Reviews of Geophysics*, 45(3).
- Phillips, F. et Castro, M. (2003). Groundwater dating and residence-time measurements. *Treatise on geochemistry*, 5, 451-497.
- Pinti, D.L., Marty, B. et Andrews, J.N. (1997). Atmosphere-derived noble gas evidence for the preservation of ancient waters in sedimentary basins. *Geology*, 25(2), 111-114.
- Pinti, D.L. et Marty, B. (1998). The origin of helium in deep sedimentary aquifers and the problem of dating very old groundwaters. *Geological Society, London, Special Publications*, 144(1), 53-68.
- Pinti, D.L., Béland-Otis, C., Tremblay, A., Castro, M.C., Hall, C.M., Marcil, J.-S., Lavoie, J.-Y. et Lapointe, R. (2011). Fossil brines preserved in the St-Lawrence Lowlands, Québec, Canada as revealed by their chemistry and noble gas isotopes. *Geochimica et Cosmochimica Acta*, 75(15), 4228-4243.
- Pinti, D.L., Castro, M.C., Shouakar-Stash, O., Tremblay, A., Garduño, V.H., Hall, C.M., Hélie, J.F. et Ghaleb, B. (2013). Evolution of the geothermal fluids at Los Azufres, Mexico, as traced by noble gas isotopes, $\delta^{18}\text{O}$, δD , $\delta^{13}\text{C}$ and $^{87}\text{Sr}/^{86}\text{Sr}$. *Journal of Volcanology and Geothermal Research* 249, 1-11.
- Plater, A., Ivanovich, M. et Dugdale, R. (1992). Uranium series disequilibrium in river sediments and waters: the significance of anomalous activity ratios. *Applied Geochemistry*, 7(2), 101-110.
- Plummer, L. et Glynn, P. (2013). Radiocarbon dating in groundwater systems. *Isotope Methods for Dating Old Groundwater, International Atomic Energy Agency (IAEA), Vienna*, 33-90.
- Porcelli, D. et Swarzenski, P.W. (2003). The behavior of U-and Th-series nuclides in groundwater. *Reviews in Mineralogy and Geochemistry*, 52(1), 317-361.
- Porcelli, D. et Baskaran, M. (2012). An overview of isotope geochemistry in environmental studies. *Handbook of Environmental Isotope Geochemistry* (11-32) : Springer.
- Reynolds, B., Wasserburg, G. et Baskaran, M. (2003). The transport of U-and Th-series nuclides in sandy confined aquifers. *Geochimica et Cosmochimica Acta*, 67(11), 1955-1972.
- Riotte, J. et Chabaux, F. (1999). ($^{234}\text{U}/^{238}\text{U}$) activity ratios in freshwaters as tracers of hydrological processes: the Strengbach watershed (Vosges, France). *Geochimica et Cosmochimica Acta*, 63(9), 1263-1275.
- Riotte, J., Chabaux, F., Benedetti, M., Dia, A., Gérard, M., Boulègue, J. et Etamé, J. (2003). Uranium colloidal transport and origin of the $^{234}\text{U}-^{238}\text{U}$ fractionation

- in surface waters: new insights from Mount Cameroon. *Chemical Geology*, 202(3), 365-381.
- Rouleau, E., Pinti, D.L., Stevenson, R.K., Takahata, N., Sano, Y. et Pitre, F. (2012). N, Ar and Pb isotopic co-variations in magmatic minerals: Discriminating fractionation processes from magmatic sources in Montréal Hills, Québec, Canada. *Chemical Geology*, 326–327, 123-131.
- Rouleau, E. et Stevenson, R. (2013). Geochemical and isotopic (Nd–Sr–Hf–Pb) evidence for a lithospheric mantle source in the formation of the alkaline Montréal Province (Quebec). *Canadian Journal of Earth Sciences*, 50(6), 650-666.
- Saar, M., Castro, M., Hall, C., Manga, M. et Rose, T. (2005). Quantifying magmatic, crustal, and atmospheric helium contributions to volcanic aquifers using all stable noble gases: Implications for magmatism and groundwater flow. *Geochemistry, Geophysics, Geosystems*, 6(3).
- Saby, M., Larocque, M., Pinti, D.L., Barbecot, F., Sano, Y. et Castro, M.C. (2016). Linking groundwater quality to residence times and regional geology in the St. Lawrence Lowlands, southern Quebec, Canada. *Applied Geochemistry*, 65, 1-13.
- Sano, Y., Horiguchi, K., Takahata, N., Shirai, K., Oda, S. et Gamo, T. (2006). Helium isotopes of seawater in adjacent sea of Japan. *Geochimica et Cosmochimica Acta*, 70(18, Supplement), A555.
- Sano, Y., Tokutake, T. et Takahata, N. (2008). Accurate measurement of atmospheric helium isotopes. *Analytical Sciences*, 24(4), 521-525.
- Sasada, T., Hiyagon, H., Bell, K. et Ebihara, M. (1997). Mantle-derived noble gases in carbonatites. *Geochimica et cosmochimica acta*, 61(19), 4219-4228.
- Schlosser, P., Stute, M., Sonntag, C. et Munnich, K. (1989). Tritiogenic ^3He in shallow groundwater. *Earth Planet. Sci. Lett*, 94, 245-256.
- Séjourné, S., Lefebvre, R., Malet, X. et Lavoie, D. (2013). Synthèse géologique et hydrogéologique du Shale d'Utica et des unités sus-jacentes (Lorraine, Queenston et dépôts meubles), Basses-Terres du Saint-Laurent, Province de Québec; Commission géologique du Canada. *Commission géologique du Canada, Dossier Public*, 7338, 165.
- Sleep, N.H. (1990). Montréal hotspot track: A long-lived mantle plume. *Journal of Geophysical Research: Solid Earth* (1978–2012), 95(B13), 21983-21990.
- Smith, S. et Kennedy, B. (1983). The solubility of noble gases in water and in NaCl brine. *Geochimica et Cosmochimica Acta*, 47(3), 503-515.

- Solomon, D., Hunt, A. et Poreda, R. (1996). Source of radiogenic helium 4 in shallow aquifers: Implications for dating young groundwater. *Water Resources Research*, 32(6), 1805-1813.
- Stuart, F.M., Lass-Evans, S., Fitton, J.G. et Ellam, R.M. (2003). High $^3\text{He}/^4\text{He}$ ratios in picritic basalts from Baffin Island and the role of a mixed reservoir in mantle plumes. *Nature*, 424(6944), 57-59.
- Takaoka, N. et Mizutani, Y. (1987). Tritiogenic ^3He in groundwater in Takaoka. *Earth and Planetary Science Letters*, 85(1), 74-78.
- Tokarev, I., Zubkov, A., Rumynin, V.G., Polyakov, V., Kuznetsov, V.Y. et Maksimov, F. (2006). Origin of high $^{234}\text{U}/^{238}\text{U}$ ratio in post-permafrost aquifers. Dans *Uranium in the Environment* (p. 847-856) : Springer.
- Tolstikhin, I. et Kamenskiy, I. (1969). Determination of ground-water ages by the ^3He Method. *Geochemistry International*, 6, 810-811.
- Tolstikhin, I., Lehmann, B., Loosli, H. et Gautschi, A. (1996). Helium and argon isotopes in rocks, minerals, and related ground waters: A case study in northern Switzerland. *Geochimica et cosmochimica acta*, 60(9), 1497-1514.
- Tolstikhin, I. et Marty, B. (1998). The evolution of terrestrial volatiles: a view from helium, neon, argon and nitrogen isotope modelling. *Chemical Geology*, 147(1), 27-52.
- Torgersen, T. (1980). Controls on pore-fluid concentration of ^4He and ^{222}Rn and the calculation of $^4\text{He}/^{222}\text{Rn}$ ages. *Journal of Geochemical Exploration*, 13(1), 57-75.
- Torgersen, T. (1993). Defining the role of magmatism in extensional tectonics: Helium 3 fluxes in extensional basins. *Journal of Geophysical Research: Solid Earth (1978–2012)*, 98(B9), 16257-16269.
- Torgersen, T. et Clarke, W.B. (1985). Helium accumulation in groundwater, I: An evaluation of sources and the continental flux of crustal ^4He in the Great Artesian Basin, Australia. *Geochimica et Cosmochimica Acta*, 49(5), 1211-1218.
- Torgersen, T. et Jenkins, W. (1982). Helium isotopes in geothermal systems: Iceland, the geysers, raft river and steamboat springs. *Geochimica et Cosmochimica Acta*, 46(5), 739-748.
- Torgersen, T. et O'Donnell, J. (1991). The degassing flux from the solid earth: release by fracturing. *Geophysical Research Letters*, 18(5), 951-954.
- Torgersen, T., Drenkard, S., Farley, K., Schlosser, P. et Shapiro, A. (1994). Mantle helium in the groundwater of the Mirror Lake Basin, New Hampshire. USA In

- Noble Gas Geochemistry and Cosmochemistry*, ed. J. Matsuda, 279-292 : Tokyo: Terra Scientific Publishing Co.
- Torgersen, T., Drenkard, S., Stute, M., Schlosser, P. et Shapiro, A. (1995). Mantle helium in ground waters of eastern North America: Time and space constraints on sources. *Geology*, 23(8), 675-678.
- Torgersen, T. et Stute, M. (2013). Helium (and other noble gases) as a tool for understanding long time-scale groundwater transport. Isotope methods for *Dating old groundwater*, IAEA, Vienna, 179-216.
- Tran Ngoc, T., Lefebvre, R., Konstantinovskaya, E. et Malo, M. (2014). Characterization of deep saline aquifers in the Bécancour area, St. Lawrence Lowlands, Québec, Canada: Implications for CO₂ geological storage. *Environmental geology*, 72(1), 119-146.
- Tremblay, A. et Castonguay, S. (2002). Structural evolution of the Laurentian margin revisited (southern Quebec Appalachians): Implications for the Salinian orogeny and successor basins. *Geology*, 30(1), 79-82.
- Tremblay, A., Roden-Tice, M.K., Brandt, J.A. et Megan, T.W. (2013). Mesozoic fault reactivation along the St. Lawrence rift system, eastern Canada: Thermochronologic evidence from apatite fission-track dating. *Geological Society of America Bulletin*, 125(5-6), 794-810.
- Tricca, A., Porcelli, D. et Wasserburg, G. (2000). Factors controlling the groundwater transport of U, Th, Ra, and Rn. *Journal of Earth System Science*, 109(1), 95-108.
- Tricca, A., Wasserburg, G., Porcelli, D. et Baskaran, M. (2001). The transport of U- and Th-series nuclides in a sandy unconfined aquifer. *Geochimica et Cosmochimica Acta*, 65(8), 1187-1210.
- Vautour, G., Pinti, D.L., Méjean, P., Saby, M., Meyzonnat, G., Larocque, M., Castro, M.C., Hall, C.M., Boucher, C., Roulleau, E., Barbecot, F., Takahata, N. et Sano, Y. (2015). ³H/³He, ¹⁴C and (U-Th)/He groundwater ages in the St. Lawrence Lowlands, Quebec, Eastern Canada. *Chemical Geology*, 413, 94-106.
- Weisse, S. et Moser, H. (1987). Groundwater dating with helium isotopes. *Isotope techniques in water resources development*. IAEA, Vienna, 105-126.
- Wen, J., Bell, K. et Blenkinsop, J. (1987). Nd and Sr isotope systematics of the Oka complex, Quebec, and their bearing on the evolution of the sub-continental upper mantle. *Contributions to Mineralogy and Petrology*, 97(4), 433-437.
- Witherspoon, P. (2010). Validity of cubic law for fluid flow in a deformable rock fracture. *Lawrence Berkeley National Laboratory*. Water Resources Research, LBNL Paper LBL-9557.

Zurevinski, S.E. et Mitchell, R.H. (2004). Extreme compositional variation of pyrochlore-group minerals at the Oka carbonatite complex, Quebec: evidence of magma mixing? *The Canadian Mineralogist*, 42(4), 1159-1168.

ANNEXE A

U-TH DATING OF BROKEN SPELEOTHEMS FROM CACAHUAMILPA CAVE, MEXICO: ARE THEY RECORDING PAST SEISMIC EVENTS?

Pauline Méjean¹, Victor-Hugo Garduño², Daniele L. Pinti¹, Bassam Ghaleb¹, Laura Bouvier^{1,3}, Martha G. Gomez-Vasconcelos², Alain Tremblay¹

¹GEOTOP et département des Sciences de la terre et de l'Atmosphère, Université du Québec à Montréal, C.P.8888, Succ. Centre-Ville, Montréal, Qc, H3C 3P8

² UMSNH-IIM, INICIT, Michoacan, 58060, Mexico

³ Now at Department of Earth and Environmental Sciences, University of Michigan, Ann Arbor, MI 48109-1005, USA

Keywords: speleothems; seismothem; speleoseismology; cacahuamilpa cave; nevado del toluca.

Article publié dans Journal of South American Earth Sciences (2015), 57, 23-31

ABSTRACT

Cacahuamilpa cave is one of the largest karst systems in Central Mexico. The cave contains numerous massive speleothems broken and fallen following oriented directions, damaged during cataclysmic geological events. One fallen and two broken speleothems were sampled in the Cacahuamilpa cave for dating the rupture event using measured U-Th disequilibrium ages. A total of eight small carbonate cores were drilled perpendicular and longitudinal to the rupture surface. Results showed three groups of ages (weighted average): 0.95 ± 0.02 ka, 28.8 ± 0.2 ka and 88.0 ± 0.7 ka. This indicates that the construction of the Cacahuamilpa karst system, for which no absolute ages existed before this study, initiated at least since Late Pleistocene. The first two groups of ages might be related to two distinct episodes of intense seismic activity. Calculated minimum horizontal ground acceleration and frequency values of the seismic events needed to create the rupture of the stalagmites dated at 0.95 ± 0.02 ka and 28.8 ± 0.2 ka range between 1.3 to 2.0 $m\ s^{-2}$ and between 13.4 to 20.8 Hz, respectively. These parameters are compatible with earthquakes of magnitude equal or higher than 7 M, with an epicentral distance between 50 and 100 km from the Cacahuamilpa cave. The stalagmite rupture dated at 88.0 ± 0.7 ka might result from the invasion of the cave by one of the older lahars deposits of the nearby volcano Nevado del Toluca, and successively fell by gravity instability.

.1 INTRODUCTION

In Central Mexico, the intense seismic activity has left a clear imprinting in the history of this country, as witnessed by the devastating earthquakes of 1858 ($M = 7$), 1912 ($M = 6.9 - 7$) and 1985 ($M = 8.1$) (García Acosta et Suárez, 1996). The first two earthquakes were related to movements of the Morelia-Acambay Fault System (Fig. 1), while the last one was related to the subduction of the Cocos plate (Fig. 1). Data

regarding the 1858's earthquake were obtained with macro-seismic analysis (Singh *et al.*, 1996); the second with poor instrumental records and thanks to recent paleoseismological studies (Rodríguez-Pascua *et al.*, 2012); the last one was localized with the most advanced instrumentation. To create a reliable earthquake catalogue of Mexico, paleoseismology studies needs to be developed, such as the geochronology of fallen and broken speleothems, which is the focus of this paper.

Speleothems are calcite deposits in caves. Water infiltrates through soils and seeps into caves via cracks, where it dissolves calcium carbonate. The dissolution rate depends on the amount of carbon dioxide held in solution, on temperature, and on other environmental parameters related to the climatic conditions. When the solution reaches an air-filled cave, a discharge of carbon dioxide causes the precipitation of the minerals out of solution. Over time, the accumulation of these precipitates forms speleothems and growth rate of the stalagmite could be reconstructed. Speleothems are excellent high-resolution paleoclimatic recorders. Carbon and oxygen isotopes measured in speleothems, coupled with measured U-Th disequilibrium ages (Genty *et al.*, 2003; Marshall *et al.*, 2009), can trace back climatic oscillations in the Quaternary (Wang *et al.*, 2001). But chronology of speleothems can have other useful applications. In archaeology, dating of a calcite deposited on a cave floor in France was used to reconstruct period of the cave collapse (Genty *et al.*, 2004). Damaged or fallen speleothems often observed in caves (named seismotheems), are supposed to be related to the occurrence of past earthquakes (e.g., Forti et Postpischl, 1984; Postpischl *et al.*, 1991; Bini *et al.*, 1992; Quinif, 1996; Gilli, 1999; Gilli et Serface, 1999; Becker *et al.*, 2006; 2012; Kagan *et al.*, 2005; Forti, 2001). This recent branch of paleoseismology, which aims to obtain information on ancient earthquakes from the karstic record in caves, is called speleoseismology (see Gilli, 2005; Becker *et al.*, 2006 for a review).

The cave environment is ideal for paleoseismological investigations because earthquake damage is often fossilized by calcification and preserved from erosion (e.g., Gospodarić, 1977; Gilli, 1999; Gilli et Serface, 1999). Phenomena often related to seismic activity in caves include new-formed speleothems on fallen deposits (e.g., Postpischl *et al.*, 1991); collapsed ceilings (Gilli, 1999a; 1999b) and the occurrence of horizontal displacement between stalactites and stalagmites caused by a fault movement either slow, or rapid during a seismic event (e.g., Bini *et al.*, 1992; Quinif, 1996; Postpischl *et al.*, 1991; Gilli, 2005). It is worth noting that several processes, independent from seismic activity, can generate similar deformations: human and animal activities; creep movement of sediments or ice; and violent floods (e.g., Gilli, 1999b; Gilli, 2004; Delaby, 2001; Becker *et al.*, 2006). Further speleothem ruptures during seismic events have been never directly observed.

Here we present preliminary results on U-Th disequilibrium ages obtained on calcite cores drilled from three selected stalagmites in the Cacahuamilpa cave in the state of Guerrero, Central Mexico. Cacahuamilpa is one of the largest cave systems in Mexico, opened to the public in 1967 and where a variety of damaged speleothems have been recently mapped (Garduño-Monroy *et al.*, 2011). Cacahuamilpa cave is a pristine environment to study speleoseismology, because anthropic activities have not substantially modified the karst system. Further, the western entrance of the cave has been closed by volcanic debris flows and lahars () more than 45 ka ago (Capra et Macías, 2000; Capra *et al.*, 2002). The eastern, and only entrance is perched at 1230 m asl (Enjalbert, 1964) and against-slope, preserving the cave from episodes of sediment infilling which might damage speleothems.

.2 GEOLOGICAL SETTING AND SAMPLE DESCRIPTION

Cacahuamilpa cave is located in the Guerrero State of Mexico, ca. 160 km south of Mexico City (Fig. 1) and ca. 20 km NE from the town of Taxco. It is located within

the NW-SE elongated Ixtapan Valley which is 60 km long and 40 km wide. The Cacahuamilpa cave is part of a karst system denoted La Estrella Karstic System (LAKS). Two main fluvial channels running NW-SE form the LAKS: the San Jeronimo and the Chontalcoatlán (Fig. 2). The cave system is developed within a calcareous complex of Cretaceous age (Fig. 2) and particularly in the 900 m-thick limestone and dolostone deposits of the Morelos Unit from the Lower Cretaceous (Fries, 1960) N-S folds with W vergence affect Middle and Upper Cretaceous limestone. Faults and major fractures have a NNW-SSE strike and mostly two types of movement components, strike slip and reverse faults (Fig. 1). Quaternary volcanic andesitic rocks and basalts cap these Cretaceous units forming large plateaus (Fig. 2). Most of the volcanic products in this area are from the Nevado del Toluca, a 4,565 m high stratovolcano located at the intersection of a three faults system, 55 km north of the cave (García-Palomo *et al.*, 2002). Individual eruptions of the volcano were dated with radiocarbon chronology (García-Palomo *et al.*, 2000): a vulcanian eruption at about 28 ka ago that produced thick, cold and lithic lahars; a plinian eruption that deposited Lower Toluca Pumice fall ca. 24 ka ago; other plinian eruptions that generated the Upper Toluca Pumice ca. 11.6 ka ago. Non-dated debris flows and lahars preceded these eruptions (Capra *et al.*, 2002). The Chontalcoatlán river valley and the western flank of the Cerro Grande (or Cerro de la Corona), the calcareous mountain ridge where the Cacahuamilpa cave developed (Fig. 2) has been completely submerged by volcanic products of the Nevado del Toluca (Enjalbert, 1964; Capra et Macías, 2000). The volcanic products belong to two debris flows (lahars): “El Pilcaya” and “El Mogote” (Capra et Macías, 2002) which have been stratigraphically dated to be older than 40-45 ka (Capra *et al.*, 2002).

On the basis of geomorphological evidences and comparison with other karstic systems in Mexico, Enjalbert (1964) suggested that the LAKS developed at the end of Tertiary time. At that time, a “paleo-San Jeronimo” river excavated an underground tunnel from the western flank of the Cerro Grande. By eroding rapidly non-

consolidated volcanic deposits, the San Jeronimo River base level subsided, leaving behind a perched large horizontal phreatic tube with semicircular cross section in the calcareous massif (Figs. 3a,b) (Enjalbert, 1964; Bonet, 1971). A few alluvium deposits, often masked by carbonate concretions support the existence of this past subterranean stream (Bonet, 1971). The cave had two entrances: the western one was completely blocked by broken stalagmites, alluvium, and volcanoclastic deposits from the Nevado del Toluca (Enjalbert, 1964) (Figs. 3a,b). These deposits completely filled the Cacahuamilpa cave (Enjalbert, 1964) and successively were eroded. Presently, a 1 meter-thick lahar deposit, probably belonging to one of these two units, can be observed for a few meters at the middle of the cave, preserved on its southern flank (Fig. 3b). The eastern entrance, partially filled with landslide sediments cemented by stalagmitic incrustations (Enjalbert, 1964; Bonet, 1971) (Fig. 3a), is perched at 1230 m asl, 80 meters above the bottom of a calcareous karstic circus (Fig. 3a). With only one open entrance on its eastern flank, the perched stream tunnel became the karstic Cacahuamilpa cave after the last invasion of debris flow from the Nevado del Toluca.

The Cacahuamilpa cave develops through 90 successive salons, 80-120 m wide and 20-70 m high. Only twenty of these salons on 1400 meters are opened to the public (Figs. 3a,b). Stalactites are rare in the cave (Enjalbert, 1964) and the smaller ones are often broken, while enormous stalagmites (dripstones) are found all along the cave. Well-known are the “Botella de Champán”, the greatest stalagmite, which is 36 m high, and the most spectacular fallen dripstone “Calendario Azteca” (Sun Stone) which is 13 m (length) by 3.5 m (diameter) and with an estimated weight of 330 tons (Fig. 3b).

Three sites where fallen and broken stalagmites were previously mapped (Garduño-Monroy *et al.*, 2011) have been selected for this study: GC, CC-A and CC-B (Fig. 3b). The GC site is the innermost one, located ca. 1100 meters from the east entrance

(Fig. 3b) in the salon called “*Puerto del Aire*” (Fig. 3b). The site is formed by a group of 4 stalagmites broken to their stumps and some also in the middle (Fig. 4). On the stump of the larger sampled stalagmite, a neo-formed stalagmite developed with a total length of ca. 0.4 m (Fig. 4). The fallen stalagmites of site GC lie on an acclivity climbing towards the north flank of the cave (Fig. 3b). They fall northward (N 0-20°), i.e. perpendicular to the main E-W axis direction of the cave. They fell parallel each other and perpendicular to the slip side, which suggests that bending and gravity instability is not the main cause of the rupture (in this case they have more chances to fall 90° westward). The fallen stalagmites are between 4.2 and 1.7 m long, with a diameter between 0.57 and 0.4 m (Fig. 4) (Garduño-Monroy *et al.*, 2011).

The CC-A site is located at 630 m from the entrance of the cave at the salon “*de los querubines*” (Fig. 3b) and it consists of a cauliflower-like stalagmite with a variable diameter from 0.8 m at its broken base to 1.2 m at its largest section (Fig. 5). The total length of the broken stalagmite is ca. 4 meters. The stalagmite has fallen following a SE-NW direction (N105°) (Fig. 3b) but possibly rolled from its supposed stump (Fig. 5).

The CC-B site is located at 700 m from the entrance of the cave also at the salon de “*los querubines*” (Fig. 3b). At CC-B site, a large stalagmite (1 m of diameter and 1.5 meter high) is broken and faces west (N 270°) next to his stump. The stalagmite is broken 1 meter higher than the base of its stump. Originally, this large stalagmite bent of 32° SW (Fig. 6).

.3 MATERIELS AND METHOD

At site GC, four samples from the same stalagmite (samples GC-1, GC-2, GC-3 and GC-4) were collected in February 2013 using a core driller (Fig. 4). The use of the core driller was dictated by the fact that Cacahuamilpa cave is a national park and we

have not authorization to remove stalagmites from the site to obtain polish sections for observing the growth of the speleothems. Recovered core samples at all sites are 2 cm in diameter for ca. 12 cm long.

Site GC was chosen for its accessibility and the presence of several collapsed stalagmites, their stumps, and regrowth stalagmites that were available for drilling (Fig. 4). By dating the youngest part of the fallen stalagmite and the new stalagmite growth on the stump, a maximum and a minimum age for the stalagmite rupture can be obtained.

Sample GC-1 corresponds to the last group of precipitated laminae before the break, hypothetically the oldest age corresponding to the rupture of the stalagmite. GC-4 was taken at the base of the stalagmite, close to the stump, and should correspond to an earlier stage of precipitation. GC-2 and GC-3 samples represent the stalagmite growth on the post-breaking portion, formed following the rupture. Following this reasoning, GC-4 should be older than GC-1, while GC-1 should be older than GC-2 and GC-3 (Fig. 4).

A second field trip was carried out in May 2013 in the same cave in order to sample two additional stalagmites, 300 m from the first sampled site (sites CC-A and CC-B; Figs. 5 and 6). During this collection survey, the last precipitated laminae were sampled at the top of the fallen stalagmite. Two samples were taken from each speleothem in order to measure U-Th disequilibrium ages. Cores were taken parallel and perpendicular to the axis of growth with the target of intercepting the final laminae that formed prior to the rupture. Because of the inaccessibility of the stump for the heavy core driller at these two sites (CC-A and CC-B) we cannot sample properly the regrown phase on the stumps.

U-series determination of stalagmites samples was carried out at the radiogenic laboratory of the GEOTOP research center, Montréal, Canada. Stalagmite pieces (5-6

g) were cut using an abrading device (Dremel® rotary tool). We want to stress here the fact that the external layer of all recovered samples was removed in order to reduce the risk of contamination by ^{230}Th -bearing detrital particles. Presence of non-authigenic ^{230}Th in such samples requires that a correction be applied to the calculated U-Th disequilibrium ages (Bischoff et Fitzpatrick, 1991; Pons-Branchu, 2001). The removal of the external layer allowed avoiding dating neo-formed layers on the surface of the stalagmites, after they felt.

The stalagmite sample was dissolved in 7N HNO_3 in Teflon beakers and a known amount of spike (^{233}U , ^{236}U , and ^{229}Th) was added to determine U and Th isotopes by isotope dilution technique. Around 15 mg of Fe carrier was added to this solution. In order to concentrate the U and Th elements from the bulk solution, a Fe(OH)_3 precipitate was created by adding a solution of ammonium hydroxide until a pH between 7 and 9 was obtained. The precipitate was recovered by centrifugation and then dissolved in 6M HCl.

The U-Th separation based on Edwards *et al.* (1987) was conducted using an AG1X8 anionic resin bed. The Th and U-Fe fractions were retrieved by elution with 6 N HCl and H_2O , respectively. The purification of the U fraction was done using 0.2 ml U-Teva (Eichrom® Industries) resin volume. The U-Fe separation was performed by elution using 3 N HNO_3 (Fe fraction) and 0.02 N HNO_3 (U fraction). The purification of Th was performed by elution using a 2 ml AG1X8 resin in 7 N HNO_3 and elution with 6 N HCl. A final purification of Th was carried out on a 0.2 ml AG1X8 resin in 7N HNO_3 and Th was eluted with 6 N HCl. The U and Th fractions were deposited on Re filament between two layers of graphite and measured using a Triton plus mass spectrometer (TIMS) with ion counter. Mass fractionation for U was corrected by the double spike ($^{236}\text{U}/^{233}\text{U}=1.132$), while mass fractionation for Th was considered negligible with respect to analytical error. The overall analytical reproducibility, as estimated from replicate measurements of standards, is usually better than 0.5% for U

concentration and $^{234}\text{U}/^{238}\text{U}$ ratios, and ranges from 0.5% to 1% for $^{230}\text{Th}/^{234}\text{U}$ ratios (2 σ error range).

.4 RESULTS

U-series data and calculated U-Th disequilibrium ages for all samples are presented in Table 1. Uranium concentrations are relatively high and vary between 0.5 ppm and 3 ppm while thorium concentrations are below ppb levels in all analyzed samples with the exception of sample GC-3 that shows higher ^{232}Th content. This indicates that a part of the measured ^{230}Th is related to a detrital contamination. Therefore it is expected that the calculated age is older than the true age. In order to account for the ^{230}Th from the detrital fraction, a correction was done in a manner resembling the one used by Ludwig and Paces (2012). Specifically, we used ^{232}Th as an index and assumed a typical crustal Th/U ratio, with ($^{234}\text{U}/^{238}\text{U}$) and ($^{230}\text{Th}/^{238}\text{U}$) activity ratios near secular equilibrium. In this model, the isotope and the activity ratios used were ($^{232}\text{Th}/^{238}\text{U}$) = $1.21 \pm 50\%$, ($^{234}\text{U}/^{238}\text{U}$) = $1 \pm 10\%$ and ($^{230}\text{Th}/^{238}\text{U}$) = $1 \pm 10\%$. The corrected ($^{230}\text{Th}/^{238}\text{U}$) and ($^{234}\text{U}/^{238}\text{U}$) activity ratios were then used to calculate the corrected ages (Table 1). The consequence of such correction results in higher errors on the corrected age and in particular for younger ages where the errors on the corrected ages become significant.

Because of recoil effect, the initial ($^{234}\text{U}/^{238}\text{U}$)₀ activity ratios are all higher than the secular equilibrium value. Calculated corrected ages show a cluster around 0.95 ± 0.02 ka, 28.8 ± 0.2 ka and 88.0 ± 0.7 ka for samples GC-1-3, CC-A and CC-B, respectively (Table 1). The only exception is sample GC-4 which yields an older age (1.711 ± 0.036 ka) compared to those measured in GC-1 (0.999 ± 0.022 ka), GC-2 (0.828 ± 0.028 ka) and GC-3 (0.927 ± 0.155 ka) (Table 1).

No detritus correction was required to calculated U-series disequilibria ages except for sample GC-3 where a measured activity ratio ($^{230}\text{Th}/^{232}\text{Th}$) <50 implied detritus contamination during precipitation of the calcite. The sample collected at the base of the fallen speleothem (GC-4), a few centimeters from the root of the stump has the oldest calculated age of 1.711 ± 0.036 ka which corresponds to calcite precipitated at the beginning of the formation of the speleothems. The last calcite precipitated at the top of the fallen stalagmite, before the rupture, corresponds to an apparent age of 0.999 ± 0.022 ka (GC-1). Two samples were collected from the new-formed deposits and correspond to the youngest ages measured: GC-2 and GC-3 with respective ages 0.828 ± 0.028 ka and 0.927 ± 0.155 ka.

Closed system behavior for the stalagmite CC-A (Fig. 5) and the stalagmite CC-B (Fig. 6) is indicated by similar ages obtained on both samples collected in each stalagmite (as previously described, the first sample was parallel to growth axis, CC-A-01 on the stalagmite CC-A and CC-B-01 on the stalagmite CC-B; the second was perpendicular to the growth axis: CC-A-02 and CC-B-02; Figs. 5 and 6). Calculated ages are presented in Fig. 7 and highlight two different periods. In the stalagmite CC-A, the last ages recorded were 28.717 ± 0.427 ka and 28.769 ± 0.210 ka. The oldest ages were measured in the third stalagmite (CC-B): CC-B-01 with 87.615 ± 1.188 ka and CC-B-02 with 88.224 ± 0.795 ka.

Initial activity ratios ($^{234}\text{U}/(^{238}\text{U})_0$) calculated in the stalagmite GC are similar and higher than 1, from 1.272 ± 0.010 (GC-2) to 1.309 ± 0.012 (GC-3). Activity ratios ($^{234}\text{U}/(^{238}\text{U})_0$) estimated at the moment of the precipitation are similar in both samples of the stalagmite CC-A and equal to 1.969 ± 0.005 in CC-A-01 and to 1.967 ± 0.019 in CC-A-02. Despite similar calculated ages, samples from stalagmite CC-B differ in initial activity ratio. CC-B-01 initial activity ratio of 1.093 ± 0.004 is lower than that of 1.264 ± 0.003 measured in the second sample CC-B-02.

A major caveat for this study is that it can be hard to distinguish the CaCO₃ precipitation regime of fallen stalagmites. It is possible that the newly formed stalagmites (Fig. 4) cannot be attributed to a period immediately after the rupture event. This is the case, for example, when a seismic event alters the water drainage pattern within the cave (Charmoille *et al.*, 2005). As mentioned above, we tried to sample the last layer formed before the rupture and if we assume a positive hydric budget (continuous growing of CaCO₃) then the ages obtained correspond to a maximum age for these events. The initial activity ratios of (²³⁴U/²³⁸U)₀ yield more or less constant values in each studied stalagmite with the exception of sample CC-B. The two sub-samples analyzed which yield statistically different initial values may be explained by geologic events that affected the water source supplying uranium into the water. The initial activity ratio (²³⁴U/²³⁸U)₀ may record changes in the hydrologic outflow with time, as previously observed (Ersek *et al.*, 2009): (²³⁴U/²³⁸U)₀ deviates from secular equilibrium at lower growth rate and approaches secular equilibrium at higher grow rate (Zhou *et al.*, 2005).

.5 DISCUSSION

.5.1 U-Th dating on speleothems: a preliminary record of the cave's lifetime

Although not directly the focus of this study, the obtained U-series disequilibrium ages are important for understanding the evolution of the Cacahuamilpa cave. Indeed, except for one published age of 1.5 ka obtained by U-Th disequilibrium in one of the speleothems by Garduño-Monroy *et al.* (2011), there are not geochronological records of this extended karst system. This system initiated as a subterranean stream probably at the end of the Tertiary (Enjalbert, 1964) and then rapidly developed as a karstic system.

The older obtained U-Th disequilibrium age on stalagmite CC-B (~88 ka) is certainly a minimum age for the cave, because we sampled small stalagmites which growth in a shorter time lapse compared the giant ones. It is to expect that giant speleothems, such as the 36m-high “Botella de Champán” took much more time to growth to the actual size than the sampled specimen. Taking into account the presence of these giant speleothems, that the growth and development of a karst system can be discontinuous in time, pending the climatic conditions and the active hydrological system natural variations, we could speculate that Cacahuamilpa cave lasted since Early Pleistocene, as suggested by the morphological studies of Enjalbert (1964).

A.6.1 Processes other than seismic in Cacahuamilpa cave

The rupture of exposed stalagmites, several centimeters from their basis, can be caused by several processes. If soil acceleration during a seismic event is probably the most appealing one among these processes, Gilli (1999b) and Becker *et al.* (2006) observed that other natural or anthropic causes could be the source of the observed damages on speleothems in caves. Main causes are human and animal activities, collapse of rocks or ice from the ceiling of the cave, sediments and glacial creeping (e.g., Gilli, 2004).

In the case of Cacahuamilpa cave, human and animal activities can be excluded. Cacahuamilpa cave has been partially inhabited by pre-Columbian Indians and visited rarely by local explorers between 1776 and 1793. The cave was fully explored in 1847 but it was partially opened to public only in 1920 and then entirely in 1967. Local fauna is composed of small animals such as armadillos, rabbits and raccoons that are of modest dimensions to produce damages on so large and heavy stalagmites.

Ice creeping during glaciations can be also excluded. Glaciers never reach these low altitudes (entrance is at 1230 m asl; Fig. 3a). The lowest altitude reached by a glacier

in Mexico is 3000 m, 195 ka ago (Vázquez-Selem et Heine, 2004). During Last Glacial Maximum, glaciers from nearby Nevado del Toluca reached average ELA (Equilibrium Line Altitudes) of 3800-3400 m (Vázquez-Selem et Heine, 2004) well above the altitude of the Cacahuamilpa cave.

Sediment creeping could have partially damaged speleothems in the Cacahuamilpa cave, especially when the cave was a perched stream tube and the west entrance was opened and face to successive invasions of debris flows and lahars from the nearby Nevado del Toluca. Capra et Macias (2000) detailed two debris avalanche deposits (El Picaya and El Mogote) which extend E-SE from the volcano to a distance of 55 to 75 km, surrounding the western side of the Cerro de la Corona (Fig. 2). Capra *et al.* (2002) estimated the age of these two lahars to be older than 40-45 ka. This episode could have caused the invasion of the cave from west to east by the lahars deposits and likely the complete obstruction of the west entrance of the cave (Enjalbert, 1964). U-Th disequilibrium ages of speleothems at Cacahuamilpa (this study) predate or postdate this episode. The CC-B stalagmite, with an age of 88.0 ± 0.7 ka could have been damaged by invasion of volcanoclastic sediments in the cave that was at that time still open to the west. Prior of the El Picaya and El Mogote lahar episode, there is an interbedded sequence of debris flow and lahars called "Older lahars of Nevado" on the flank of the volcano (Garcia-Palomo *et al.*, 2002) for which there are not dates available. We cannot exclude the possibility that 88 ka ago some lahars from Nevado del Toluca invaded the cave and broke the CC-B stalagmite, although river erosion of the cave did not leave trace of surrounding creeping sediments. The CC-B faces opposite (W; Fig. 3b) to the supposed direction of sediment movement (from W to E), but because the strong bending on its stump (32°), the sediment creeping could have just provoked the break of the stalagmite that felt, by gravity instability, to the same direction of the bending.

Invasion of volcanoclastic products from the Nevado del Toluca after the passage of the El Picaya-El Mogote debris flow seems to be excluded. The U-Th disequilibrium ages of 28.769 ± 0.210 ka of the stalagmite CC-A coincide interestingly with one of the episodes of block-and-ash flow (BAF) of the Nevado del Toluca (Garcia-Palomo *et al.*, 2002). However, the maximum distance reached S-SE by these BAF units is the town of Ixtapan de la Sal, which is 30 km north of the Cacahuamilpa cave (Garcia-Palomo *et al.*, 2002).

Recent invasion of sediments from the east entrance is unlikely. The east entrance is partially covered by old consolidated landslide deposits but it is unlikely that a large amount of sediments could have entered deep inside the Cacahuamilpa cave, being the entrance perched at 1230 m, in a steep karst circle and against-slope (Fig. 3a). Invasion of sediments and successive speleothems burial is an unlikely cause for the rupture of stalagmites at site GC. Speleothems are too deep inside the cave compared to the eastern entrance. They lie down perpendicular to the supposed E-W direction undertaken by a sediment flow in this section of the cave (Fig. 3b). Further to be completely covered by sediments and be broken, the stalagmites at site GC should have been buried under a 6-meter high sediment deposit (the stalagmites are 4 meters high but stand on an acclivity, ca. 2 meters above the cave floor). Assuming an average U-Th disequilibrium age of 0.947 ± 0.017 ka for the episode of the stalagmite rupture at site GC, we should assume an improbable erosion rate of 6000 m/Ma, in a karst system without an active stream and in presence of a flat morphology. This erosion rate is 2-3 orders of magnitude higher than those normally observed in active stream karst systems (e.g., Bono et Percopo, 1996; Granger *et al.*, 1997).

A.6.2 Stalagmite rupture by seismic events: geotechnical considerations

If other causes than a seismic event have not damaged the dated stalagmites (with the possible exception of CC-B) then we should test whether they can be effectively broken during the passage of a seismic wave. On the basis of rupture tests on

stalagmites and stalactites, it has been concluded that most of large speleothems could not be broken by oscillations during a seismic event (Gilli *et al.*, 1999; Cadorin *et al.*, 2001; Lacave *et al.*, 2000). On the basis of their measurements, Cadorin *et al.* (2001) concluded that only very thin speleothems with a ratio between their height (H) and their diameter (D) higher than 8 can be broken by large earthquakes, able to produce a maximum peak ground acceleration (PGA) of 10 m s^{-2} . Lacave *et al.* (2000) measured natural frequencies in stalactites. They concluded that most of speleothems do not suffer dynamic amplification phenomena, because their natural frequencies are much higher than the seismic frequency range (around 0.1 to 30 Hz). Only very elongated and thin speleothems could undergo such amplification that might lead to their rupture.

Cadorin *et al.* (2001) related the PGA to the H/D ratio of a speleothem, which is actually misleading. The static, horizontal ground acceleration (a_g in m s^{-2}) resulting in the speleothems failure is calculated as follows (Cadorin *et al.*, 2001; Szeidovitz *et al.*, 2008):

$$a_g = \frac{D\sigma_u}{4\rho H^2} \quad (\text{A.4})$$

where σ_u is the tensile failure stress (in MPa or $10^6 \text{ kg m}^{-1} \text{ s}^{-2}$) which in speleothems range between 0.4 (Cadorin *et al.*, 2001) to 3.8 MPa (Szeidovitz *et al.*, 2008; Gribovszki *et al.*, 2013); and ρ is the density of speleothems ($2300\text{-}2500 \text{ kg m}^{-3}$).

Similarly, the natural frequency (f in Hertz) of a stalagmite (Szeidovitz *et al.*, 2008) can be calculated by the cantilever beam theory as:

$$f \approx \frac{1}{\pi} \sqrt{\frac{3.1ED^2}{16\rho H^4}} \quad (\text{A.5})$$

where E is the Young's modulus of elasticity that for speleothems ranges between 21 and 24 GPa (Cadorin *et al.*, 2001; Szeidovitz *et al.*, 2008; Gribovszki *et al.*, 2013).

From eq. (1) and (2), it derives that both the a_g and the f are linearly dependent of the D/H^2 ratio (e.g., Gribovszki *et al.*, 2013). Although larger, the speleothems sampled at site GC and CC-A could have been broken by large earthquakes (>7 M) with reasonable PGA and frequencies. The GC sampled speleothem has a height (H) of 4.2 m and a diameter (D) of 0.57 m with a resulting D/H^2 ratio of 0.032. Assuming an average density of 2500 kg m^{-3} , a σ_u of 0.4 MPa (Cadorin *et al.*, 2001) and an average E of 22000 MPa (Cadorin *et al.*, 2001), then GC speleothem could break if the PGA of the seismic event is equal or higher than 1.3 m s^{-2} and its frequency is 13.4 Hz. Assuming an average σ_u of 1.62 MPa, as suggested by Szeidovitz *et al.* (2008), the resulting average PGA of the seismic event would be 5.2 m s^{-2} . Similarly, for the stalagmite CC-A ($D = 0.8 \text{ m}$ and $H = 4 \text{ m}$; $D/H^2 = 0.050$) the PGA and frequency f to be reached by the earthquake for the stalagmite rupture are $2.0\text{-}8.1 \text{ m s}^{-2}$, pending the σ_u values chosen (0.4-1.62) and 20.8 Hz, respectively. Lower estimates of PGAs are compatible with the occurrence of large seismic events with magnitude 7-8 M, in a radius of 50-100 km from the Cacahuamilpa cave (PGA of 0.5 to 2 m s^{-2} ; Fukushima et Tanaka, 1990; García *et al.*, 2007; Norini *et al.*, 2010). Average estimates of PGAs could be reached for seismic events with magnitude between 7 and 8 M but located at shorter epicentral distances of less than 10 km (PGA of 2 to 8 m s^{-2} ; García *et al.*, 2007; Norini *et al.*, 2010).

The Cacahuamilpa cave could have been affected by large subduction zone earthquakes, similar to that of Michoacán (1985) of 8.1 M (Suárez *et al.*, 1990) or the earthquake of 1787 (estimated magnitude of 8.6 M; Suárez et Albini, 2009); or by intraplate earthquakes such as those of the great Oaxaca of 1931 (8.1 M), the historic earthquake of Michoacán of 1858 (7.5 M) (Singh *et al.*, 1996) and the Acambay earthquake of 1912 (7.0 M) (Rodríguez-Pascua *et al.*, 2012). Therefore, normal and

strike-slip faults (e.g. the Morelia-Acambay Fault System, the Chapala-Oaxaca Fault System; Fig. 1) (Garduño-Monroy *et al.*, 2009) could have generated sufficiently large local earthquakes to damage speleothems within the Cacahuamilpa cave. More interesting there is a very poor knowledge of the occurrence and frequency of these intraplate earthquakes. Thus Cacahuamilpa cave could became an interesting historical archive for documenting on these past seismic events.

On the other side, the dimensions of the CC-B stalagmite ($D= 1 \text{ m}$ and $H= 1.5 \text{ m}$) requires a PGA and a frequency f of the seismic event from 17.8 up to 72.2 m s^{-2} pending the value of σ_u chosen, and 184 Hz which are unconceivable also for the strongest earthquake (Cadorin *et al.*, 2001; Lacave *et al.*, 2000). It is thus possible that this massive stalagmite could have been broken by some volcanoclastic creeping, rather than a seismic event.

.6 CONCLUSIONS

Speleothems from Cacahuamilpa cave provide independent evidence of extreme geological events that occurred in the last 90 ka. Three distinctive events that provoked stalagmite ruptures were identified using calculated U-Th disequilibrium ages, specifically at $0.95 \pm 0.02 \text{ a}$, $28.8 \pm 0.2 \text{ ka}$ and $88.0 \pm 0.7 \text{ ka}$. The first two rupture ages of stalagmites could be related to strong intraplate seismic events ($>7 \text{ M}$) in the region. However, detailed studies of the geotechnical characteristics of the sampled stalagmites, such as the determination of the tensile failure stress are critical to confirm or infirm these hypotheses. The third stalagmite's rupture is possibly related to local phenomena such as sediment creeping when the cave was still opened on both sides and invaded regularly by volcanoclastic sediments from nearby Nevado del Toluca volcano.

A greater number of U-Th disequilibrium ages are required on seismothems from Cacahuamilpa cave in order to create a significant historical database. Sampling in caves surrounding Cacahuamilpa cave (as the nearby Carlos Pacheco Cave and La Estrella; Bonet, 1971) and stratigraphy studies of the lakes from the lower subterranean floor of the Cacahuamilpa karst system could be used to support preliminary hypotheses presented in this work. The specific ages of ruptures obtained from different stalagmites with similar orientations could help identify massive events capable of damaging speleothems.

Though a detailed morphological study of this cave is required together with a complete stratigraphy of the sedimentary deposits, this preliminary work provides a pathway for future experimental design to retrace the geochronology of caves and could be a key argument to support independent near-fault paleoseismic records.

ACKNOWLEDGMENTS

We wish to thank an anonymous reviewer for his careful review that greatly improved this manuscript. We thank the officers of the Grutas de Cacahuamilpa National Park for permitting to sample inside the cave and the local guides that helped during collection. M. Laithier is thanked for her original drawings of the sampled stalagmites and R. Bartnett for correcting English. This work has been supported by the XIII Quebec-Mexico Working Group funded from the Ministry of International Relations of Quebec and CONACYT (project 13-30).

REFERENCES

- Becker, A., Häuselmann, P., Eikenberg, J. et Gilli, E. (2012). Active tectonics and earthquake destructions in caves of northern and central Switzerland. *International Journal of Speleology*, 41(1), 35-49. doi: 10.5038/1827-806x.41.1.5
- Bini, A., Quinif, Y., Sules, O. et Uggeri, A. (1992). Les mouvements tectoniques récents dans les grottes du Monte Campo dei Fiori (Lombardie, Italie). *Karstologia*, 19(1), 23-30.
- Bischoff, J.L. et Fitzpatrick, J.A. (1991). U-series dating of impure carbonates: an isochron technique using total-sample dissolution. *Geochimica et Cosmochimica Acta*, 55(2), 543-554.
- Bonet, F. (1971). *Espeleología de la región de Cacahuamilpa, Gro.* : Instituto de Geología.
- Bono, P. et Percopo, C. (1996). Flow dynamics and erosion rate of a representative karst basin (Upper Aniene River, Central Italy). *Environmental Geology*, 27(3), 210-218.
- Bourdon, B., Turner, S., Henderson, G.M. et Lundstrom, C.C. (2003). Introduction to U-series geochemistry. *Reviews in Mineralogy and Geochemistry*, 52(1), 1-21.
- Cadorin, J.-F., Jongmans, D., Plumier, A., Camelbeeck, T., Delaby, S. et Quinif, Y. (2001). Modelling of speleothems failure in the Hotton cave (Belgium). Is the failure earthquake induced? *Geologie en Mijnbouw*, 80(3/4), 315-322.
- Capra, L. et Macías, J. (2000). Pleistocene cohesive debris flows at Nevado de Toluca Volcano, central Mexico. *Journal of Volcanology and Geothermal Research*, 102(1), 149-167.
- Capra, L., Macías, J., Scott, K., Abrams, M. et Garduño-Monroy, V. (2002). Debris avalanches and debris flows transformed from collapses in the Trans-Mexican Volcanic Belt, Mexico—behavior, and implications for hazard assessment. *Journal of Volcanology and Geothermal Research*, 113(1), 81-110.
- Charmoille, A., Fabbri, O., Mudry, J., Guglielmi, Y. et Bertrand, C. (2005). Post - seismic permeability change in a shallow fractured aquifer following a ML 5.1 earthquake (Fourbanne karst aquifer, Jura outermost thrust unit, eastern France). *Geophysical Research Letters*, 32(18).
- Delaby, S. et Quinif, Y. (2001). Palaeoseismic investigations in Belgian caves. *Geologie en Mijnbouw*, 80(3/4), 323-332.

- Edwards, R.L., Chen, J. et Wasserburg, G. (1987). ^{238}U ^{234}U ^{230}Th ^{232}Th systematics and the precise measurement of time over the past 500,000 years. *Earth and Planetary Science Letters*, 81(2), 175-192.
- Enjalbert, H. (1964). Phénomènes karstiques au Mexique et au Guatemala. *Bulletin de l'Association de géographes français*, 41(324-325), 30-58.
- Ersek, V., Hostetler, S.W., Cheng, H., Clark, P.U., Anslow, F.S., Mix, A.C. et Edwards, R.L. (2009). Environmental influences on speleothem growth in southwestern Oregon during the last 380000 years. *Earth and Planetary Science Letters*, 279(3), 316-325.
- Forti, P. (2001). Seismotectonic and paleoseismic studies from speleothems: the state of the art. *Geologica belgica*, 4(3-4), 175-185.
- Forti, P. et Postpischl, D. (1984). Seismotectonic and paleoseismic analyses using karst sediments. *Marine geology*, 55(1), 145-161.
- Fries Jr, C. (1960). Geología del Estado de Morelos y de partes adyacentes de México y Guerrero, región central meridional de México.-Inst. geol. *Univ. Nac. Autón. Mex., Bol.*, 60.
- García-Palomo, A., Macías, J., Arce, J., Capra, L., Garduño, V. et Espíndola, J. (2002). Geology of Nevado de Toluca volcano and surrounding areas. *Central Mexico, Geological Society of America*, 26.
- García, S.R., Romo, M.P. et Mayoral, J.M. (2007). Estimation of peak ground accelerations for Mexican subduction zone earthquakes using neural networks. *Geofísica internacional*, 46(1), 51-62.
- Garduño-Monroy, V., Pérez-López, R., Israde-Alcantara, I., Rodríguez-Pascua, M., Szynkaruk, E., Hernández-Madrigal, V., García-Zepeda, M., Corona-Chávez, P., Ostroumov, M. et Medina-Vega, V. (2009). Paleoseismology of the southwestern Morelia-Acambay fault system, central Mexico. *Geofísica internacional*, 48(3), 319-335.
- Garduño-Monroy, V., Pérez-López, R., Rodríguez-Pascua, M., Mayordomo, J.G., Israde-Alcántara, I. et Bischoff, J. (2011). Could large palaeoearthquakes break giant stalactites in Cacahuamilpa Cave?(Taxco, Central Mexico). Dans *2nd INQUA-IGCP-567 Proc.* (Vol. 2, p. 50-53).
- Genty, D., Blamart, D., Ouahdi, R., Gilmour, M., Baker, A., Jouzel, J. et Van-Exter, S. (2003). Precise dating of Dansgaard-Oeschger climate oscillations in western Europe from stalagmite data. *Nature*, 421(6925), 833-837.
- Genty, D., Ghaleb, B., Plagnes, V., Causse, C., Valladas, H., Blamart, D., Massault, M., Geneste, J.-M. et Clottes, J. (2004). Datations U/Th (TIMS) et ^{14}C (AMS) des stalagmites de la grotte Chauvet (Ardèche, France): intérêt pour la

- chronologie des événements naturels et anthropiques de la grotte. *Comptes Rendus Palevol*, 3(8), 629-642.
- Gilli, E. (1999). Rupture de spéléothèmes par fluage d'un remplissage endokarstique. L'exemple de la grotte de Ribièvre (Bouches-du-Rhône). *Comptes Rendus de l'Académie des Sciences-Series IIA-Earth and Planetary Science*, 329(11), 807-813.
- Gilli, E. (2004). Glacial causes of damage and difficulties to use speleothems as palaeoseismic indicators. *Geodinamica Acta*, 17(3), 229-240.
- Gilli, É. (2005). Review on the use of natural cave speleothems as palaeoseismic or neotectonics indicators. *Comptes Rendus Geoscience*, 337(13), 1208-1215.
- Gilli, E. et Serface, R. (1999). Evidence of palaeoseismicity in the caves of Arizona and New Mexico (USA). *Comptes Rendus de l'Académie des Sciences-Series IIA-Earth and Planetary Science*, 329(1), 31-37.
- Gospodarič, R. (1977). Collapsing of speleothems in Postojna cave system. In: Proc. 7th INt. Speleol. Congr. Sheffield, 223-225.
- Granger, D.E., Kirchner, J.W. et Finkel, R.C. (1997). Quaternary downcutting rate of the New River, Virginia, measured from differential decay of cosmogenic ^{26}Al and ^{10}Be in cave-deposited alluvium. *Geology*, 25(2), 107-110.
- Gribovszki, K., Bokelmann, G., Szeidovitz, Gy, Paskaleva, I., Brimich, L., Kovacs, K., Monus, P. (2013). Comprehensive investigation of intact, vulnerable stalagmites to estimate an upper limit on prehistoric horizontal ground acceleration. Vienna congress on recent advances in earthquake engineering and structural dynamics.
- Kagan, E.J., Agnon, A., Bar-Matthews, M. et Ayalon, A. (2005). Dating large infrequent earthquakes by damaged cave deposits. *Geology*, 33(4), 261. doi: 10.1130/g21193.1
- Lacave, C., Levret, A., Koller, M. (2000). Measurements of natural frequencies and damping of speleothems. Proc. of the 12th World Conference on Earthquake Engineering, Auckland, New-Zealand, paper.
- Ludwig, K. (2012). User's Manual for Isoplot 3.75: A Geochronological Toolkit for Microsoft Excel. Berkeley Geochronology Centre Special Publication No. 5.
- Ludwig, K.R., Paces, J.B. (2002). Uranium series dating of pedogenic silica and carbonate, Crater Flat, Nevada. *Geochim. Cosmochim. Acta* 66, 487-506
- Marshall, D., Ghaleb, B., Countess, R. et Gabities, J. (2009). Preliminary paleoclimate reconstruction based on a 12,500year old speleothem from Vancouver Island, Canada: stable isotopes and U-Th disequilibrium dating. *Quaternary Science Reviews*, 28(23-24), 2507-2513.

- Norini, G., Capra, L., Borselli, L., Zuniga, F., Solari, L. et Sarocchi, D. (2010). Large scale landslides triggered by Quaternary tectonics in the Acambay graben, Mexico. *Earth Surface Processes and Landforms*, 35(12), 1445-1455.
- Pons-Branchu, E. (2001). *Datation haute résolution de spéléothèmes (230 Th/234 U et 226 Ra/238 U): application aux reconstitutions environnementales autour des sites du Gard et du Meuse/Haute Marne*. Aix-Marseille 3.
- Postpischl, D., Agostini, S., Forti, P. et Quinif, Y. (1991). Palaeoseismicity from karst sediments: the “Grotta del Cervo” cave case study (Central Italy). *Tectonophysics*, 193(1), 33-44.
- Quinif, Y. (2010). Enregistrement et datation des effets sismo-tectoniques par l'étude des spéléothèmes. *Annales de la Société géologique de Belgique*.
- Rodríguez-Pascua, M., Garduño-Monroy, V., Pérez-López, R., Perucha-Atienza, M. et Isdrade-Alcántara, I. (2012). The Acambay earthquake of 1912, revisited 100 years after. Dans *3rd INQUA-IGCP-567 Proc* (p. 157-160).
- Suárez, G. et Albini, P. (2009). Evidence for great tsunamigenic earthquakes (M 8.6) along the Mexican subduction zone. *Bulletin of the Seismological Society of America*, 99(2A), 892-896.
- Suárez, G., Monfret, T., Wittlinger, G. et David, C. (1990). Geometry of subduction and depth of the seismogenic zone in the Guerrero gap, Mexico. *Nature*, 345(6273), 336-338.
- Szeidovitz, G., Surányi, G., Gribovszki, K., Bus, Z., Leél-Óssy, S. et Varga, Z. (2008). Estimation of an upper limit on prehistoric peak ground acceleration using the parameters of intact speleothems in Hungarian caves. *Journal of Seismology*, 12(1), 21-33.
- Vázquez-Selem, L. et Heine, K. (2004). Late quaternary glaciation of Mexico. *Developments in Quaternary Sciences*, 2, 233-242.
- Wang, Y.-J., Cheng, H., Edwards, R.L., An, Z., Wu, J., Shen, C.-C. et Dorale, J.A. (2001). A high-resolution absolute-dated late Pleistocene monsoon record from Hulu Cave, China. *Science*, 294(5550), 2345-2348.
- Zhou, J., Lundstrom, C.C., Fouke, B., Panno, S., Hackley, K. et Curry, B. (2005). Geochemistry of speleothem records from southern Illinois: Development of $(^{234}\text{U})/(^{238}\text{U})$ as a proxy for paleoprecipitation. *Chemical Geology*, 221(1), 1-20.

FIGURES

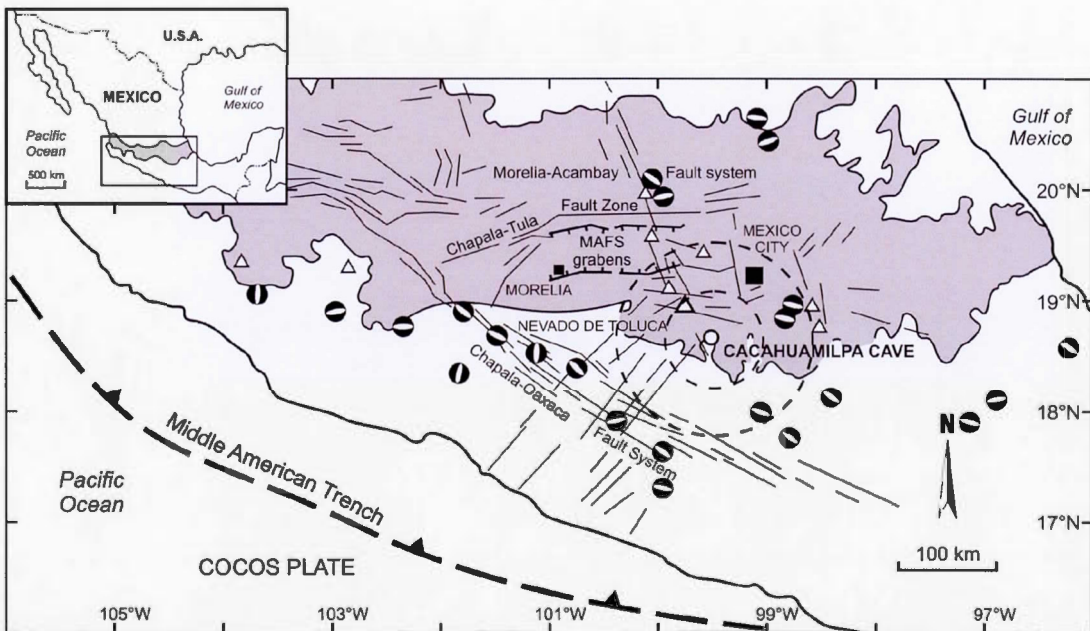


Figure A.1 Simplified map with the localization of Cacahuamilpa cave within the Transmexican Volcanic Belt TMVB (in grey color). The NE-SW and NW-SE trending fault systems belonging to the Morelia-Acambay Fault System and the Nevado de Toluca Volcano are also reported. Two circles with radius of 50 and 100 km are reported to indicate the region where seismic events possibly originated and induced ruptures in stalagmites of the Cacahuamilpa cave. Focal mechanisms of the major intraplate earthquakes occurring in the region have been also reported (beachball plot). Redrawn and modified from Garduño-Monroy *et al.* (2011).

Figure A.2 Simplified geo-morphological map of the area of the Cacahuamilpa cave with the San Jeronimo and Chontalcoatlán river systems that developed the La Estrella Karstic System (LAKS). The position of the Cacahuamilpa cave (plan profile) has been also drawn. Redrawn and modified from Enjalbert (1964).

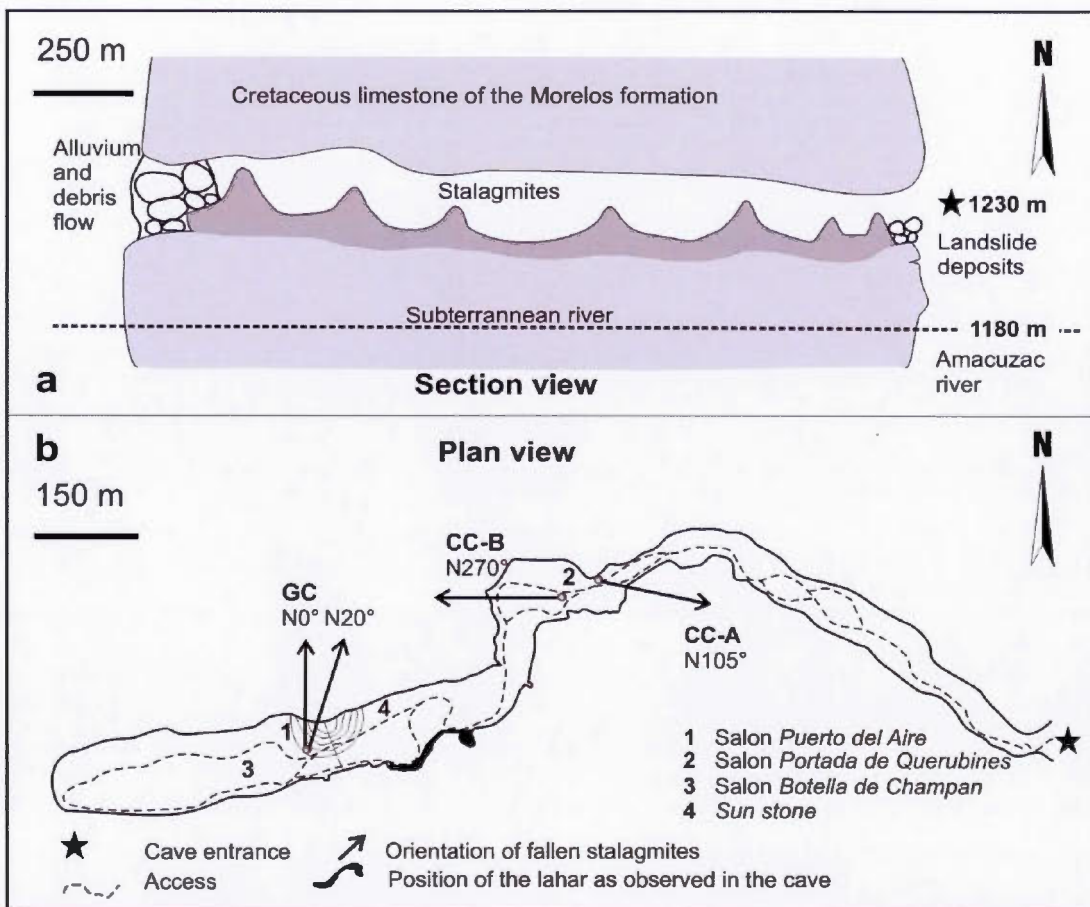
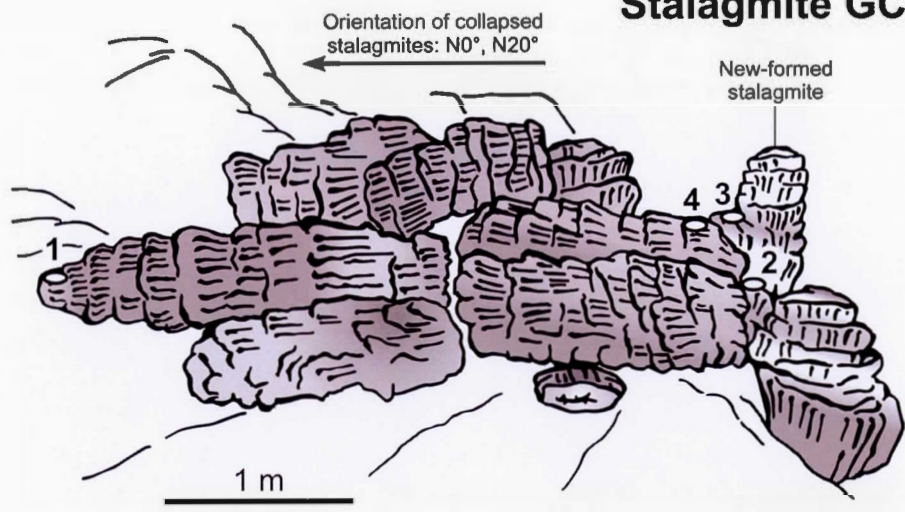


Figure A.3 Profile (a) and plan (b) view of the Cacahuamilpa cave. The position and orientation of the dated stalagmites are reported together with the position of the small outcrop of lahar deposits from the Nevado del Toluca volcano. Redrawn and

modified from Enjalbert (1964) and Bonet (1971).

Stalagmite GC



GC-1: 0.999 ± 0.022 ka

GC-3: 0.927 ± 0.155 ka

GC-2: 0.828 ± 0.028 ka

GC-4: 1.711 ± 0.036 ka

Figure A.4 Fallen and oriented stalagmites on the site GC. Sample GC-1 corresponds to the last calcite precipitated before rupture of the stalagmite. Sample GC-4 records the oldest age in the stalagmite. Sample GC-2 and sample GC-3 are from the stalagmite formed on the hung.

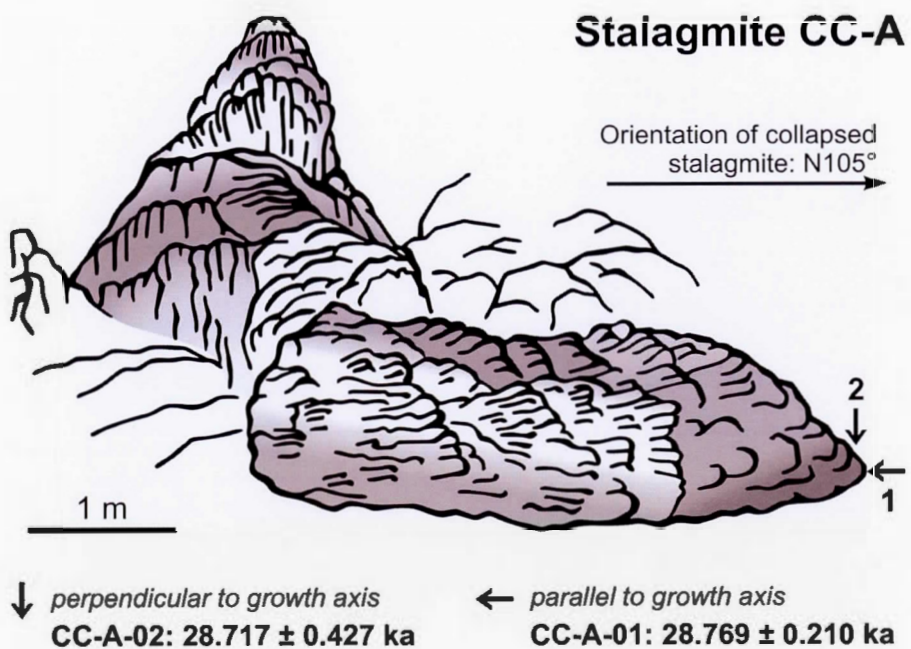


Figure A.5 Drilled-cores acquired on the site CC-A. The first sample (1) was collected parallel to the growth axis of the stalagmite. The second sample (2) was taken perpendicular to the growth axis.

Stalagmite CC-B

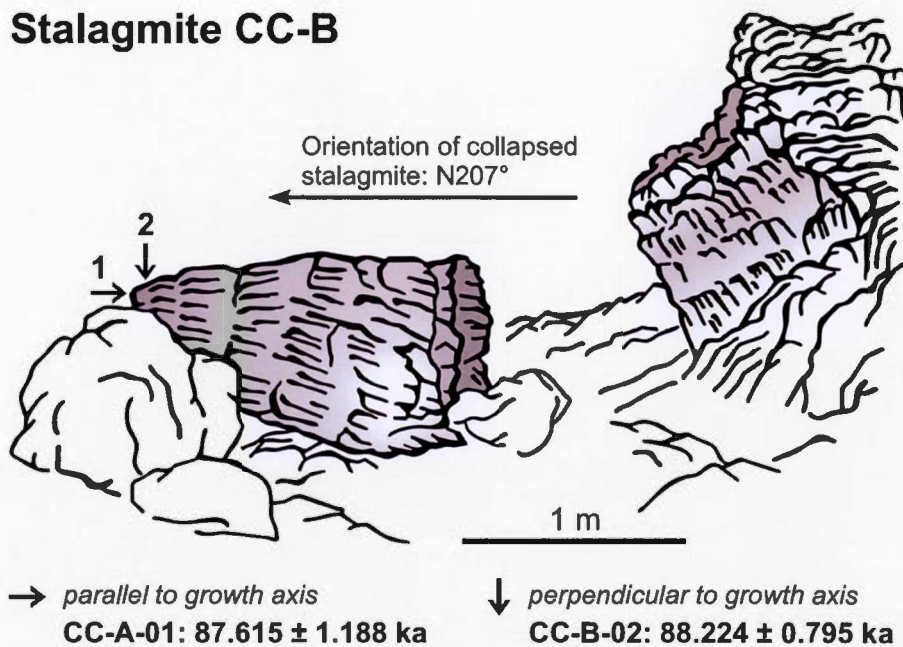


Figure A.6 Drilled-cores acquired on the site CC-B. The first sample (1) was collected parallel to the growth axis of the stalagmite. The second sample (2) was taken perpendicular to the growth axis.

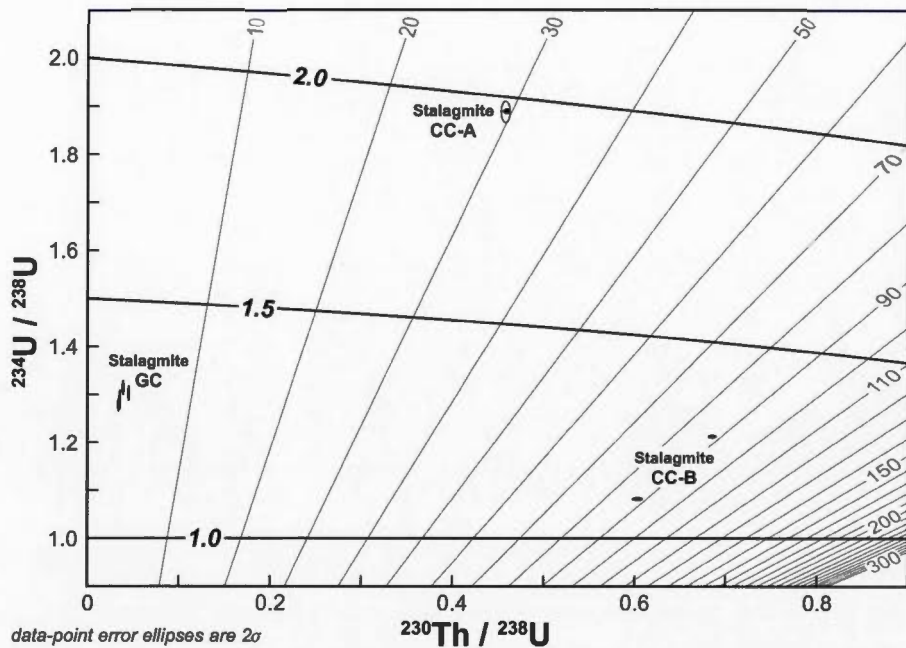


Figure A.7 U-Th disequilibrium ages calculated on stalagmite GC, CC-A and CC-B with corresponding $(^{234}\text{U}/^{238}\text{U})$ and $(^{230}\text{Th}/^{238}\text{U})$ activity ratios. The plot was drawn using ISOPLOT 3.7 (Ludwig, 2012).

Tableau A.1 U/Th disequilibrium data with calculated and corrected ages.

Sample	^{238}U ppm	\pm	^{232}Th ppb	\pm	$^{234}\text{U}/^{238}\text{U}$	\pm	$^{230}\text{Th}/^{234}\text{U}$	\pm
GC 1	1.045	0.006	0.6250	0.0020	1.2834	0.0147	0.0092	0.0002
GC 2	0.969	0.005	0.5486	0.0028	1.2716	0.0104	0.0077	0.0003
GC 3**	0.904	0.005	11.1291	0.0557	1.3076	0.0123	0.0110	0.0003
GC 4	0.895	0.005	1.5361	0.0080	1.2958	0.0112	0.0160	0.0003
GC weighted average age***								
CC-A-01	0.636	0.003	0.1105	0.0100	1.8935	0.0046	0.2370	0.0014
CC-A-02	0.542	0.005	0.6252	0.0034	1.8916	0.0185	0.2366	0.0016
CC-A weighted average age								
CC-B-01	3.110	0.019	0.2660	0.0031	1.0722	0.0034	0.5576	0.0046
CC-B-02	1.845	0.010	0.8170	0.0080	1.2053	0.0025	0.5669	0.0032
CC-B weighted average age								

* Detritus correction using crustal model, the isotope and the activity ratios used were ($^{232}\text{Th}/^{238}\text{U}$)=1.21 \pm 50%, ($^{234}\text{U}/^{238}\text{U}$)=1 \pm 10% and ($^{230}\text{Th}/^{238}\text{U}$)=1 \pm 10%

**Sample corrected for detritus

*** The outliers GC 4 age has been excluded. The GC weighted average age including GC 4 would be 1.271 \pm 0.018 ka

$^{230}\text{Th}/^{238}\text{U}$	\pm	$^{230}\text{Th}/^{232}\text{Th}$	\pm	Calculated age ka	\pm	$(^{234}\text{U}/^{238}\text{U})_0$	\pm	Corrected age* ka	\pm
0.0119	0.0002	60.6	0.9	1.013	0.021	1.284	0.015	0.999	0.022
0.0098	0.0003	52.8	1.8	0.841	0.027	1.272	0.010	0.828	0.028
0.0144	0.0004	3.6	0.1	1.204	0.035	1.309	0.012	0.927	0.155
0.0207	0.0003	36.9	0.6	1.750	0.030	1.297	0.011	1.711	0.036
								0.947	0.017
0.4488	0.0027	790.2	9.6	28.795	0.210	1.969	0.005	28.769	0.210
0.4475	0.0039	1187.5	9.9	28.735	0.427	1.967	0.019	28.717	0.427
								28.759	0.189
0.5978	0.0049	21343.4	325.4	87.617	1.188	1.093	0.004	87.615	1.188
0.6832	0.0038	4713.2	58.4	88.234	0.795	1.264	0.003	88.224	0.795
								88.037	0.661

* Detritus correction using crustal model, the isotope and the activity ratios used were $(^{232}\text{Th}/^{238}\text{U})=1.21 \pm 50\%$, $(^{234}\text{U}/^{238}\text{U})=1 \pm 10\%$ and $(^{230}\text{Th}/^{238}\text{U})=1 \pm 10\%$

**Sample corrected for detritus

*** The outliers GC 4 age has been excluded. The GC weighted average age including GC 4 would be 1.271 ± 0.018 ka